

ASSESSING THE EFFECT OF NEAR SURFACE ENVIRONMENTAL CONDITIONS ON UNSATURATED SLOPE INSTABILITY

by

Nelson John Ferreira

A Thesis
Submitted to the Faculty of Graduate Studies
in Partial Fulfillment of the Requirements for the Degree of

Master of Science

Department of Civil Engineering
University of Manitoba
Winnipeg, Manitoba

August, 2002



National Library
of Canada

Acquisitions and
Bibliographic Services

395 Wellington Street
Ottawa ON K1A 0N4
Canada

Bibliothèque nationale
du Canada

Acquisitions et
services bibliographiques

395, rue Wellington
Ottawa ON K1A 0N4
Canada

Your file Votre référence

Our file Notre référence

The author has granted a non-exclusive licence allowing the National Library of Canada to reproduce, loan, distribute or sell copies of this thesis in microform, paper or electronic formats.

The author retains ownership of the copyright in this thesis. Neither the thesis nor substantial extracts from it may be printed or otherwise reproduced without the author's permission.

L'auteur a accordé une licence non exclusive permettant à la Bibliothèque nationale du Canada de reproduire, prêter, distribuer ou vendre des copies de cette thèse sous la forme de microfiche/film, de reproduction sur papier ou sur format électronique.

L'auteur conserve la propriété du droit d'auteur qui protège cette thèse. Ni la thèse ni des extraits substantiels de celle-ci ne doivent être imprimés ou autrement reproduits sans son autorisation.

0-612-79952-2

THE UNIVERSITY OF MANITOBA
FACULTY OF GRADUATE STUDIES

COPYRIGHT PERMISSION

**ASSESSING THE EFFECT OF NEAR SURFACE ENVIRONMENTAL CONDITIONS ON
UNSATURATED SLOPE INSTABILITY**

BY

NELSON JOHN FERREIRA

**A Thesis/Practicum submitted to the Faculty of Graduate Studies of The University of
Manitoba in partial fulfillment of the requirement of the degree**

of

MASTER OF SCIENCE

NELSON JOHN FERREIRA © 2002

Permission has been granted to the Library of the University of Manitoba to lend or sell copies of this thesis/practicum, to the National Library of Canada to microfilm this thesis and to lend or sell copies of the film, and to University Microfilms Inc. to publish an abstract of this thesis/practicum.

This reproduction or copy of this thesis has been made available by authority of the copyright owner solely for the purpose of private study and research, and may only be reproduced and copied as permitted by copyright laws or with express written authorization from the copyright owner.

Abstract

The shear strength of soils can be significantly increased when matric suction is present in the soil matrix. In reference to highways, this increase in soil strength is reflected as an increase in stability. However, the increased strength associated with soil suction cannot be expected to exist over the entire life of the slope as it will fluctuate or even be removed when subjected to certain weather conditions. With the employment of unsaturated/saturated soil mechanics into finite element and limit equilibrium methods, the influences of matric suction and weather conditions on slope stability can be quantitatively evaluated.

In 1999, after a period of extensive rainfall, two slope failures developed within the right-of-way of Provincial Road 259 near Virden, Manitoba. It is postulated that extensive rainfall events in 1999 caused dissipation of soil suction that reduced total shear strength triggering failure. Following the slides, a research project was initiated between the Geotechnical Group at the University of Manitoba and the Manitoba Department of Highways and Transportation to determine the cause of failure. A detailed research program that included the assessment of the geology, geomorphology, site conditions, field conditions, laboratory testing, and numerical modelling was undertaken to quantitatively identify the cause of failure.

A transient coupled seepage analysis and slope stability computer model was constructed to analyze the impact and contribution of matric suction and the

weather conditions on slope stability. The Seep/W and Slope/W computer programs from GeoSlope Int. (Calgary, Alberta) were used in the analysis. Three seven-month periods (April 1 to November 1) 1998, 1999, and 2000 were analyzed with the seven-month period in 2000 used as the calibration year.

The results showed that during typical conditions the highway cut was stable due to the contribution of matric suction to total shear strength. Following the non-typical rainfall events of 1999, the highway cut became unstable as a result of dissipation of matric suction due to infiltration into the soil.

Acknowledgements

I would like to thank Dr. J. Blatz, P.Eng. and Dr. J. Graham, P.Eng. for their patience and guidance during my time in post-graduate studies. Their relentless encouragement and support helped me to grow academically and professionally. I enjoyed my time under their supervision and look forward to a continued collaboration in the future.

I thank Dr. R. Kenyon of KGS Group for his support and advice during this research project. His assistance is appreciated greatly.

Special thanks go to all the graduate students who helped me through discussions on my research and their friendship; Paula Kennedy, Blair Garinger, Grant Ferguson, Kate Franklin, and David Anderson. Also I would like to thank the support and work done by two summer students, Ritchie Armstrong and Greg Siemens.

I acknowledge financial support from the Natural Sciences and Engineering Research Council of Canada, the department of Civil Engineering, the Canadian Geotechnical Society, the friends and colleagues of Neil Burgess, and the Department of Highways and Transportation (MB), specifically Said Kass, Tony Ng, and Ray Van Cauwenberge, who funded the field component of this research project.

I would like to finally thank my parents João Carlos and Maria dos Anjos Ferreira, my two sisters Suzana Maria da Silva, Michelle Thomas, and my two cousins Marco Augusto Carreira and Roberto Luis Carreira who took my mind off my research as much as possible. Finally I would like to especially thank Margherita Gagliardi for her endless patience, encouragement, and support during my research.

Table of Contents

Abstract	i
Acknowledgements	iii
Table of Contents	iv
List of Tables and Figures	vii
 Chapter 1: Introduction	 1
1.0 General Overview	1
1.1 Hypothesis and Objectives	2
1.2 Organization of Thesis	2
 Chapter 2: Literature Review	 6
2.0 Introduction	6
2.1 Strength of Soils	7
2.1.1 Phase Relationship	8
2.1.2 Stress-State of a Soil	8
2.2 Soil Suction	10
2.2.1 Osmotic Suction	12
2.2.2 Matric Suction	12
2.3 Predication of the Soil Water Characteristic Curve from Grain Size Distributions	14
2.3.1 Theoretical Predictive Methods for the Soil Water Characteristic Curve	16
2.3.2 Calculating the Air Entry Value	18
2.3.3 Prediction of the SWCC Using the Kovács Method (1981)	19
2.3.4 The Modified Kovács Method of Predicting Soil Water Characteristic Curve	23
2.4 Prediction of the Conductivity Function from the SWCC	26
2.4.1 Closed-form Equation Presented by van Genuchten (1980)	26
2.5 Shear Strength	28
2.5.1 Shear Strength Equation for Saturated Soil	29
2.5.2 Shear Strength Equation for Unsaturated Soil	30
2.6 Slope Instability	31
2.6.1 Infinite Slope Analysis	32
2.6.2 Limit Equilibrium Method of Slices	34
2.6.2.1 Development of Safety Factor Equations	36
2.6.2.2 Spencer's Method of Slope Stability Equations	38
2.7 Seepage Modeling Using a Finite Element Model	39
2.7.1 Governing Equations for the Finite Element Seepage Software	41
2.8 Summary	43
 Chapter 3: Site Conditions	 45
3.0 General Overview of Site	45
3.1 Site Geology and Geomorphology	48

Chapter 4: Field Investigation	52
4.0 Introduction	52
4.1 Topographic Survey	53
4.2 Hand Augured Holes	53
4.3 Test Pits	57
4.3.1 <i>In-Situ</i> Suction Profile	59
4.4 Borehole and Standpipe installation	59
4.5 Summary	62
Chapter 5: Laboratory Testing	64
5.0 Introduction	64
5.1 Soil Classification	64
5.1.1 Atterberg Limits and Moisture Contents	65
5.1.2 Specific Gravity	66
5.1.3 Grain Size Determination	66
5.2 Flexible Wall Permeameter Tests	67
5.3 CIU Triaxial Tests	68
5.4 Direct Shear Tests	70
Chapter 6: Integrated Seepage and Slope Stability Modeling	73
6.0 Introduction	73
6.1 Preliminary Integrated Model	74
6.1.1 Seep/W Modeling	74
6.1.2 Slope/W Modeling	76
6.1.3 Results from the Preliminary Model	78
6.2 Integrated Transient Model	79
6.2.1 Transient Seepage Analysis	80
6.2.1.1 Construction of Seep/W Transient Model	80
6.2.1.2 Soil Properties	84
6.2.1.3 Initial Boundary Conditions	87
6.2.1.4 Calibration of the Transient Seep/W Model	91
6.2.2 Transient Slope Stability Analysis	94
6.3 Results	96
6.3.1 Seep/W Results	96
6.3.2 Slope/W Results	97
6.4 Sensitivity Analyses	100
Chapter 7: Summary and Conclusions	104
7.0 Summary	104
7.1 Conclusions	110
7.2 Limitations of the Research	111

References

Appendix A: Hand Augured Field Logs

Appendix B: Test Pits Field Logs

Appendix C: Field Borehole Logs

Appendix D: Borehole Logs
Appendix E: Grain Size Distribution
Appendix F: Gould Report

List of Tables and Figures

Tables:

- Table 6.01 Comparison of water levels for fall 2001 used in preliminary seepage analysis.
- Table 6.02 Factors of Safety for preliminary Slope/W model.
- Table 6.03 Runoff coefficients used in calibrated transient Seep/W model.

Figures:

- Figure 2.01 Stress-state variables for an unsaturated soil (Fredlund and Rahardjo 1993).
- Figure 2.02 The capillary tube (Fredlund and Rahardjo 1993).
- Figure 2.03 Varying capillary rise due to variation of pore size (Fredlund and Rahardjo 1993).
- Figure 2.04 Hysteresis of the SWCC (adapted from Gonzalez and Adams 1980).
- Figure 2.05 Comparison of calculated AEV using the Brooks and Corey method (1964) *versus* measured AEV (Aubertin *et al.* 1998).
- Figure 2.06 Comparison of the a) Kovács model to b) the modified Kovács to experimental results for the SWCC (Aubertin *et al.* 1998).
- Figure 2.07 Observed (open circles) and calculated curves (solid lines) of the hydraulic conductivity function for Hygiene Sandstone (van Genuchten 1980).
- Figure 2.08 Observed (open circles) and calculated curves (solid lines) of the hydraulic conductivity function for Touchet Silt Loam G.E. 3 (van Genuchten 1980).
- Figure 2.09 Observed (open circles) and calculated curves (solid lines) of the hydraulic conductivity function for Silt Loam G.E. 3 (van Genuchten 1980).
- Figure 2.10 Observed (open circles) and calculated curves (solid lines) of the hydraulic conductivity function for Beit Netofa Clay (van Genuchten 1980).
- Figure 2.11 Observed (open circles) and calculated curves (solid lines) of the hydraulic conductivity function for Guelph Loam (van Genuchten 1980).
- Figure 2.12 Mohr-Coulomb failure envelope for a saturated soil (Fredlund and Rahardjo 1993).
- Figure 2.13 Mohr-Coulomb failure surface for an unsaturated soil (Fredlund and Rahardjo 1993).
- Figure 2.14 Non-linearity of unsaturated failure envelope (Fredlund and Rahardjo 1993).
- Figure 2.15 Infinite slope analysis (Graham 1984).
- Figure 2.16 Free body diagram of forces acting on a soil slice (Graham 1984).

- Figure 2.17 Parameters used to resolve force and moment limit equilibrium equations (Fredlund and Krahn 1977).
- Figure 2.18 Relationship between the two limit equilibrium equations, F_f and F_m , and the interslice inclination using Spencer's method of slope stability analysis (Fredlund and Krahn 1977).
- Figure 3.01 East Failures of 1999 and 2000.
- Figure 3.02 West Failure summer of 1999.
- Figure 3.03 New West Failure 2001.
- Figure 3.04 Aerial photograph of study area taken November 1999.
- Figure 3.05 Toe of West Failure, summer 2001.
- Figure 3.06 Toe of failure north of PR 259.
- Figure 3.07 Assiniboine drainage basin (Klassen 1975).
- Figure 3.08 Assiniboine Valley cross-sections (Klassen 1975).
- Figure 3.09 Bedrock geology (Betcher 1983).
- Figure 3.10 Bedrock topography (Betcher 1983).
- Figure 3.11 Surficial deposits (Betcher 1983).
- Figure 4.01 Topographic map of study area.
- Figure 4.02 Cross-section A-A.
- Figure 4.03 Cross-section B-B.
- Figure 4.04 Cross-section C-C.
- Figure 4.05 Cross-section D-D.
- Figure 4.06 Cross-section E-E.
- Figure 4.07 Cross-section F-F.
- Figure 4.08 Hand augered holes interpreted soil profile.
- Figure 4.09 Borehole and hand augered holes interpreted soil profile.
- Figure 4.10 Hand augered holes standpipe installation.
- Figure 4.11 Standpipe installation in boreholes and hand augered holes.
- Figure 4.12a Test pit 1.
- Figure 4.12b Close up of Test pit 1.
- Figure 4.13 Test pit 2 and backhoe.
- Figure 4.14 Failure surface at the bottom of Test pit 2.
- Figure 4.15 Possible failure surface on west wall of Test pit 2.
- Figure 4.16 Possible failure on east wall of Test pit 2.
- Figure 4.17 Tensiometer from Soilmoisture Inc..
- Figure 4.18 Tensiometer schematic.
- Figure 4.19 Variation of matric suction with depth.
- Figure 4.20 BH-2-5 - fracture at a depth of 3.71 metres below ground surface.
- Figure 4.21 BH-3-6 - slickensided fracture at a depth of 3.81 metres.
- Figure 4.22 Undrained shear strength *versus* depth using Torvane.
- Figure 4.23 Undrained shear strength *versus* depth using Pocket Penetrometer
- Figure 5.01 Plasticity chart for material retrieved from the study area.
- Figure 5.02 Grain size distribution of "till-like soil".

- Figure 5.03 A example of a failure plane developed under undrained triaxial conditions.
- Figure 5.04 Stress-strain results for all triaxial specimens.
- Figure 5.05 Deviator stress *versus* confining stress for all triaxial specimens.
- Figure 5.06 Normally consolidated failure envelope from triaxial tests.
- Figure 5.07 Residual failure envelope from direct shear tests.
-
- Figure 6.01 Seep/W domain used in preliminary analysis.
- Figure 6.02 Slope/W domain used in preliminary analysis.
- Figure 6.03 Pore water pressure profile used in preliminary study.
- Figure 6.04 Detailed Seep/W domain used in transient analysis.
- Figure 6.05 Finite element mesh used in transient Seep/W model.
- Figure 6.06 The silty fine sand seam after the re-failing of the 'West Failure'.
- Figure 6.07 SWCC and hydraulic conductivity function for weathered clay layer. SWCC function was based on sample BH-3-7.
- Figure 6.08 SWCC and hydraulic conductivity function for sand seam layer. SWCC function was based from BH-2-4.
- Figure 6.09 SWCC and hydraulic conductivity function for unweathered clay layer. SWCC function was determined from sample BH-3-7.
- Figure 6.10 Return period for rainfall events at Virden, Manitoba.
- Figure 6.11 Seep/W result with no applied environmental flux boundary.
- Figure 6.12a Calibrated environmental flux function for April 1, 2000 to November 1, 2001.
- Figure 6.12b Shifted SWCC for the weathered clay layer.
- Figure 6.13 BH-2 measured groundwater levels *versus* modeled groundwater levels for April 1 to November 1, 2000.
- Figure 6.14 A-4 measured groundwater levels *versus* modeled groundwater levels for April 1 to November 1, 2000.
- Figure 6.15 A-4 measured groundwater levels *versus* modeled groundwater levels for April 1 to November 1, 2000
- Figure 6.16 Modeled groundwater levels *versus* Measured groundwater levels for all standpipes.
- Figure 6.17 Measured *versus* Modeled suction profile.
- Figure 6.18 Slope/W domain used in detailed transient analysis.
- Figure 6.19 Groundwater profile modelled in Seep/W for 1998.
- Figure 6.20 1998 - Total head *versus* time for node 693 plotted on the primary axis (left). Environmental flux function *versus* time is plotted on the secondary axis (right).
- Figure 6.21 1999 - Total head *versus* time for node 693 plotted on the primary axis. Environmental flux function *versus* time is plotted on the secondary axis.
- Figure 6.22 2000 - Total head *versus* time for node 693 plotted on the primary axis. Environmental flux function *versus* time is plotted on the secondary axis.

- Figure 6.23 1998 – Suction versus time for a node 674 plotted on the primary axis. Environmental flux function *versus* time is plotted on the secondary axis.
- Figure 6.24 Factor of safety with respect to time for 1998, 1999, and 2000.
- Figure 6.25 Factor of safety with respect to time for May and June for both 1998, and 1999.
- Figure 6.26 Pore water pressure distribution along failure surface for two simulations.
- Figure 6.27 Frictional and suction component of available shear strength.
- Figure 6.28 Factor of safety *versus* percent change in evapotranspiration for May 15, 1999.
- Figure 6.29 Factor of safety *versus* change in head at the left boundary of the detailed model domain for May 15, 1999.
- Figure 6.30 Factor of safety *versus* ϕ of the silty fine sand seam for May 15, 1999.
- Figure 6.31 Factor of safety *versus* ϕ of the weathered and unweathered clay for May 15, 1999.

Chapter 1

Introduction

1.0 General Overview

The influence of soil suction on the stability of slopes is an important field of study considering the abundance of unsaturated soils in populated areas of the world (Fredlund and Rahardjo 1993). Specific case studies from Hong Kong, Singapore, Malaysia and more recently Canada have shown examples where instability was related to a loss of suction caused by weather conditions.

In 1999, after a period of substantial rainfall, two relatively shallow, bowl-shaped failures developed along the right-of-way of Provincial Road 259, 4 kilometres northeast of Virden MB. The movements are located along a highway cut slope near the top of the west side of the Assiniboine River Valley. Movements in both slide areas occurred along a 200 metre section of the highway. The two failures are referred to as the West Failure and the East Failure.

1.1 Hypotheses and Objectives

Hypothesis:

Extensive rainfall caused dissipation of soil suction (negative pore water pressures) in the soil profile of the slope, that in turn reduced the total effective shear strength which triggered failure.

Objective of Research:

A research project was initiated between the University of Manitoba and the Manitoba Department of Highways and Transportation to determine the cause of failure. The objective was to obtain a better understanding of why these slopes failed after 25 years of remaining stable. The results will be used to examine methods of preventing future instabilities along similar highway cuts and to properly assess improvements that can be realized from different remediation techniques.

1.2 Organization of the Thesis

The literature review in Chapter 2 provides descriptions, comparisons, and concepts of appropriate theories published in literature pertaining to this thesis. This chapter also describes the fundamentals behind the modeling tools used in this research project. The concepts include the stress-states of soils, soil suction,

predictive models for both the soil water characteristic curve and the unsaturated hydraulic conductivity function, shear strength of soils, slope stability analysis, and the fundamentals of numerical modelling and the finite element method.

Chapter 3 presents a general overview of the study area and includes a description of the soil types and information on the geology and geomorphology. The chapter also describes the location and geometry of the slope failures, including details about the surficial deposits and groundwater conditions. Other local failures are described along with their relevance to the study area. The study area is located within a complex geological sequence produced by numerous geomorphologic processes. These processes and the associated physical formations are discussed in detail in the Geology and Geomorphology section of this chapter.

Chapter 4 discusses the field investigation component of the research. The field investigation consisted of a site survey, excavation of test pits, four boreholes, and several hand augured holes. All the boreholes and most of the hand augured holes included installation of standpipe piezometers to measure the groundwater conditions. Information gathered from the field investigation is shown to be a major key to understanding the site conditions and the factors that influence slope instability. The knowledge gathered from the field investigation is used in subsequent components of this research project.

Chapter 5 presents description, and results for all laboratory tests undertaken in this research program. The laboratory tests included traditional soil classification tests, flexible wall permeameter tests, triaxial tests, and direct shear tests. The traditional soil classification tests included Atterberg limits, specific gravities, and grain size distributions. For the most part, the soil was medium plastic in nature with the majority of the soil being classified as a "till like" clay. The permeability was determined to range between 5.6×10^{-10} m/sec to 3.7×10^{-11} m/sec based on intact, lab specimens. *In-situ* permeability could be expected to be significantly higher due to weathering and freeze/thaw cycles. The normally consolidated (critical state) friction angle from the triaxial test results was selected based on the blocky/friable nature of the material retrieved from the study area and was interpreted as being 22.3° with an assumed cohesion of zero. Since the slope has undergone past instability and the nature of the material would result in cohesion near zero, the interpreted shear strength envelope was forced through the origin for simplicity. The internal friction angle determined from triaxial tests was verified with shear strength results from direct shear tests.

Chapter 6 provides details on seepage and slope stability model construction calibration, and analysis under steady-state and transient conditions. The seepage and slope stability models were used to predict the stability of the PR 259 highway cut at the study location. The preliminary seepage and slope stability model incorporated one soil profile with averaged field and laboratory soil

parameters under steady-state conditions. No flux boundary was defined along the slope face. A transient seepage and stability model included four soil types and their associated soil properties determined or inferred from laboratory and field results. A defined environmental flux boundary along the slope face was included in the detailed model allowing for evaluation of the time-dependant dissipation phenomenon. Calibration and sensitivity studies using the model are also presented in this chapter.

Chapter 7 summarizes all the major conclusions of the research project, including a discussion of the results from the transient seepage and slope models for 1998, 1999, and the calibration year 2000. In addition, this chapter concludes with a discussion of the limitations of the work undertaken and the directions for future research.

Chapter 2

Literature Review

2.0 Introduction

The most important concept in soil mechanics required to understand the instability issues for PR 259 is unsaturated soil mechanics. In the last 25 years there has been a significant increase in the volume of literature on unsaturated soils and numerical modeling. One reason for the increase in research activity is the improvement in laboratory testing procedures for obtaining unsaturated soil parameters to verify theoretical concepts. Better experimental data produced a stronger basis for applying the theory of unsaturated soil mechanics in practical applications. A second reason for the increase in unsaturated soils research is the ability, with the aid of the personal computer, to apply unsaturated soil mechanics to solve engineering problems. In terms of computer-aided numerical modeling research, the increase in published literature is strictly due to the increase in computational power and availability of commercial software. This allows for an increase in complexity and precision of solutions for engineering problems. Finite element and limit equilibrium numerical methods are the two

most widely used methods that have been incorporated into computer-aided numerical modelling for geotechnical engineering.

All unsaturated soil theories used in this research project are described, compared, and selected in this chapter. The chapter also describes the fundamentals inherent in the modeling tools used in the research project. This chapter provides necessary background information needed to comprehend the work that has been presented.

2.1 Strength of Soils

Soil behaviour, in general, is directly related to the stress-state to which it is subjected. Varying the stress-state of a soil element will affect its strength and volume state. Since volume change of a soil is not incorporated into limit equilibrium slope stability analysis or finite element seepage analysis, the theoretical concepts are addressed only briefly in this literature review.

The stress-state of a soil can be best defined as a combination of stress variables exerting either external or internal stresses on a soil element. The number of stress variables needed to describe the state of stress of a soil element is dependent on the number of phases present in the soil mass (Fredlund and Rahardjo 1993).

2.1.1 Phase Relationship

Soils generally exist either as two-phase systems or three-phase systems. A soil incorporates soil particles and pore spaces (which include pore fluid and/or pore air). In a two-phase soil system, either fluid or gas occupies all pore spaces within the soil element. A two-phase soil system incorporating only pore fluid, usually water, is generally referred to as a saturated soil. A two-phase soil system that incorporates only soil particles and gas, usually air is referred to as a fully dry soil. A three-phase system incorporates pore fluid, pore air, and soil particles. A three-phase soil system is referred to by many as “partially saturated” soil. However, the term “partially saturated” is used out of context. The technical definition of the term “partially saturated” describes a soil where a portion of the soil structure is saturated while the remaining part of the soil is unsaturated. An example is bimodal compacted high plastic clay. The term “unsaturated” is the more accepted term to use when describing a three-phase soil mass and will be used in this thesis for this purpose.

2.1.2 Stress-State of Soil

The stress-state for saturated soil incorporates two stress-state variables, while the stress-state for unsaturated soils incorporates three stress-state variables. There are many different ways to define the stress-state of a soil mass for saturated and unsaturated soils. The choice of the stress-state variables

presented by Fredlund and Morgenstern (1977) is generally accepted in current geotechnical practice and will be used in this research project. The stress-state variables chosen by Fredlund and Morgenstern (1977) are as follows: $(\sigma - u_a)$, $(u_a - u_w)$, and (u_a) (Figure 2.01, Figures can be found after each chapter). The stress variables are total stress (σ) , pore water pressure (u_w) , and pore air pressure (u_a) . Total stress is the force per unit area exerted on a soil mass externally, including gravitational forces. Pore water pressure is the stress exerted internally by the pore water against the soil particle matrix, while pore air pressure is the internal force per unit area exerted by the pore air.

The three stress-state variables can be incorporated into an unsaturated stress tensor to define soil behaviour (Figure 2.01). The saturated stress tensor can be regarded as a special case based on a modified unsaturated stress tensor (Fredlund and Rahardjo 1993). The unsaturated stress tensor is written as follows:

$$\begin{pmatrix} (\sigma_x - u_a) & \tau_{yx} & \tau_{zx} \\ \tau_{xy} & (\sigma_y - u_a) & \tau_{zy} \\ \tau_{xz} & \tau_{yz} & (\sigma_z - u_a) \end{pmatrix} \quad \text{eq. 2.01}$$

$$\begin{pmatrix} (u_a - u_w) & 0 & 0 \\ 0 & (u_a - u_w) & 0 \\ 0 & 0 & (u_a - u_w) \end{pmatrix} \quad \text{eq. 2.02}$$

The $(\sigma_i - u_a)_{y,z}^x$ terms in the unsaturated stress tensor are referred to as the net normal stress, while $(u_a - u_w)$ is referred to as matric suction. Matric suction is discussed in detail in section 2.2.

The stress tensor for a saturated soil is a simplification of the unsaturated stress tensor (equation 2.02). As the soil becomes fully saturated the matric suction approaches zero since the pore water pressure (u_w) begins to equalize with the pore air pressure (u_a). This equalization generates a zero term in the second stress tensor eliminating the second stress tensor completely (equation 2.02). The first unsaturated stress tensor remains unchanged with the pore water and pore air variables being interchangeable. The unsaturated stress tensor in equation 2.02 simplifies to equation 2.01 for saturated soil.

2.2 Soil Suction

Soil suction can be referred to as the free energy state of soil water (Edlefsen and Anderson 1943). Soil suction can be calculated using the thermodynamic relationship of partial pressure (Richards 1965) which is written as:

$$\psi = \frac{-RT}{v_w \omega_v} \ln \left(\frac{\bar{u}_v}{\bar{u}_{v0}} \right) \quad \text{eq. 2.03}$$

where:

ψ = soil suction or also known as total potential, (kPa)

R = molar gas constant, 8.31432 J/(mol K)

T = absolute temperature, (K)

v_w = specific volume of water, $1/\rho_w$ (m^3/kg)

$\bar{\omega}_v$ = molecular mass of water vapour, 18.016 (kg/ kmol)

\bar{u}_v = partial pressure of pore water vapour, (kPa)

\bar{u}_{v0} = saturation pressure of the water vapour over a flat surface of pure water at temperature T , (kPa)

The \bar{u}_v / \bar{u}_{v0} term in equation 2.03 represents relative humidity. Relative humidity is directly proportional to soil suction since all other terms in equation 2.03 are constants. It is difficult to calculate the relative humidity in a soil. In particular, it is difficult to calculate the partial pressure in a soil. Adding to the complexity is the fact that partial pressure in a soil is due to two independent mechanisms, osmotic suction and matric suction (see equation 2.04). Total suction is taken as the sum of the two components. Total suction is written as:

$$\psi = (u_a - u_w) + \pi \quad \text{eq. 2.04}$$

where:

$(u_a - u_w)$ = matric suction

π = osmotic suction

2.2.1 Osmotic Suction

Pore water in many applications includes dissolved salts such as Na^+ , Ca^{2+} , and Mg^{2+} . The vapour pressure of water over a solution of dissolved salts is less than the vapour pressure of water vapour over pure water. The difference in partial pressures between a solvent and pure water decreases the relative humidity of the soil thus increasing the overall soil suction. Since the soil retrieved from the study area is suspected of having low concentration of salts and was exposed to the same pore fluid at all times, the osmotic component is expected to have little impact on total suction. Osmotic suction was not considered in this program.

2.2.2 Matric Suction

Matric suction is based on the capillary rise phenomenon related to surface tension of water. Surface tension is due to the interaction of molecules within the contractile skin at liquid/air interfaces. All liquids have a unique surface tension value. The best example of the capillary phenomenon is demonstrated by a capillary tube (Figure 2.02). Within the capillary tube all water above atmospheric pressure (Point A) is under a negative pressure or in other words is in tension. This negative pressure is due to the surface tension that acts along the circumference of the meniscus at a specific contact angle. The contact angle depends on the contact material and the liquid used. Using the summation of forces in the y-direction, the capillary rise is as follows:

$$2\pi r T_s \cos \alpha = \pi r^2 h_c \rho_w g \quad \text{eq. 2.05}$$

where

r = radius of capillary tube, (m)

T_s = surface tension of fluid, (kg/s²)

α = contact angle, (degrees)

h_c = capillary height, (m)

ρ_w = density of fluid, (kg/m³)

g = gravity, 9.806 (m/s²)

Equation 2.05 can be re-written as:

$$h_c \rho_w g = 2T_s \cos \alpha / r \quad \text{eq. 2.06}$$

$h_c \rho_w g = (u_a - u_w)$ and $\cos \alpha \approx 0$ for water therefore;

$$(u_a - u_w) = 2T_s / r \quad \text{eq. 2.07}$$

Equation 2.07 states that the matric suction is inversely proportional to the radius of the capillary tube. Pore spaces within the soil can be broadly thought of as acting like small diameter capillary tubes (Figure 2.03). The radius of a pore space will affect the height of the raised pore water. Therefore the pore space structure of the material (clay, silt, sand, etc.) will inherently affect the magnitude of matric suction that is developed at specific water contents.

The capillary rise phenomenon and the associated equation (2.07) is the theoretical basis for determining the soil water characteristic curve for a soil (SWCC). The soil water characteristic curve is the most important unsaturated soil property for examining unsaturated/saturated flow and the increase in soil strength due to suction. The procedures used for determining the SWCC for this research project are presented in the following section.

2.3 Prediction of the Soil Water Characteristic Curve from Grain Size Distributions

Section 2.2 illustrated how pore size of a soil affects capillary rise of the pore fluid, which in turn affects the magnitude of matric suction. All soils contain a varying pore size distribution resulting in a range of suctions depending on the water content. Adding to the complexity is an understanding that smaller pore sizes may be completely saturated while larger pore sizes are unsaturated for any given moisture content. Varying pore size distribution and the fact that certain pores will be saturated while others are unsaturated produces a functional relationship between suction and water content known as the soil water characteristic curve.

The SWCC depends on whether the soil is undergoing a wetting phase or drying phase. When a soil is undergoing wetting from a dry state (high suctions/large negative pressures) the smaller size pore spaces will fill first while the larger

pores fill last. Conversely, when a soil is fully saturated and undergoes drying, the larger pores will empty first, while smaller pores empty more slowly. The difference in the mechanics of wetting and drying phases produces two independent SWCC curves for a specific material, one for each direction (wetting/drying, Figure 2.04). For simplicity, most predictive SWCC models average the wetting and drying phases to produce one curve.

Currently, experimental tests using salt solutions and desiccators produce the most accurate measurements of the SWCC. Equations have been developed to calculate functions that fit experimental data for the SWCC. The most common fitting equations were developed by Brooks and Corey (1964, 1966) and van Genuchten (1980). Theoretically based predictive methods have and are currently being developed to calculate the SWCC through non-experimental means with promising results. In general, two types of theoretically based predictive approaches have been developed.

The first type involves using a mathematical equation to represent a grain size distribution. The grain size distribution function is then in turn converted into a pore size distribution. This pore size distribution function can be transformed into a SWCC using the theoretical principles such as capillary rise (equation 2.07). Unfortunately, calculated soil water characteristic curves need to be adjusted to archived experimental results of similar material using fitting parameters. This

method can be useful when an experimentally attained SWCC is not available for a particular soil that its SWCC has been archived.

The second type of theoretical approach involves a more scientifically based method using a mathematical function to create the SWCC based on basic material properties derived from a grain size distribution. The second approach is attractive due to its scientific rigour and well-developed formulation. The limitations of the second approach are that some empirical constants are still required.

Both the experimental and predictive approaches for obtaining the SWCC were considered in this project. Since the heterogeneity of the material encountered at the study area would require numerous lengthy tests and the limited amount of soil samples, it provided arguments against using the experimental approach for obtaining the SWCC for this project. Therefore, SWCC curves were determined using theoretically based predictive models.

2.3.1 Theoretical Predictive Methods for the Soil Water Characteristic Curve

Several predictive models were examined, with two particular methods being explored in further detail. The two methods examined in detail were the Fredlund and Xing (1994) method, and the Kovács method (1981).

Fredlund and Xing (1994) developed a theoretical method of predicting the SWCC based on a surface tension equation and an equation fitted to the pore size distribution. The pore size distribution is developed from a fitted grain size distribution. The first difficulty encountered was calculating reasonable air entry values for the material type retrieved from the study area using the equation presented by Fredlund and Xing (1994). The second difficulty was producing an empirical equation to represent the grain size distribution. The third difficulty was to determine what equation and assumptions were required to convert the fitted grain size distribution to a pore size distribution. The grain size to pore size conversion equation needed to incorporate the density and packing of the soil particles. In addition, the equation needed to represent the soil particle shape distribution from the flaky nature of clay particles to the angular nature of granular materials. Overall this method produced unreasonable results when used to calculate the SWCC for the material retrieved from the study area and will not be considered further.

The second method (Kovács 1981) produced reasonable results when used to predict the SWCC for several samples of soil retrieved from the study area and was attractive because of the ease to which the method could be applied to any type of soil material. For these reasons the Kovács method was selected for calculating the SWCC for this project.

Aubertin *et al.* (1998) examined the Kovács method (1981) and compared it with other methods. The authors selected the Kovács method for their study because of its simplicity, its physical significance, and its lesser reliance on empirical constants compared with other models. The lack of reliance on empirical constants is important when constructing a “theory based” predictive model. In addition to examining, comparing, and verifying the Kovács model, Aubertin *et al.* (1998) also presented a comparison of several methods of calculating the air entry value. One of these methods was selected for evaluating the air entry value for material retrieved from the study area. Results are discussed in the following section.

2.3.2 Calculating the Air Entry Value (AEV)

The air entry value (AEV) is the suction value where the largest pores within the soil begin to drain and air begins to enter the soil. Several methods of calculating the AEV were presented by Aubertin *et al.* (1998). After reviewing the paper and its results, the Brooks and Corey (1964) method of determining the AEV was adopted for this research. It was preferred because of its simplicity and its common use in engineering practice. The Brooks and Corey (1964) method assumes that two straight lines in semi-log space can represent the SWCC. The intersection point of the two straight lines is considered the AEV.

Estimation of the AEV provides an “anchor point” where the predicted SWCC can be adjusted to match experimental values. The AEV estimation equation presented by Bear (1972) was selected. The equation is a simplified form of the Polubarinova-Kockina equation as follows:

$$\psi_{AEV} = \frac{b}{eD_{10}} \quad \text{eq. 2.08}$$

where:

b = a constant based on the Brooks and Corey method (1964) from experimental SWCC, $b = 4.0$

e = void ratio of the soil

D_{10} = diameter for which 10 % of the weight passed a sieve size, (mm)

ψ_{AEV} = the suction value where the largest pores begin to drain, (kPa)

The constant b is an empirical constant derived from air entry values calculated using the Brooks and Cory method (1964) from experimental soil water characteristic curves. Aubertin *et al.* (1998) showed acceptable correlations between the estimated AEV and the calculated AEV from experimental results (Figure 2.05).

2.3.3 Prediction of the SWCC Using the Kovács Method (1981)

Kovács proposed that the soil water characteristic curve was based on the following equation:

$$S_r = S_c + S_a(1 - S_c) \quad \text{eq. 2.09}$$

where:

S_r = saturation ratio, θ/θ_s , θ = volumetric water content, θ_s = saturated water content

S_c = component of saturation due to capillary forces

S_a = component of saturation due to adhesive forces

The two components of the S_r equation are saturation due to capillary forces (S_c) and saturation due to adhesive forces (S_a). The S_c component of the SWCC dominates the curve from the saturated water content, θ_s , to the water content where the water characteristic curve begins to flatten out at larger suction values. Between this range, the water content and the capillary rise depends on the pore size distribution of the soil. The S_c equation is as follows:

$$S_c = 1 - \left[\left(\frac{h_{co}}{\psi} \right)^2 \right] \exp \left[- \left(\frac{h_{co}}{\psi} \right)^2 \right] \quad \text{eq. 2.10}$$

The h_{co} term represents the pore water rise between the AEV and the residual volumetric water content, θ_r . The h_{co} is a constant and is calculated using the following equation:

$$h_{co} = a_2 \left(\frac{1-n}{n} \right) \left(\frac{\alpha_k}{D_h} \right) \quad \text{eq. 2.11}$$

The S_c equation given in equation 2.10 is a probability function that represents the pore size frequency. The probability function is an exponential function that has been simplified from a gamma function or also referred to as Euler's second integral which is an improper integral.

The a_2 term in equation 2.11 represents an averaged empirical constant suggested by Kovács to be 0.75. The n term represents the porosity of the soil, which is assumed to be equal to θ_s . The α_k/D_h term is the ratio of the particle shape factor α_k to the effective grain size D_h . The shape factor α_k , defines the shape of the soil particles between a sphere (rounded material such as granular, $\alpha_k = 6$) and tetrahedron (flaky material such as clay, $\alpha_k = 18$). The shape factor parameter cannot be determined from any basic soil properties and thus has to be estimated based on the soil material present. The D_h term represents the Kozeny's effective grain size, which is the diameter of a perfect spherical particle of soil that has been converted from the real non-spherical soil particle. The Kozeny equation is given in equation 2.12 where:

$$D_h = (1.17 \log C_u + 1) D_{10} \quad \text{for } C_u \leq 50 \quad \text{eq. 2.12}$$

where C_u is the uniformity coefficient, D_{60}/D_{10} .

The adhesive component, S_a of equation 2.09 is associated with a thin film of pore water that covers the interlocking soil grains. The interlocking soil grains can

be considered conceptually as a solid wall (Helmholtz Double Layer). This film of water creates an attractive force between the film and the solid wall due to electrostatic charges and the dipolar characteristic of water molecules (eg. Hillel 1980: Mitchell 1993). The S_a equation is as follows:

$$S_a = a_1 \left(\frac{1-n}{n} \right) \psi^{-\beta_1} \left(\frac{\alpha_k}{D_h} \right)^{\beta_2} \quad \text{eq. 2.13}$$

a_1 , β_1 , β_2 are empirical model coefficients equal to 2.5×10^{-3} , $1/6$, $2/3$ respectively. The values used for the empirical coefficients are average values suggested by Kovács.

The two components of the saturation equation can be combined into one equation representing the relationship between soil suction and volumetric water content. The combined equation is given below:

$$\theta = n - \left[\left(\frac{h_{co}}{\psi} \right)^2 + 1 \right] \exp \left[- \left(\frac{h_{co}}{\psi} \right)^2 \right] \times \left[n - 1.4 \times 10^{-2} \left(\frac{h_{co}}{\psi} \right)^{1/6} (n^2 - n^3)^{1/3} (h_{co})^{1/2} \right] \quad \text{eq. 2.14}$$

The equation is considered representative for:

$$50 < \frac{\alpha_k}{D_h} < 25 \times 10^3$$

Using equation 2.14, Kovács (1981) and Aubertin *et al.* (1998) compared the calculated and experimental soil water characteristic curves with good results. However, the Kovács method of predicting soil water characteristic curves is limited in its ability to represent the experimental soil water characteristic curves because of the estimated empirical parameters. One example of a parameter that limits the accuracy of the Kovács equation is estimating meaningful values for the α_k term. Fortunately, slight modifications to the Kovács model produces better correlations to experimental soil water characteristic curves while removing some irregularities in the SWCC curve (Aubertin *et al.* 1998).

2.3.4 The Modified Kovács Method of Predicting Soil Water Characteristic Curve

The first modification that was performed by Aubertin *et al.* (1998) on the Kovács model is to equation (2.09):

$$S_r = S_c^v + S_a^w (1 - S_c^v) \quad \text{eq. 2.15}$$

The v and w are fitting parameters with $v = 0.2$ and $w = 1$ for most soils. Using fitting parameters somewhat defeats the purpose of a physically based model.

Even with the addition of the fitting parameters v and w , the modified Kovács model is still more physically based than any other predictive SWCC model that has been considered.

This first modification to the Kovács model affects the capillary component of the model (equation 2.10). The S_c equation was modified with the addition of an adjustment parameter, m , which produces a pore size distribution intermediate to a gamma and exponential distribution. The new S_c equation is given below:

$$S_c = 1 - \left[\left(\frac{h_{co}}{\psi} \right)^2 \right] \exp \left[-m \left(\frac{h_{co}}{\psi} \right)^2 \right] \quad \text{eq. 2.16}$$

In addition to the adjustment parameter (m), the h_{co} parameter can be based on the AEV and not on the α_k/D_h term, which can be difficult to estimate. The h_{co} term can be assumed to be linear with the air entry value with $h_{co} = 1.25 - 2.5\psi_{AEV}$. This assumption limits the possible range of h_{co} thus limiting the range of the S_c component of suction to unknown parameters.

The second modification to the Kovács model was to the adhesive component of the model (equation 2.13). This modification ensures that the SWCC reaches a fully dry state at some finite suction. The modification includes a material parameter correction developed by Fredlund and Xing (1994). The modified S_a equation is as follows:

$$S_a = C_\psi \frac{a}{e^{1/3} \psi^{1/6}} h_{co}^{2/3} \quad \text{eq. 2.17}$$

where:

$$C_\psi = \frac{1 - \ln(1 + \psi / \psi_r)}{\ln(1 + \psi_o / \psi_r)} \quad \text{eq. 2.18}$$

The 'a' term in equation 2.17 is based on a_1 of equation 2.13 and is empirically derived by fitting, with an average value equal to 0.006. In equation 2.18, developed by Fredlund and Xing (1994), the ψ_o term represents the suction value for a completely dry soil, which is equal to 10^7 cm of water (Ross *et al.* 1991). The ψ_r term represents the suction value for the residual water content, θ_r . The residual suction value, ψ_r , of 15×10^3 cm was observed for the material studied in Aubertin *et al.* (1998). This residual suction value was used in this research project since the material studied in Aubertin *et al.* (1998) is very similar in nature to the material retrieved from the study area in terms of grain size distribution. Since the studied failures are shallow, the S_a component of the SWCC is of little importance in terms of its impact at low suction values.

Overall the modified Kovács model better represents the experimental data when compared to the Kovács model. Figure 2.06 compares the two models against experimental results. The modified Kovács model was used to calculate the SWCC for the soil retrieved from the author's study area.

2.4 Prediction of the Conductivity Function from the SWCC

As with matric suction, the hydraulic conductivity of a soil depends on the water content and whether the soil is undergoing drying or wetting. The hydraulic conductivity function can be obtained by experimental or numerical means. Obtaining the hydraulic conductivity function from experiments was once more not considered because of the wide variability and limited amount of the material retrieved from the study area. The only reasonable option was to use the SWCC to predict the hydraulic conductivity function. Two predictive models were considered, Fredlund *et al.* (1994) and van Genuchten (1980). The van Genuchten (1980) method was selected because of its simplicity, ease of application and the fact that an equation is first fitted to the existing SWCC using fitting parameters. The same fitting parameters are then used in a second equation to predict the hydraulic conductivity function. Using two separate equations with the same fitting parameters allows for calibration of the fitting parameters when applied to the SWCC, which in turn increases the confidence in the predicted hydraulic conductivity.

2.4.1 Closed-form Equation Presented by van Genuchten (1980)

van Genuchten (1980) presented a closed-form equation for predicting the hydraulic conductivity of a soil at different suction values. The closed-form equation was based on Mualem's model (1976). As explained above, van

Genuchten first predicted and fitted a SWCC to an existing SWCC. The equation used to predict and fit the SWCC is:

$$\theta_v = (n - \theta_r) \times \left[\frac{1}{1 + (\alpha\psi)^n} \right]^m + \theta_r \quad \text{eq. 2.19}$$

where $m = 1 - 1/n$ and α, n are fitting parameters (note: here n is different from $n = \theta_s$)

The n -parameter affects the slope of the SWCC between AEV and the residual water content while the α -parameter adjusts the location of the AEV. After using equation 2.19 to predict and fit a SWCC to SWCC data, the fitting parameters are incorporated into a function developed by van Genuchten that predicts the hydraulic conductivity distribution. The function is based on a partial incomplete beta function (Euler's second integral). The function is given below:

$$k_{(\theta)} = \frac{\left\{ 1 - (\alpha\psi)^{n-1} \left[1 + (\alpha\psi)^n \right]^{-m} \right\}^2}{\left[1 + (\alpha\psi)^n \right]^{n/2}} \quad \text{eq. 2.20}$$

van Genuchten (1980) compared results from equation 2.20 against all types of soils with good results. Figure 2.07-2.11 presents results of those comparisons.

In addition van Genuchten (1980) compared his closed-form equation against a model presented by Brooks and Corey (1964). The Brooks and Corey (1964) model developed a general equation for predicting the hydraulic conductivity from a large database of SWCC's. The Brooks and Corey (1964) model is based on the Burdine model (1953), which is very similar to Mualem's model (1976). At large suction values, the van Genuchten (1980) model simplifies to the Brooks and Corey (1964) model, producing an identical SWCC relationship. However, at smaller suction values, the Brooks and Corey (1964) model produces a curved SWCC while the van Genuchten (1980) model is somewhat bi-linear creating a discrepancy. Both models are very similar and are equally accepted in practice.

2.5 Shear Strength

Many geotechnical failures, including the shallow instability examined in this thesis, are directly related to reduction of shear strength in a soil. The shear strength of a soil in any plane is related to the stress-state of the soil. The stress-state of a soil, as described in a previous section depends on two stress-state variables, net normal stress, $(\sigma - u_a)$, and matric suction, $(u_a - u_w)$. As with most theoretical principles in soil mechanics, the saturated case is presented first because of its relative simplicity.

2.5.1 Shear Strength Equation for a Saturated Soil

The shear strength of a saturated cohesive soil can be defined by the Mohr-Coulomb failure criterion and the effective stress principle (Terzaghi 1936). The shear strength of a soil is defined as:

$$\tau = c' + (\sigma - u_w) \tan \phi' \quad \text{eq. 2.21}$$

The Mohr-Coulomb failure criterion assumes the soil is at failure once the maximum principal stress ratio is reached for a specific normal stress level. The criterion can be applied to intact soil (peak strength) or soils that have previously undergone deformation and are now completely remolded (residual strengths). Equation 2.21 defines a straight line referred to as the Mohr-Coulomb failure envelope (Figure 2.12). Equation 2.21 can be represented graphically through the construction of at least two (preferably more) Mohr circles representing different stress conditions that produce failure in a soil. A Mohr circle describes the interaction between shear stress and normal effective stress on a variety of different orientations at a point. With the construction of Mohr circles at failure, a straight line can be drawn tangent to the circles defining the failure envelope. The slope of the line represents the internal friction angle, ϕ' , and the intercept on the τ -axis represents the effective cohesion, c' (in overconsolidated soils failure envelopes are generally bi-linear and additional tests are needed).

The shear strength of a two-phase soil mass depends on the effective stress concept. The effective stress concept for saturated soils is as follows:

$$\{\sigma'\} = \{\sigma\} - u_w \{I\} \quad \text{eq. 2.22}$$

The effective stress concept is widely accepted and at times regarded as a law (Fredlund and Rahardjo 1993). The effective stress concept is independent of soil properties, meaning it is applicable to all soils (sands, silts and clays).

2.5.2 Shear Strength Equation for an Unsaturated Soil

The shear strength of an unsaturated soil, like the saturated case, uses the Mohr-Coulomb failure criterion and the effective stress concept, but with an additional stress-state variable. Fredlund *et al.* (1978) presented a shear strength equation for unsaturated soils that has become widely accepted. The equation is given by:

$$\tau = c' + (\sigma - u_a) \tan \phi' + (u_a - u_w) \tan \phi^b \quad \text{eq. 2.23}$$

The shear strength equation for an unsaturated soil is an extension of the saturated case (equation 2.21) with addition of the $(u_a - u_w)$ stress-state variable and the ϕ^b strength parameter. With two stress-state variables, the Mohr-

Coulomb failure envelope becomes three-dimensional (Figure 2.13). The $(u_a - u_w)$ term defines the third orthogonal axis.

The ϕ^b parameter is the parameter that represents the increase in shear strength associated with an increase in matric suction. This is the most important parameter in unsaturated soil mechanics. The ϕ^b parameter was initially thought to be constant for a specific soil, but recent evidence has shown that it varies with matric suction level up to the air entry value. This produces the curved envelope shown in Figure 2.14. At suction values greater than the air entry value, the ϕ^b parameter is constant and less than ϕ' . The $\tan(\phi^b)$ function is currently represented by a bi-linear function with the air entry value being the inflection point (Fredlund and Rahardjo 1993). Morris *et al.* (1992) has suggested that $\phi^b = \phi' - 4^\circ$, as a global approximation, while up to the air entry value, Vanapalli *et al.* (1996) has suggested value of $\phi^b = \phi'$.

2.6 Slope Instability

The concept of using limit equilibrium slope stability analysis is well established. The development of analytical methods for slope stability has only recently seen a method that produces a deterministic solution. Recently, further improvements have been achieved with the aid of computers in the accuracy and precision of slope instability analysis.

For the most part, slope instability analysis is based on the effective stress principle and the Mohr-Coulomb failure criterion discussed and presented in sections 2.5.1 and 2.5.2. Both of these ideas are incorporated into limit equilibrium analysis. A limit equilibrium solution is based on summation of forces or moments acting on a soil mass at the point of failure. Limit equilibrium includes forces and strengths, but does not include displacement. In order to produce the most accurate solution, a good site investigation and site survey needs to be undertaken to adequately determine the groundwater conditions and soil strength properties (Graham 1984). Thus, slope stability analysis incorporates many aspects of geotechnical engineering practice.

2.6.1 Infinite Slope Analysis

Infinite slope stability analysis is a determinate simplified solution where the failure surface is assumed to act parallel to the ground surface. These types of failures most often occur in natural hillsides due to softening, weathering, high groundwater pressures, and/or toe unloading (Skempton 1964).

The analysis assumes the slope surface is uniform and any element or slice represents the mechanics of the entire slope failure. For each slice, the soil properties and pore water pressures remain constant (Figure 2.15). The forces acting on the slice are as follows: W is the self-weight of the slice, P is the normal force acting at the base of the slice, T is the shear force acting at the base of the

slice, and Q_L and Q_R are the interslice forces acting at an angle β to the horizontal. The interslice forces can be assumed to be equal and opposite if all slices are assumed to be identical. The forces described above are defined as follows:

$$W = \gamma bz \quad P = \gamma bz \cos \beta \quad T = \gamma bz \sin \beta$$

Letting the length of the base of a slice $JK = b \sec \beta$ and converting the forces into stresses:

$$\sigma_N = \gamma z \cos^2 \beta \quad \tau_N = \gamma z \sin \beta \cos \beta$$

Therefore the safety factor against sliding is simply the ratio of mobilized shear strength to required shear strength:

$$S.F. = \tau_{Req} / \tau_{Mob} = \frac{c' + (\gamma z \cos^2 \beta - u) \tan \phi'}{\gamma z \sin \beta \cos \beta} \quad \text{eq. 2.24}$$

where:

$$u = \gamma_w m \cos^2 \beta \quad \text{eq. 2.25}$$

where:

m = the percentage of the slice height that is fully saturated, (0 to 1.0).

If previous movements have occurred in the slope, ϕ' will be reduced and cohesion will be at or near zero. If the slope is fully saturated then equation 2.24 simplifies into:

$$S.F = \left(\frac{\gamma - \gamma_w}{\gamma} \right) \frac{\tan \phi'}{\tan \beta} \quad \text{eq. 2.26}$$

Using equation 2.26, under natural conditions fissured clay in a periglacial slide mass at a slope angle of $\phi'_r/2$ will have a safety factor of 1.0 (Prior and Graham 1974). The conditions described by Prior and Graham (1974) are very similar to the conditions observed in the field and laboratory component of this thesis.

2.6.2 Limit Equilibrium Method of Slices

It is common in slope stability analysis to equally divide the failed soil mass into individual slices. These slices are then analyzed on an individual basis in terms of forces and moments acting on a slice (Figure 2.16). The forces that act on a slice are as follows:

1. Self-weight, defined as W
2. Interslice resultant forces, Q_L and Q_R acting at some angle θ_L and θ_R to the horizontal, as well as the horizontal pore water forces, U_L and U_R
3. Forces acting on the base of a slice, including total normal force, P , pore water pressure, U , and shear force, S_m , acting at some angle α from horizontal along the base of the slice

The following unknowns need to be calculated for n number of slices of a sliding mass:

Forces:

n	normal forces, P
$n - 1$	interslice forces, Q_L and Q_R
$n - 1$	interslice angles, θ_L and θ_R
<hr/>	
$3n - 2$	total unknowns

Moments:

n	e distances of P
$n - 1$	f distances of Q_L and Q_R
<hr/>	
$2n - 1$	total unknowns

Σ Total $5n - 3$ unknowns

It is assumed that pore water pressures are known for each slice. The sliding mass can be analyzed with two force and one moment equilibrium equations solving for $3n$ of the unknowns. Subtracting $3n$ values from $5n - 3$ values leaves $2n - 3$ unknowns. In order to make the problem statically determinate you need $2n - 3$ assumptions. One assumption is that P acts at the centre of each slice when the slices are selected thin enough thereby eliminating unknown e and reducing the unknowns by n . The last assumption deals with interslice angle, θ , reducing the unknowns by $n - 1$ values. These two assumptions produce $2n - 1$ values, where only $2n - 3$ unknowns are required. This over simplification of unknowns produces two independent solutions to a slope stability problem depending on whether a force or moment limit equilibrium equation is used. The θ assumption creates a non-rigorous solution allowing an infinite number of solutions to be developed based on the choice for the interslice assumption incorporated into the analysis. Luckily, the interslice angle assumption, θ , does not significantly affect the safety factor, especially when using moment limit equilibrium equations (Fredlund and Krahn 1977).

2.6.2.1 Development of Safety Factor Equations

The principle of limit equilibrium states that the sum of driving forces (or moments) equals the resisting force (or moments). When considering circular sliding surfaces it is convenient to analyze the problem at a center of rotation producing an average mobilized shear strength along the failure surface required

to maintain equilibrium. The development of limit equilibrium force and moment equations assuming no earthquake effects, line loads, tension cracks, or partial submergence of the slope (Figure 2.17) is as follows:

Summation of forces in the y-direction for a slice gives:

$$W - S_m \sin \alpha - P \cos \alpha - (X_L - X_R) = 0 \quad \text{eq. 2.27}$$

Where $S_m = l(\tau_{\text{req}}) = (c'l + (P - ul)\tan\phi')/F$ and rearranging equation 2.27 in terms of P:

$$P = \left(W - \frac{c'l \sin \alpha}{F} + \frac{ul \tan \phi' \sin \alpha}{F} - (X_L - X_R) \right) / m_\alpha \quad \text{eq. 2.28}$$

where $m_\alpha = (\cos \alpha + \tan \phi' \sin \alpha / F)$

Assuming no earthquake effects, line loads, tension cracks, or partial submergence of the slope and solving the forces horizontally:

$$\sum P \sin \alpha - \sum (c'l + (P - ul)\tan\phi')/F + \sum (E_R - E_L) = 0 \quad \text{eq. 2.29}$$

The force equilibrium equation therefore is:

$$F_f = \frac{\sum (c' + (P - ul) \tan \phi') \cos \alpha}{\sum P \sin \alpha + \sum (E_R - E_L)} \quad \text{eq. 2.30}$$

where P is determined from equation 2.28 thus producing an iterative process of solving for the safety factor. The summation of moments at the center of the base of each slice gives the moment equilibrium equation as follows:

$$F_m = \frac{\sum (c'R + (P - ul)R \tan \phi')}{\sum Wx - \sum Pf + \sum (E_R n - E_L o)} \quad \text{eq. 2.31}$$

The two equilibrium equations are independent of each other and will produce two independent safety factors. The moment equation is considerably less sensitive to the interslice force assumption (Graham 1984).

2.6.2.2 Spencer's Method of Slope Stability Equations

The Spencer's method of slope stability analysis assumes that there is a constant interslice inclination of θ for the interslice forces Q where:

$$\tan \theta = X_L / E_L = X_R / E_R \quad \text{eq. 2.32}$$

This assumption allows us to use $X_L - X_R = (E_L - E_R) \tan \theta$ in equation 2.27. Both the F_f and F_m equations are solved individually by varying θ till both equations produce the same answer. The relationship for each of the limit equilibrium equations versus θ were plotted by Fredlund and Krahn (1977). A sample of

Fredlund and Krahn's results are presented in Figure 2.18. As previously mentioned, the moment limit equilibrium equation will produce a narrow banded range of safety factors for varying θ , while the force limit equilibrium equation produces a large band of safety factor results. The Spencer method of slope stability analysis is incorporated into the slope stability analysis of this thesis because of the planar nature of the two slides.

2.7 Seepage Modeling Using a Finite Element Model

The finite element method has been used in engineering for many years. Only recently since the advancement of the personal computer, has the power of the finite element approach been fully utilized. A finite element model approximates numerical solutions for complex physical systems. The model is used to approximate the response of a physical system subjected to external loading (force, temperature, etc.) conditions. An example of an applied external condition in terms of seepage analysis is infiltration or evapotranspiration.

There are four basic conditions that need to be satisfied in the finite element method. They are as follows:

1. Equilibrium conditions (mass transfer)
2. Compatibility conditions (flow)
3. Soil property relationships – (ex. soil water characteristic curve, hydraulic conductivity, etc.)

4. Boundary conditions – (No flow boundary)

All these conditions need to be satisfied before physically representative approximations to the response of a real system can be obtained.

The concept behind the finite element method is as follows:

1. Divide the domain into smaller sub-domains (triangular or rectangular elements).
2. Define rules/relationships for the behaviour of each individual sub-domain.
3. Apply external “loads” and then allow elements to respond or share external loads between sub-domains as necessary until all four basic conditions are satisfied.
4. Combine the response of each of the sub-domains to evaluate the bulk response of the system.

While the approach of the finite element method is simple in theory, hand calculations are tedious and time consuming. The nature of the finite element method demonstrates the need for computers when constructing a model to represent the behaviour of a physical system. Currently, there are several finite element software packages that are designed to analyze seepage through soils. Generally the packages are user-friendly and do not require much knowledge of

the inherent mathematics used in the finite element method. The following section outlines the form of FEM solutions for seepage analysis. Details of the finite element method are not discussed in this thesis (see the Geoslope Seep/W manual for further information)

2.7.1 Governing Equations for Finite Element Seepage Software

The governing equation used in two dimensional finite element seepage analysis, in particular Seep/W, is a second order partial differential equation.

$$\frac{\partial}{\partial x} \left(k_x \frac{\partial H}{\partial x} \right) + \frac{\partial}{\partial y} \left(k_y \frac{\partial H}{\partial y} \right) + Q = \frac{\partial \theta_v}{\partial t} \quad \text{eq. 2.33}$$

where:

k_x = hydraulic conductivity in the horizontal direction

k_y = hydraulic conductivity in the vertical direction

H = total head

Q = external boundary flux

θ_v = volumetric water content

t = time

The above equation states that the rates of change in flow for both the x and y direction (in addition to the applied boundary flux) is equal to the rate of change of the volumetric water content with respect to time. This is the definition for the transient flow condition.

As previously mentioned in section 2.1, the stress-state of saturated and unsaturated soils depends on two stress-state variables, $(\sigma - u_a)$ and $(u_a - u_w)$. The Seep/W finite element software makes two assumptions in terms of these stress-states. The first is that the soil is under a constant total stress. A change in the total stress would result in a volume change and a change in the volumetric water content. The second is that during transient analysis the pore air pressure is atmospheric. These two assumptions create a constant $(\sigma - u_a)$ term in the stress state tensor, simplifying the mathematics that lead to equation 2.33. With a constant u_a , the change in volumetric water content of a sub-domain can be related directly to the change in pore water:

$$\partial\theta_v = a_w \partial u_w \quad \text{eq. 2.34}$$

where a_w is the slope of the hydraulic conductivity function with respect to soil suction.

Total hydraulic head is defined by:

$$H = h_p + h_e \quad \text{eq. 2.35}$$

where:

h_p = hydraulic head, (m)

h_e = elevation head, (m)

Equation 2.35 can be redefined as:

$$H = \frac{u_w}{\gamma_w} + h_e \quad \text{eq. 2.36}$$

solving for u_w and substituting in equation 2.34 gives:

$$\partial \theta_v = a_w \gamma_w \partial (H - h_e) \quad \text{eq. 2.37}$$

Equation 2.37 can be simplified since the elevation is constant, resulting in the derivative of elevation with respect to time being eliminated. Substituting the simplified equation 2.37 into equation 2.33 gives the following equation:

$$\frac{\partial}{\partial x} \left(k_x \frac{\partial H}{\partial x} \right) + \frac{\partial}{\partial y} \left(k_y \frac{\partial H}{\partial y} \right) + Q = a_w \gamma_w \frac{\partial H}{\partial t} \quad \text{eq. 2.38}$$

Equation 2.38 is the partial differential equation that is used in the formulation of the Seep/W finite element software (Geoslope Seep/W user manual).

2.8 Summary

This chapter has outlined the theories and methods that were used to examine the failure of the PR 259 slopes. The background information presented in this

chapter will provide the reader with the necessary background to understand the methodology and analysis undertaken in this research project.

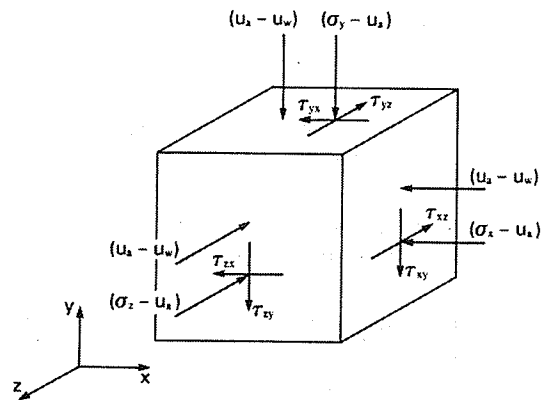


Figure 2.01 Stress-state variables for an unsaturated soil (Fredlund and Rahardjo 1993).

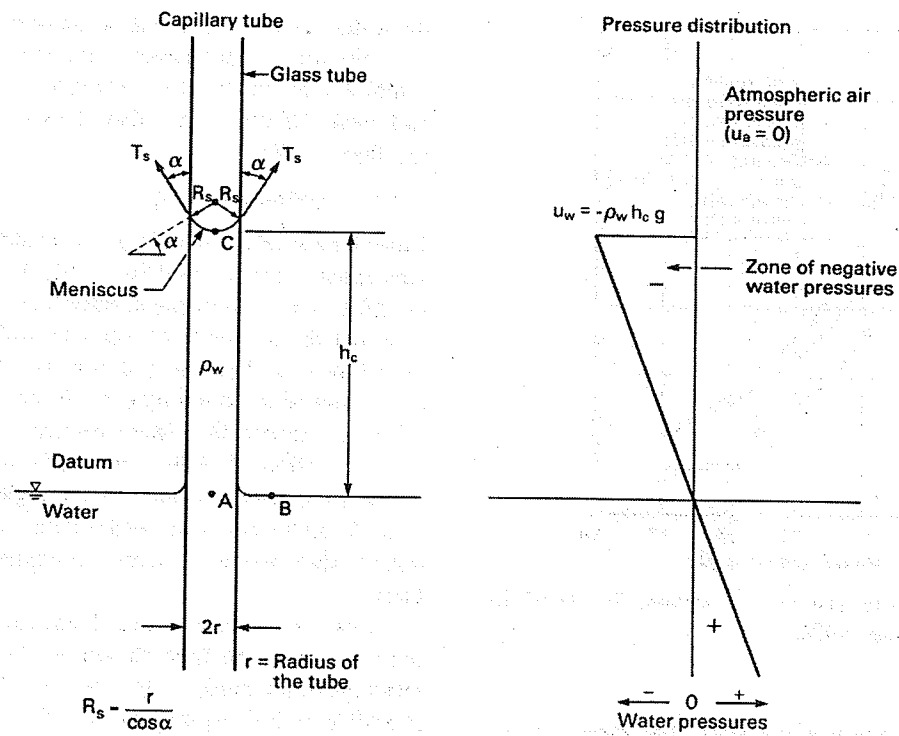


Figure 2.02 The capillary tube (Fredlund and Rahardjo 1993).

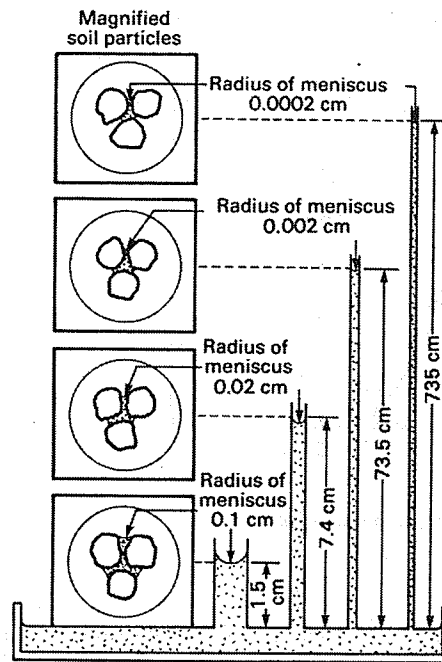


Figure 2.03 Varying capillary rise due to variation of pore size (Fredlund and Rahardjo 1993).

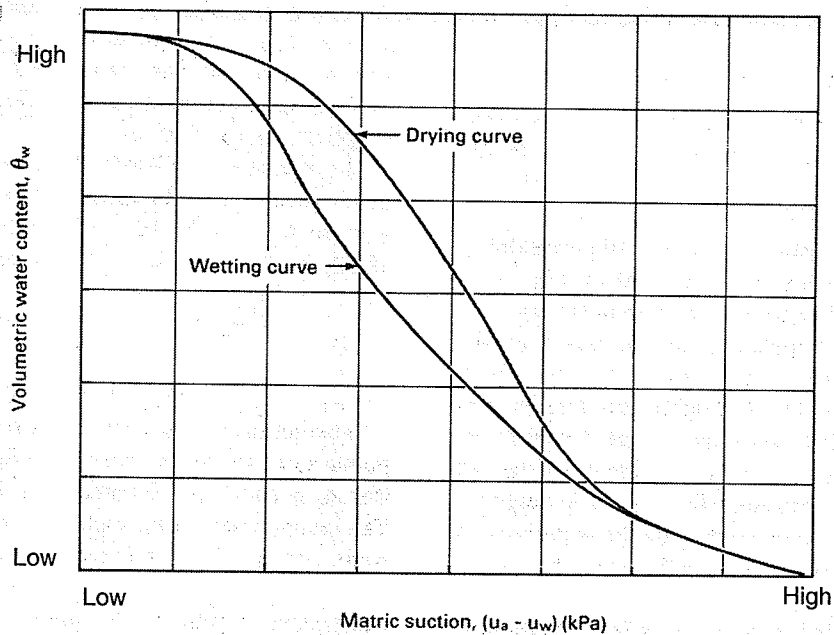


Figure 2.04 Hysteresis of the SWCC (adapted from Gonzalez and Adams 1980).

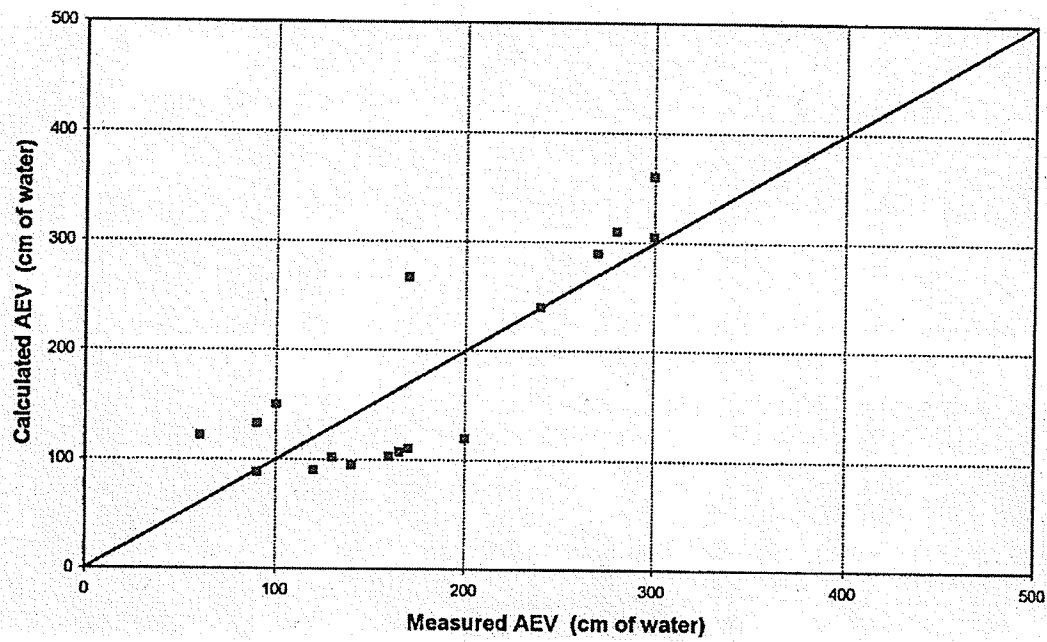


Figure 2.05 Comparison of calculated AEV using the Brooks and Corey method (1964) *versus* measured AEV (Aubertin *et al.* 1998).

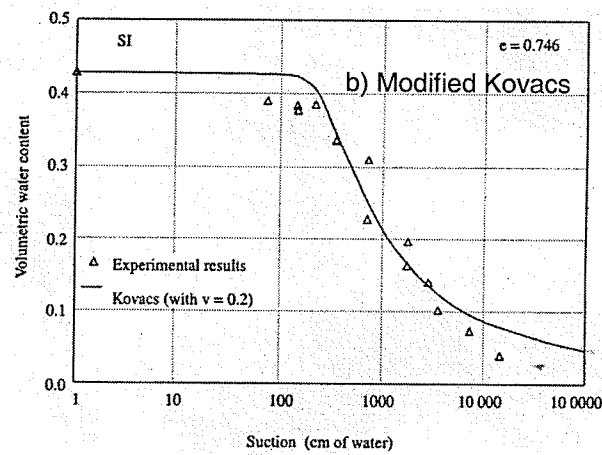
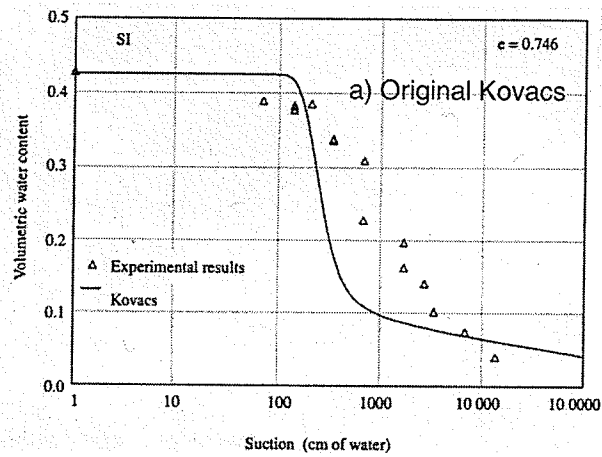


Figure 2.06 Comparison of the a) Kovács model to b) the modified Kovács to experimental results for the SWCC (Aubertin *et al.* 1998).

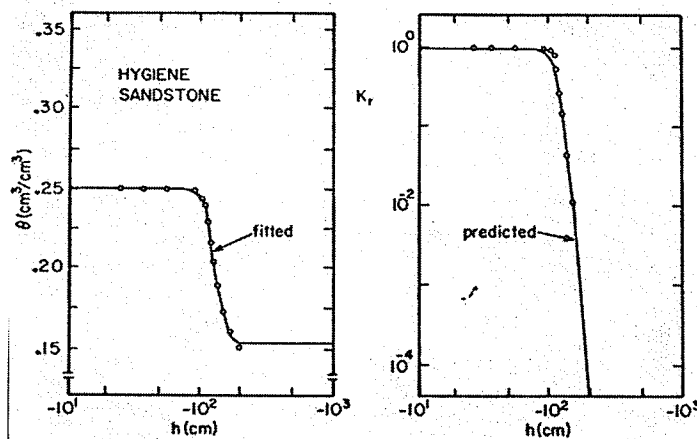


Figure 2.07 Observed (open circles) and calculated curves (solid lines) of the hydraulic conductivity function for Hygiene Sandstone (van Genuchten 1980).

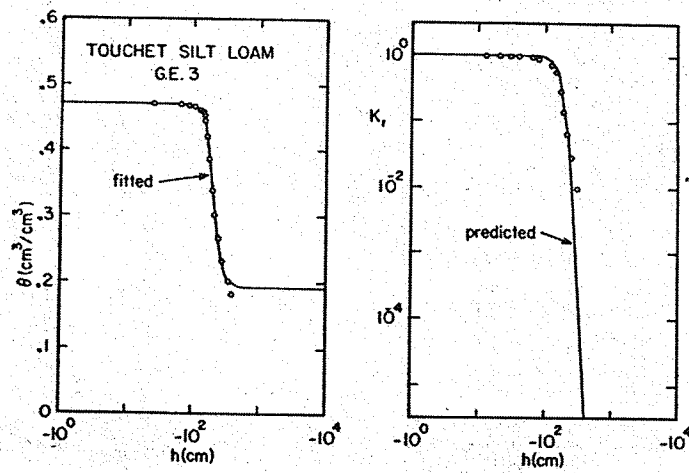


Figure 2.08 Observed (open circles) and calculated curves (solid lines) of the hydraulic conductivity function for Touchet Silt Loam G.E. 3 (van Genuchten 1980).

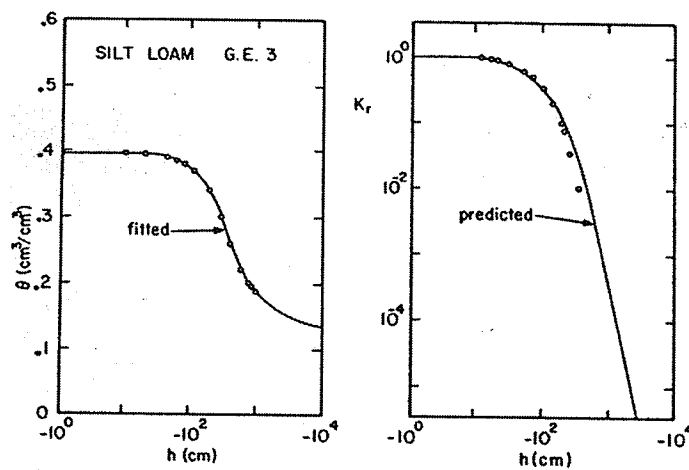


Figure 2.09 Observed (open circles) and calculated curves (solid lines) of the hydraulic conductivity function for Silt Loam G.E. 3 (van Genuchten 1980).

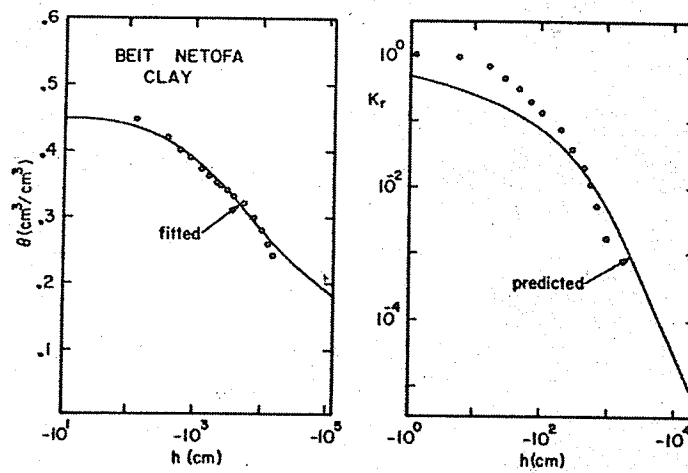


Figure 2.10 Observed (open circles) and calculated curves (solid lines) of the hydraulic conductivity function for Beit Netofa Clay (van Genuchten 1980).

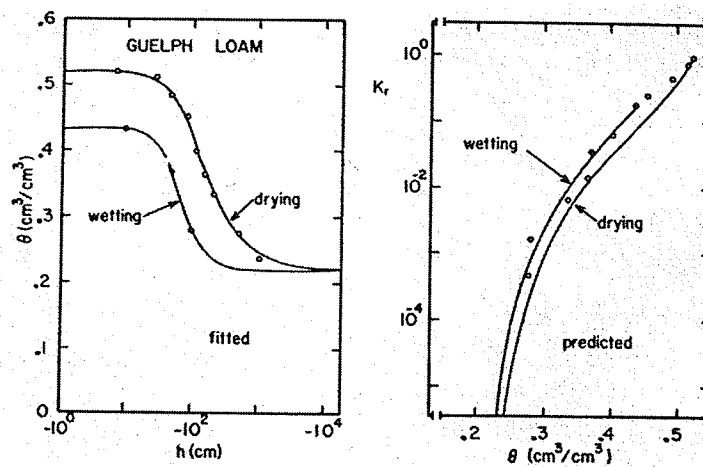


Figure 2.11 Observed (open circles) and calculated curves (solid lines) of the hydraulic conductivity function for Guelph Loam (van Genuchten 1980).

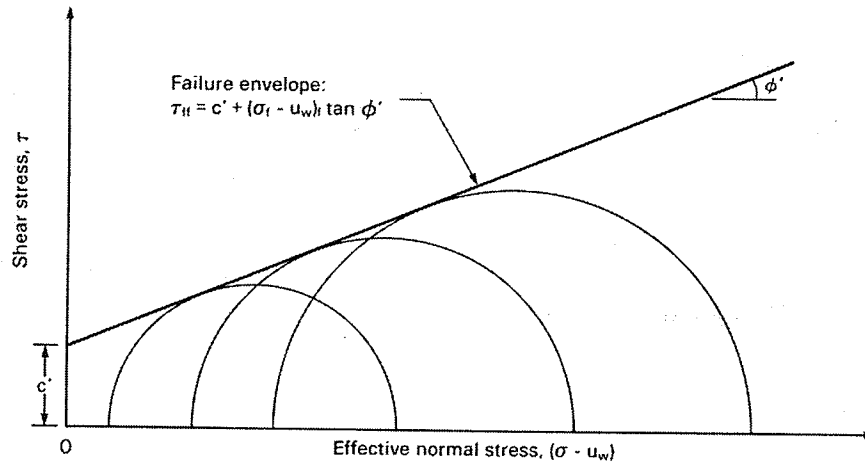


Figure 2.12 Mohr-Coulomb failure envelope for a saturated soil (Fredlund and Rahardjo 1993).

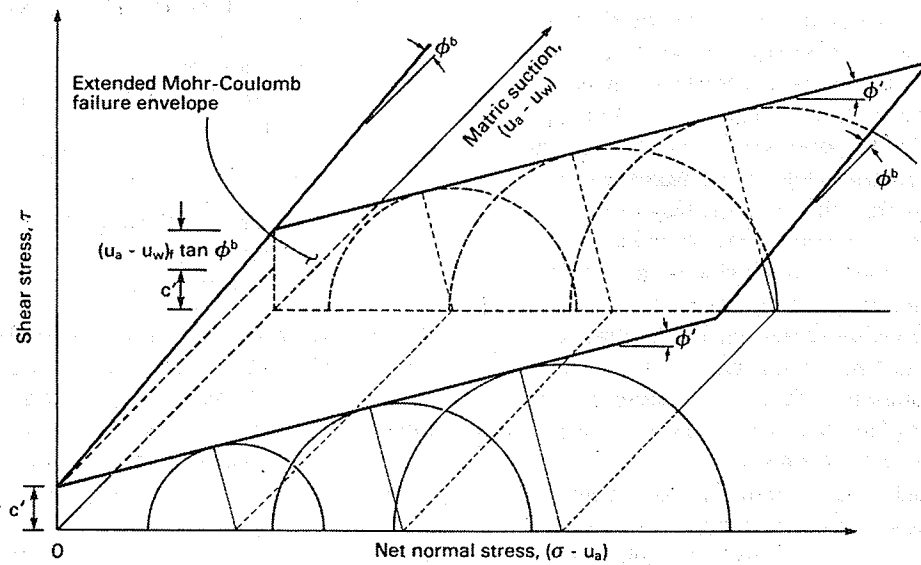


Figure 2.13 Mohr-Coulomb failure surface for an unsaturated soil (Fredlund and Rahardjo 1993).

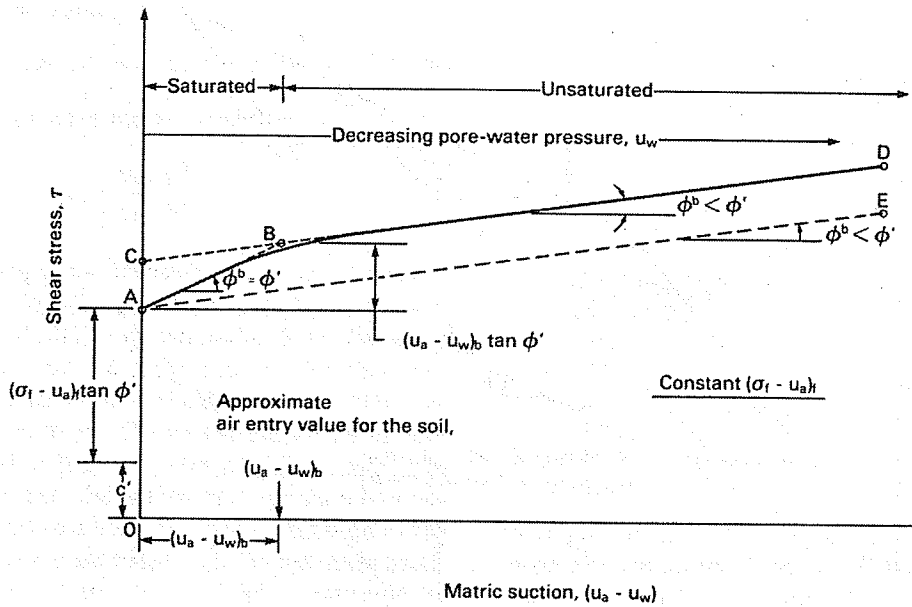


Figure 2.14 Non-linearity of unsaturated failure envelope (Fredlund and Rahardjo 1993).

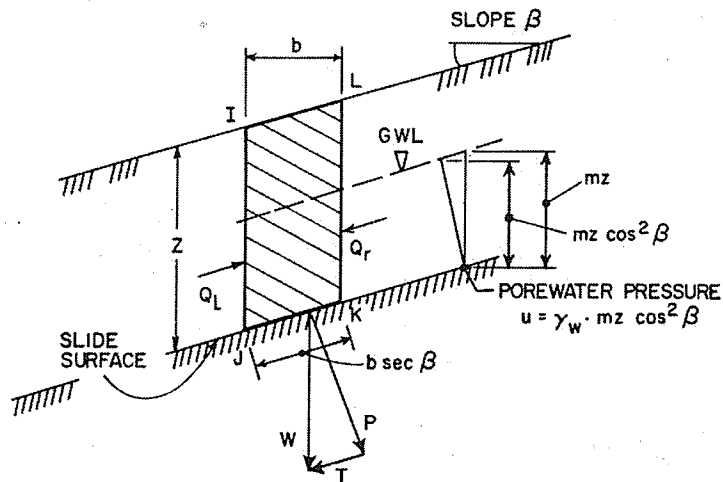


Figure 2.15 Infinite slope analysis (Graham 1984).

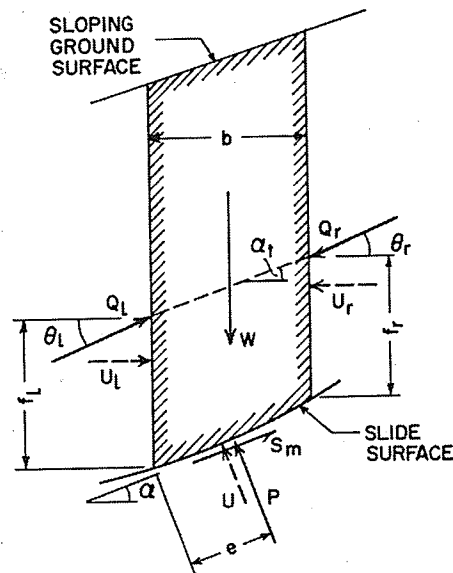


Figure 2.16 Free body diagram of forces acting on a soil slice (Graham 1984).

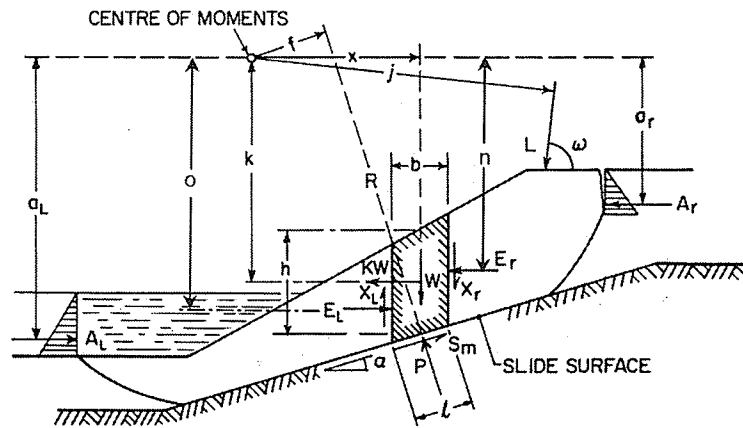


Figure 2.17 Parameters used to resolve force and moment limit equilibrium equations (Fredlund and Krahn 1977).

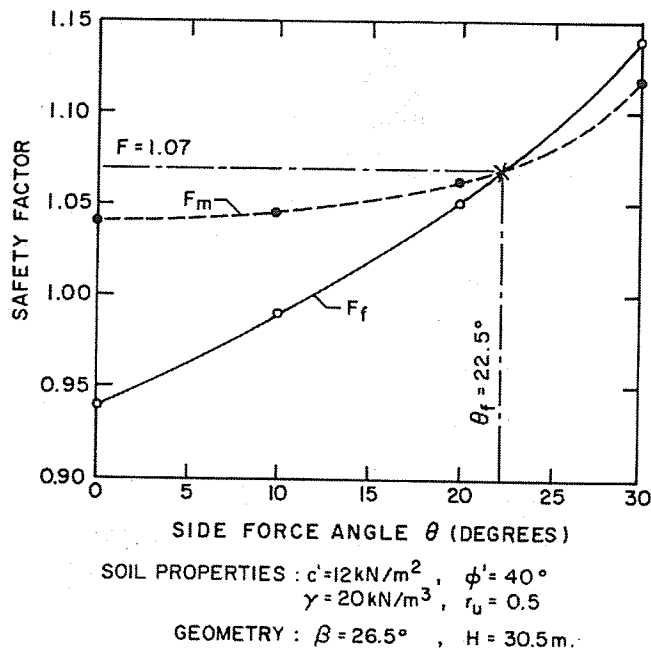


Figure 2.18 Relationship between the two limit equilibrium equations, F_f and F_m , and the interslice inclination using Spencer's method of slope stability analysis (Fredlund and Krahn 1977).

Chapter 3

Site Conditions

3.0 General Overview of Site

The study area is located near the top of the Assiniboine Valley, 4 kilometers Northeast of the town of Virden (MB). Two slope failures occurred in the spring of 1999 on a 3.4H:1V north-facing slope. It was initially thought that the movements were the first cases of slope instability in the area. However, discussion with local residents indicate past instability occurred roughly 30 years ago, most likely immediately- or shortly-following construction of the highway.

Both the 1999 failures have shallow, bowl-shaped geometries, ranging in maximum depth from two to four metres. The two failures are referred to as the West Failure and East Failures. Generally the failure scarp is at or below the crest and the failures exit above the toe. The geometry of the failures suggest a combined sliding and rotational movement. Between the summers of 1999 and 2000, the two failures were repaired by Manitoba Highways to improve their appearance. The West Failure was benched approximately mid-way up the slope

(Figure 4.01), while the East Failure was simply reworked back to original grade with no additional stabilization measures (Figure 4.01).

Since the slope repairs, both the "East" and "West" have re-failed. The East Failure moved again in the spring of 2000. The new movement of the East Failure was approximately half the size of the original mass and approximately the same depth (Figure 3.01).

The West Failure moved yet again after substantial rainfall during early July 2001 (Figure 3.02, Figure 3.03). There were some differences in vegetation cover that outlined the new movement. From aerial photos taken after the slope failures, the re-failed West Failure appears to be approximately the same size as the original slope failure (Figure 3.04). The new movement produced a head scarp that dropped vertically approximately 2-3 metres with numerous tension cracks along the slope above the bench. The toe of the movement occurred at an elevation just above the highway ditch and moved upwards approximately 2-3 metres in height (Figure 3.05). During the new West Failure movements, several existing standpipes were destroyed.

Before the failures, the study area was well vegetated with grass and a few sporadic trees and tree patches. The surficial soil along the slope face is a clayey silt loam with some weathered clay-shale and other gravel-sized debris including rock fragments of igneous and metamorphic origin. The presence of

sedimentary, igneous, and metamorphic lithology is evidence of glacial activity within the study area. At and beyond the slope crest the surficial deposits consist typically of glacial till that include clay- to boulder-sized material.

The drainage ditch along the highway showed no indication of groundwater draining from the failed slope during the field investigation. This was most likely due to the hot, dry weather during the time of and directly preceding the field investigation. However, surficial water was noted midway up the slope at the location of the reworked West Failure bench. Beyond the slope crest, depressions produced by glacial activity showed evidence of water retention for extended periods by the species, maturity and density of the vegetation.

Outside the study area, there are numerous failures within the Assiniboine River Valley. The largest of these failure that occurred along the PR 259 highway cut on the east side of the main river valley, opposite to the location of the study area. This major failure appears to be linked to a weathered clay shale unit with an average strike of N39°W and an average dip of 18 degrees from horizontal taken from a compass and inclinometer. This weathered clay shale failure is at present still moving and is a significant threat to the operation of the highway. It appears to be geologically dominated and not related to the study area on the west side of the valley.

One local failure that appears to be similar to the studied failures is located North of PR 259 about 50 metres to the west of the study area. It is approximately the same shape, size, and depth and is along the highway fill. The surficial material at this failure is identical to the studied failures except for the lack of gravel-sized debris. Due to the terrain and location of this failure it was not incorporated into the research project (Figure 3.06).

3.1 Site Geology and Geomorphology

The geology at the location of the failures encompasses a complex geological profile produced by several geomorphological processes. The study area is located within the Souris Basin physiographic division near the edge of the Assiniboine River Valley. The local overburden material includes water-laid glacial till, alluvium, lacustrine clays, and silts all deposited about 12,000 – 14,000 years before present (Klassen and Wyder 1970).

During the last glaciation, ice at its farthest extent covered a significant portion of southwestern Manitoba, including the study area. A small area in southwestern Manitoba occupied by the present day Souris River Valley remained free of ice (Klassen 1975). At the time of glaciation, the present day Souris River Valley was occupied by glacial Lake Souris (Figure 3.07). As the ice retreated, Lake Souris expanded northward, terminating slightly north of the study area before draining eastward. Upon further retreat of the ice, the Assiniboine spillway

channeled melt-water from glaciers in the north. The most recent glaciation ended more than 14,000 years ago with the entire area being ice-free about 12,000 years ago. Comparing historic flows during lake drainage with today's normal river conditions, the Assiniboine river is an under-fit river occupying a larger valley than current flows could form.

Between Kamsack SK and Brandon MB, the Assiniboine Valley is trench shaped, about 45 – 85 metres deep, and 1.2 – 2.4 km wide. Figure 3.08 shows a cross-section of the Assiniboine River Valley at the approximate location of the failures. The Assiniboine River Valley system in general is of glacial origin, evident through the shape and position of valleys that are parallel to the regional slope and ride over topographic highs. The valley, for the most part, was formed before the last glaciation, during the Early Wisconsin age. There are several locations along the river, including the study area, where the Assiniboine Valley breaks away from the ancestral valley referred to as the Virden Valley (Figures 3.09, 3.10, 3.11). The Virden Valley where it coincides with the Assiniboine River Valley, is evident through the nature, thickness and distribution of older fill material underlying recent Assiniboine Valley sediments along the valley bottom, walls and beneath certain terraces (Klassen and Wyder 1970). The study area is located between the ancestral Virden Valley that lies to the west and the Assiniboine Valley to the east.

The bedrock geology in the vicinity of the study area is comprised of the Upper Cretaceous Riding Mountain Formation. The Upper Cretaceous Riding Mountain Formation consists of two members; the Odanah member and Milwood member (Figure 3.09). The Odanah member consists of a hard gray siliceous shale. It lies beneath the study area and exists on the east side of the Assiniboine River Valley with outcrops along the east valley wall which coincides with the large shale slope movement previously mentioned. The Milwood member, consists of a soft greenish brown bentonite silt shale and is located on both the west and east of the study area. The Milwood member outlines the location of the Assiniboine River Valley and the Ancestral Virden Valley due to its erodable nature. The bedrock topography also outlines the two valleys (Figure 3.10)

Surficial deposits along the Assiniboine River Valley include till, glaciolacustrine clay, silt, alluvium, colluvium, sand and gravel, and occasional bedrock outcrops. Figure 3.11 shows a map of surficial deposits in the region (Betcher 1983). The study area is in a transition zone consisting of glacial till and alluvium/colluvium deposits. Aerial photos taken October 20, 1999 show several glacial topographic features such as hummocky and kettle topography surrounding the study area. In addition there is evidence of ice scours beyond the scarp of the study area. Figure 3.04 consists of two aerial photos in stereoscopic position of the East and West Failures. The soil profile at the study area incorporates varying geological deposits produced by these varied geomorphological processes. However the

shallow nature of the movements suggests that geological complexity does not play a major role in the development of the failures.



Figure 3.01 East Failures of 1999 and 2000.



Figure 3.02 West Failure summer of 1999.



Figure 3.03 New West Failure 2001.

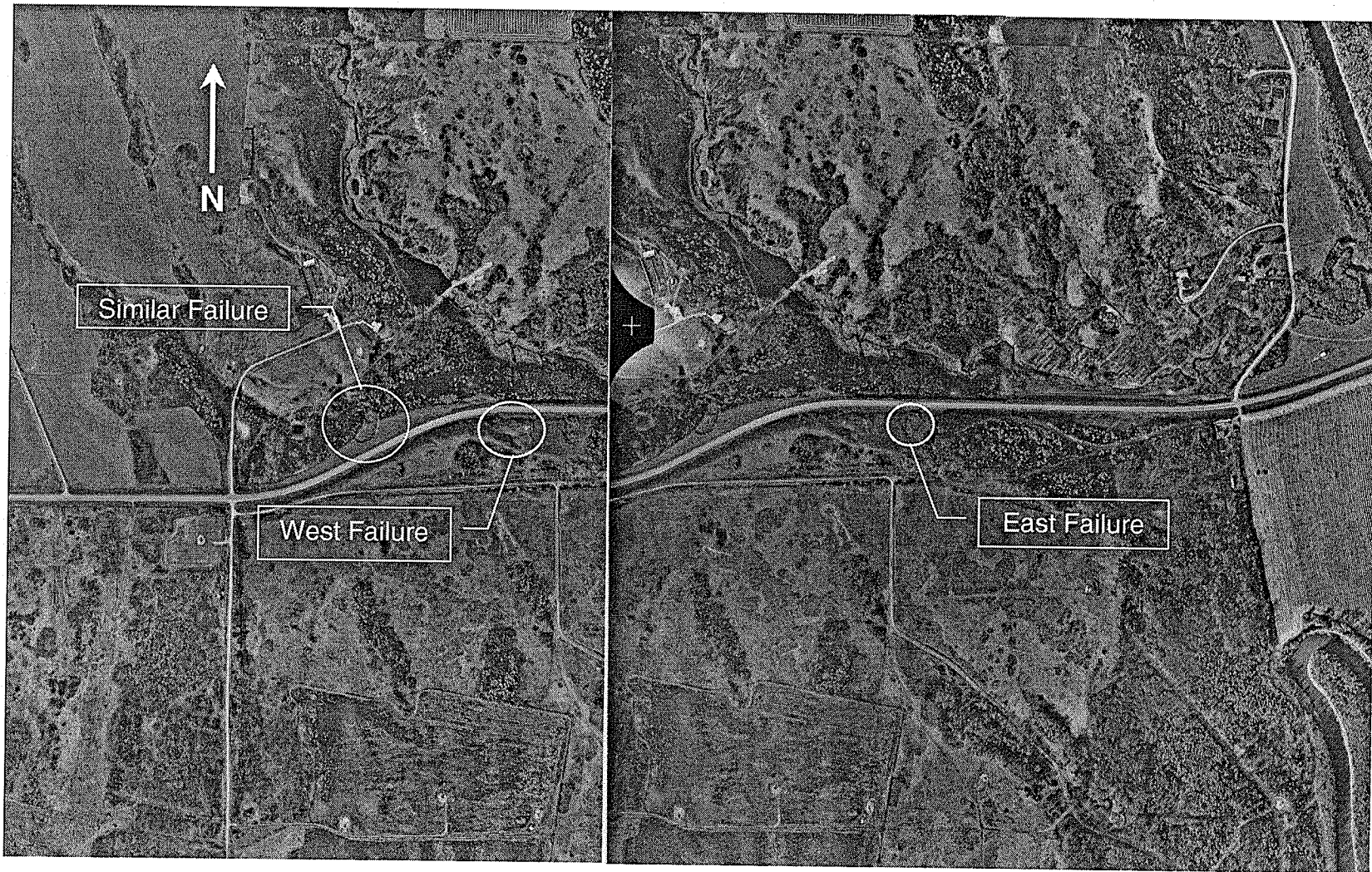


Figure 3.04 Aerial photograph of study area taken November 1999.



Figure 3.05 Toe of West Failure, summer 2001.



Figure 3.06 Toe of failure north of PR 259.

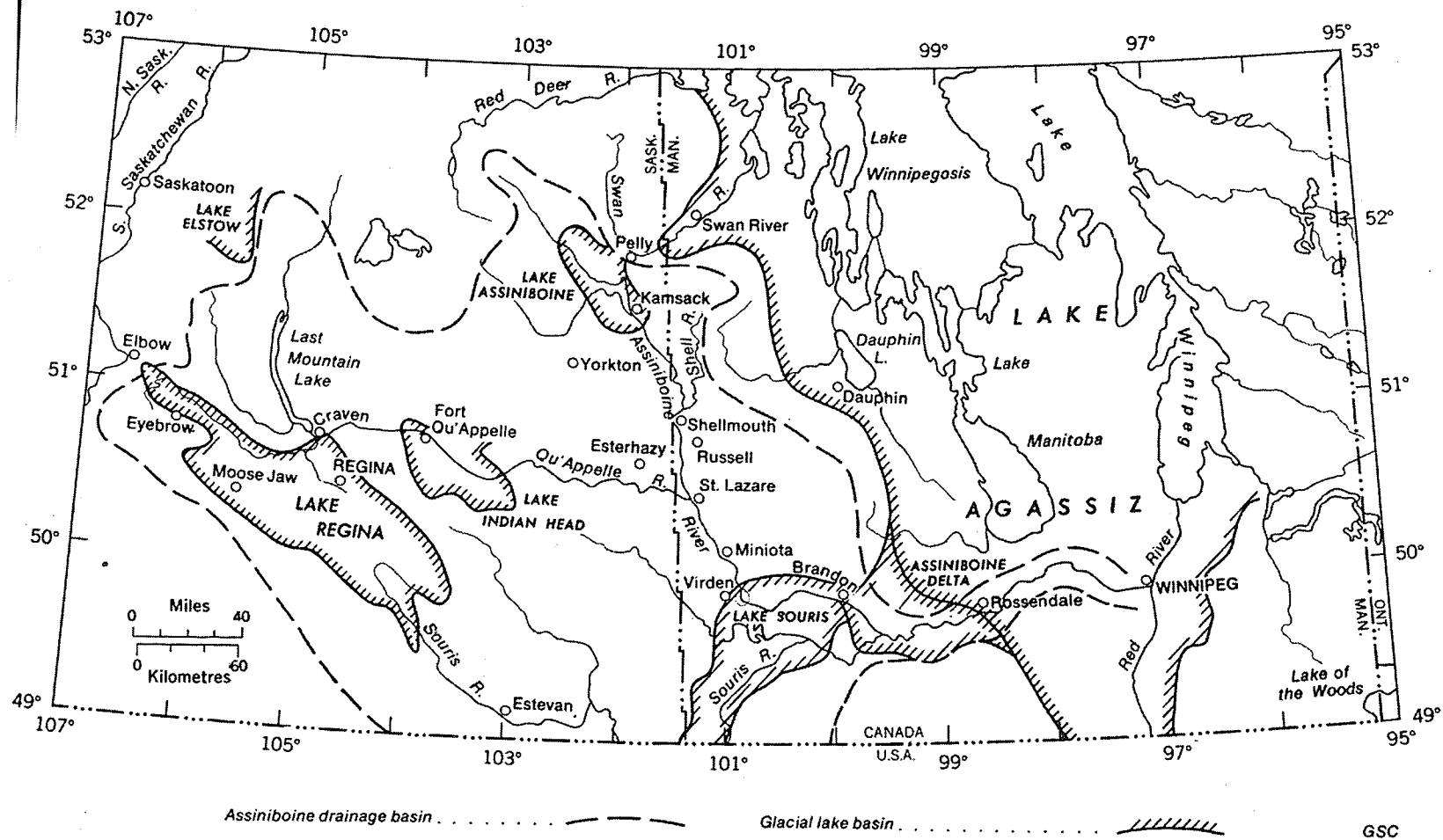
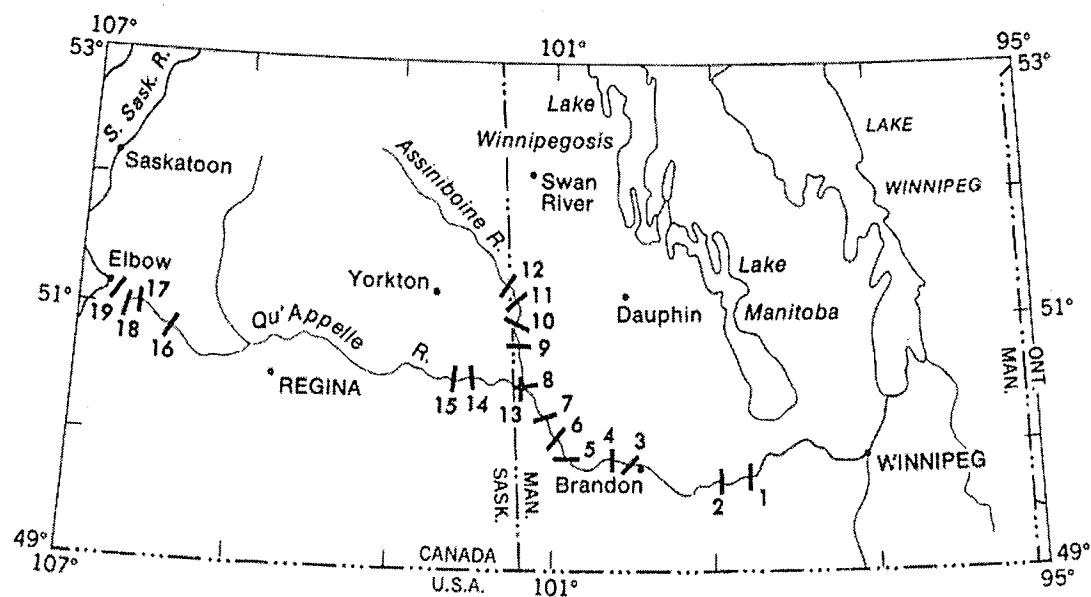


Figure 3.07 Assiniboine drainage basin (Klassen 1975).



Index map showing locations of valley cross-sections.

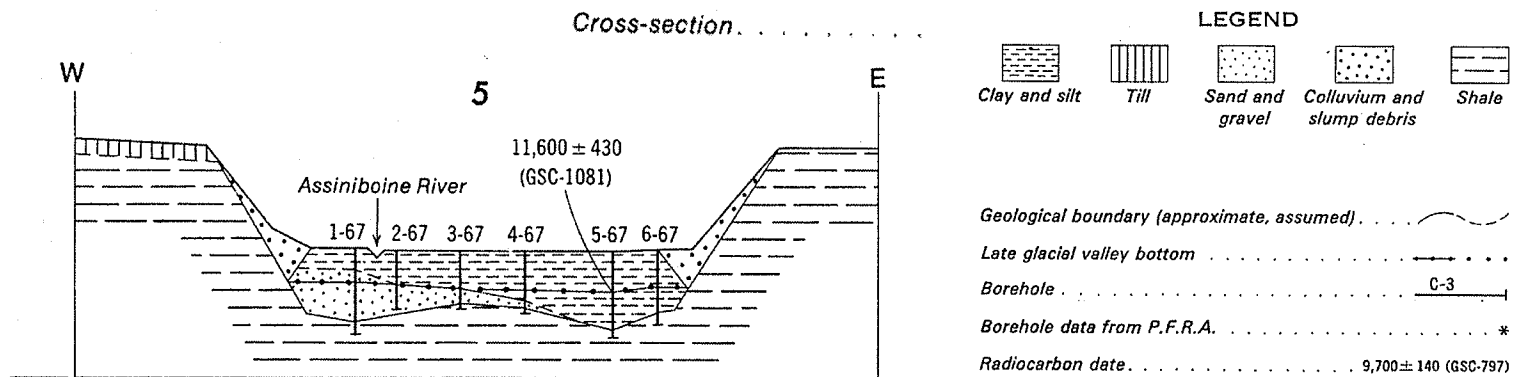


Figure 3.08 Assiniboine Valley cross-sections (Klassen 1975).

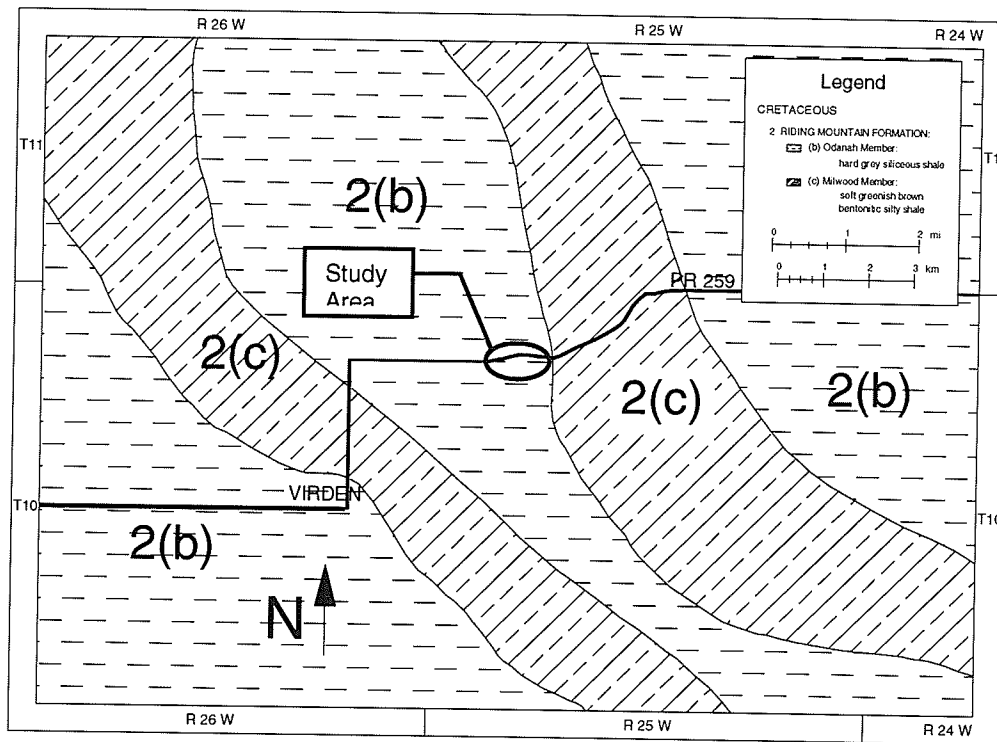


Figure 3.09 Bedrock geology (Betcher 1983).

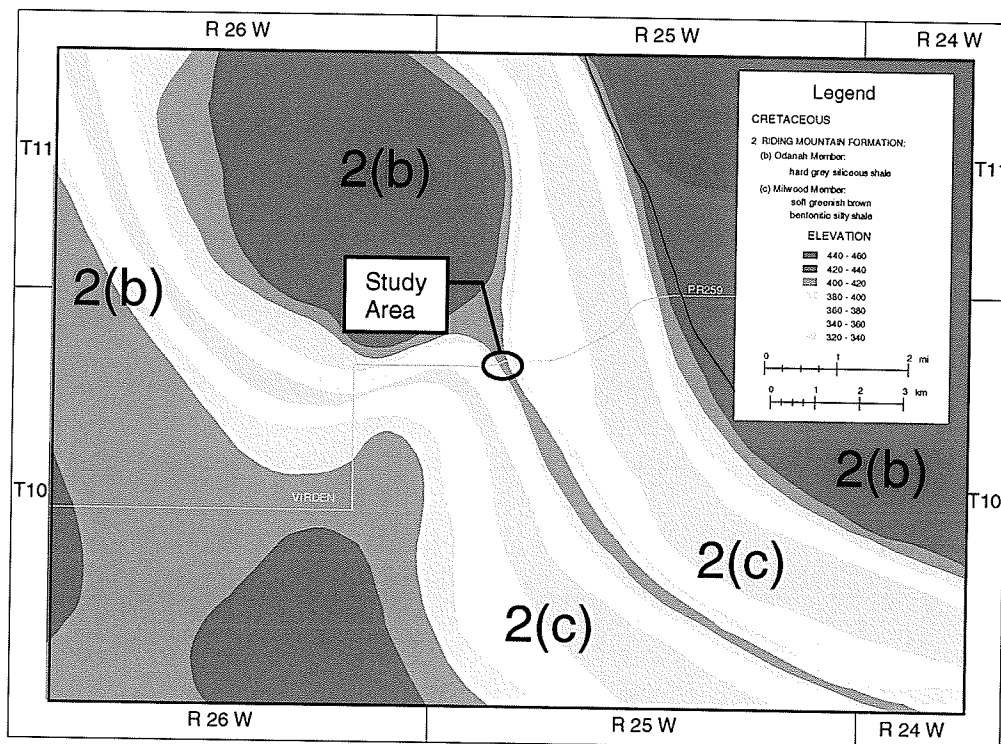


Figure 3.10 Bedrock topography (Betcher 1983).

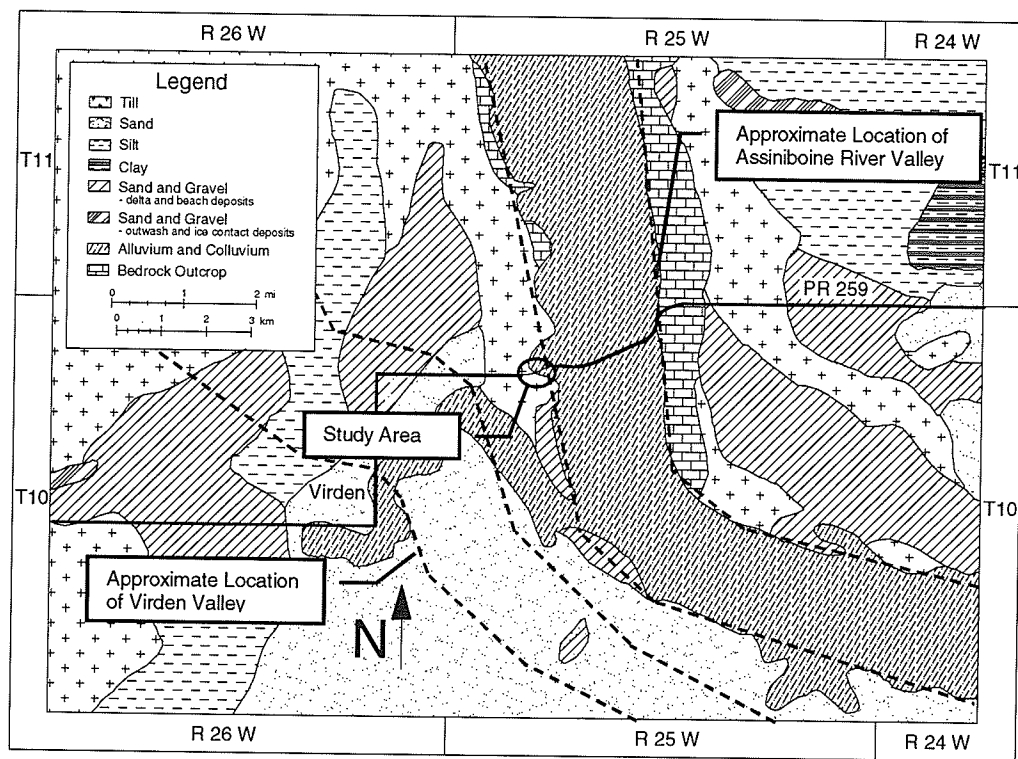


Figure 3.11 Surficial deposits (Betcher 1983).

Chapter 4

Field Investigation

4.0 Introduction

Prior to the field investigation program, a preliminary site reconnaissance visit was undertaken. A hand augered hole was drilled into the West Failure to obtain grab samples for classification and to install a shallow standpipe (Appendix A: Hand Augered Field Logs). Results from the initial reconnaissance were used to develop a more-detailed investigation program that included two test pits and four boreholes with piezometer installations. In addition to the test pits and boreholes, a detailed survey of the site with a total station was planned. The detailed field investigation was conducted in July 2000. A few weeks after the detailed field investigation, four additional hand augered holes were drilled including three standpipe installations.

4.1 Topographic Survey

The study area was surveyed with a TOPCON GTS-605AF total station. A local coordinate system was established for Northings and Eastings while the elevations were taken relative to a marker located by the local Department of Highway and Transportation (MB) staff. Cross-sections of the site were selected in order to create a topographic map of the study area using the Eagle Point software application (Figure 4.01). The cross-sections were spaced approximately at 10 metre intervals, with each cross-section commencing from the centerline of PR 259 and ending beyond the crest of the slope. After all the survey data was compiled and inputted into Eagle Point, a topographic map (Figure 4.01) and six cross-sections (Figures 4.02 – 4.07) were generated.

4.2 Hand Augered Holes

The preliminary investigation included an inspection on foot over the study area and a hand-augered hole (A-1) to depth of 3.3 metres below ground surface. (Figure 4.08). To further complement the drilling program, a day trip to the study area was undertaken a few weeks after completion of field investigation to drill four additional hand augered holes (A-2 to A-5) including installation of three additional standpipes piezometers to better characterize the groundwater conditions at the site. Figure 4.08 and Figure 4.09 show the soil profile interpreted from the hand augered holes. Almost all of the hand augered holes

were drilled approximately mid-way up the slope at or near the bench elevation. The hand augered holes terminated at a depth of approximately 3.3 metres below ground surface due to difficulties in drilling further. Field logs from the hand augered holes are included in Appendix A. Appendix B and C include the test pit field logs and field borehole logs, while Appendix D has the borehole logs of the hand augered holes, test pits and field boreholes.

The first hand augered hole was located 12.9 metres west of BH-3 at approximately the same elevation (Figure 4.01). While BH-3 for the most part consisted of silty clay, the hand augered hole, A-1, consisted of silty clay material to a depth of 2.0 metres below ground surface. Below 2.0 metres, the soil profile consisted of silty fine sand to a depth of 3.3 metres, which corresponds to the bottom of the borehole. The differences between A-1 and BH-3 show how variable the soil profile is within the study area. This difference in the first metre of the soil profiles between BH-3 and A-1 is mostly likely linked to the fact that the slope was reworked. A-1 showed evidence of a watertable through sloughing and free water in the cuttings. The watertable was estimated to be at a depth of 2.1 metres below ground surface. Below the apparent watertable, the extracted samples were very soft and consistently sloughed in. Due to the nature of the material below 2.1 metres, it is difficult to be confident that the extracted material came from the bottom of the hole and was not material scraped off the walls of the borehole. As previously mentioned, surficial water was also observed in the

vicinity of A-1. This was the only location within the study area that surficial water was evident.

On the day trip after the detailed field investigation, A-2 was drilled close to the hand Augered hole, A-1. Hole A-2 was drilled to a depth of 3.8 metres, 0.5 metres below the bottom of A-1. For the additional 0.5 metres the soil consisted of low plastic silty clay with some partially oxidized fine sand, and trace gypsum. Free water was observed in A-2 but was significantly less than in the A-1 hole. Hole A-2 was drilled close to A-1 to facilitate installation of a standpipe in the coarse material. A standpipe enclosed with a filter sock was installed at a depth of 3.8 metres in A-2. Slots were cut into the bottom 0.3 metres of the standpipe. Water levels have been observed between 1.3 and 2.1 metres below ground surface in this installation. Installation details for the standpipes are shown in Figure 4.10.

The third hand augered hole, A-3 was drilled within 0.10 metres of BH-1. The soil profile was not logged for this hole. The purpose of re-drilling at this location was for installation of a standpipe. The standpipe installation was similar to the installation in A-2. A standpipe enclosed with a filter sock was installed to a depth of 3.8 metres in A-3. Slots were cut into the bottom foot of the standpipe. A standpipe installed at 4.9 metres depth has shown no readings as of August 1, 2001. A detailed illustration of the standpipe installation is given in Figure 4.11.

The fourth hole (A-4) was hand augered approximately 12.9 metres west of BH-3 and 7.7 metres up from A-2 along the slope. The first metre of the soil profile consisted of a silty fine sand with trace medium sand to coarse gravel. In addition, there were trace organics, gypsum, and oxidation. Below the upper layer, the soil consisted of silty clay with trace fine sand to coarse gravel. The coarser material consisted for the most part of clay shale. The clay layer was low to medium plasticity to a depth of 2.1 metres. At this depth the plasticity of the clay reduced to low plastic in nature to the bottom of the hole at a depth of 3.4 metres. There was evidence of the watertable at a depth of 2.1 metres below ground surface where there was an evident change in plasticity due to the increase in water content. As with the other hand augered holes, a standpipe was installed to a depth of 3.1 metres below ground surface. Water levels have been observed between 1.1 and 1.8 metres below ground surface in this installation. A detailed illustration of the standpipe installation is given in Figure 4.10.

The last hand augered hole, A-5 was drilled approximately 7.5 metres up from BH-3 along the slope. The soil profile consisted of intermittent layers of silty fine sand and silty clay. As well, throughout the entire profile there was trace fine gravel. The hand augered hole A-5 was cut short due to a boulder/cobble encountered at a depth of 2.0 metres below ground surface.

4.3 Test Pits

Two test pits were excavated mid-way up the slope with a backhoe mounted on a front-end loader. Test pit 1 (TP-1), just west of the East Failure, was in intact (unfailed) material, while Test pit 2 (TP-2) was excavated in slide material within the East Failure (Figure 4.01). Field logs for the two test pits are included in Appendix B, while Appendix D has the borehole logs of the test pits.

Test pit 1 was excavated to 5.0 metres depth (Appendix B: Test Pit Field Logs, Appendix D: Borehole Logs, Figure 4.12a, 4.12b). The profile comprised silty clay material of low to medium plasticity with a blocky/friable structure. Some clay shale and fine sand was encountered at a depth of 3.4 metres. A possible failure surface was identified at approximately 2.7 metres depth. The failure surface was interpreted from material retrieved by the backhoe but was not visible in the walls of the pit. The failure surface dipped at 15 degrees from horizontal, which roughly matched the inclination of the ground surface ($\sim 17^\circ$). Below 3.4 metres, the silty clay became significantly slickensided, with several distinct failure planes being evident. The plasticity also increased from low-medium to medium plasticity, with additional evidence of free water. Since Test pit 1 was outside the zone of failed material, the presence of failure planes suggests past movements.

In Test pit 1, block samples were taken at 1.5 and 2.5 metre depths for laboratory use. Block samplers allow for retrieval of large volumes of intact material (44 cm

x 22 cm x 22 cm) with minimal disturbance to the majority of the sample (Domaschuk 1977). The block sampler used at the University of Manitoba is a thin-walled rectangular tube that is pushed into the soil, in this case, using the bottom of the backhoe bucket. The end walls of the block sampler are reinforced to prevent damage while pushing.

Test pit 2 showed a similar soil profile, although with greater variability near the surface than the profile in test pit 1 (Appendix B: Test Pit Field Logs, Appendix D: Borehole Logs, Figure 4.13). This variability was likely caused by slope re-grading. Test pit 2 was excavated to a depth of 3.8 metres. A slickensided surface was visible on the walls and bottom of the Test pit at a depth of 2.9 metres (Figure 4.14). The appearance of the failure surface on the west wall was a lighter gray than the soil above and below (Figure 4.15). On the east wall of the test pit, the failure surface was significantly slickensided, oxidized with a blocky/friable structure (Figure 4.16). The failure surface dipped at approximately 22 degrees from the horizontal. A block sampler was pushed at 2.7 metres depth to capture a large specimen that included the failure surface. After extruding the block sample in the laboratory, an additional failure surface was found at 3.1 metres depth. The failure surface at 3.1 metres was more distinct and visible than the slip surface at 2.7 metres.

4.3.1 *In-situ* Suction Profile

A Quickdraw tensiometer¹ (Figure 4.17) was used to measure matric soil suction in the Test pits every 0.5 metres below ground surface until a zero suction reading was obtained. A tensiometer is a hand-held instrument used to measure suction with a high-air-entry ceramic stone tip attached to a hollow metal tube filled with water (Figure 4.18). Attached to the other end of the metal tube is a vacuum gauge calibrated to read in kPa. When the instrument's ceramic tip comes into contact with soil, water is drawn out of the hollow metal tube, thereby causing a vacuum (matric suction) that is measured by the gauge (Krahn *et al.* 1989). Prior to the detailed field investigation, the Tensiometer was calibrated using a manometer set-up capable of generating negative pore water pressure up to 40 kPa. Figure 4.19 shows the variation of tensiometer readings with depth in the two test pits. Suctions decreased from approximately 75 kPa (0.5 – 1.0 metres depth) near the surface to zero at 2.0 – 2.5 metres depth.

4.4 Boreholes and Standpipe Installation

The first borehole (BH-1) was drilled from the top of the slope to a depth of 24.4 metres (Figures 4.01, Appendix D: Borehole Logs). The other three boreholes (BH-2, BH-3, BH-4) were drilled to 5.2 - 7.2 metres depth long the location of the re-graded West Failure. Standpipes with Casagrande tips were installed in each hole. Figure 4.09 shows the soil profile with depth interpreted from all boreholes

¹The Quickdraw tensiometer was purchased from Soilmoisture Incorporated, Santa Barbara, California

and some of the hand augered holes, while Figure 4.11 illustrates the associated standpipe installations.

Borehole BH-1 was used to give an overall understanding of the local geology below the depth of the shallow failures. The first 2.5 metres consisted of silty clay material with organics, boulders, and cobbles decreasing with depth. Between 1 metre and 2.5 metres depth, the soil was blocky/friable in nature. Several fracture surfaces were encountered from 1.2 - 1.6 metres below ground surface. Along these fractures, traces of fine sand, organics and gypsum with significant oxidation were noted. A hollow stem auger bit was used for this hole but due the presence of cobbles and boulders, which made it difficult and nearly impossible to drill, the auger bit was switched from hollow to solid stem for the remaining depth. Using a solid stem auger eased the drilling process, but made it difficult to be accurate when recoding the soil profile. The transition between the two types of auger bits left a section of the soil profile un-logged. For the remaining depth, the material ranged between medium plastic silty clay to silty fine sand. This is thought to be a combination of deposits from glacial Lake Souris and the buried Virden Valley (or the Assiniboine spillway)(Figures 3.07, 3.08 3.10). No free water or watertable was encountered. A standpipe installed at 4.9 metres depth showed no groundwater readings up to November, 2001.

Borehole BH-2, was drilled to a depth of 5.2 metres (Appendix D: Borehole Logs, Figure 4.01 for location). The material in the initial 1.5 metres consisted of a

clayey silt loam with trace fine sand and coarse gravel. Shelby tubes were used to collect samples for the remaining depth. After extruding material from the Shelby tubes in the laboratory, the soil profile from 1.5 metres to 4.6 metres was found to be a mix of silty clay of medium plasticity. The silty clay, for the most part, was firm to stiff in nature with a blocky/friable structure. There was evidence of two slip surfaces, one at 3.7 metres and the other at 3.8 metres (Figure 4.20). Both slip surfaces were in-filled with fine sand with trace oxidation and organics showing evidence of water movements along the fractures. The failure planes were slightly blocky/friable. Below 4.6 metres, the stratigraphy consisted of water bearing silty fine sand with trace of fine gravel. A standpipe was installed to a depth of 5.2 metres below ground surface. Water levels have been observed between 2.5 and 3.5 metres below ground surface in this installation. A more detailed description of BH-2 and the standpipe installation is included in Appendix C.

Borehole BH-3 was drilled to a depth of 7.6 metres (Appendix D: Borehole Logs). The first metre consisted of low plastic silty clay loam with small fissures. Below 1.0 metre depth, the profile showed silty clay of medium to high plasticity with fissures, as well as numerous failures with a slightly blocky/friable structure. For the most part, the failures are slickensided in nature or in-filled with fine sand and traces of gypsum (Figure 4.21). Some of the in-filled fine sand was oxidized. Most fractures dipped at roughly 20° to 24° from horizontal, with the remaining fractures being horizontal. A standpipe installed in BH-3 showed no evidence of

water up to November, 2001. A more detailed description of BH-3 and the standpipe installation is included in Appendix C.

BH-4 was drilled to a depth of 6.0 metres (Appendix D: Borehole Logs). The top layer of the soil profile consisted of silty clay loam to a depth of 0.5 metres. Underlying the silty clay loam, the soil consisted of fine sandy silt to a depth of 6.1 metres, which corresponds to the bottom of the test hole. At times the soil unit was varved or laminated in nature with traces of oxidation. A standpipe installed to 6.0 metres below ground surface showed no evidence of water as of November, 2001. A more detailed description of BH-4 and the standpipe installation is included in Appendix C.

Several field measurements were taken at the ends of the samples contained within Shelby tubes. Torvane and pocket penetrometer readings were obtained at selected depths (Figure 4.22, Figure 4.23). Several readings obtained by the pocket penetrometer were beyond the range of the instrument. In general the pocket penetrometer and torvane results classify the soil as stiff to very stiff in nature.

4.5 Summary

Plotting a cross-section of the borehole information showed, as expected, that the soil profile was highly variable. In particular, the logs from BH-2, BH-3 BH-4

and the hand augered holes do not correspond well with information from BH-1. Groundwater measurements were also variable, with only some standpipes (including borehole and hand augered installations) showing evidence of water in the slope. The variability in the boreholes confirms the complex nature of the deposits and geomorphological processes that formed the area.

The soil profile observed at all boreholes and hand augered holes displayed little compatibility. However, there are roughly 4 major units that can be interpreted from the observed soil profile. They are as follows; (1) a near surface clay layer with a weathered zone, (2) a silty fine sand seam below the clay from the crest to approximately mid-slope, (3) a unweathered layer beneath the weathered zone and the silty fine sand seam and (4) a silt/fine sand layer beneath the clay layer at a considerable depth relative to the slope failures.

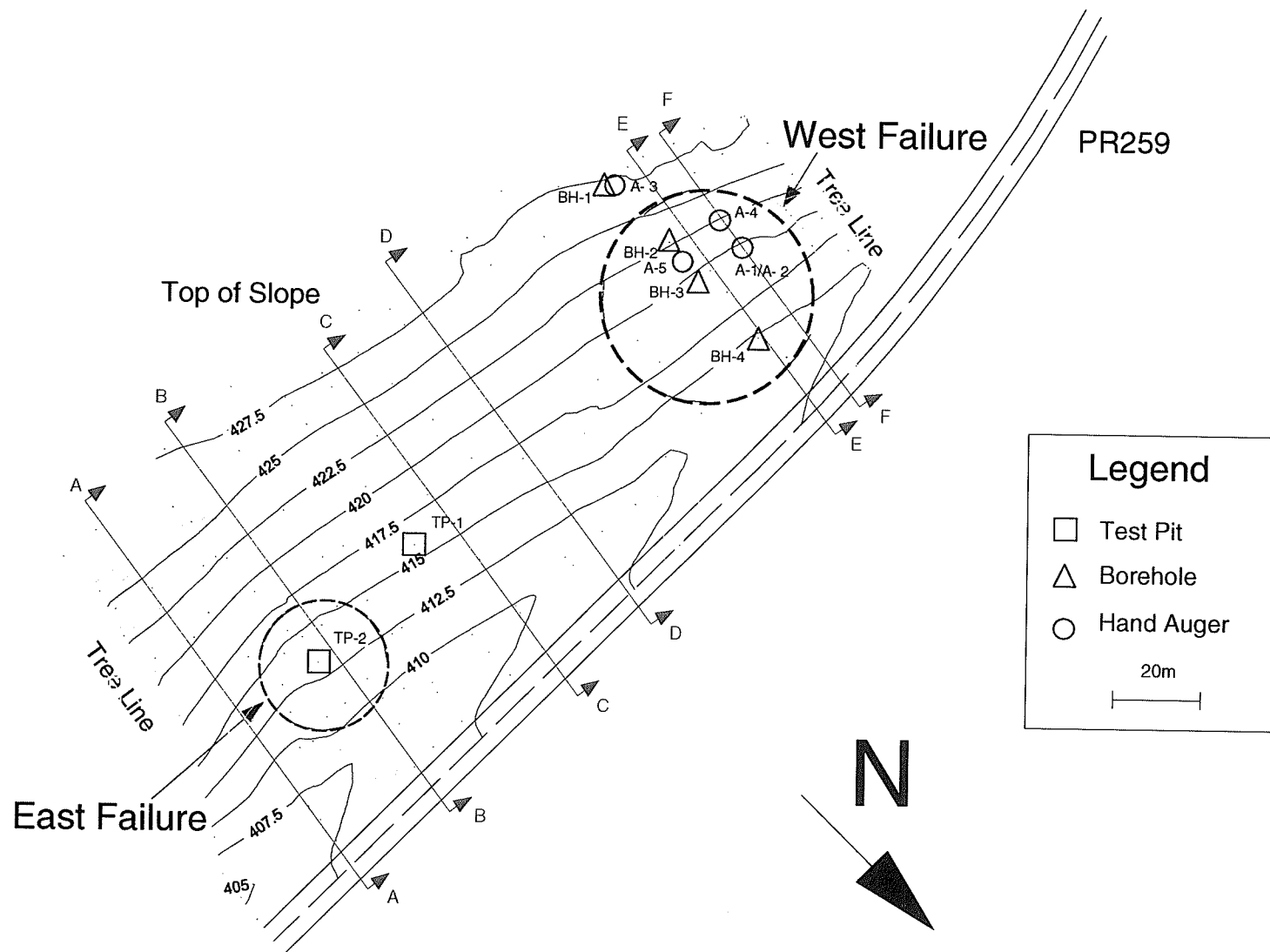


Figure 4.01 Topographic map of study area.

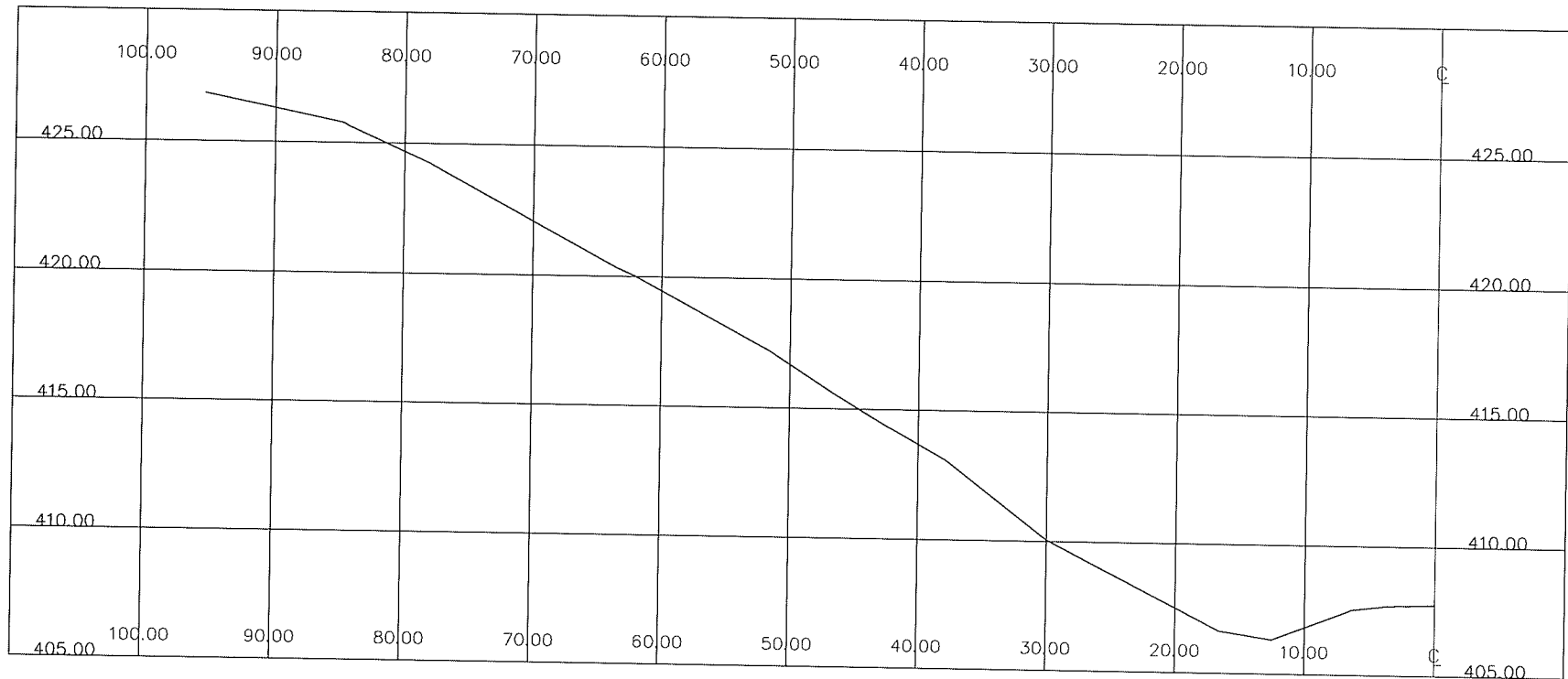


Figure 4.02 Cross-section A-A.

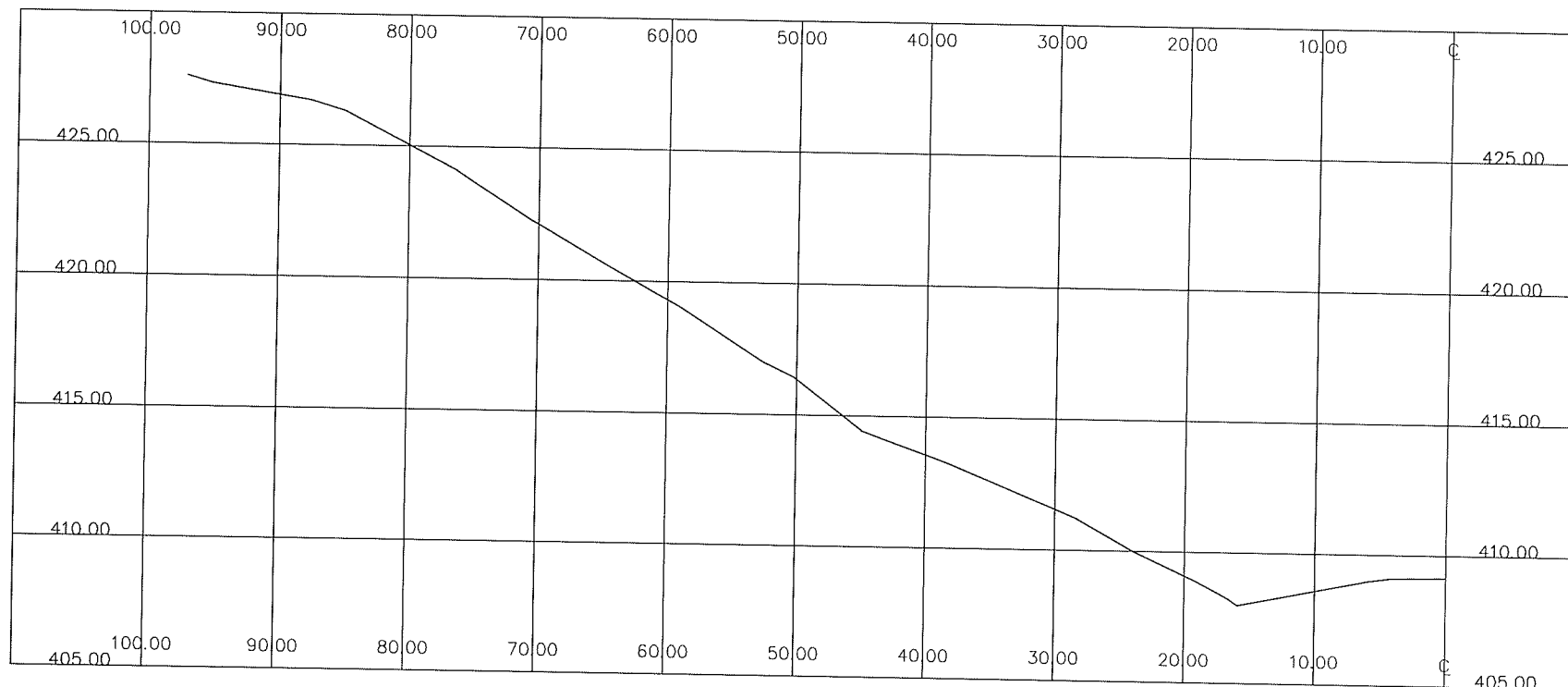


Figure 4.03 Cross-section B-B.

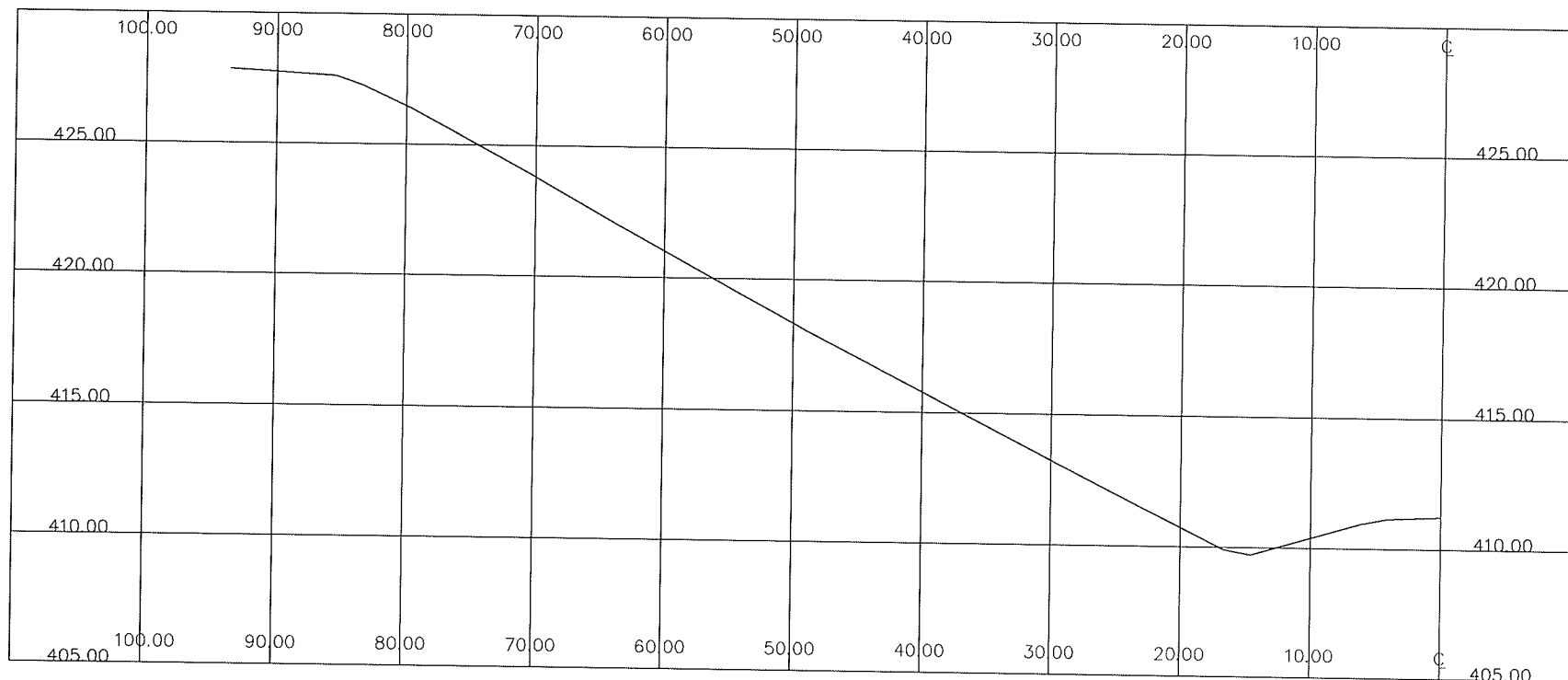


Figure 4.04 Cross-section C-C.

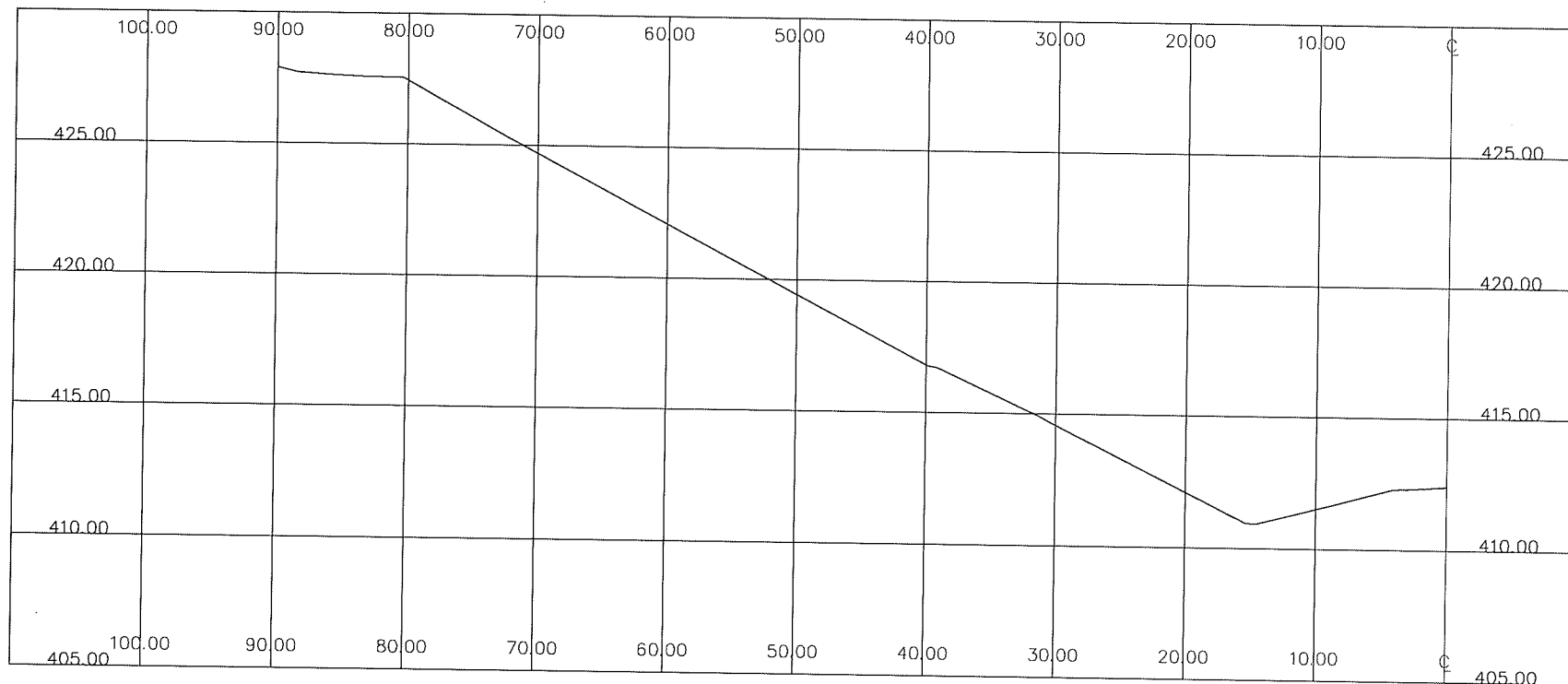


Figure 4.05 Cross-section D-D.

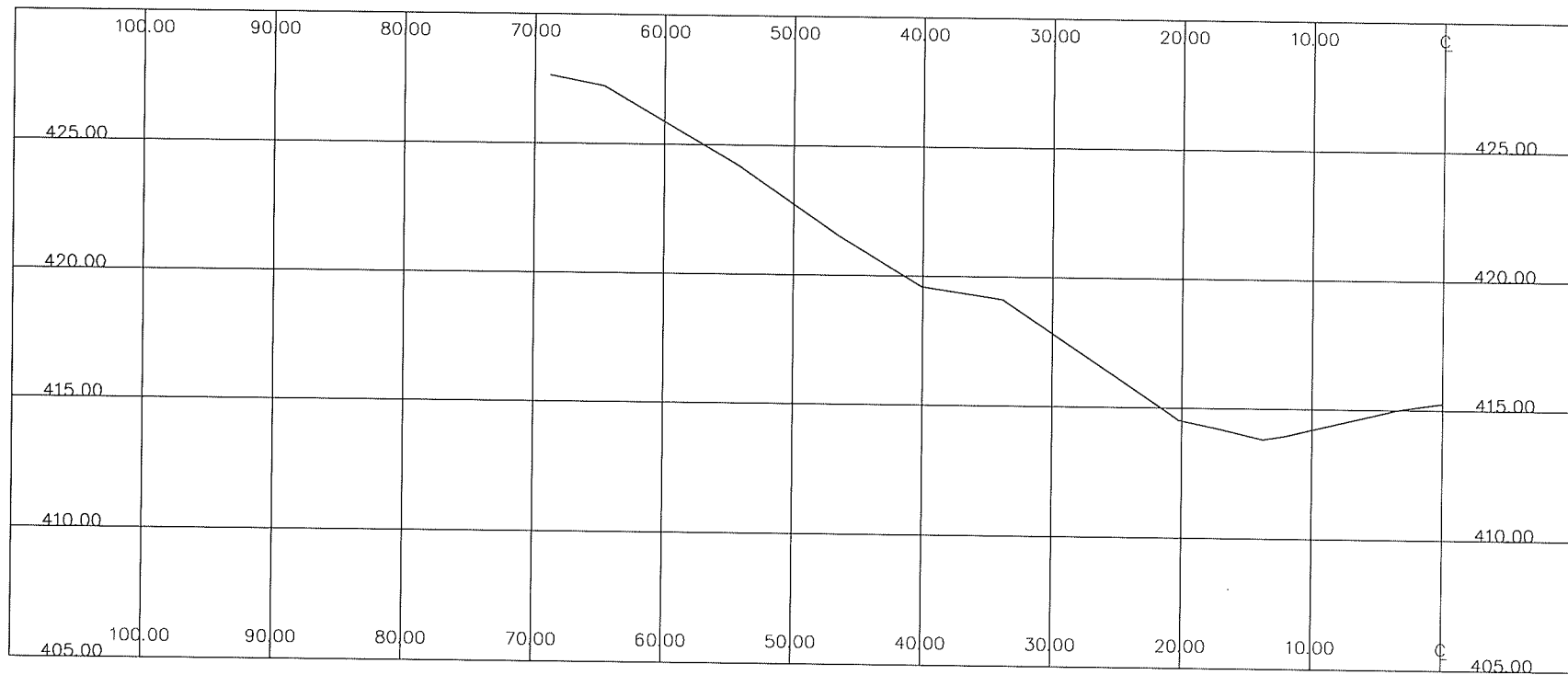


Figure 4.06 Cross-section E-E.

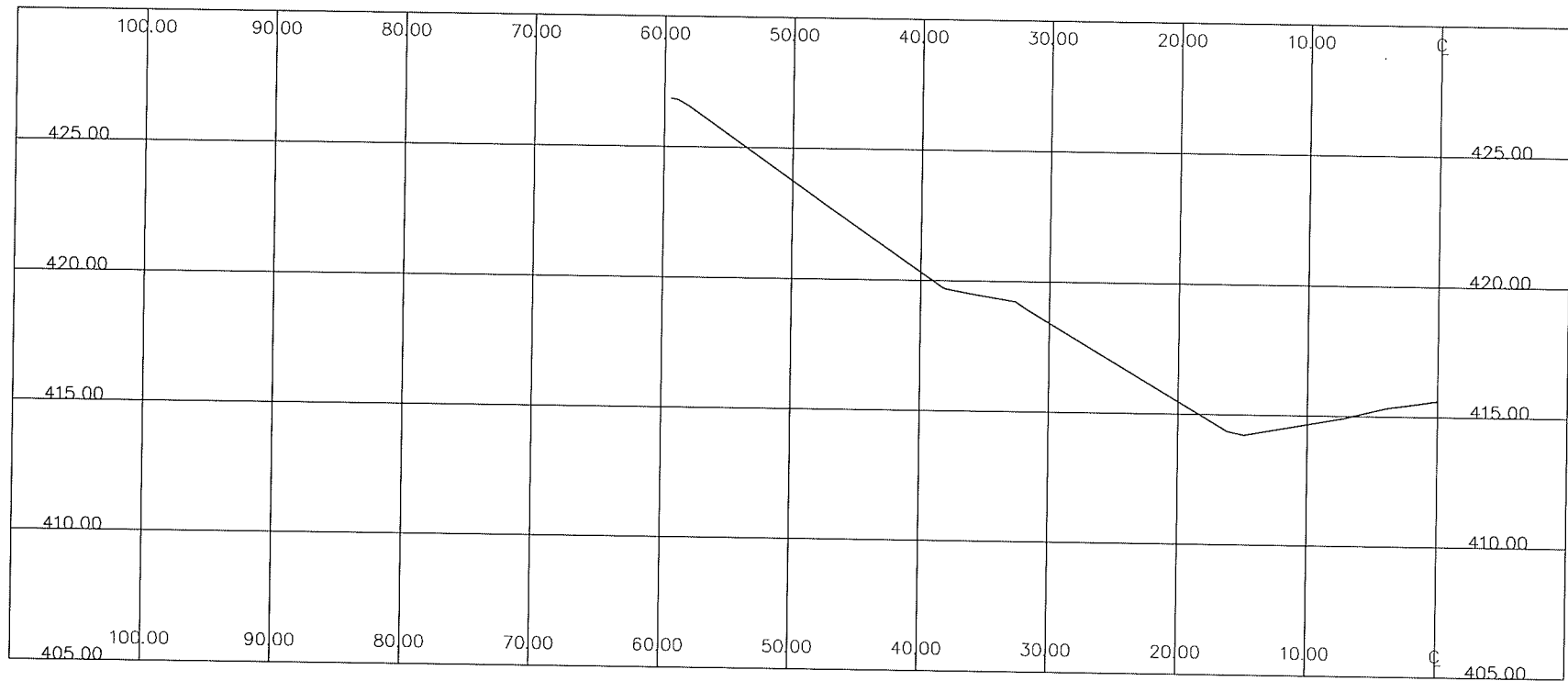


Figure 4.07 Cross-section F-F.

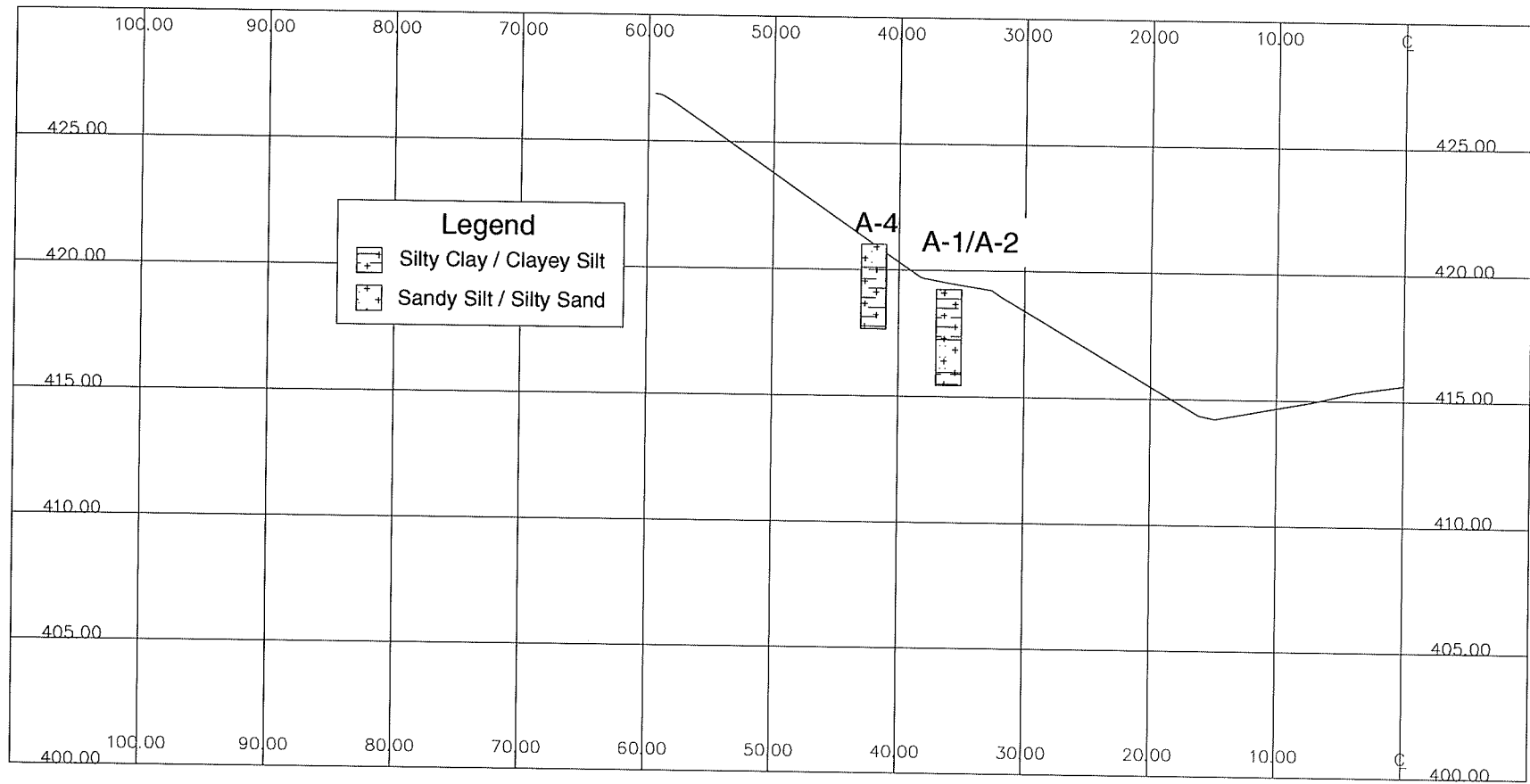


Figure 4.08 Hand augered holes interpreted soil profile.

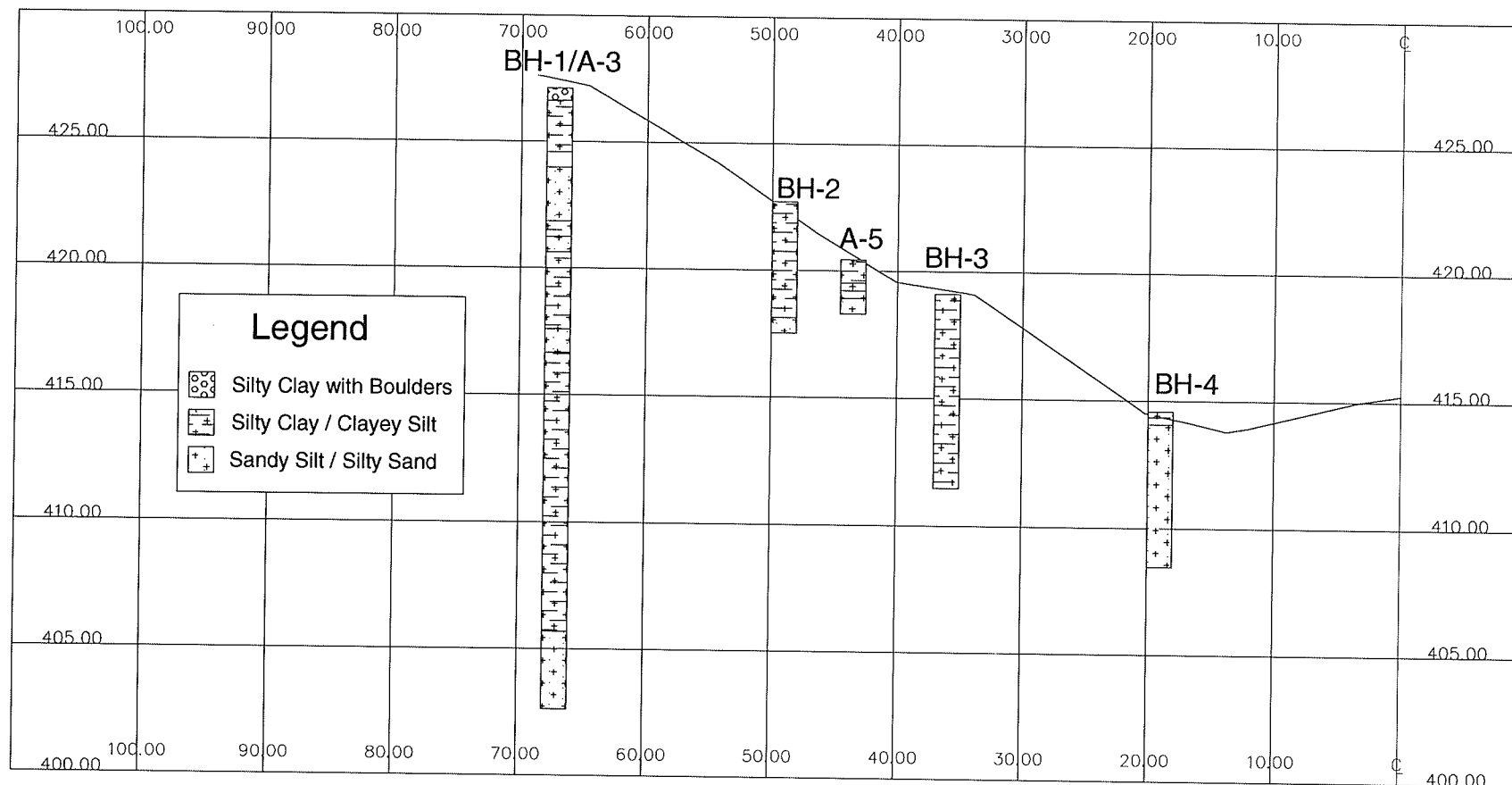


Figure 4.09 Borehole and hand augered holes interpreted soil profile.

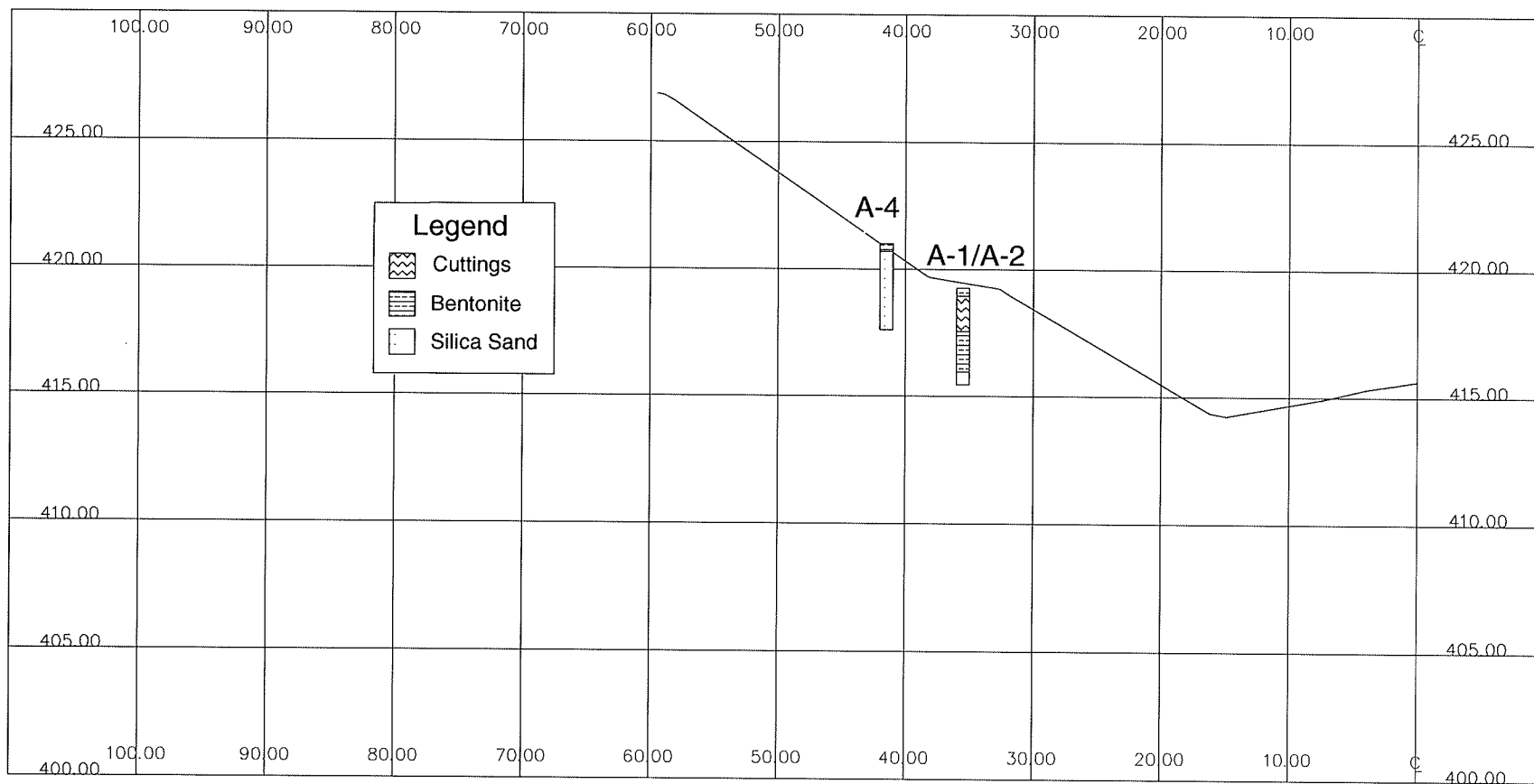


Figure 4.10 Hand augered holes standpipe installation.

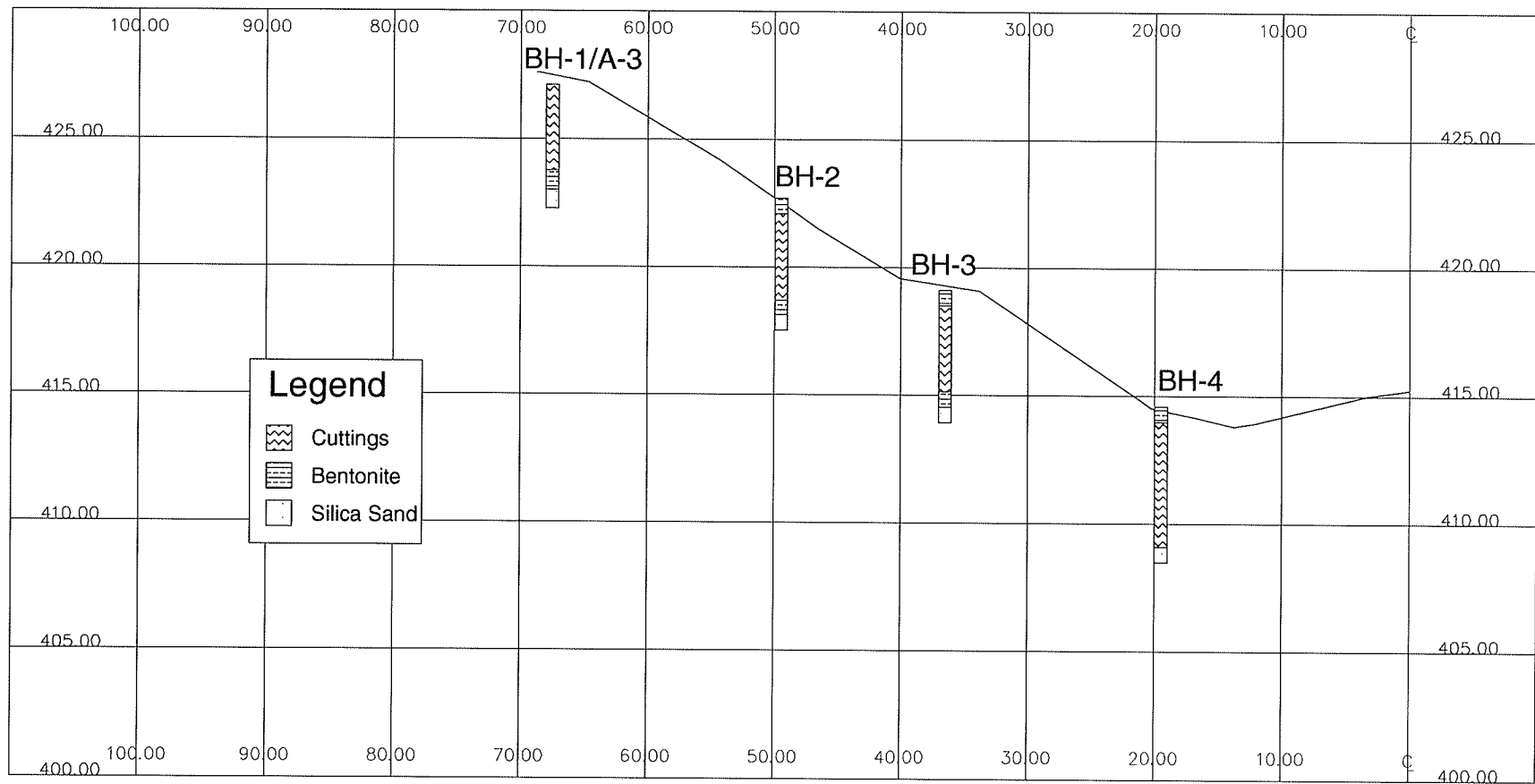


Figure 4.11 Standpipe installation in boreholes and hand augered holes.

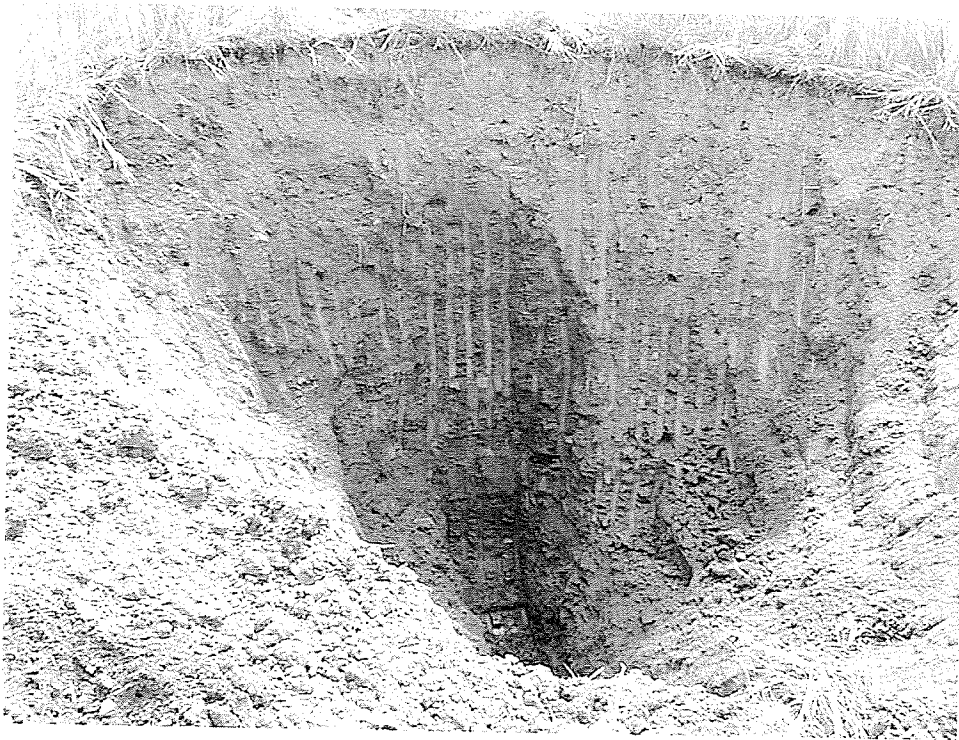


Figure 4.12a Test pit 1.



Figure 4.12b Close up of Test pit 1.



Figure 4.13 Test pit 2 and backhoe.



Figure 4.14 Failure surface at the bottom of Test pit 2.

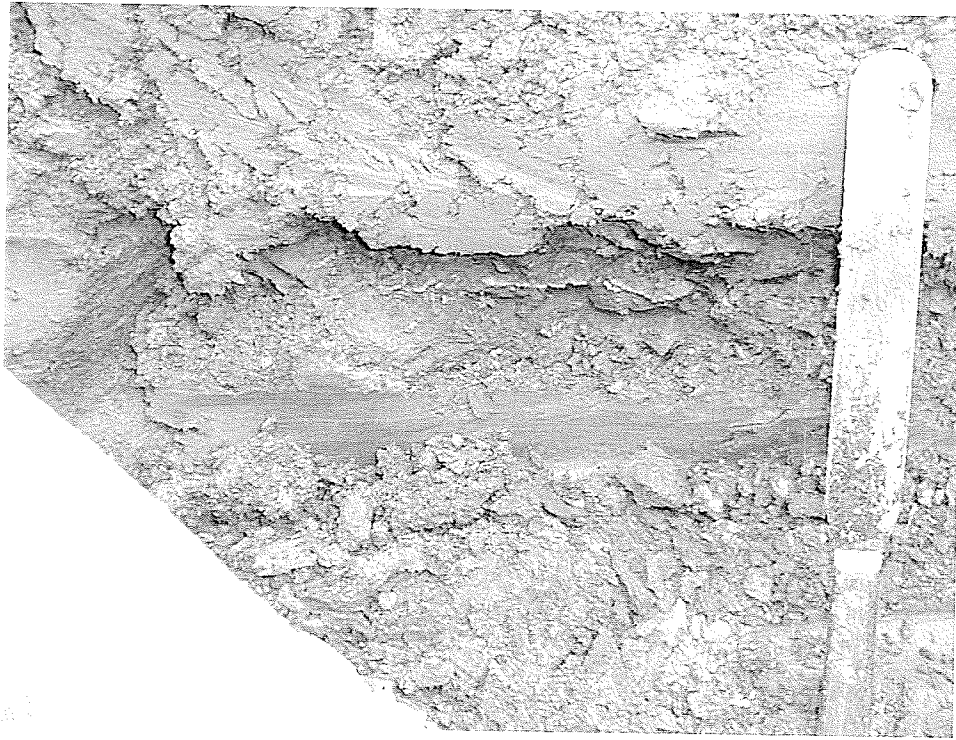


Figure 4.15 Possible failure surface on west wall of Test pit 2.



Figure 4.16 Possible failure on east wall of Test pit 2.

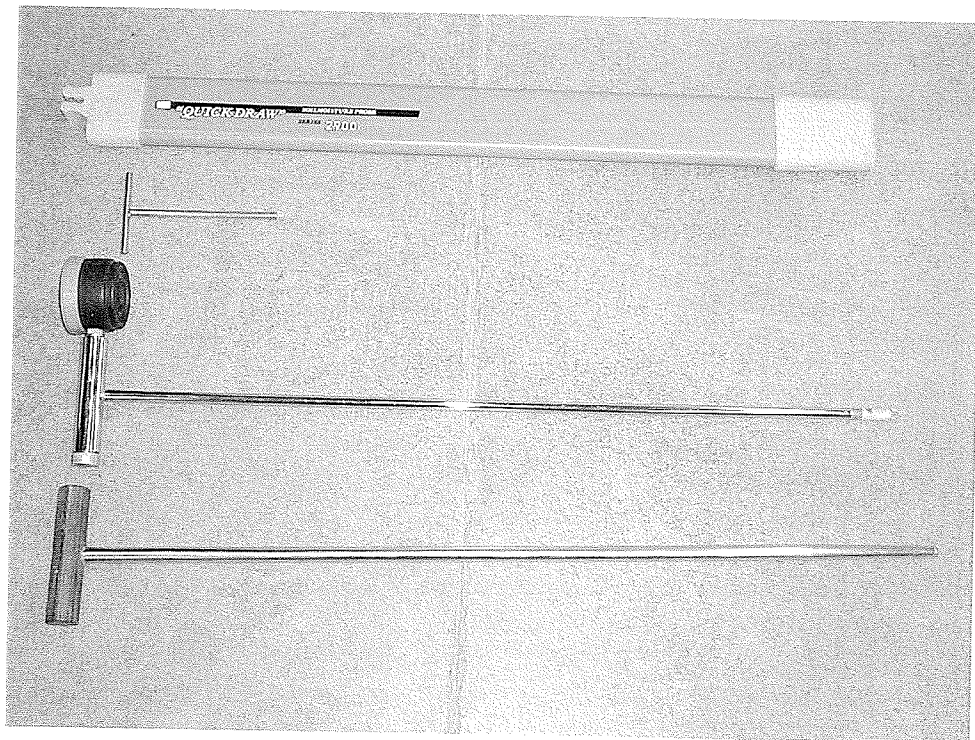


Figure 4.17 Tensiometer from Soilmoisture Inc..

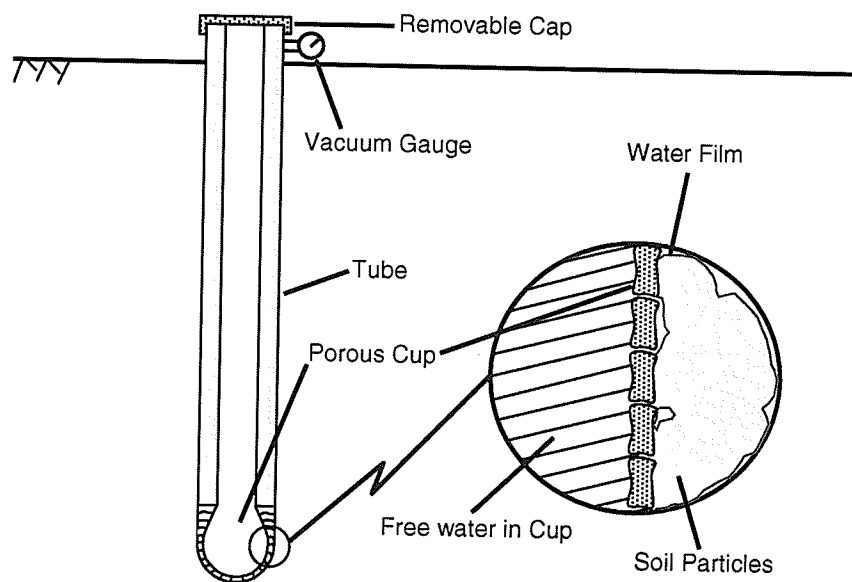


Figure 4.18 Tensiometer schematic.

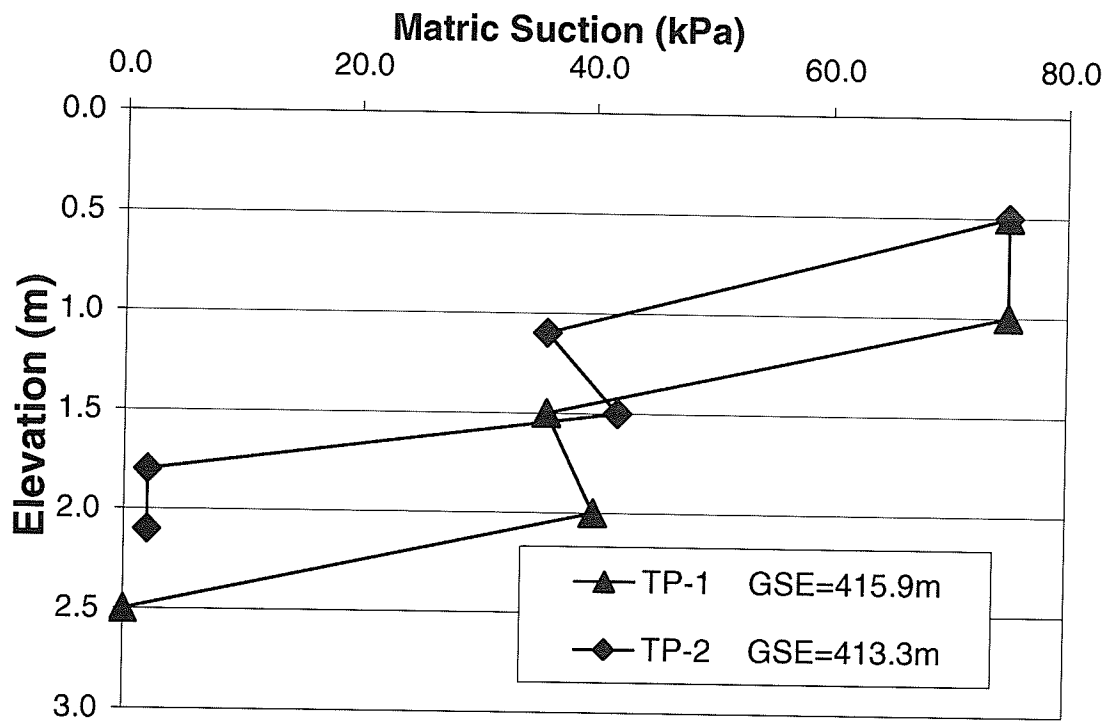


Figure 4.19 Variation of matric suction with depth.

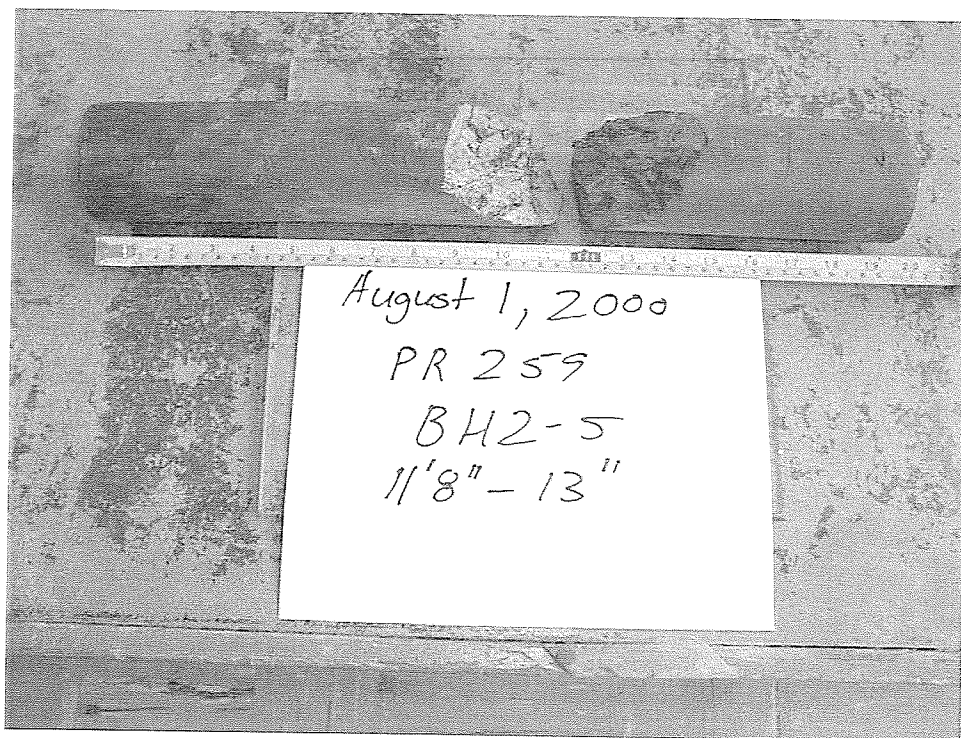


Figure 4.20 BH-2-5 - fracture at a depth of 3.71 metres below ground surface.

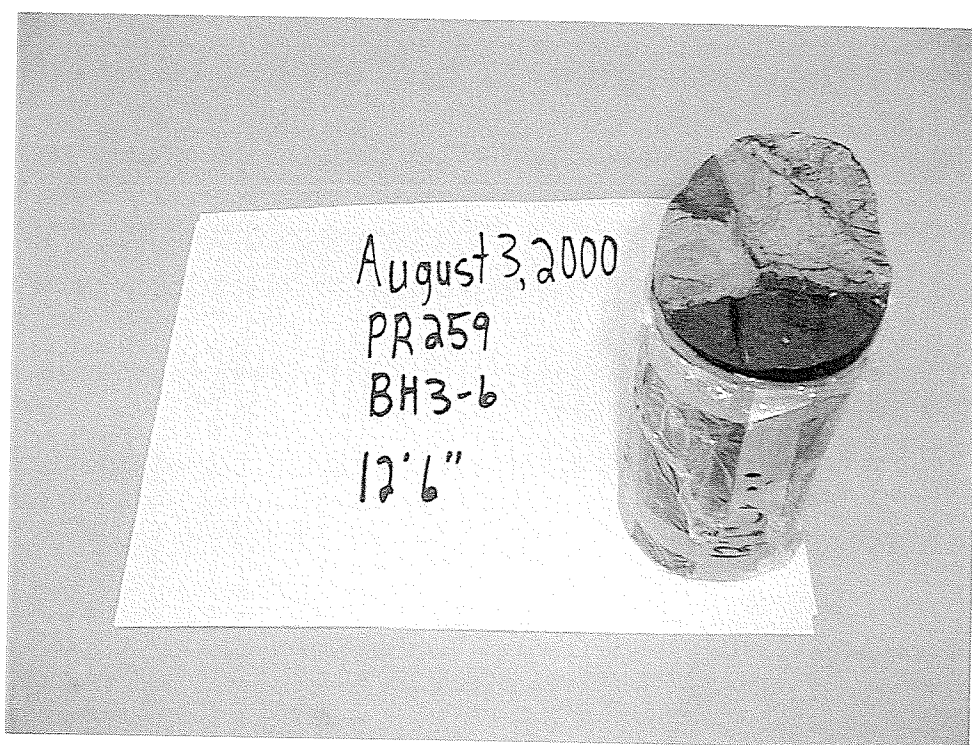


Figure 4.21 BH-3-6 – slickensided fracture at a depth of 3.81 metres.

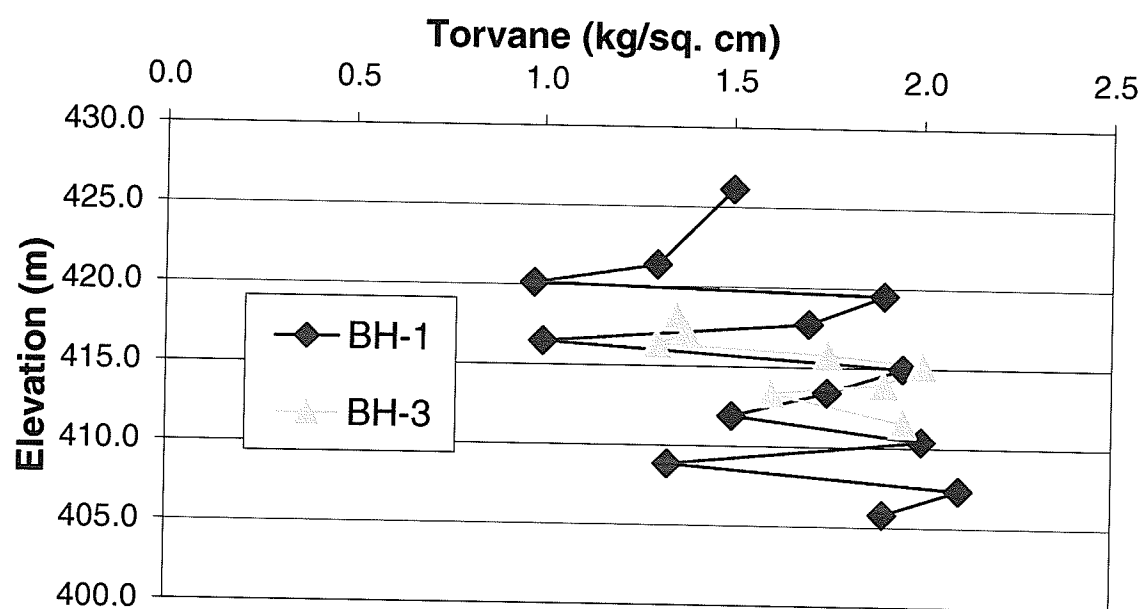


Figure 4.22 Undrained shear strength *versus* depth using Torvane.

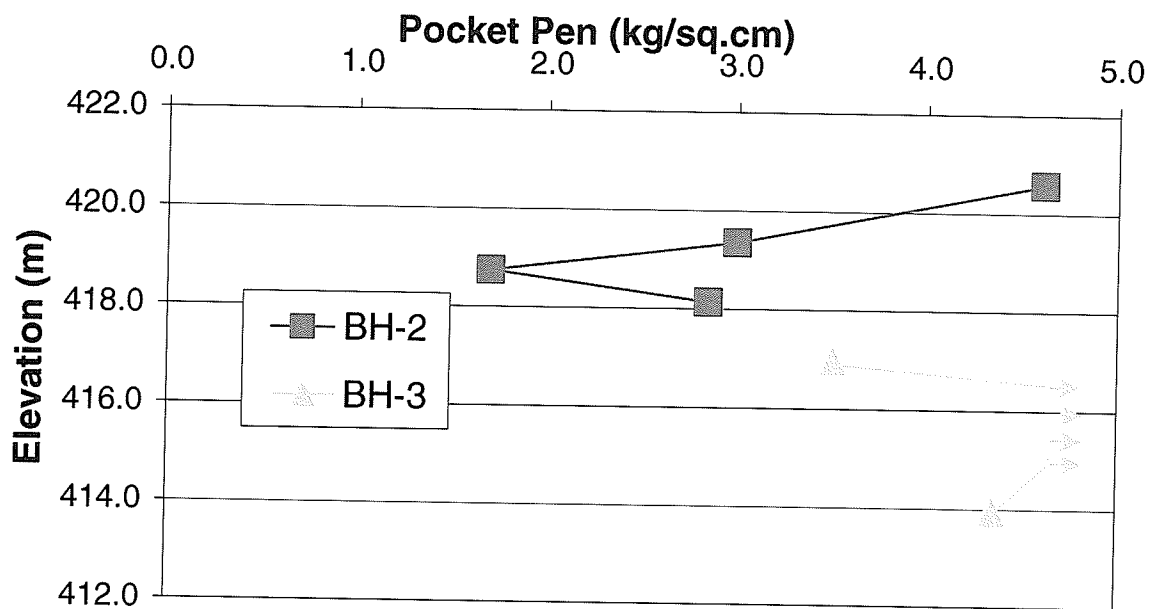


Figure 4.23 Undrained shear strength *versus* depth using Pocket penetrometer.

Chapter 5

Laboratory Testing

5.0 Introduction

The laboratory testing component of the project consisted of traditional soil classification tests, flexible wall permeameter tests, triaxial tests, and direct shear tests to determine parameters required for numerical modeling.

5.1 Soil Classification

In total, over 30 classification tests were performed on material retrieved during the field investigation. Tests included Atterberg limits, average specific gravity, hydrometer, and sieve analysis. In addition, water contents were taken for most of the soil samples.

5.1.1 Atterberg Limits and Moisture Contents

Atterberg limits (ASTM D 4318) classify the behaviour of a soil based on index properties termed the plastic and liquid limit. Atterberg limits do not give a direct measurement of strength or compressibility. They are however useful as an indicator of soil behaviour and the associated strength and compressibility. The best way to classify soil is to plot the Atterberg limits on a plasticity index *versus* liquid limit plot referred to as the Plasticity Chart (Figure 5.01). Soil from the study area ranges from low plastic to high plastic clay (Figure 5.01) with a few medium to high plastic silts/organics samples lying below the A-line. Most of the samples classified within the medium plastic clay range.

Moisture contents ranged from 20 - 40 % for almost all samples retrieved from the study area. Referring to the borehole logs (Appendix D) the moisture contents are at, near or just below the plastic limit producing in general very stiff material. The majority of liquid limits ranged between 50 - 60 %, while the majority of plastic limits ranged between 18 - 30%. The plasticity index, which is simply the difference between the plastic and liquid limits, ranged between 20 - 40 % for the majority of the samples, representing intermediate plasticity.

5.1.2 Specific Gravity

A total of eleven specific gravity tests (ASTM D 854) were performed on specimens retrieved from BH-1, BH-2, BH-3. The specific gravities ranged from 2.69 to 2.74 with an average specific gravity of 2.70.

5.1.3 Grain Size Determination

The grain size distribution of a soil is another tool geotechnical engineers use to classify soils and predict their behaviour. Determining the grain size distribution involves two independent testing methods for fine and coarse fractions. The first method is referred to as mechanical sieve analysis (ASTM D 422). The sieve analysis determines the percent distribution of coarse particles from fine sand to cobbles using specified sieve size intervals. The finer particle size distribution is determined by a hydrometer test (ASTM D 422). The hydrometer tests determine the percent distribution of finer soil particles. The two sets of percent distributions are combined into a total grain size distribution. Once the grain size distribution is known it can be used to verify and alter the field descriptions of the soil interpreted by field personnel.

In total, 34 grain size distributions were performed on soil retrieved from the study area. The grain size distributions were used to verify the field classification completed during drilling and were used to determine the AEV for the soil

(Section 2.3.2). The grain size distributions verified that the site was heterogeneous and was predominantly a “till-like soil”. The till-like soil grain size distribution is especially evident in BH-2 (Figure 5.02, Appendix E: Grain Size Distribution).

5.2 Flexible Wall Permeameter Tests

Since the influence of rainfall infiltration combined with groundwater fluctuations was considered a key relationship for analyzing the instability of these slopes, hydraulic conductivity of the material was measured using six flexible wall permeameter tests (ASTM D50 84 –90). Tests on samples from shallow depths of 1.7 metres to 4.4 metres produced results ranging from 5.6×10^{-10} m/sec to 3.7×10^{-11} m/sec.

Hydraulic conductivity of this low magnitude would not facilitate rainfall infiltration. The hydraulic conductivity results represent the permeability of intact specimens under imposed stress conditions (confinement) necessary to run the test. As discussed in the previous chapter, to an approximate depth of 2.5 metres the soil profile consists of a blocky/friable structure with, at several locations, fractures and fissures. This structure suggests a weathered zone due to frost action and drying/wetting cycles that would produce a higher bulk permeability allowing increased infiltration consistent with a suction dissipation mechanism. Several authors have studied the effect of weathering on intact samples. Shaw and Henry (1998) compared field and laboratory permeability results in oxidized (weathered)

and unoxidized clay till. Their field slug test results on unoxidized clay till were in the magnitude of 5.4×10^{-11} m/s, which correlated with their laboratory results of 2.7×10^{-11} m/s. As for the oxidized clay till, the permeability results were substantially different from slug results on the unoxidized clay till. The slug tests on the oxidized till, produced hydraulic conductivities between 6.5×10^{-9} to 1.3×10^{-8} m/s. That is a permeability increase between 160 and 320 times. Viklander (1998) subjected till specimens to 10-18 freeze-thaw cycle in a laboratory environment increasing the permeability close to two fold. The limited amount of freeze-thaw cycles resulted in a small change in permeability. Both of the papers showed significant increases in permeability in clay till due to weathering and freeze/thaw cycles.

5.3 CI \bar{U} Triaxial Tests

In total, seven isotropically consolidated undrained triaxial compression tests with pore water pressure measurement (CI \bar{U} tests) were performed on Shelby-tube samples from BH-2 and BH-3. In addition to the seven CI \bar{U} tests, two drained triaxial tests were performed on specimens retrieved from BH-2.

Testing procedures followed ASTM D 4767. Due to the shallow nature of the slides, relatively low effective stresses of 70, 130, 150, 190 kPa were selected for the confining pressures. The specimens were 71.1 mm in diameter which corresponded to the diameter of the Shelby tubes. As a result of the stiffness and

gravel content in most of the samples, trimming to a smaller diameter for testing was avoided. Lengths (heights) of the specimens ranged from 108 to 128 mm. Figure 5.03 shows well-developed conjugate failure planes in specimen BH-3-8 following shearing.

The stress-strain behaviour of the soil retrieved from the study area was, for almost all the samples, non-linear in nature. Figure 5.04 shows deviator stress *versus* axial strain plots for all the triaxial specimens tested, including the two drained tests. All peak strengths of the undrained samples leveled off before 4% axial strain, with a limited number of specimens exhibiting a small amount of strain hardening. Figure 5.05 shows the deviator stress *versus* mean stress behaviour for all triaxial tested specimens with the circles identifying the test end points. All of the undrained triaxial samples exhibited anisotropic elastic behaviour visually evident through the non-vertical stress paths in q, p' space.

All results for the 'critical state' (normally consolidated) strengths of the $CI\bar{U}$ specimens produced ϕ' values that deviated widely by ± 8 degrees over a 150 kPa range of confining pressure. A linear best-fit line produced $\phi'_{nc} = 22.3^\circ$ assuming $c'_{nc} = 0$ (cohesion was close to zero when the interpreted failure envelope was not forced through the origin, Figure 5.06). Five of the seven specimens showed results that were within two degrees of the best-fit line. The ϕ'_{nc} parameter was chosen due to the blocky structure of the material. Rivard and Lu (1978) demonstrated that the ϕ'_{nc} more appropriately defines the shear

strength at the Shellmouth Dam upstream of the study area along the Assiniboine River, as opposed to ϕ'_{oc} . An average value of ϕ'_{nc} was selected since the material itself is highly heterogeneous and failures can be expected to develop when 'averaged' shearing resistance has been generated.

5.4 Direct Shear Tests

To verify the triaxial test results, seven direct shear tests were performed on samples retrieved from the study area. Six specimens were trimmed from samples extracted from Shelby tubes from BH-2 and BH-3, while the remaining specimen was trimmed from one of the block samples retrieved from Test pit 1.

Trimming a block sample into a useable, undisturbed direct shear sample was very difficult due to the blocky/friable nature of the material and the awkward size of the block sample. A diamond bladed table saw that is usually used to cut concrete was used to cut the block sample since the sample contained some gravel size particles. The block sample was first tightly wrapped in duct tape to add confinement prior to cutting. This confinement reduced the amount of disturbance to the sample during cutting. However, even with the confinement, the sample was subjected to a substantial amount of disturbance. After cutting the sample into a workable size, it was placed in a hydraulic press apparatus where the direct shear cutting shoe was inserted into the workable sample. In the end, the test pit specimen results did not compare well with the direct shear

results from the borehole samples. The difference between the two sets of results could not be distinguished between sample disturbance or material differences. The lack of confidence in material differences lead to the results from the block sample being discarded due to sample disturbance.

The direct shear testing procedure followed ASTM D 3080. The samples were tested at vertical pressures that partially overlapped the lower range of confining pressures used in the triaxial tests. This was done to extend and verify shear strength parameters determined in the triaxial test results. The vertical stresses used in the direct shear tests are as follows; 30 kPa, 60 kPa, and 90 kPa. As with the samples used in the triaxial test apparatus, the direct shear samples were only slightly trimmed. The specimens were 70.9 mm in diameter, which is 0.2 mm smaller than the diameter of the Shelby tubes. The small amount of trimming was required in order to produced a circular specimen required for a snug fit in the shear box. The average height of the direct shear samples used was 28.3 mm.

The six samples retrieved from BH-2 and BH-3 correlated well with the triaxial results. Figure 5.07 shows results for residual strength envelopes. The first best-fit envelope with a slope of 0.48 is for all six tests. It is clear that one of the 90 kPa normal stress points can be considered an outlier. When this is neglected, a best-fit envelope with a slope of 0.38 is obtained based on the remaining five pertinent points. The two shear strength envelopes correspond to internal residual friction angle (ϕ_r) of 25.7°, and 20.9° respectively. The second shear

strength envelope is comparable to the shear strength results from the triaxial tests of $\phi'_{nc} = 22.3^\circ$ adding further confidence to the results from the triaxial test program.

Plasticity Chart (Unified Soil Classification System)

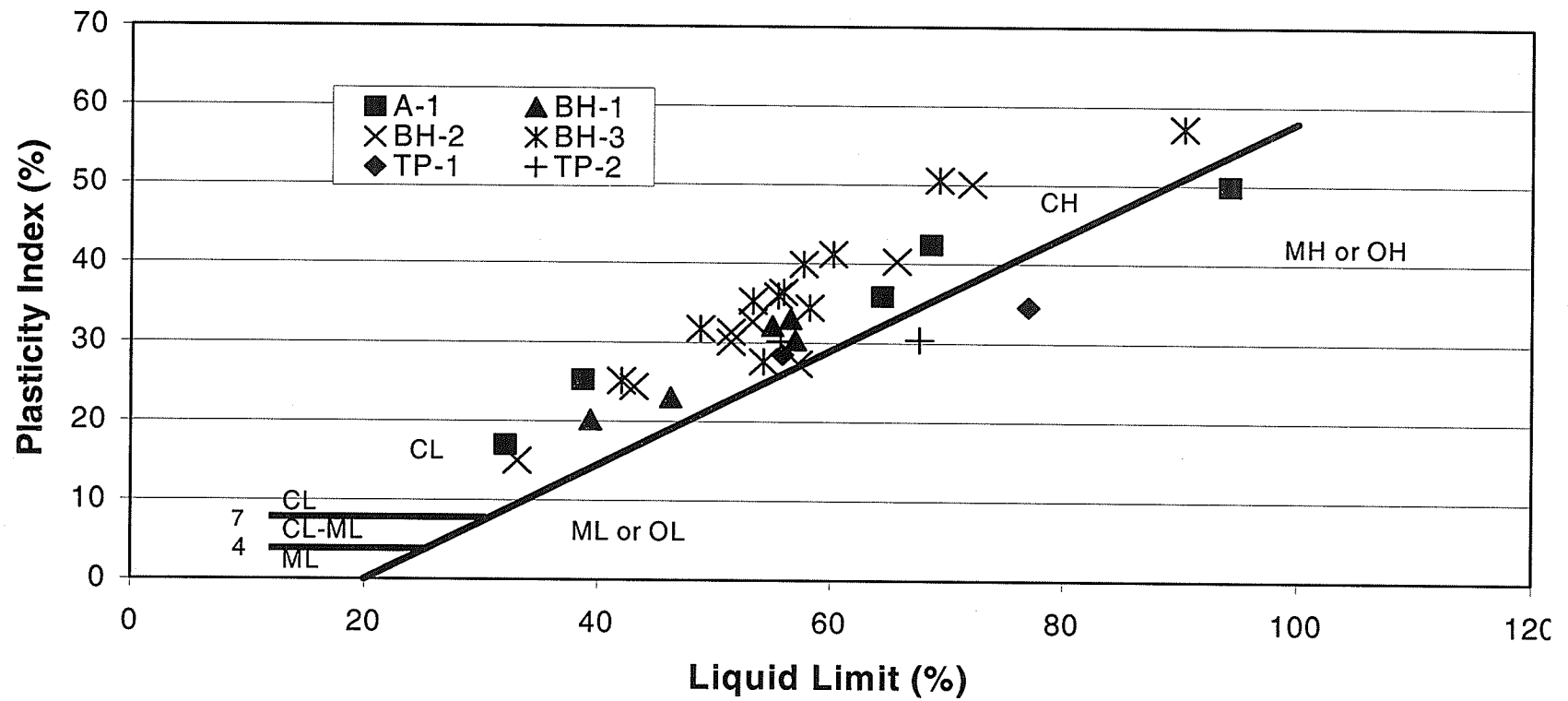


Figure 5.01 Plasticity chart for material retrieved from the study area.

Project: PR259
Sample: BH-2-2(2) Depth:1.96 - 2.13 m
Date: April 18, 2001

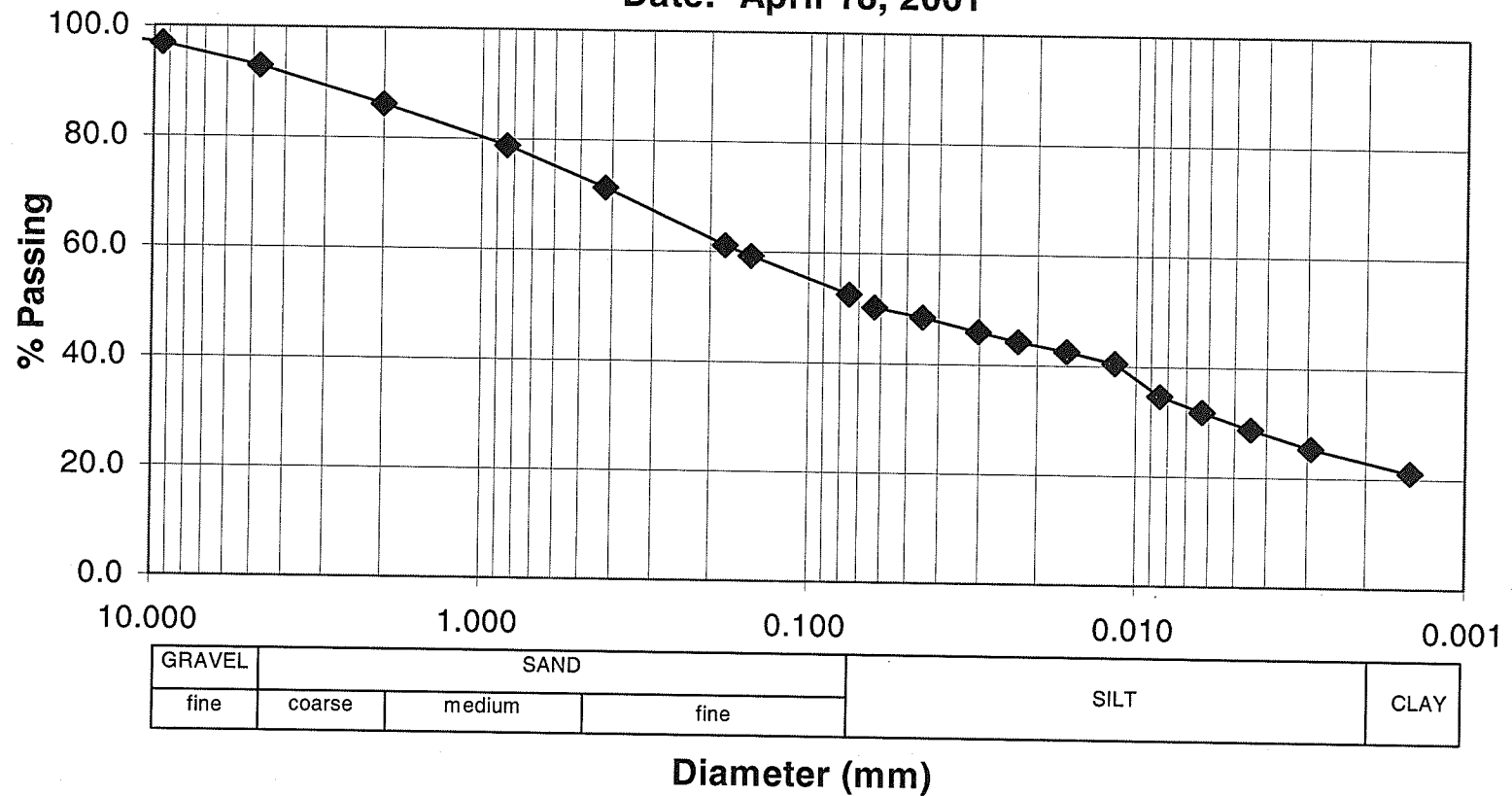


Figure 5.02 Grain size distribution of "till-like soil".

PR 259
BH-3-8
Depth: 4.57 –4.70

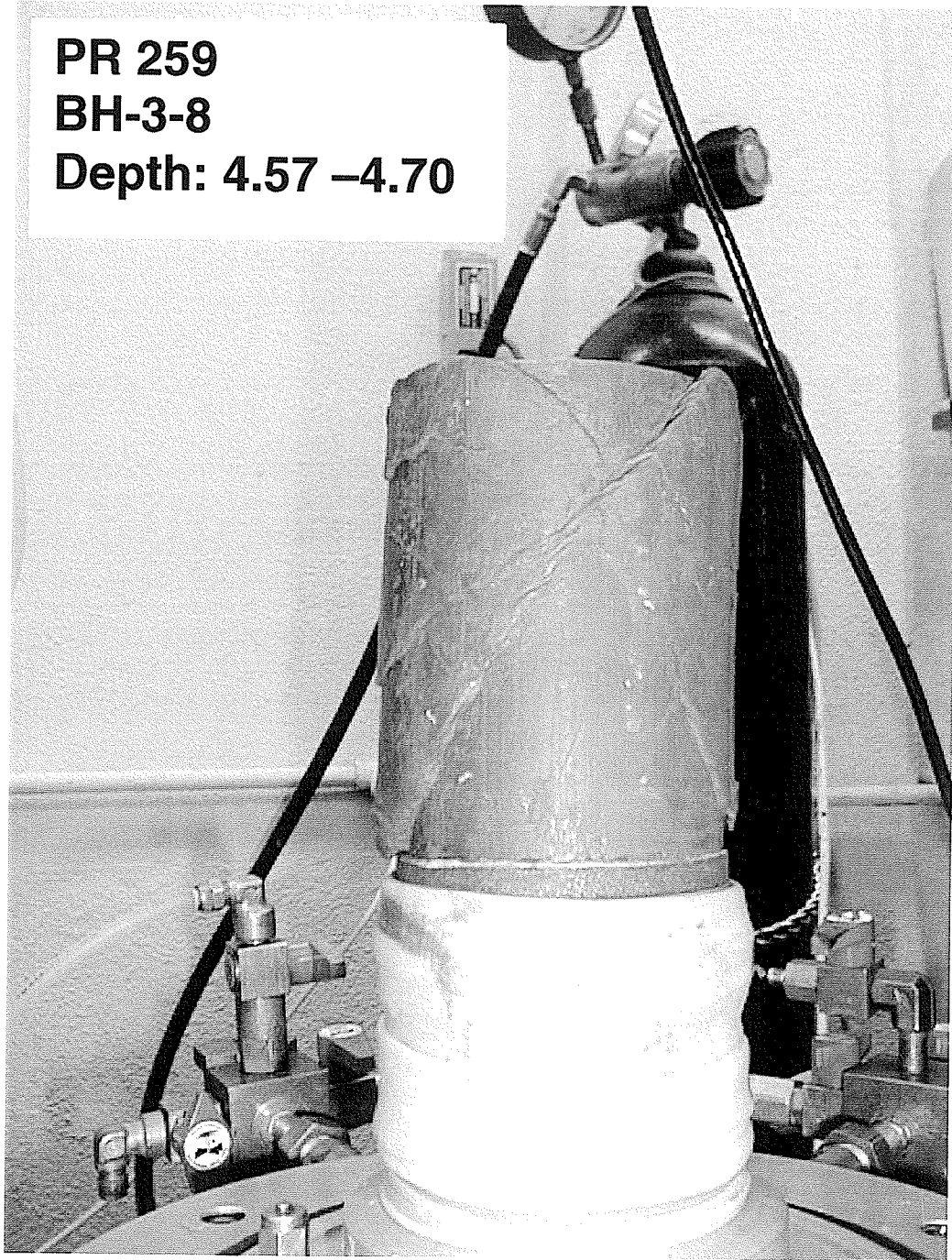


Figure 5.03 A example of a failure plane developed under undrained triaxial conditions.

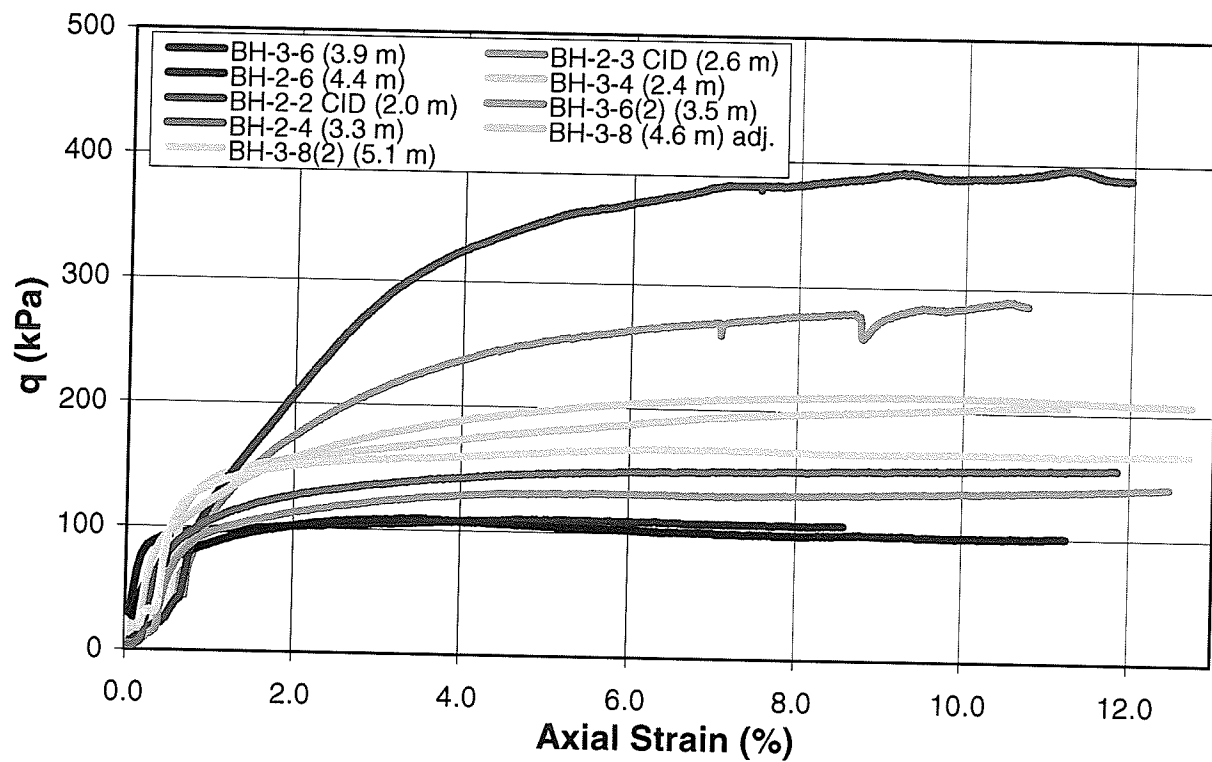


Figure 5.04 Stress-strain results for all triaxial specimens.

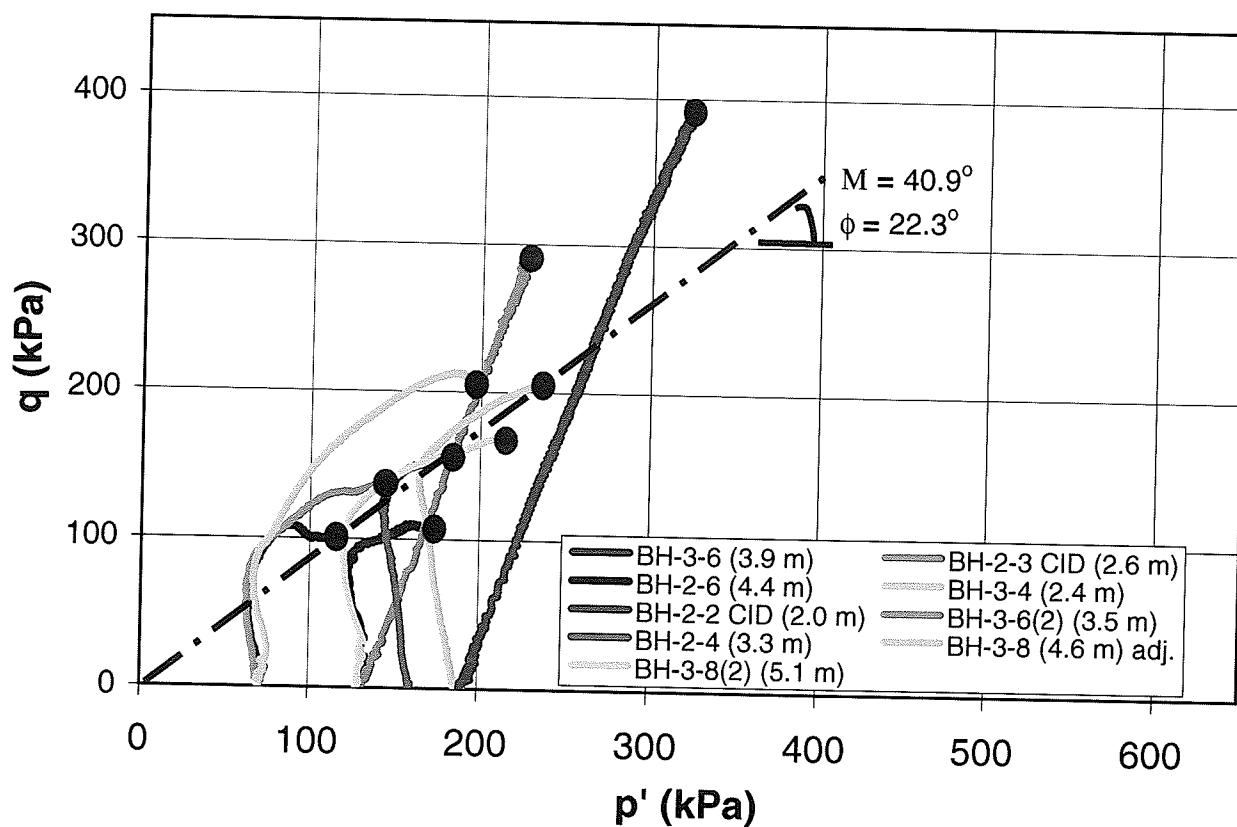


Figure 5.05 Deviator stress *versus* confining stress for all triaxial specimens.

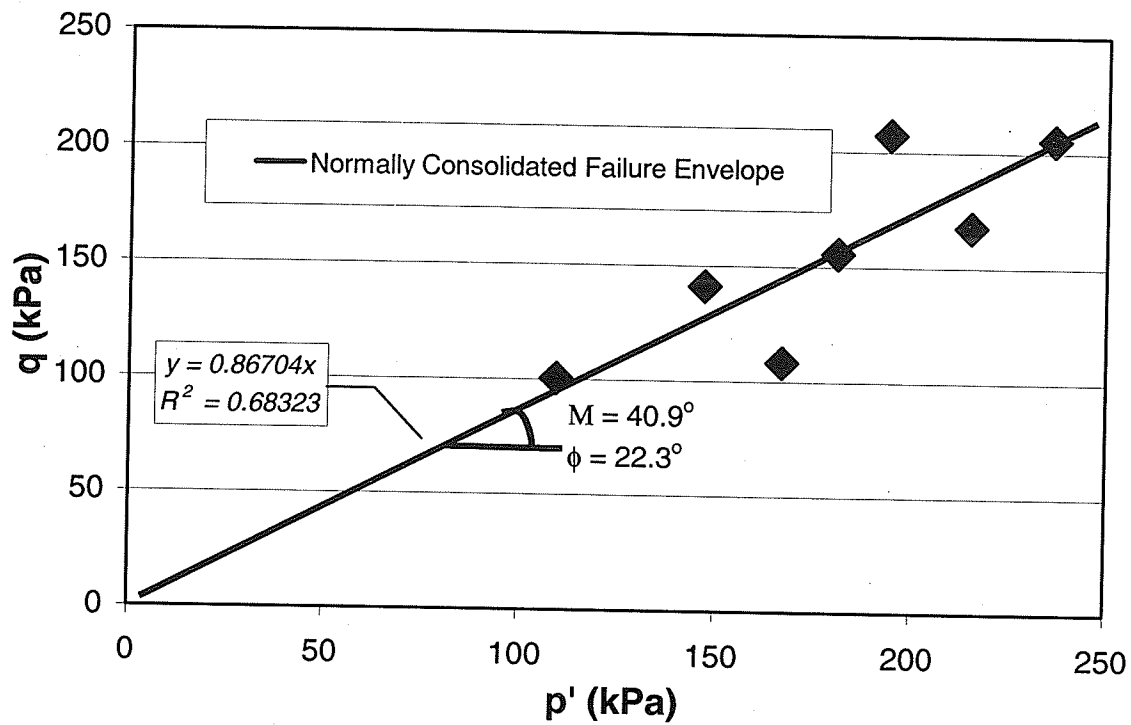


Figure 5.06 Normally consolidated failure envelope from triaxial tests.

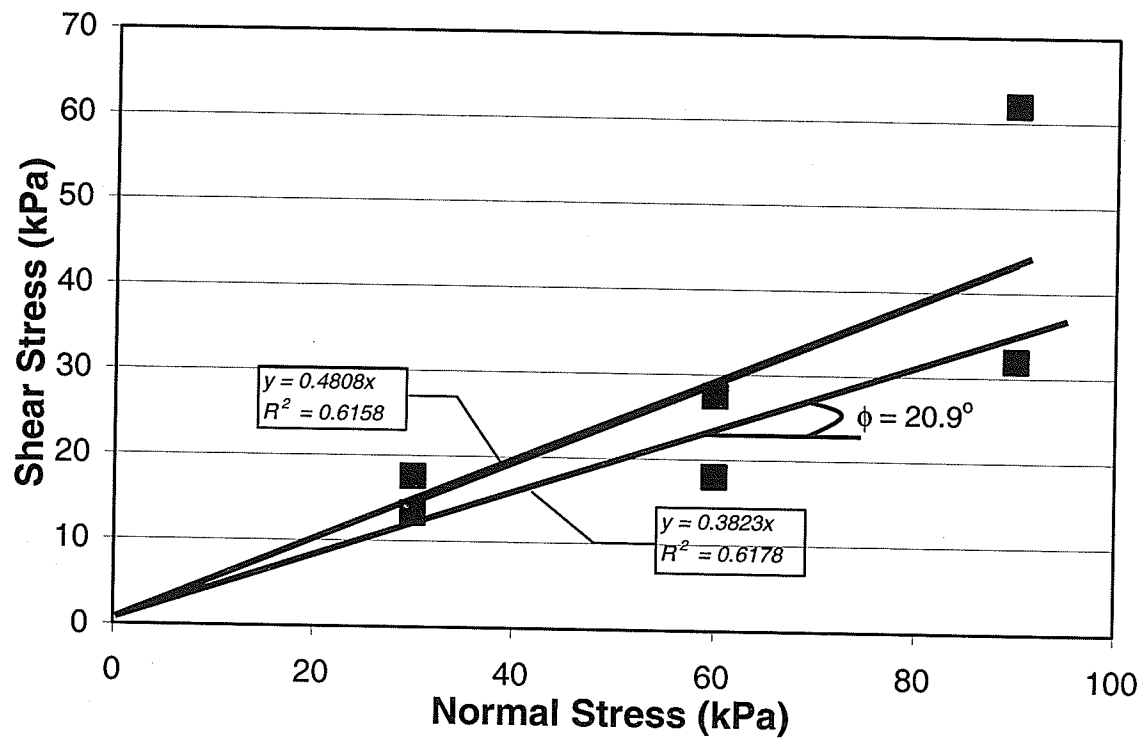


Figure 5.07 Residual failure envelope from direct shear tests.

Chapter 6

Integrated Seepage and Slope Stability Modeling

6.0 Introduction

Integrated seepage and limit equilibrium slope stability analyses were used to model the failures at PR 259 using the results of the field and laboratory investigations. The modeling was performed using the Seep/W and Slope/W products from GeoSlope International (Calgary, AB). The modeling included a preliminary analysis using steady-state conditions. The preliminary study used one soil type with averaged soil properties. The analysis was later extended to a more detailed and representative transient analysis, an approach which is believed to be unique in Manitoba and forms the principal original component of this thesis document. The transient model incorporated four soil types and associated soil properties. Due to the heterogeneity of the site, most parameters used in the integrated transient analyses were averaged within a soil type for simplicity.

6.1 Preliminary Integrated Model

Preliminary analysis was performed to better understand the mechanisms and soil/water conditions affecting stability and to ensure that the complexity of the model was within the limits of the author's understanding of the problem. The preliminary analysis provided evidence that the dissipation of soil suction due to a rainfall infiltration was most likely the mechanism that triggered failure. The results were sufficiently interesting that they were presented to the 54th Canadian Geotechnical Conference in Calgary in 2001 (Ferreira *et al.* 2001).

With a better understanding of the site/water conditions and the behaviour of the slope, a detailed transient model was then constructed to further confirm the results from the preliminary analysis and verify the postulated failure mechanism.

6.1.1 Seep/W Modeling

The geometry used in the preliminary Seep/W analysis was taken from the measured cross-section E-E in Figure 4.06. The element size in Seep/W was generally 1 m² or smaller. Figure 6.01 illustrates the finite element mesh for the Seep/W analysis. From the laboratory tests, an average hydraulic conductivity of $K = 2.1 \times 10^{-10}$ m/s was used for the conductivity function when pore water pressures were positive (higher than atmospheric). When pore water pressures were negative (lower than atmospheric), the hydraulic conductivity was reduced

by two orders of magnitude over a suction range of 0.5 kPa. The boundary conditions included a 'no flow' boundary along the bottom of the domain, two constant head boundaries at the left boundary and right boundary of the domain, and one variable flux boundary reviewed by elevation along the slope face. The variable flux boundary was incorporated into the model to allow water to exit the domain along the slope face as required. Three seepage cases were analyzed. Each case involved different assumptions regarding the head boundary condition at the left side of the model. The head boundary condition at the toe of the slope beside the highway ditch was held constant.

The first case (Case 1) modeled the groundwater conditions during a three-month period from August 2000 to October 2000 when water levels had been measured in the field. A head condition at the left boundary (crest of the slope) of 423.5 metres above sea level produced model results that were close to the measured water levels (Table 6.01). The other two cases simply increased the head condition on the left boundary by 0.75 metres and 1.5 metres respectively. These three cases were chosen to bracket physically representative groundwater conditions during the normal operating condition of the slope. All three cases were modeled assuming steady-state flow conditions.

6.1.2 Slope/W Modeling

Results from the preliminary Seep/W modeling were imported into Slope/W using the same geometry (Figure 6.02). The data file of heads computed by Seep/W was used by Slope/W to calculate pore water pressures at the base of each of the slices in the limit equilibrium analysis. The parameters used in Slope/W were averaged values from laboratory results; $c'_{nc} = 0$, $\phi'_{nc} = 22^\circ$, and $\gamma_{bulk} = 19.6 \text{ kN/m}^3$. When incorporating suction, ϕ^b (the material parameter that describes the increase in strength with suction) was taken as $0.5 \times \phi'_{nc}$ as a lower limit. This assumption will produce conservative results (lower contributions) for suction less than the air entry value. Vanapalli *et al.* (1996) suggested that $\phi^b = \phi'$ up to air entry (Vanapalli *et al.* 1996). The upper limit for the slope stability analysis used $\phi^b = \phi'$. The Morgenstern-Price method (1965) was used in the stability analysis with a constant interslice force inclination function ($\theta = \text{constant}$, which gives Spencer's solution 1967).

For modeling, a fully-specified slip surface was defined based on information gathered from the field regarding the position and shape of the observed failure surface (Figure 6.02). The location of the slip surface was known from BH-1 and BH-2, but less obvious in BH-3 due to numerous fracture surfaces that were observed (Figure 6.02, Appendix D: Borehole Logs). For the fully-specified failure surface, the position of the toe of the failure was determined using aerial photographs, which showed toe movements just above the highway ditch (Figure

3.04). Since the failure was shallow, the centre of rotation for the Slope/W model was located far away from the slope face to produce stable, numerically-accurate results.

For each of the three groundwater conditions mentioned in section 6.1.1, three additional suction conditions were incorporated into the model; 1) suctions measured by tensiometer (Figure 4.19), 2) suctions calculated by Seep/W, and 3) a 'no-suction' condition. These suction distributions are illustrated in Figure 6.03.

In order to incorporate tensiometer suctions into the model, the authors made adjustments to the Seep/W output head file (This is also an original contribution to slope analysis in Manitoba.). The preliminary Seep/W model produced results that were lower than the measured suction values due to the lack of a defined flux boundary along the slope (Wilson *et al.* 1994). A macro was set up using Visual Basic to adjust all suction values at nodal points in the unsaturated zone by a scale factor. Suction values for nodes more than 2 metres above the water table were limited to 80 kPa based on measurements taken at the site (Figure 6.03). The final suction profile for all three cases are shown in Figure 6.03.

6.1.3 Results from the Preliminary Model

The preliminary integrated Seep/W and Slope/W modeling produced results showing the impact of matric suction on factor of safety. Results from the integrated Seep/W and Slope/W model are summarized in Table 6.02.

Results in Table 6.02 with $\phi^b = 0.5 \times \phi'_{nc}$ for measured water conditions (Case1) show that the factor of safety is greater than unity for all three suction profiles examined. As the groundwater elevation is increased (Case 2 and Case 3) the factor of safety decreases as expected. A value of unity, that is, a prediction that failure will occur, was calculated for the case where the groundwater elevation was 425.0 metres at the left boundary of the model and suction was taken as zero above the water table. At this groundwater level, incorporating the suction profile generated by Seep/W provided a 4 % increase in the safety factor. Using the measured suction profile increased the factor of safety by 16 %. In the case incorporating the measured matric suction profile, the suction component showed stable conditions for the specified hydraulic boundary conditions representing typical operating conditions for the slope. In other words, according to the model, the slope would have failed in the past had it not been for the suction contribution to strength in the unsaturated zone. When the slope was analyzed for $\phi^b = \phi'_{nc}$ the increase in factor of safety was roughly twice as much as for the $\phi^b = 0.5 \times \phi'_{nc}$ case. A fully saturated case with groundwater level coincident with the ground profile was performed and compared to hand calculated results for an

infinite slope analysis. Both cases produced safety factors of approximately 0.75. These results mean that the slope cannot be stable with phreatic surfaces at the ground surface.

Results from the integrated model showed that during dry conditions, the highway cut was stable. During wet conditions, the slope could also remain stable but only with the stabilizing contribution of matric suction. The slope angle ($\sim 17^\circ$) is close to the friction angle of the material (22°) and requires cohesive strength during wet periods to remain stable. The preliminary models demonstrate that during typical wet conditions, suction in the unsaturated zone contributes significantly to the stability of the slope. This preliminary analysis determined that matric suction significantly contributes to the stability of the highway cut. In order to verify that failure was triggered by a dissipation of suction, the model needed to be improved to demonstrate that the actual measured rainfall would in fact reduce suctions to zero.

6.2 Integrated Transient Model

The transient analysis was undertaken to extend the understanding of the failure mechanism determined in the preliminary analysis by determining if the rainfall from 1999 would cause dissipation of soil suction. This model was targeted to improve the understanding of the influence of rainfall duration and intensity in terms of dissipation of soil suction. Results of the time-dependent analysis show

how the characteristics of the environmental flux boundary condition contribute to the rate and magnitude of suction dissipation.

6.2.1 Transient Seepage Analysis

An integrated transient seepage analysis was constructed and calibrated to best represent the soil/water conditions that existed *in-situ*. After calibration, using the water levels from April 1 to November 1 for both 1998, and 1999 and the measured suction profiles, the results were incorporated into the stability analysis. The results for both years and the calibration year (2000) were incorporated into Slope/W to evaluate the stability of the highway cut during these times.

6.2.1.1 Construction of Seep/W Transient Model

The transient Seep/W model included four soil layers interpreted from the field logs and laboratory specimens. The domain of the detailed Seep/W model is shown in Figure 6.04. The layers are as follows in descending order from the slope face down; a weathered clay layer, a water bearing silty fine sand seam, an unweathered intact clay layer, and a silt/sand layer. As with the preliminary model, the transient model used a cross-section through the location of the boreholes (Figure 4.01, Cross-section E-E). The finite element size was generally 1 m² or smaller. To satisfy compatibility, triangle and squares (or close

to squares) were used for the element geometry. The finite element mesh used in the transient Seep/W model is illustrated in Figure 6.05.

The weathered clay layer was incorporated into the transient analysis because of the blocky/friable nature of the upper soil material. The thickness of the weathered zone is consistently three metres in depth along the weathered-unweathered clay interface. The weathered-unweathered interface occurs below the silty fine sand seam approximately mid-way up the slope to the highway pavement edge (Figure 6.04). From the toe of the slope to the highway pavement, no clay was encountered during the field investigation (BH-4). Since the two slope movements occurred above the toe, the effect of a clay layer beyond the toe is negligible and is only included in the model for completeness. A weathered zone to a depth of three metres is consistent with the blocky/friable nature observed in soil samples and the potential depth of frost action and drying/wetting in Manitoba. From the crest of the slope to above the day-lighting silty fine sand seam, the weathered clay layer is equal to the difference between the elevation of the slope face and the location of the top of the silty fine sand seam. It is suspected that water flowing laterally through the silty fine sand seam weathered the above clay layer from below creating a weathered zone deeper than the potential depth of frost action.

The location of the water bearing silty fine sand seam was determined from field observation made in BH-1, BH-2, A-5, A-4, A-1 (Appendix E: Grain Size

Distributions, BH-2-7). Standpipes installed in BH-2, A-4, and A-1 all produced water. Hand augured holes A-1 and A-4 were not drilled within cross-section E-E. A-1 was drilled approximately 13 metres along the slope from BH-3 (Cross-section F-F, Figure 4.01, Appendix D: Borehole Logs). Both BH-3 and A-1 were drilled on top of the reworked West Failure bench (Cross-section E-E, Figure 4.01, Appendix D: Borehole Logs). The soil profile in BH-3 showed no evidence of a sand seam, while A-1's soil profile included a water bearing silty fine sand seam. This discrepancy could not be correlated to natural *in-situ* heterogeneity or the fact that significant activity and soil movement had occurred in the vicinity of the two holes during construction of the stabilizing bench. Given that the location of the silty fine sand seam corresponded reasonably well with BH-2 and A-5, the silty fine sand seam was included at the location of BH-3. Reinforcing this assumption is the fact that during the preliminary field investigation, the stabilizing bench was fully saturated with surficial water. Saturating the stabilizing bench to this degree would only be feasible by a near surface, high permeability soil and not medium plastic clay soil as observed in BH-3.

Hand augured hole A-4 (Cross-section F-F, Figure 4.01) was drilled approximately 13 metres along slope from A-5 and included a piezometer installation that produced water. The soil profile at A-4, below two metres to the end of hole, consisted of silty clay with a significant amount of fine sand. Since the hand augured hole A-5 was terminated prematurely due to a cobble/boulder before a possible water table could be reached, water levels measured in A-4

were assumed to be the same at A-5. Water levels at A-4 could be assumed to be the same at A-5 because the hydraulic conductivity of the silty clay with fine sand determined from field slug tests was within the same magnitude as slug test results from BH-2. Having similar hydraulic conductivities would result in relatively similar phreatic surfaces.

In BH-1, the silty fine sand seam was first observed at three metres depth and was slightly over 1.75 metres thick. Figure 6.06 is a photograph of the silty fine sand seam taken after the West Failure re-failed in early July 2001. At the other borehole and hand augured hole locations, the thickness of the silty fine sand seam could not be determined as the boreholes and hand augured holes terminated within the silty fine sand seam. A thickness of 1.75 metres for the silty fine sand seam was used for the transient model. The silty fine sand seam between BH-2 and A-1 was for the most part horizontal. In the transient Seep/W model, the sand seam was assumed to be horizontal for simplicity. The sand seam was assumed to be inclined between BH-1 and 2.5 metres before BH-2 (Figure 6.04). The location where the inclination of the silty fine sand seam terminated was not known. Terminating the inclined sand segment at, or near BH-2 would have a significant impact on water levels measured at BH-2. The inclined portion of the silty fine sand seam was terminated a few metres before BH-2 because measured water levels at BH-2 were only slightly higher than water levels measured at A-4 suggesting little influence from the inclined segment of the silty fine sand seam.

In the transient model, the intact unweathered clay underlies the sand seam from the crest of the slope to approximately mid-slope. From mid-slope to the highway pavement edge, the intact unweathered clay underlies the weathered clay layer. Based on information gathered from BH-1, the intact clay layer terminates at a depth of 22 metres below the crest near the left boundary of the domain (Figure 6.04). The termination depth of the intact clay at the right hand boundary was determined from a field investigation performed by A. Dean Gould and Associates. Their report is included in Appendix F. Mr Gould's field investigation, particularly test hole 10, has the intact clay layer terminating at an elevation of 402.16 metres where a silty/sand layer begins. Test hole 10 was drilled at the toe of the slope, approximately 10 metres west of Cross-section F-F (Figure 4.01). The elevation of the bottom of the intact clay layer at the right boundary also corresponds to a water table observed by A. Dean Gould and Associates. Beneath the intact clay to the bottom of the domain, a silt/sand soil layer was observed in BH-1 and in A. Dean Gould and Associates test hole 10.

6.2.1.2 Soil Properties

For Seep/W to perform a transient analysis, the specified properties of each soil layer need to include a soil water characteristic curve (SWCC) and associated hydraulic conductivity function. The SWCC for all the soil types retrieved from the study area was determined using the modified Kovács method, while the associated hydraulic conductivity function was estimated using van Genuchten

method. Both of these methods were presented in detail in the literature review chapter, Chapter 2. The chosen SWCCs and hydraulic conductivity functions are presented in Figures 6.07, 6.08, and 6.09.

The nature of the material retrieved in the top two to three metres of the slope suggested a weathered and desiccated zone due to infiltration, root action, and freeze/thaw cycles. The upper three metres of soil warranted a separate soil layer to be included in the transient analysis to take these effects into account. The soil water characteristic curve and the hydraulic conductivity function used for the weathered soil layer were adjusted from laboratory results performed on intact, unweathered clay. The SWCC and hydraulic conductivity curves were shifted 70% from the reference point of the AEV to better represent the nature of the weathered material. The reduction resulted in an AEV just over 200 kPa consistent with a blocky/friable structure unable to maintain higher suctions. The saturated hydraulic conductivity was adjusted according to information published by two of the authors mentioned previously. Shaw and Hendry (1998) showed hydraulic conductivity differences in the magnitude of 160 to 320 times between oxidized (weathered) and unoxidized clay till, while Viklander (1998) increased the hydraulic conductivity on laboratory controlled clay till samples subjected to freeze/thaw cycles by a factor of almost two. The saturated conductivity of the weathered clay used in the transient Seep/W model, 1.84×10^{-4} m/day (2.13×10^{-9} m/s), was equal to ten times the average saturated hydraulic conductivity measured in the laboratory. Increasing the hydraulic conductivity ten fold was a

conservative adjustment based on evidence presented in the literature. Figure 6.07 is a plot of the SWCC for the weathered clay layer (modified Kovács method) and the corresponding hydraulic conductivity function (van Genuchten method).

The SWCC and the hydraulic conductivity function assigned to the silty fine sand seam layer have negligible impact on the solution since the sand seam was assumed to be continuously saturated and therefore would not use the non-linear portion of the SWCC function. The soil properties of sample BH-2-4 were used to calculate both the SWCC and hydraulic conductivity curve for the silty fine sand seam. The SWCC and hydraulic conductivity curves were shifted by 50% to reduce the AEV to one that was consistent with silty fine sand material. The saturated hydraulic conductivity was determined from slug tests performed on piezometers installed within the silty fine sand layers in BH-2 and A-4. An average saturated hydraulic conductivity of 5.69×10^{-2} m/day (6.59×10^{-7} m/s) was used in the detailed transient seepage model. Figure 6.08 is a plot of the SWCC (modified Kovács method) and the hydraulic conductivity function (van Genuchten method) for the silty fine sand seam.

The SWCC and hydraulic conductivity functions used for the unweathered clay layer were directly determined from grain size distributions of soil samples without any adjustments. The saturated hydraulic conductivity used in the detailed Seep/W model was an average of six laboratory flexible wall

permeameter tests and was 1.84×10^{-5} m/day (2.13×10^{-10} m/s). Soil properties determined from sample BH-3-7 were used in the modified Kovács method to calculate the SWCC for the unweathered clay. Figure 6.09 plots both the SWCC function and the hydraulic conductivity function used for the unweathered clay layer in the detailed transient analysis.

The silt/sand layer that underlies the intact unweathered clay has little to no effect on the near slope pore water pressure distributions or gradients that effect stability. This layer was included in the detailed analysis for completeness. The SWCC and hydraulic conductivity function were assigned to be equal to those used in the weathered clay layer.

6.2.1.3 Initial Boundary Conditions

The boundary conditions included a 'no flow' boundary along the bottom of the domain, and a 'no flow' boundary for the weathered clay layer, the intact unweathered clay layer, and the silt/sand layer at the left boundary (Figure 6.04). The left boundary was assigned a 'no flow' condition to be incorporated into the transient Seep/W model since the lateral flow in the low permeable layers would be negligible in contrast to the high permeability of the silty fine sand seam. Contrary to all other soils at the left boundary, a positive flux boundary condition was assigned to the silty fine sand seam at the left boundary. A positive flux boundary condition was incorporated into the detailed model to act as a

groundwater recharge into the silty fine sand seam since the seam is continuously saturated and expected to be draining areas behind the crest (Figure 6.04). The magnitude of the recharge was determined during calibration of the detailed model (Section: 6.2.1.4). The right boundary of the domain incorporated a constant head value of 402.16 metres based on observed water levels in test hole 10 from the A. Dean Gould and Associates report (Appendix F).

An environmental flux boundary reviewed by elevation was assigned to the slope face. This boundary condition represents the *in-situ* soil/water interaction. The environmental flux boundary function includes evapotranspiration during non-rainfall events and infiltration during rainfall events. The flux function was determined from rainfall and temperature data obtained from an Environment Canada weather station in Virden, Manitoba.

The magnitude of evapotranspiration for a vegetated area is difficult to calculate due to the complexity of the vegetation/soil/water interaction. Many factors will affect the magnitude of evapotranspiration such as vegetation type, vegetation density, humidity, temperature, wind speed, inclination of the sun (season), inclination of soil surface, soil type, and availability of groundwater. Penman (1948) stated that the rate of evapotranspiration from vegetated and bare soils is approximately equal to the rate of evaporation from a free water surface provided that the supply and availability of water to the surface is unlimited. Assuming that

the availability of water is unlimited for the study area, a simple mass transfer equation from a free water surface could be used to determine the evapotranspiration as a starting point prior to calibration. Meyer (1944) proposed a simple mass transfer equation for Minnesota lakes given below;

$$E = 0.0106(1 + 0.1u)(e_s - e_a) * 2.54 \quad \text{eq. 6.01}$$

where:

E = evaporation from free water surface, (cm/day)

u = wind speed, (mph)

e_s = saturated water vapour pressure, (mb)

e_a = actual water vapour pressure, (mb)

The saturated vapour pressure can be calculated using the following equation;

$$e_s = 2.7489 \times 10^8 \exp \left(- \frac{4278.6}{T_d + 242.79} \right) \quad \text{eq. 6.02}$$

where:

T_d = dew point temperature, ($^{\circ}\text{C}$)

The most common way to represent the magnitude of water vapour pressure in the atmosphere is by a ratio of water vapour pressure to saturated water vapour pressure referred to as Relative Humidity. The weather station at Virden,

Manitoba did not measure Relative Humidity or wind speed, two parameters needed to calculate evapotranspiration using the Meyer (1944) equation. For calculating the evapotranspiration function for the study area, wind speed and relative humidity were arbitrarily assumed to be constant at 20 km/h and 60% respectively.

Infiltration during rainfall events needed to be incorporated into evapotranspiration and runoff based on the return period of the event. The infiltration was calculated based on the following intuitive relationship.

$$I = P - E - (a \times P) \quad \text{eq. 6.03}$$

where:

I = Infiltration, (cm/day)

P = Precipitation, (cm/day)

E = Evapotranspiration calculated using eq. 6.01, (cm/day)

a = runoff coefficient based on return period, T_R

Three runoff coefficients were used in calculating runoff. The three runoff coefficients were assigned to three return period ranges. The return periods were calculated using the last 40 years of rainfall data gathered from the weather station in Virden, Manitoba. Figure 6.10 shows the rainfall event *versus* return period from data collected at the weather station at Virden, Manitoba. The first

runoff coefficient was assigned to rainfall events less than a 5 year return period in Figure 6.10. The second runoff coefficient calculated runoff for rainfall events between 5 year return period and 15 year return period. The last runoff coefficient was assigned to large rainfall events having return periods greater than 15 years. The runoff coefficients were adjusted accordingly in the calibration phase of the modeling discussed in the following section.

6.2.1.4 Calibration of the Transient Seep/W Model

The calibration phase of the transient Seep/W model consisted of adjusting the amount of recharge into the silty fine sand seam and adjusting the environmental flux function to reproduce measured *in-situ* groundwater and suction profiles. The calibration year of 2000 was modeled from April 1 to November 1 when two measurements were taken of groundwater levels and the suction profile. The transient model was sensitive to the interaction between the surficial environmental flux boundary and the recharge to the sand seam. Adjusting one of these parameters significantly affected the soil/water profiles.

The amount of recharge to the silty fine sand seam was not known and could only be estimated based on measured water levels. The recharge was held constant, producing a constant groundwater profile when no environmental flux boundary was defined (Figure 6.11). The amount of recharge to the silty fine sand seam was based on the maximum possible recharge, equal to the

conductivity of the silty fine sand seam (5.69×10^{-2} m/day). After calibration, the recharge into the silty fine sand seam was reduced to 1.82×10^{-2} , 32% of the maximum magnitude of recharge.

The second of these relationships is the environmental flux function. Figure 6.12a plots the flux function that was obtained after calibration. The calibration consisted of adjusting evapotranspiration (section 6.2.1.3) and the magnitude of the three runoff coefficients. The evapotranspiration function needed to be reduced by 96.3% to best represent the *in-situ* groundwater and suction profiles. This large reduction suggests (a) the inability of the Meyer (1944) mass transfer equation to properly estimate evaporation from a free water surface or (b) the validity of the assumption that the evapotranspiration from a bare or vegetated soil is equal to evaporation from a free water surface provided a continuous availability of water. The second assumption is likely the less realistic since numerous factors will affect the evapotranspiration in a vegetated soil. Another possibility could be the orientation of the slope. A north-facing slope like the one at PR 259 would not attract the same amount of solar radiation as a flat or south-facing exposure, thus reducing the amount of evapotranspiration. The impact of the assumed relative humidity on groundwater conditions and slope stability is examined in the sensitivity analysis discussed later in the chapter (Section 6.4). The runoff factors used in the calibrated environmental function are presented in Table 6.03.

During the initial part of the calibration exercise, the calculated groundwater profile was very sensitive to rainfall events when compared to the relatively constant water levels that were actually measured. The sensitivity was due to the fact that the AEV in the weathered clay layer was too high to allow for de-saturation of the upper soil material where there were larger suctions. A fully saturated soil would not permit primary storage capabilities in the soil peds. In addition, the lack of secondary storage, such as fissures, fractures and the block/friable structure of the weathered zone would also not be incorporated in a fully saturated soil. A storage component had to be built into the model to limit the influence of intense rainfall events. To incorporate storage capabilities and to de-saturate the upper soil, the SWCC for the weathered soil layer was shifted 65% (Figure 6.12b). Shifting the SWCC for the weathered soil significantly reduced the sensitivity of the groundwater profile to intense rainfall events. The hydraulic conductivity function was not adjusted.

Calibration results for BH-2, A-1, A-4 are presented in Figures 6.13, 6.14, 6.15 respectively. All modeled water level profiles showed, for the most part, good agreement with the measured water levels. The modeled groundwater profile for BH-2 was higher than the measured water levels by an average of 0.45 metres. The groundwater profiles for A-1 and A-4 were below measured water levels by an average of 0.19 and 0.21 metres respectively. Overall the results of the calibration exercise compared with observed potentials with time were in good agreement over the entire domain (Figure 6.16).

The modeled suction profile compared reasonably well with the two measured suction profiles from TP-1, and TP-2 (Figure 6.17). The modeled suction profile was not as steep as the measured profile, but still displayed significant non-linearity and in the negative pore water pressure range, it produced suctions that were approximately two times larger than the hydrostatic values $\gamma_w \times z$ above $\mu = p_a$. Having a modeled suction profile at a lesser slope than the slope of measured suction profile results in conservative results for the contribution of suction to stability.

At this point, calibration of the model was considered complete. Both the groundwater (at different times) and suctions were being modeled well. Improvements could no doubt be made to either the modeled groundwater profile or to the suction profile. However, the coupled nature of the saturated/unsaturated flow regime restricts adjustments since improving one aspect of the *in-situ* pore water pressures appeared to worsen another aspect. The calibrated Seep/W results using the year 2000 data were considered an acceptable modeling of the soil conditions in the slope.

6.2.2 Transient Slope Stability Analysis

Pore water pressure distributions for 1998, 1999, and 2000 modeled using Seep/W model were imported into Slope/W using the same slope geometry, and soil profiles used in Seep/W. The same fully-specified failure surface used in the

preliminary analysis was used in the detailed Slope/W model. Figure 6.18 illustrates the domain used in the detailed Slope/W model.

The soil parameters used for the weathered and unweathered clay layers were identical to the soil parameters used in the preliminary analysis. The preliminary Slope/W analysis used averaged values from laboratory results; $c'_{nc} = 0$, $\phi'_{nc} = 22^\circ$, and $\gamma_{bulk} = 19.6 \text{ kN/m}^3$. The friction angle due to suction, ϕ_b , was assumed to be equal to ϕ' (Vanapalli *et al.* 1996) based on the fact that the AEV intuitively is never reached in the weathered and unweathered clay. The effect of the ϕ_b parameter on slope stability is determined in the sensitivity section (6.4) of this chapter. The soil parameters used for the silty fine sand seam were estimated based on typical values for silty sands. The silty fine seam used the following soil properties; $c' = 0$, $\phi' = 37^\circ$, and $\gamma_{bulk} = 19.6 \text{ kN/m}^3$. The effect of these estimated soil parameters on slope stability would be limited due to the location and small thickness of the sand seam. The location and thickness of the sand seam means that only a few slice bases in the slope analysis will fall in the sand seam. Since the silty fine sand seam was assumed to be saturated, no friction angle due to suction was defined in the Slope/W model. The effect of the estimated friction angle of the silty fine sand seam on slope stability is described in the sensitivity section (6.4) of this chapter.

6.3 Results

After calibration of the Seep/W model, simulations in both Seep/W and Slope/W were executed for the periods April 1 to November 1 for 1998, 1999, and 2000. The results of for each of the three years are presented in the following section.

6.3.1 Seep/W Results

Figures 6.19 presents the modeled Seep/W groundwater profile for 1998. Figures 6.20, 6.21, 6.22 plot calculated values of total head versus time for a node (node 693) located in the center of the silty fine sand seam at BH-2 for 1998, 1999, 2000. In addition to the total head *versus* time profile, the environmental flux function for each year is plotted on the secondary axis (on the right side) in Figure 6.20, 6.21, 6.22. Plotting both the total head *versus* time for a node and the environmental flux function allows for easy comparison of trends. It can be easily seen from Figure 6.20, 6.21, 6.22 that there is direct correlation between the environmental flux function and the modeled variable head profile for any node in the domain. The virtually exact trends between the two profiles demonstrate the expected influence and impact of the environmental flux boundary on the groundwater profile as expected.

In addition to directly affecting the groundwater profile, the environmental flux boundary condition has considerable influence on the suction profile. Figure 6.23

plots modeled suction versus time (1998) for a node (674) located at the slope face at BH-2 on the primary (left) axis, while the environmental flux function for 1998 *versus* time is plotted on the secondary (right) axis. As with the groundwater profile, there is generally a strong correlation between the suction profile and the environmental flux function. However, the trend comparison between the suction profile and the environmental flux function at times did not correspond, in this way differing from the much closer comparisons observed in the groundwater profiles in Figures 6.20, 6.21, 6.22.

After the three seven-month periods were modeled, the results from the Seep/W model were used as input in Slope/W to determine the stability of the slope. The following section presents results from the transient Slope/W analysis using the Seep/W results as input.

6.3.2 Slope/W Results

Upon completion of the transient seepage analysis for 1998, 1999, 2000, the stability of the studied slope was examined using Slope/W. Figure 6.24 plots the factor of safety with respect to time for all three years. The factor of safety profile for the calibration year of 2000 is significantly above 1.0 with a minimum factor of safety of 1.72. The calibration year of 2000 displayed only small fluctuations in modeled factor of safety.

In contrast, the modeled factor of safety profile for the two wet years of 1998 and 1999 exhibited considerable variation in the factor of safety within short periods of time (a few days). For the most part, significant fluctuations in the factor of safety occur in May and June, with the 1998 profile exhibiting the largest change in factor of safety. In May and June (Figure 6.25), factor of safety profiles for both 1998 and 1999 had several simulations that were only marginally above unity ($F.S. \approx 1.04$). These marginally stable simulations suggest that the slope movements could have occurred in either 1998, 1999. However, it is suspected that the slope movements occurred in 1999 since rainfall events that produced factors of safety near unity were long in duration, low intensity events facilitating infiltration as opposed to runoff. The effect of long duration, low intensity events is reflected in gradual decreases in the modeled factor of safety from a stable factor of safety to just above unity. Rainfall events in 1998 that produced inadequate factors of safety were of short duration, high intensity events. These high intensity rainfall events decreased the factor of safety over larger ranges when compared to the range of decreases exhibited in 1999 during wet periods. In addition to the differences in the type of rainfall events, 1999 has a larger frequency of factors of safety that fall below 1.4 when compared to 1998, suggesting slope movements in 1999.

After June, all three factor of safety profiles in Figure 6.24 correspond reasonably well with each other. Having similar factors of safety after June indicates that there is a natural equilibrium for the slope. Even after periods of substantial rain

(May, June), the *in-situ* soil/water conditions tend towards this natural equilibrium and are reflected in the factor of safety profiles. Based on the wet years of 1998 and 1999, instability issues will occur in the months following spring thaw until the dry heat of mid-summer.

To evaluate how matric suction affects slope stability, two simulations of stable and unstable factors of safety were compared. The comparison was based on soil/water conditions along identical fully-specified failure surfaces. Figure 6.26 plots the pore water pressure along the slip surface *versus* slice number for May 14, 1999 (unstable) and August 28, 1999 (stable). Slice #1 is located near the crest of the slope while slice #50 is near the toe. Differences between the stable and unstable pore water pressures profiles are substantial, with the unstable pore water profile remaining almost entirely above zero. According to the effective stress concept, the difference in the pore water pressures will result in differences in effective stress. In turn, these affect the available soil strength acting along the base of each slice. The difference between the two pore water pressure profiles is reflected in the friction and suction components of soil strength (available shearing resistance) profiles plotted in Figure 6.27. The May 14, 1999 (unstable) simulation produced considerably less available frictional shear strength when compared to August 28, 1999 (stable). In addition, the soil strength increase due to suction is non-existent, for May 14, 1999, while the simulation for August 28, 1999 encompasses substantial amounts of soil strength (shearing resistance) due to suction. The reduction of frictional shear strength

and almost non-existent shear strength due to suction for the unstable simulation further confirms the important effect that rainfall events have on the examined slope.

6.4 Sensitivity Analyses

Sensitivity analyses were performed to determine the effects that adjusted, assumed or estimated model parameters have on calculated stability. The sensitivity analyses incorporated the following parameters; evapotranspiration, recharge into the silty fine sand seam, ϕ_b to ϕ' relationship, and ϕ' of the silty fine sand and unweathered clay.

The evapotranspiration component of the environmental flux boundary was altered between a range of $\pm 50\%$. The effect of changing the evapotranspiration on slope stability is plotted in Figure 6.28. May 15, 1999 was chosen for the analysis because its factor of safety of 1.14, allowed for a considerable reduction in the factor safety before reaching unity. The sensitivity results exhibit a linear change in the factor of safety between -10% change and $+40\%$. Within the linear range, the factor of safety ranged between 1.10 and 1.36. A 50% percent change in evapotranspiration over the linear range resulted in a 23% change in the factor of safety. Within the linear portion of Figure 6.28 the stability can be said to be relatively sensitive to changes in evapotranspiration. Above $+40\%$, the factor of safety *versus* percent change in evapotranspiration curve increases sharply. It

can be inferred from this relationship that the calculated stability is beginning to be dominated by the amount of recharge into the sand seam, with the influence of the environmental flux decreasing. Below -10%, the factor of safety *versus* percent change in evapotranspiration curve becomes non-linear and begins to flatten out. The groundwater profile for this portion of the curve is at the surface for most of the sliding mass except at the upper and lower ends of the sliding mass. A positive flux condition would only infiltrate at the ends of the sliding mass, with runoff occurring in the middle in the fully saturated zone. This limited the infiltration capacity and increased the runoff resulting in minimal decrease in the factor of safety with a decrease in the amount of evapotranspiration.

In order to construct the detailed Seep/W model, the magnitude of recharge into the silty fine sand seam had to be assumed since no explicit recharge data were available. Because the recharge into the silty fine sand seam contributed considerably to the groundwater profile, a sensitivity analysis was performed to determine its impact on the factor of safety. The sensitivity analysis involved altering the head at the left boundary of the seepage domain between ± 0.5 metres while the environmental flux boundary condition was not applied. Once the correct head adjustment was attained, the environmental flux boundary was then applied to the system, with the results being imported into Slope/W. Figure 6.29 plots the factor of safety *versus* change in head at the left boundary of the seepage domain for May 15, 1999. The results clearly show that the slope is only moderately sensitive to the magnitude of recharge into the silty fine sand seam.

As with reducing evapotranspiration, non-linearity is observed when the factor of safety falls below 1.10. The sensitivity is 12% for a change of input head of 1 metre.

The friction angle of the silty fine sand seam was estimated to be 37° , which is a conservative ϕ angle based on the nature of the material. The sensitivity analysis adjusted the ϕ angle by two degree increments between 29° and 39° . Figure 6.30 shows results of sensitivity analysis. It can be seen that the stability of the slope is relatively insensitive to the friction angle of the silt fine sand seam. Over the range of 10° the calculated factor of safety changed 6.5%.

In addition to analyzing the assumed ϕ' for the silty fine sand seam, the ϕ' for the weathered and unweathered clay was adjusted over a range of $\pm 4^\circ$ to determine its effect of the calculated factor of safety. A range to this extent would go well beyond all likely ϕ' angles for the material. Figure 6.31 plots factor of safety *versus* the adjusted ϕ' for the weathered and unweathered clay. It was determined that the factor of safety is moderately sensitive to the assigned ϕ' of the weathered and unweathered clay. Over a range of 8° the calculated factor of safety changed 36%. Therefore, any possible error in the interpolated failure envelope from laboratory results (Figure 5.05) would have marginal impact on the calculated factor of safety.

Another assumption that was incorporated into the Slope/W model was the relationship between ϕ_b , and ϕ' . The base model assumed that ϕ_b , was equal to ϕ' . This assumption would only affect the stability of the slope during dry conditions when the factor of safety is substantially above unity. Nevertheless, the effect of this assumption was analyzed. A relationship of $\phi_b = 0.5 \times \phi'$ was incorporated into the Slope/W model for the September 23, 1999 simulation. The base factor of safety (with of $\phi_b = \phi'$) was equal to 2.16 while the $\phi_b = 0.5 \times \phi'$ simulation had a factor of safety equal to 1.78. Reducing the friction angle for suction by 50% reduced the factor of safety by 17.5%. The $\phi_b = \phi'$ assumption does not significantly affect the slope stability results at or near unity when the slope is saturated for the most part and consequently is not important for the failure mechanism being studied.

The sensitivity analysis demonstrated, excluding evapotranspiration, that assumed, adjusted or estimated model parameters had little affect on the stability of the slope. The sensitivity of the model to changes in evapotranspiration was acceptable. The confidence level in the evapotranspiration parameter could be greatly improved with improved estimation method (96.2% reduction on estimated evapotranspiration).

Standpipe ID	Distance From Centerline (metres)	Measured Total Head (metres)	Modeled Total Head (metres)
BH-2	50	420.30	420.70
A-4	43	419.33	419.40
A-1	37	418.40	418.33

Table 6.01 Comparison of water levels for fall 2000 used in preliminary seepage analysis.

Suction Conditions		Groundwater Conditions		
		Case 1 423.50 m	Case 2 424.25 m	Case 3 425.00 m
No Suction		1.13	1.07	1.01
$\phi^b = 0.5$ $\times \phi'_{nc}$	Seep/W Suction	1.21	1.12	1.04
	Measured Suction	1.44	1.30	1.16
$\phi^b = \phi'_{nc}$	Seep/W Suction	1.31	1.18	1.08

Table 6.02 Factors of safety for preliminary Slope/W model.

Return Period, T_R	Runoff Coefficient
< 5 years	0.97
5 years < x > 15 years	0.98
> 15 years	0.99

Table 6.03 Runoff coefficients used in calibrated transient Seep/W model.

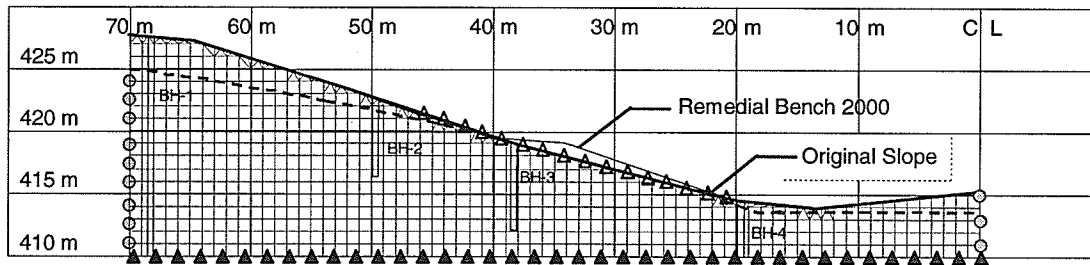


Figure 6.01 Seep/W domain used in preliminary analysis.

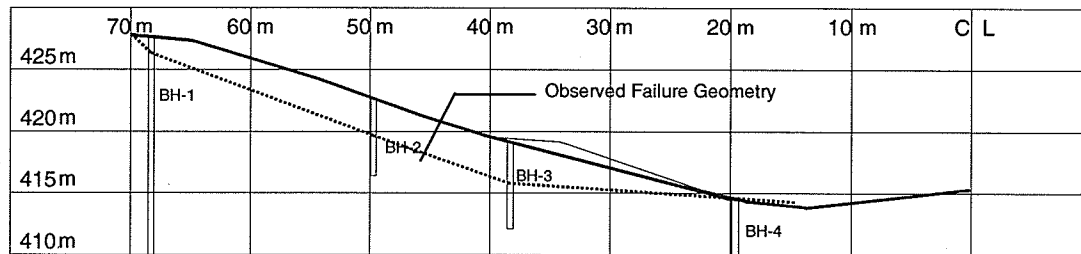


Figure 6.02 Slope/W domain used in preliminary analysis.

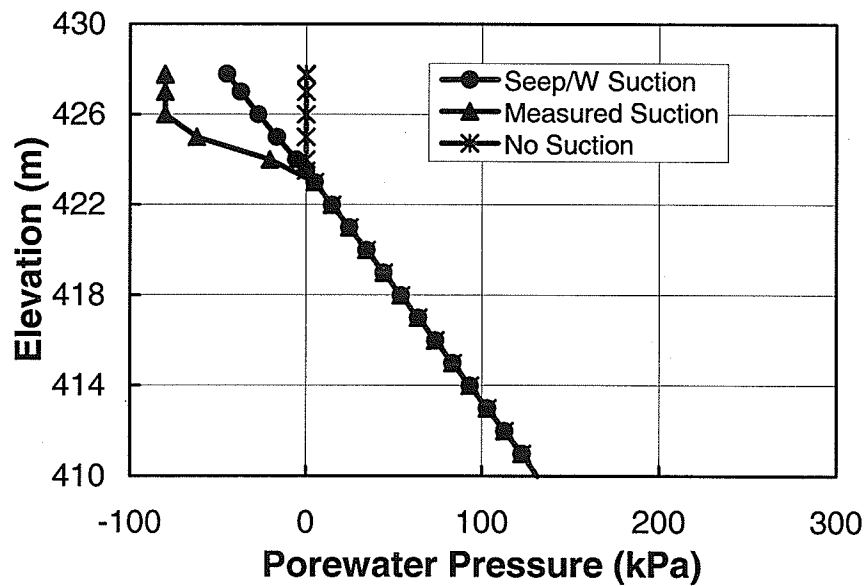


Figure 6.03 Pore water pressure profile used in preliminary study.

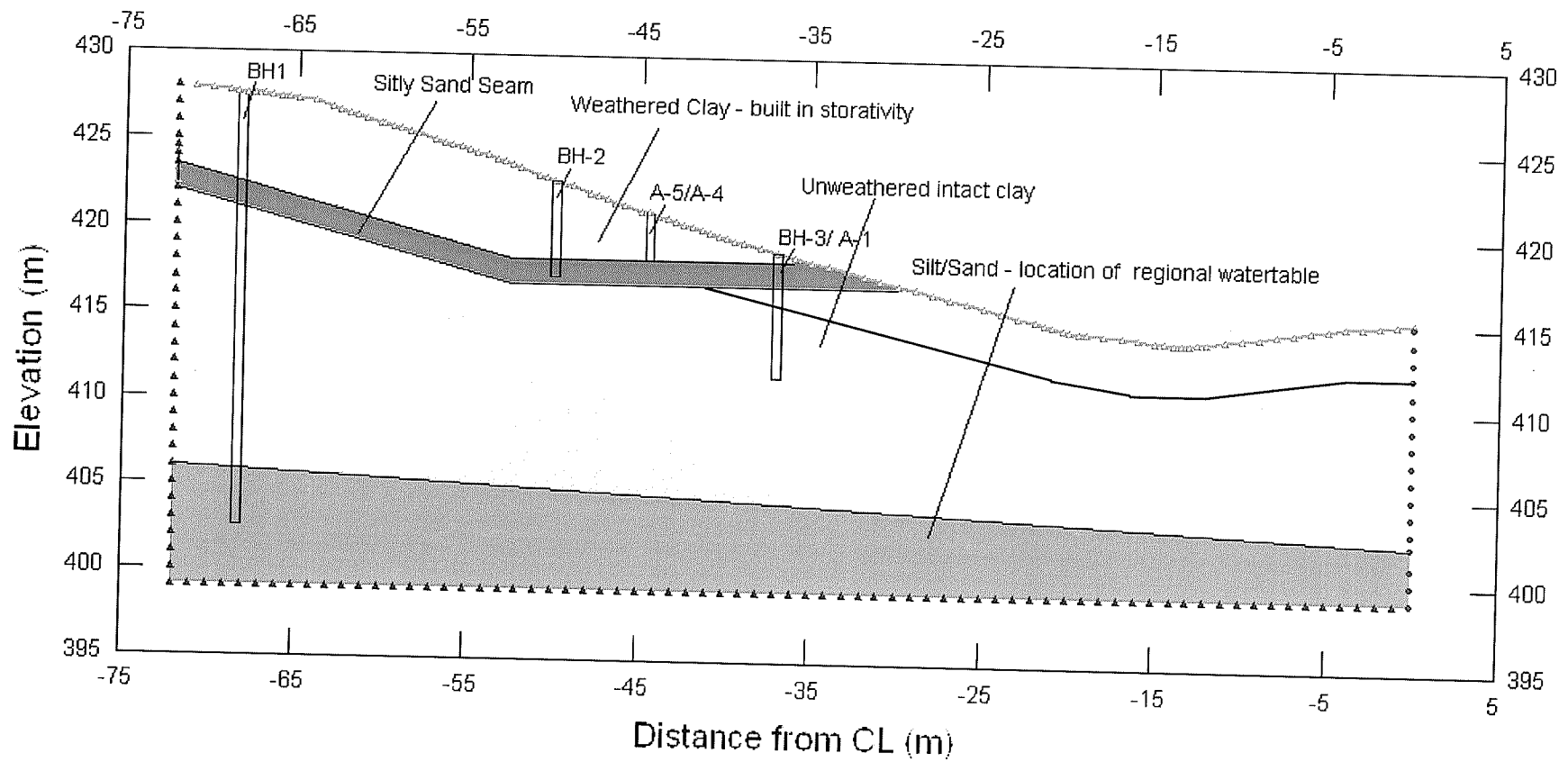


Figure 6.04 Detailed Seep/W domain used in transient analysis.

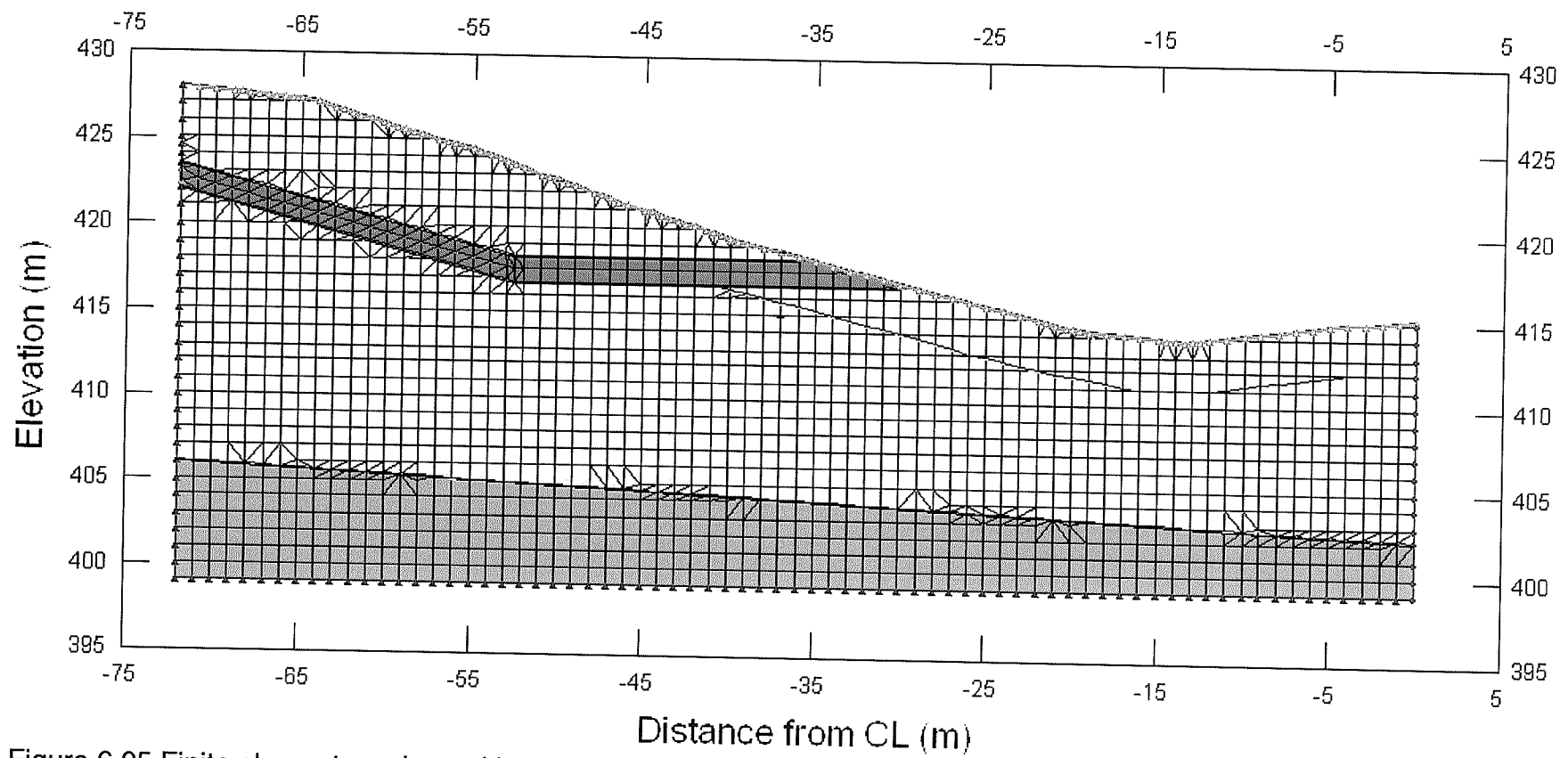


Figure 6.05 Finite element mesh used in transient Seep/W model.



Figure 6.06 Silty fine sand seam after re-failing of the West Failure in July 2001.

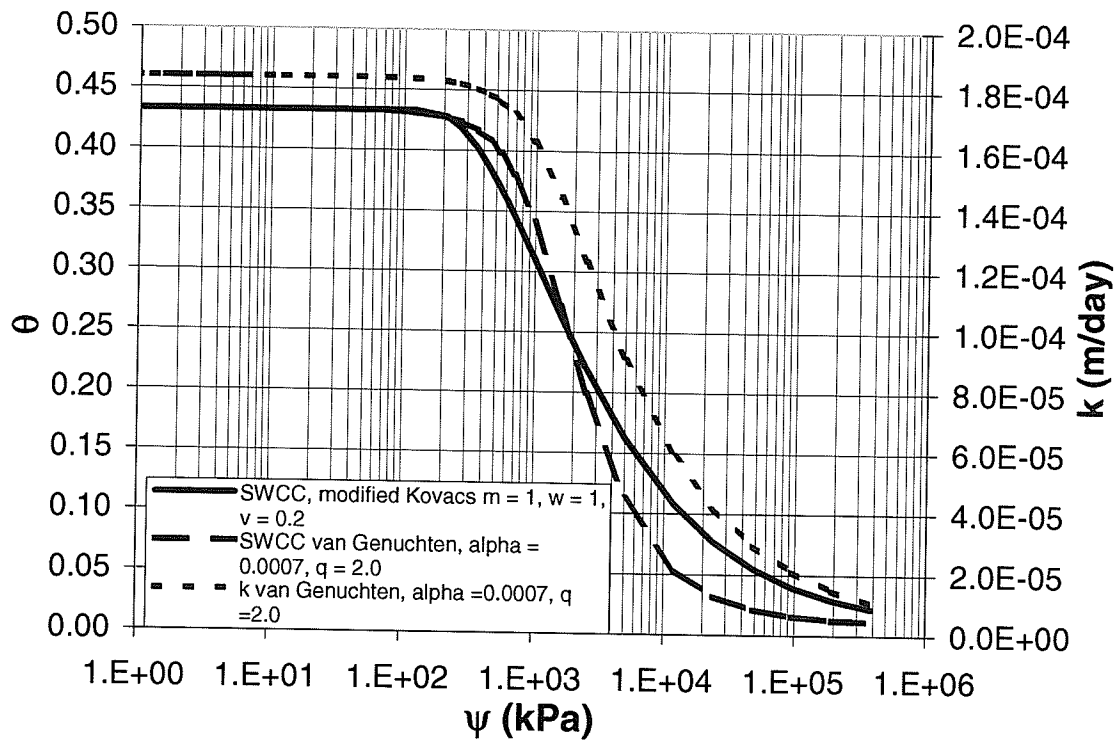


Figure 6.07 SWCC and hydraulic conductivity function for weathered clay layer. SWCC function was based on sample BH-3-7.

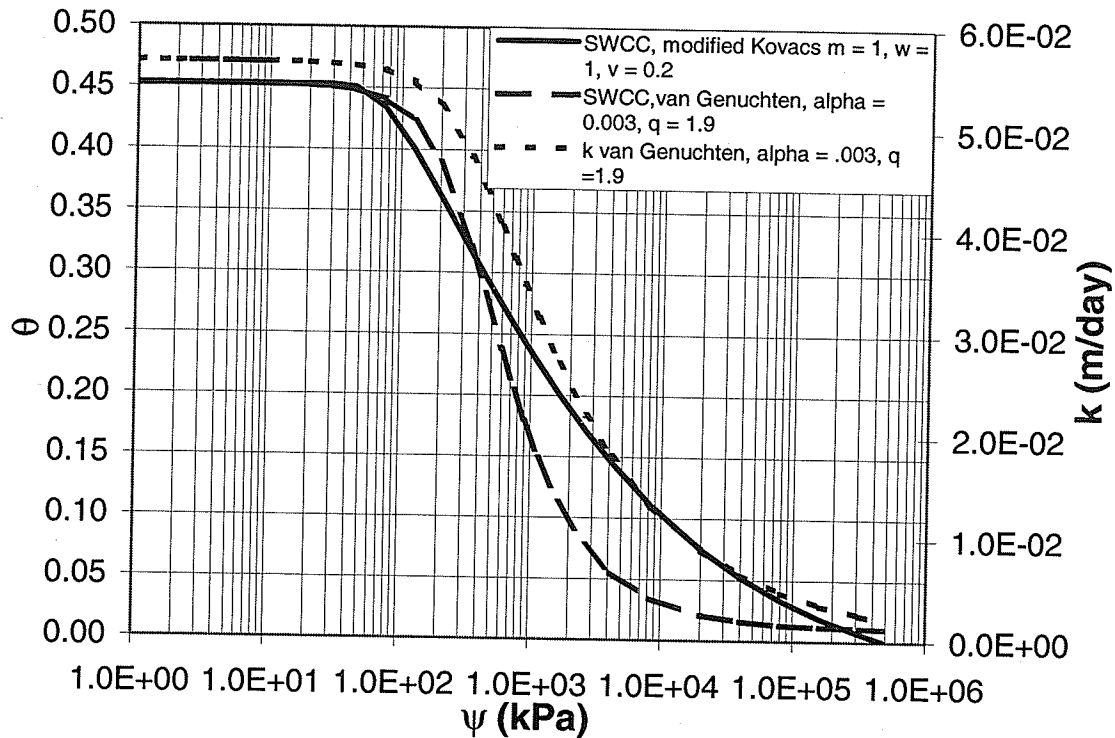


Figure 6.08 SWCC and hydraulic conductivity function for sand seam layer. SWCC function was based from BH-2-4.

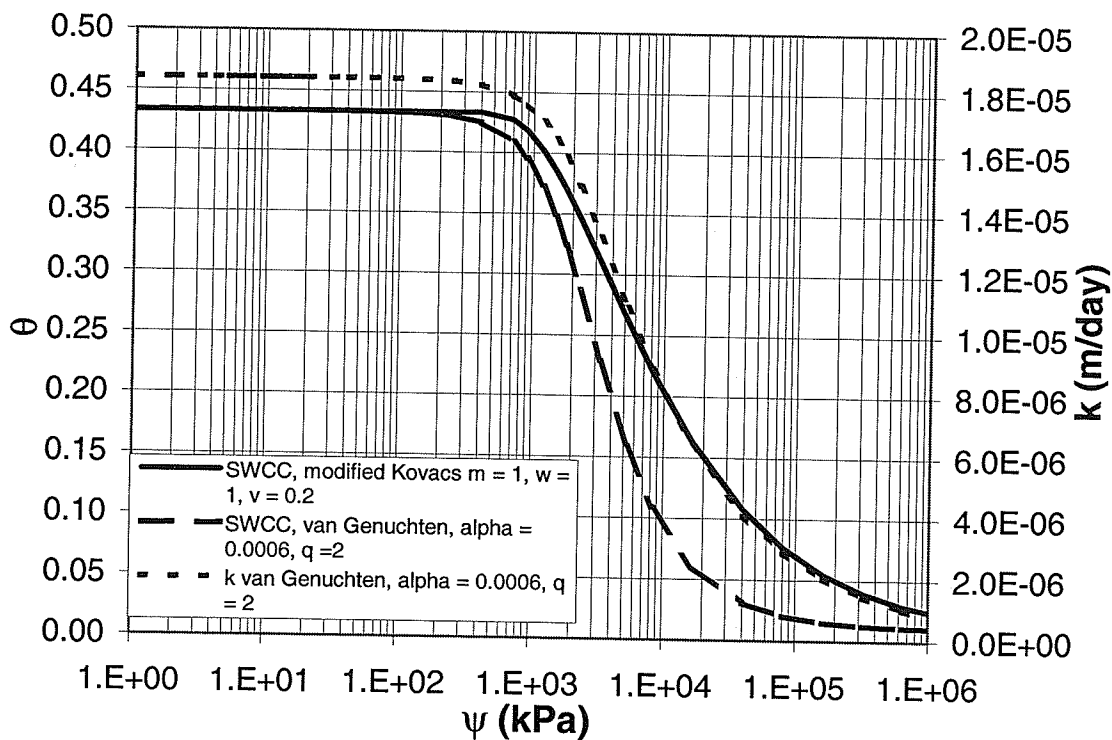


Figure 6.09 SWCC and hydraulic conductivity function for unweathered clay layer. SWCC function was determined from sample BH-3-7.

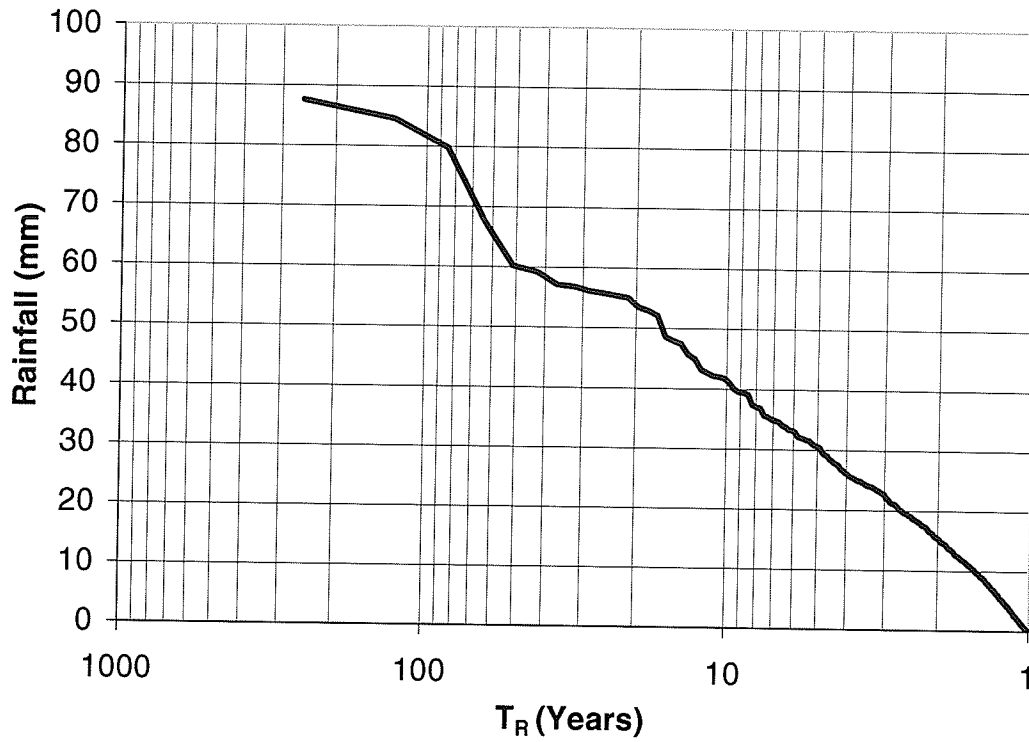


Figure 6.10 Return period for rainfall events at Virden, Manitoba.

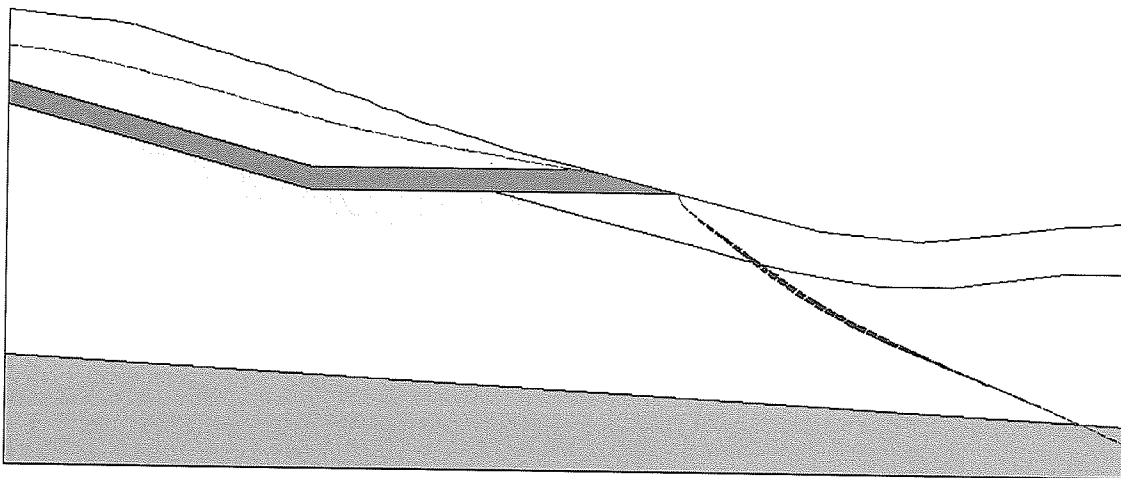


Figure 6.11 Seep/W result with no applied environmental flux boundary.

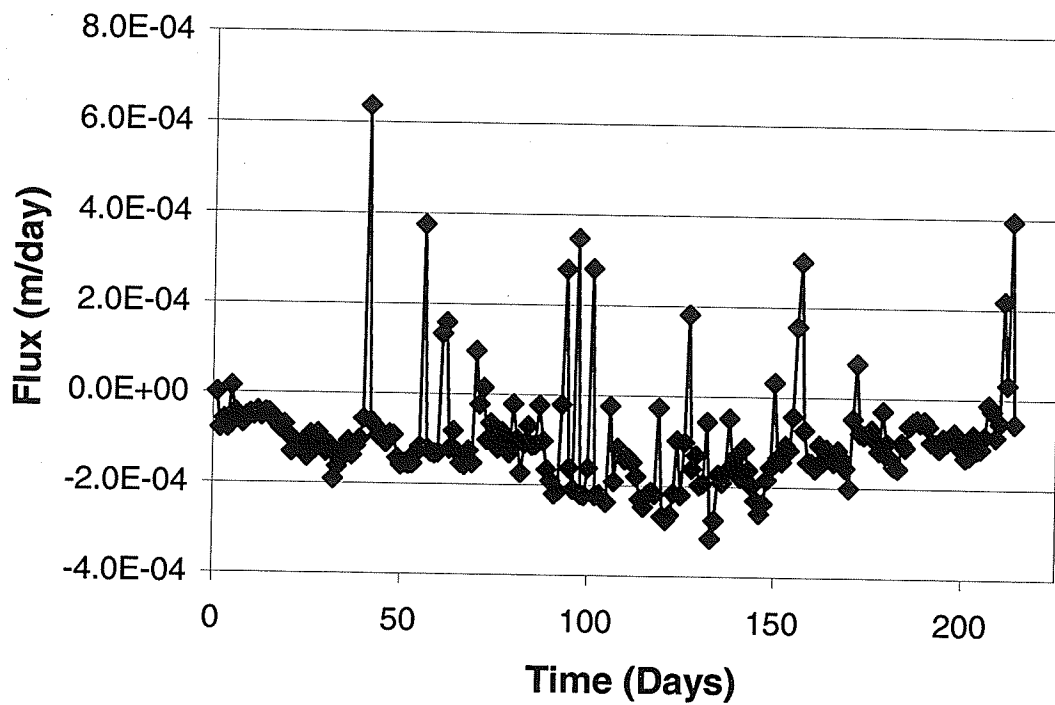


Figure 6.12a Calibrated environmental flux function for April 1, 2000 to November 1, 2001.

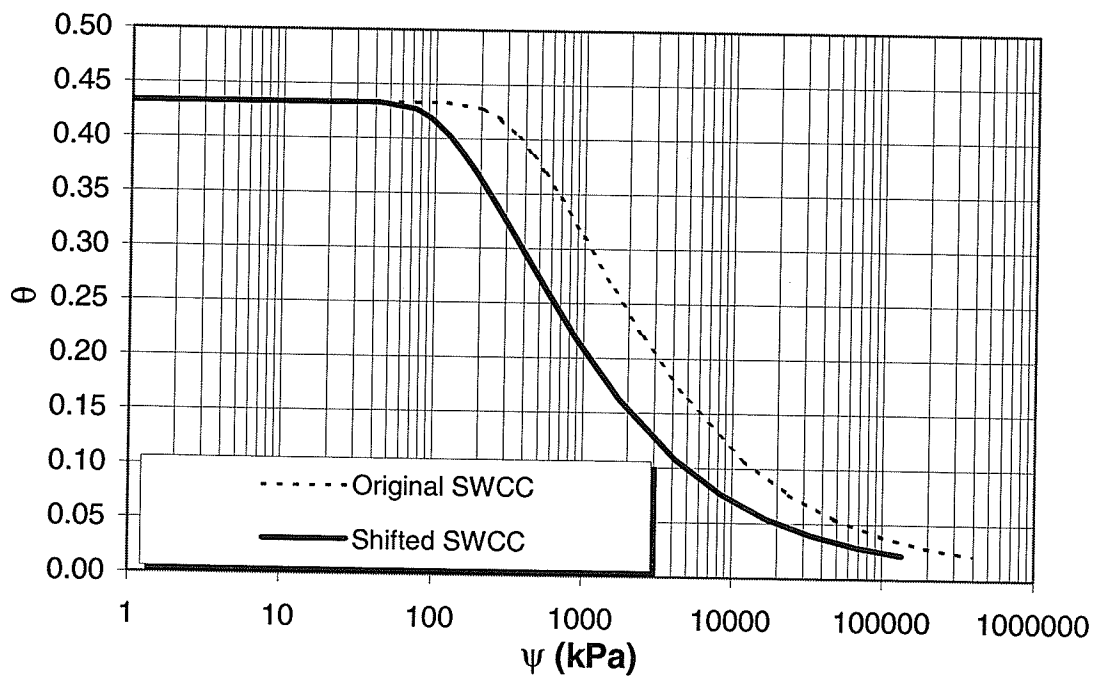


Figure 6.12b Shifted SWCC for the weathered clay layer.

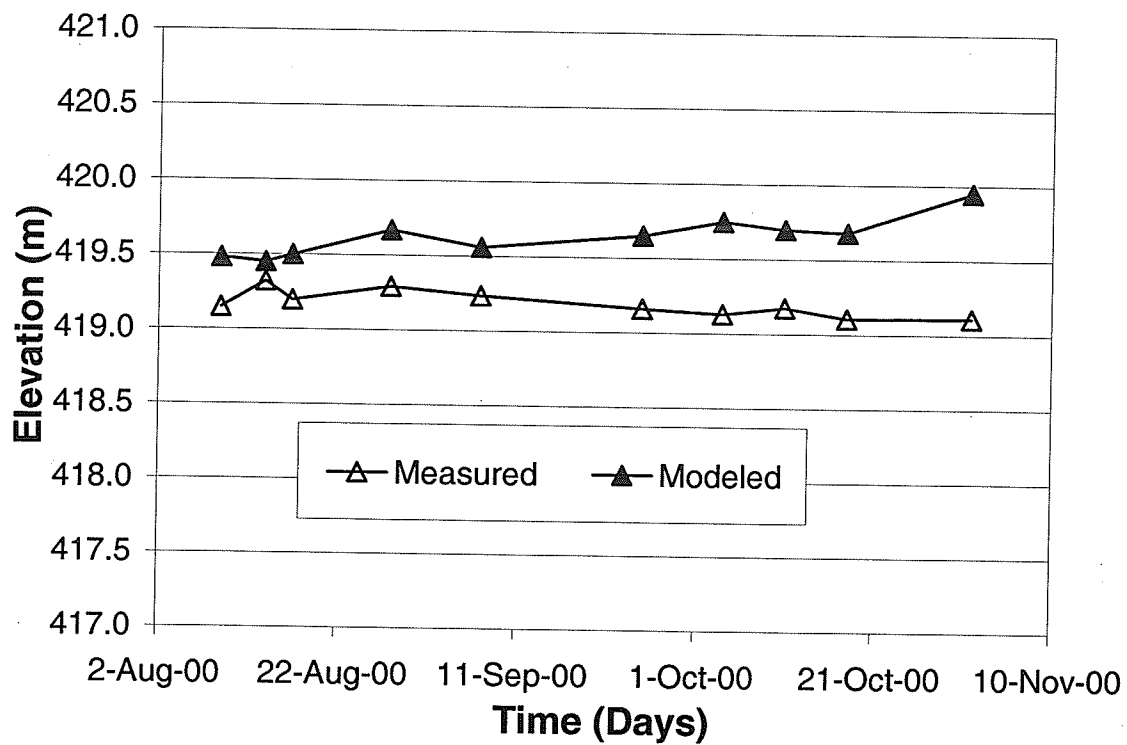


Figure 6.13 BH-2 measured groundwater levels *versus* modeled groundwater levels for April 1 to November 1, 2000.

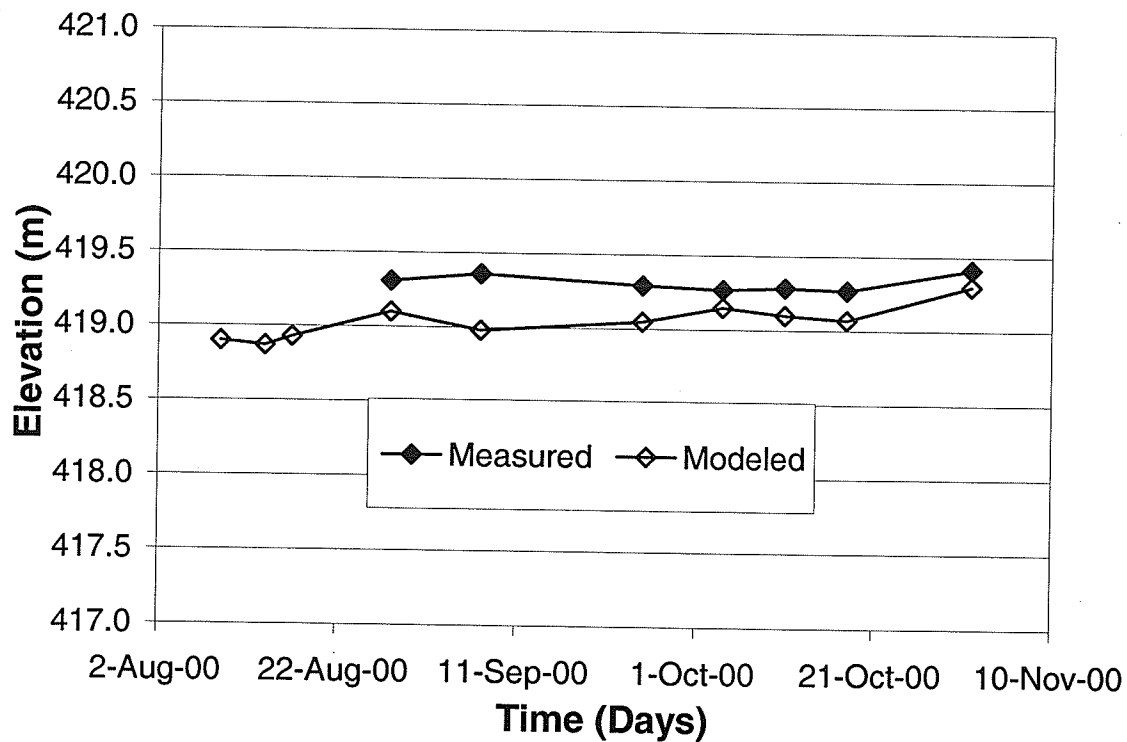


Figure 6.14 A-4 measured groundwater levels *versus* modeled groundwater levels for April 1 to November 1, 2000.

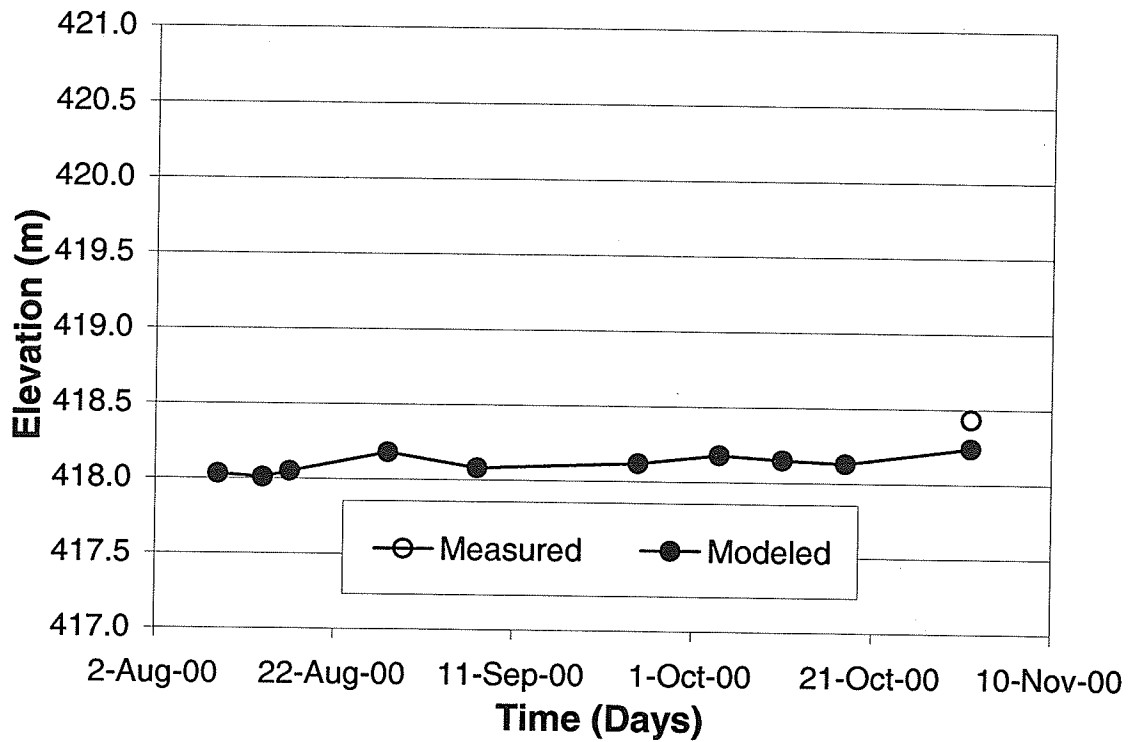


Figure 6.15 A-2 measured groundwater levels *versus* modeled groundwater levels for April 1 to November 1, 2000

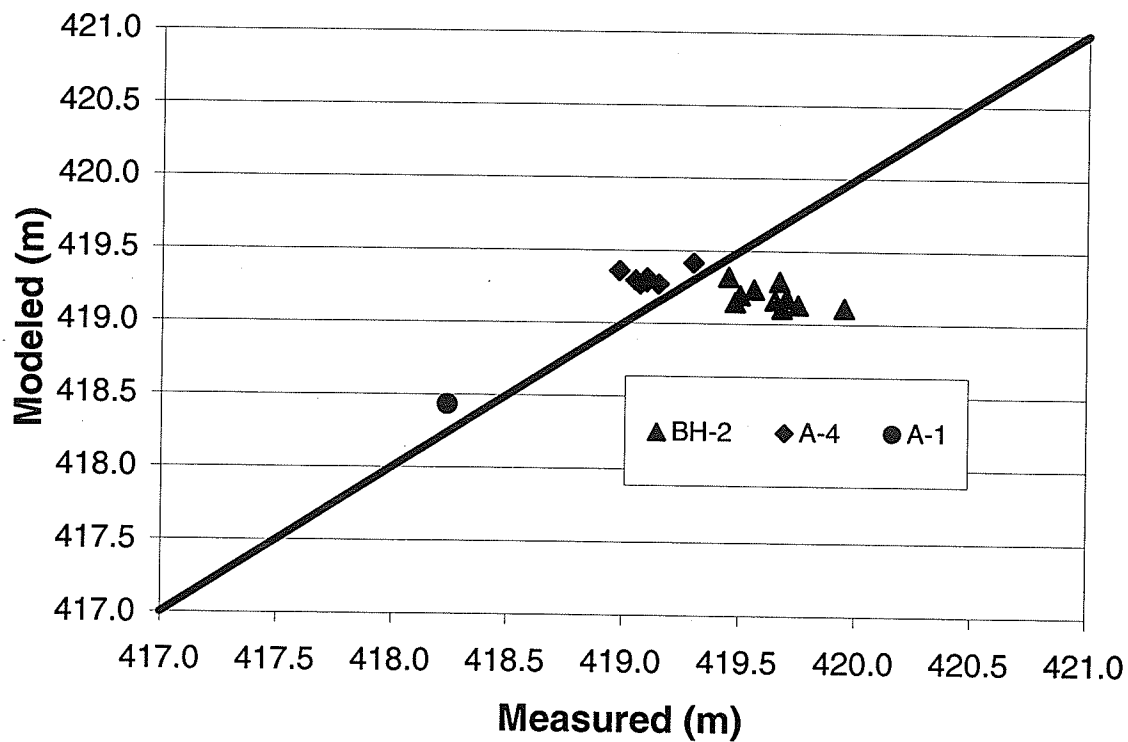


Figure 6.16 Modeled groundwater levels *versus* Measured groundwater levels for all standpipes.

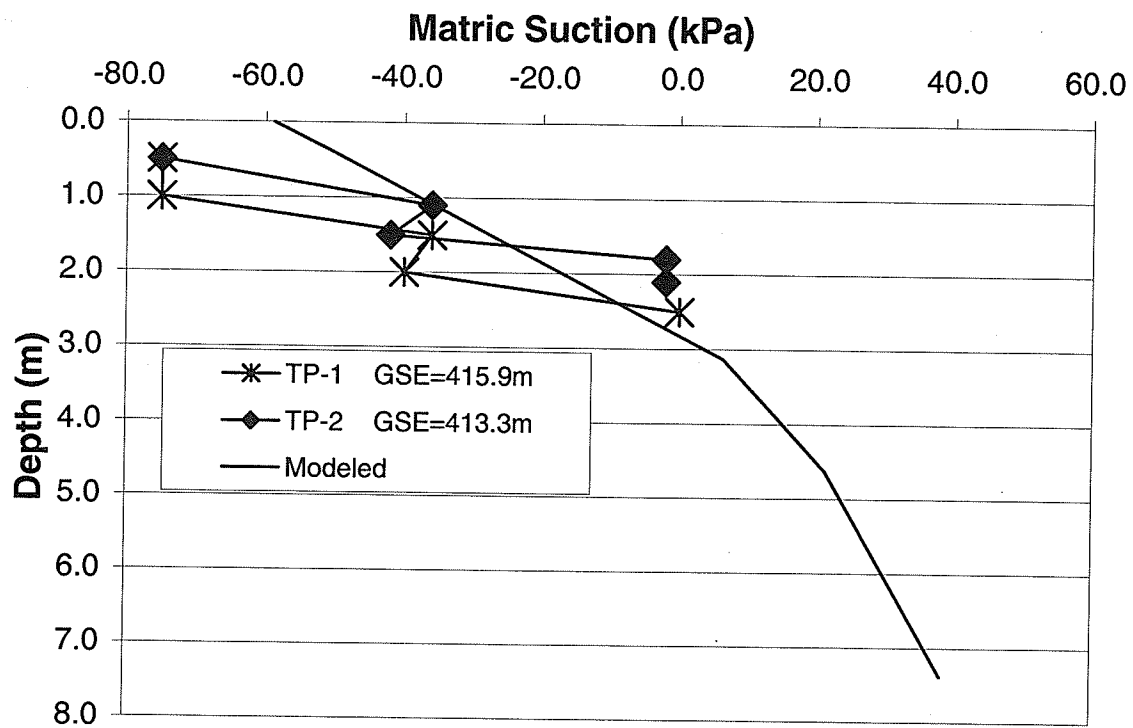


Figure 6.17 Measured *versus* Modeled suction profile.

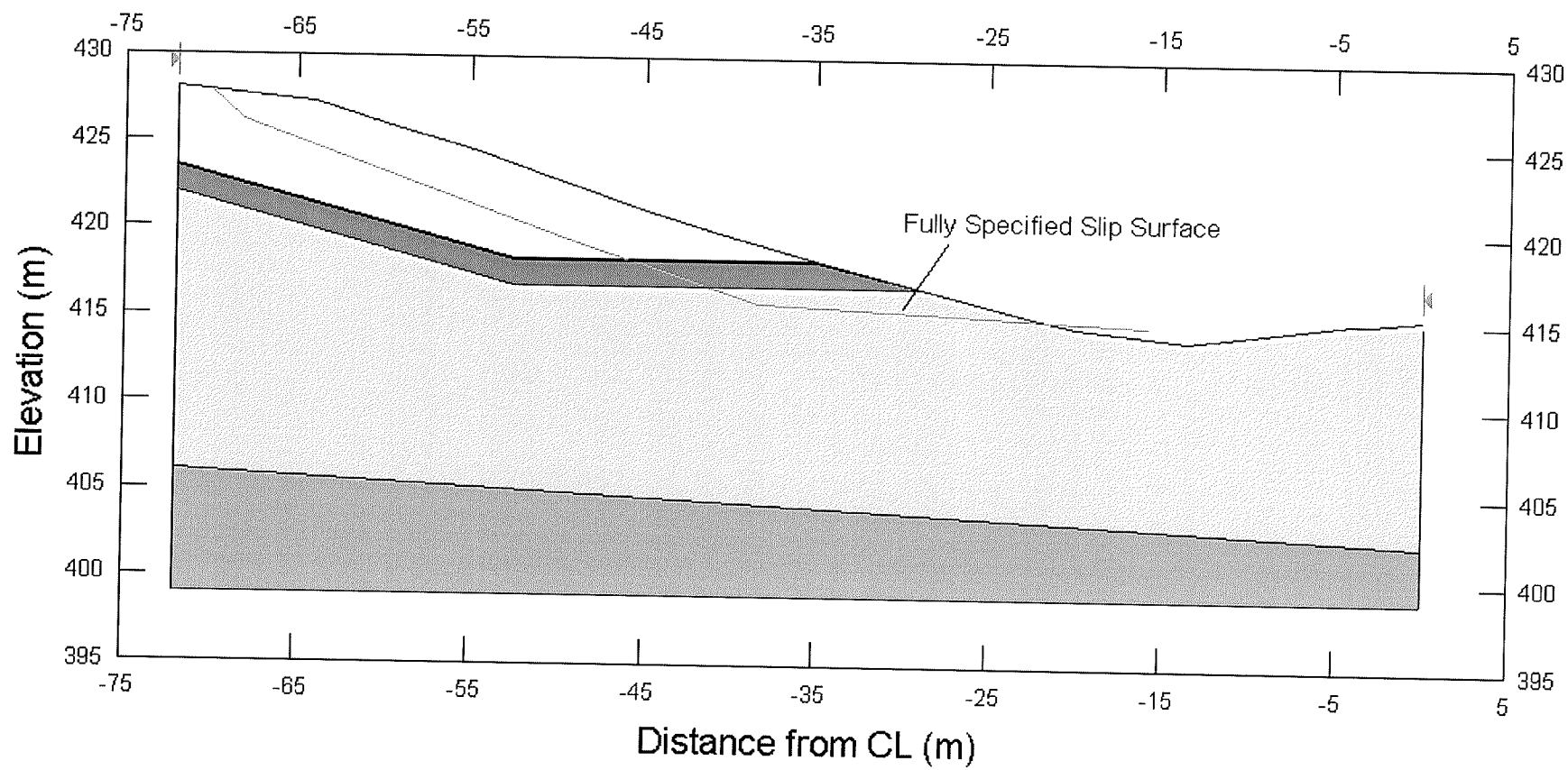


Figure 6.18 Slope/W domain used in detailed transient analysis.

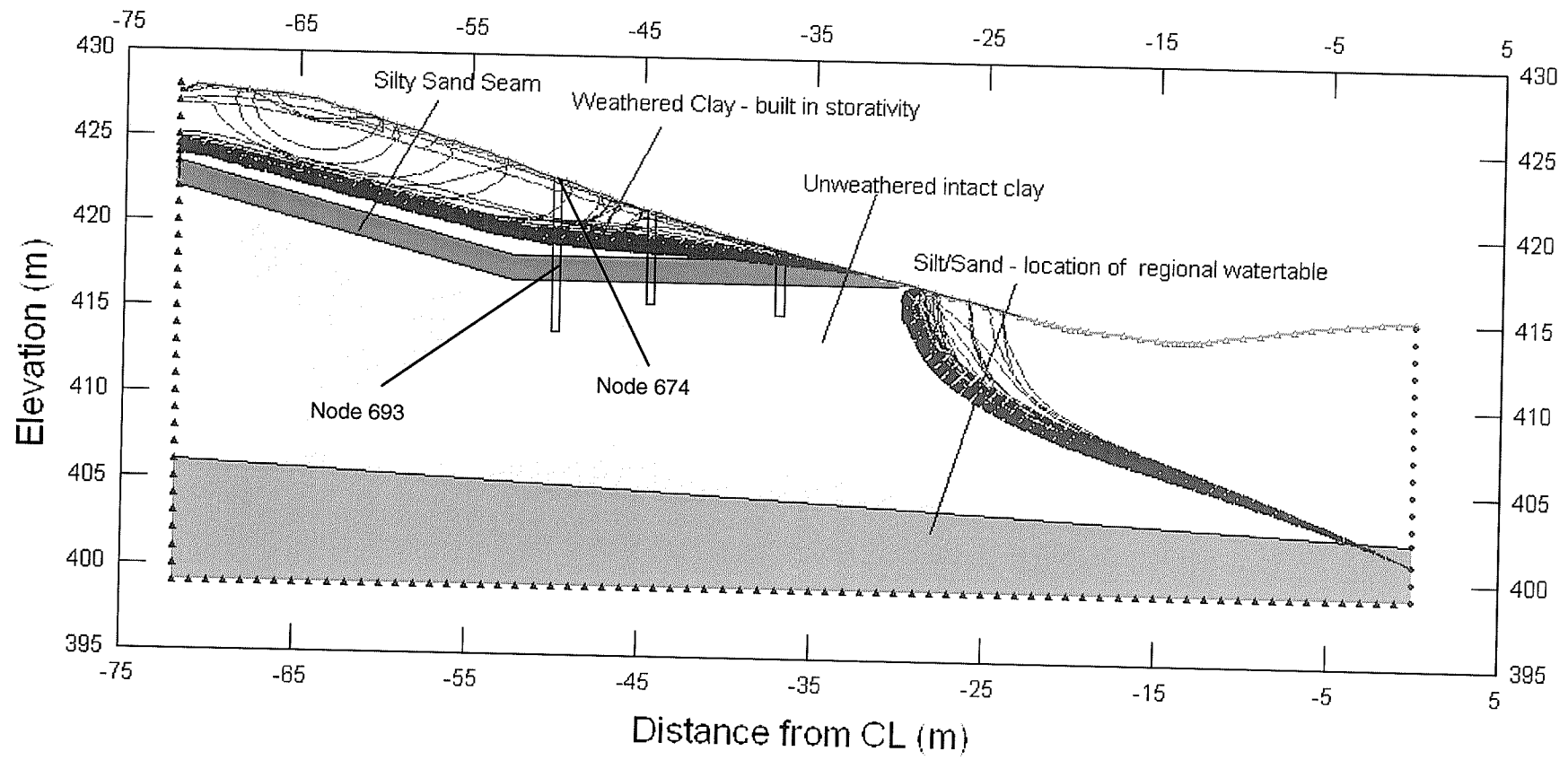


Figure 6.19 Groundwater profile modelled in Seep/W for 1998.

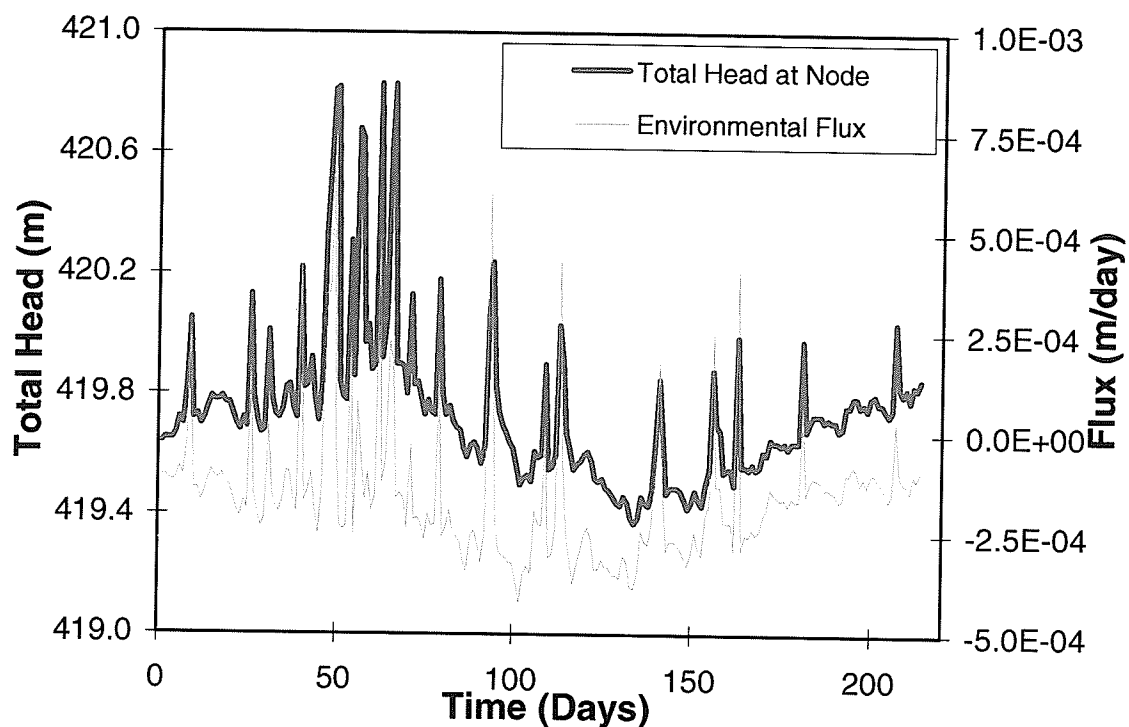


Figure 6.20 1998 - Total head versus time for node 693 plotted on the primary axis (left). Environmental flux function *versus* time is plotted on the secondary axis (right).

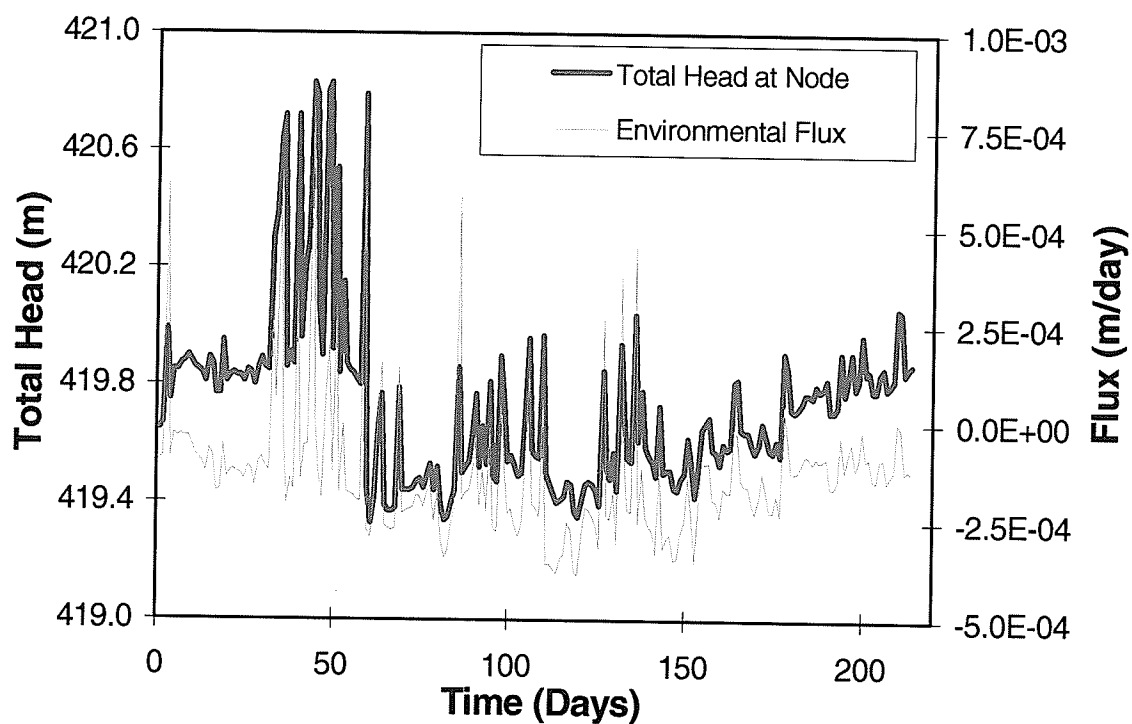


Figure 6.21 1999 - Total head versus time for node 693 plotted on the primary axis. Environmental flux function *versus* time is plotted on the secondary axis.

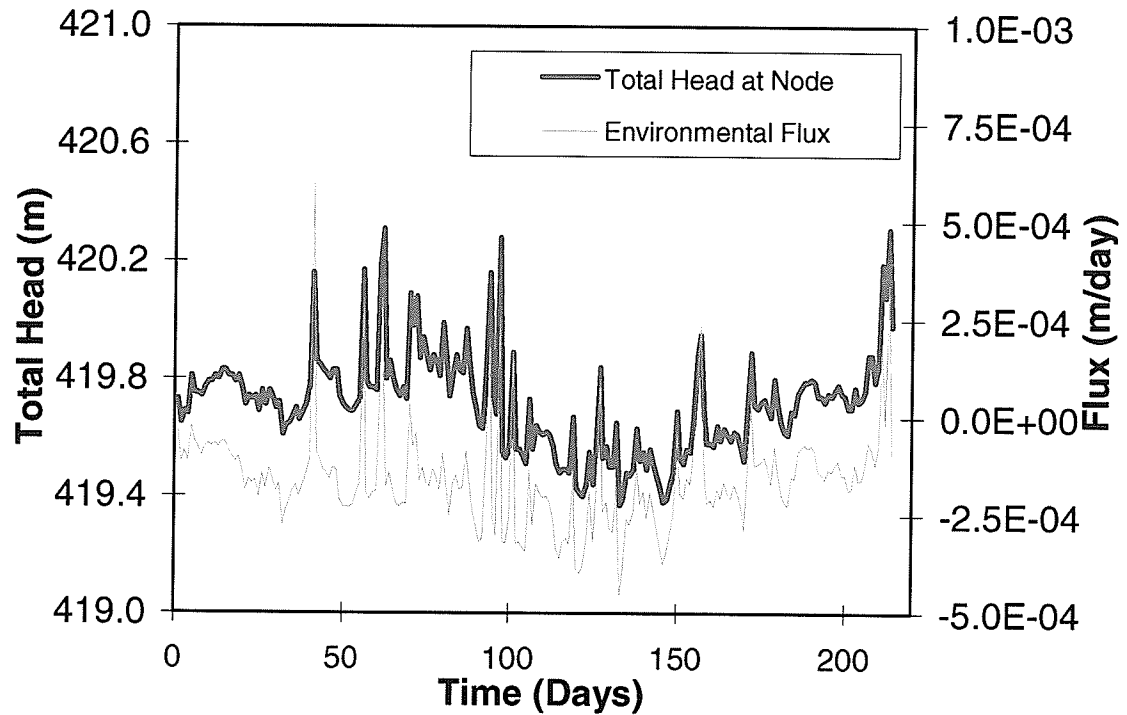


Figure 6.22 2000 - Total head versus time for node 693 plotted on the primary axis. Environmental flux function *versus* time is plotted on the secondary axis.

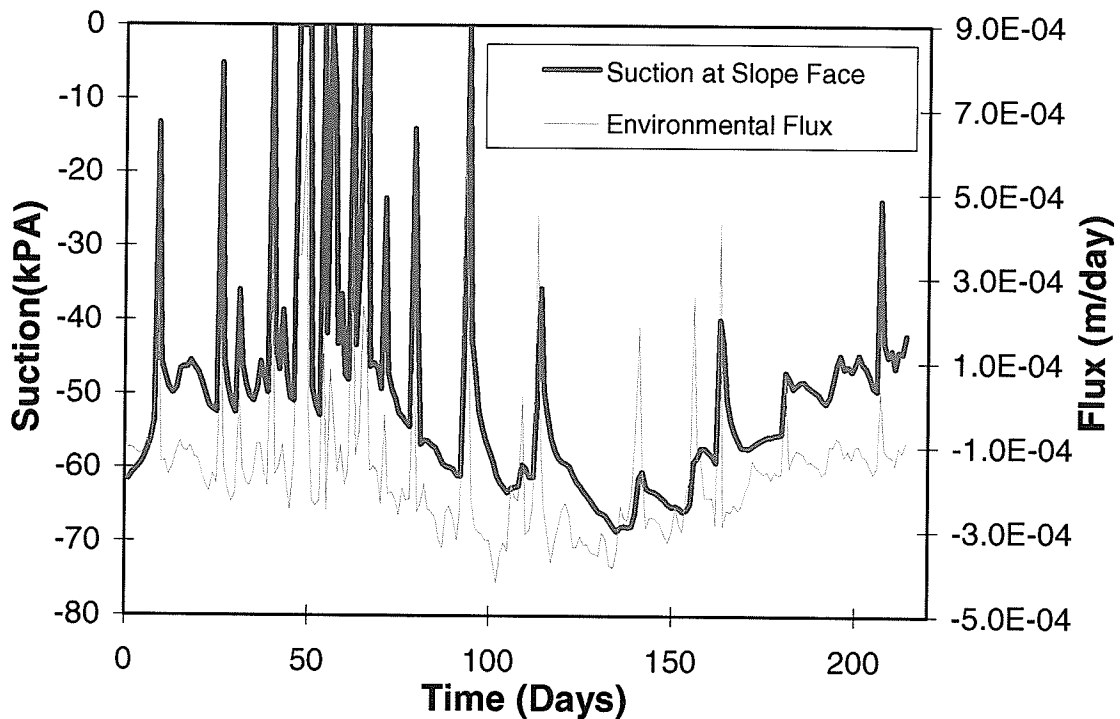


Figure 6.23 1998 – Suction versus time for node 674 plotted on the primary axis. Environmental flux function *versus* time is plotted on the secondary axis.

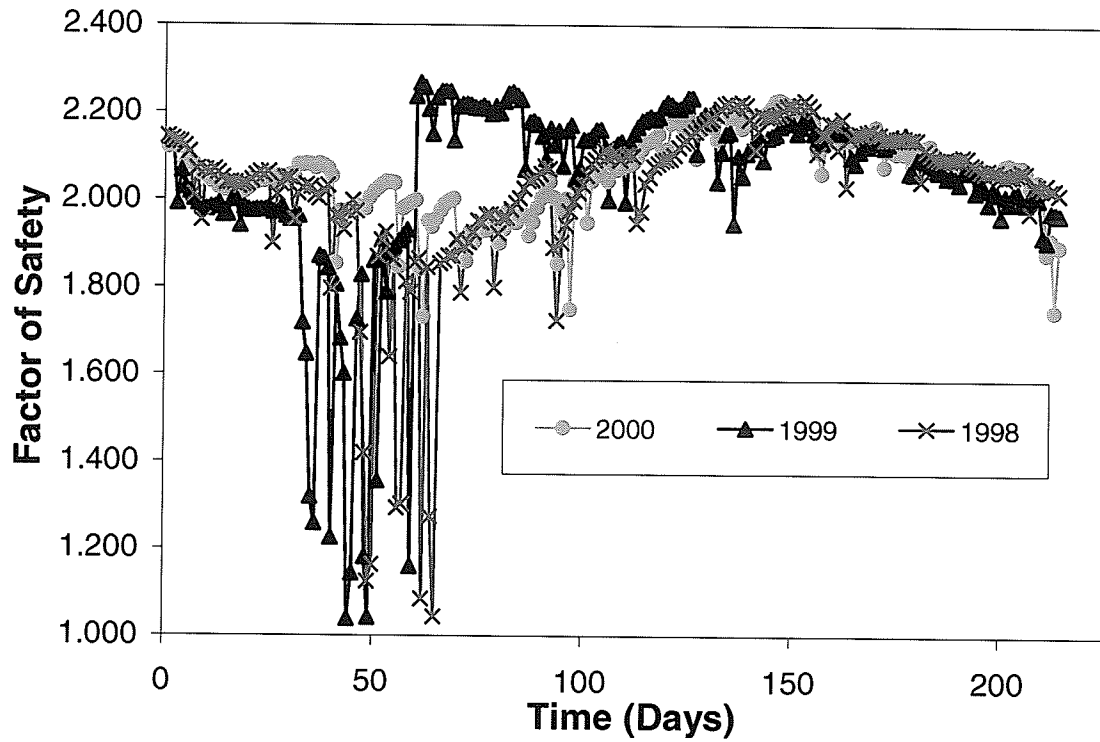


Figure 6.24 Factor of safety with respect to time for 1998, 1999, and 2000.

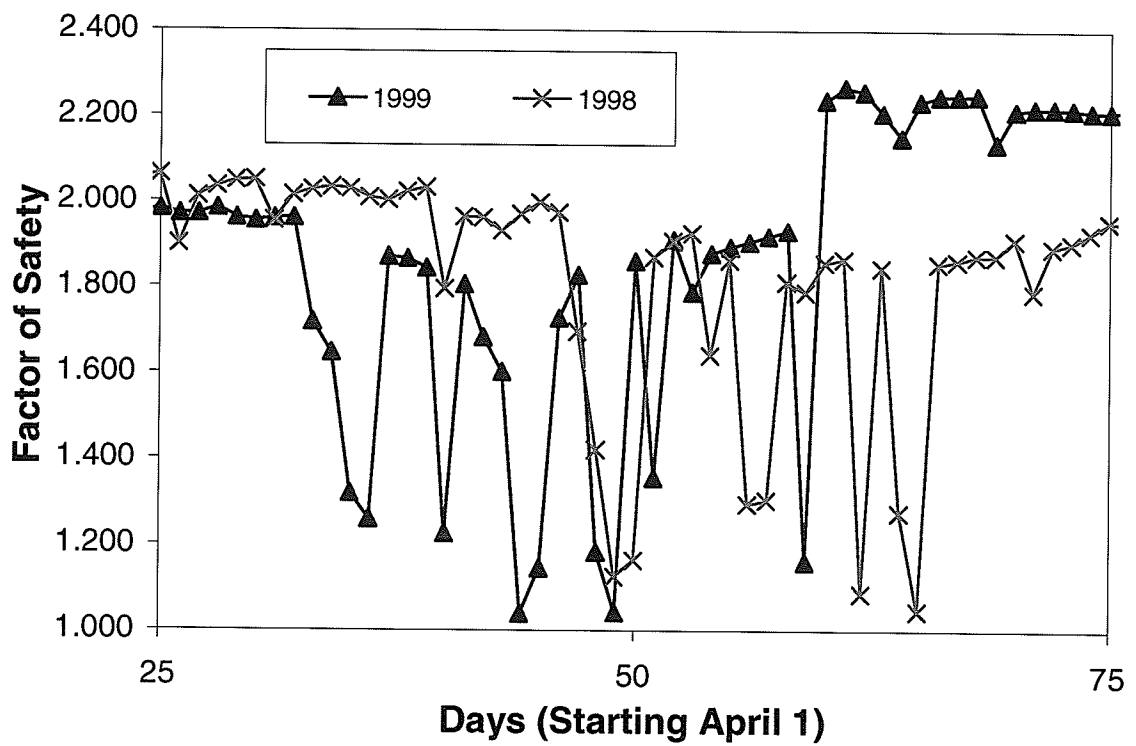


Figure 6.25 Factor of safety with respect to time for May and June for both 1998, and 1999.

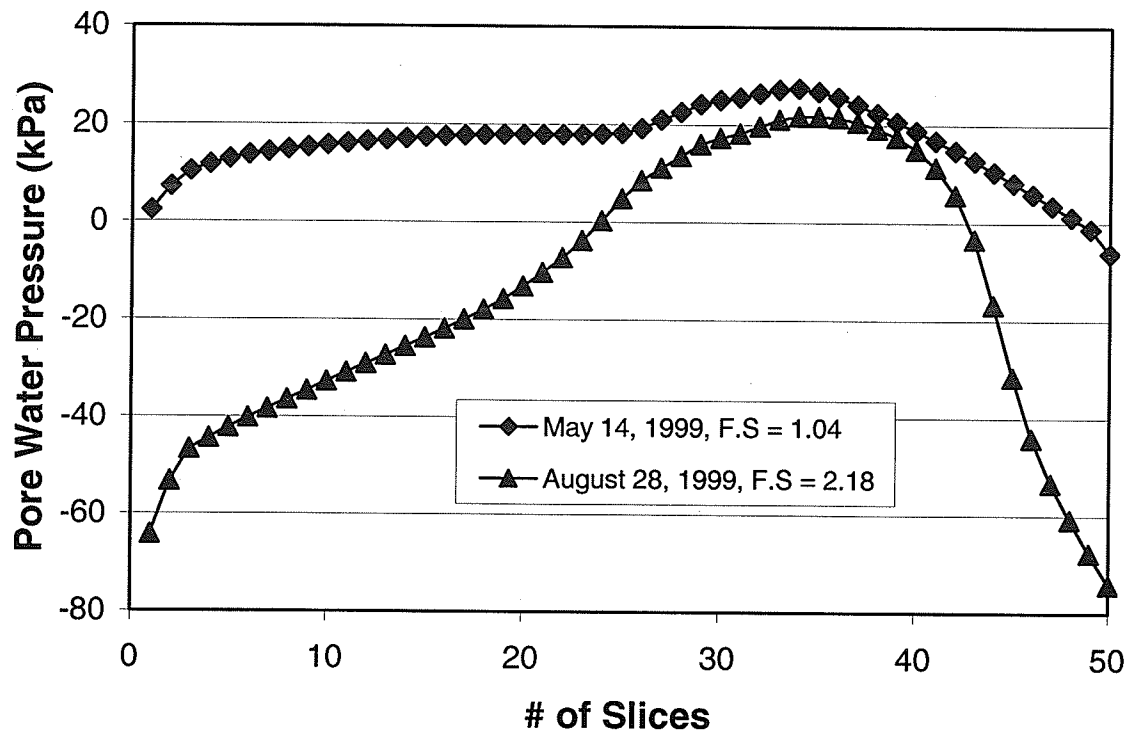


Figure 6.26 Pore water pressure distribution along failure surface for two simulations.

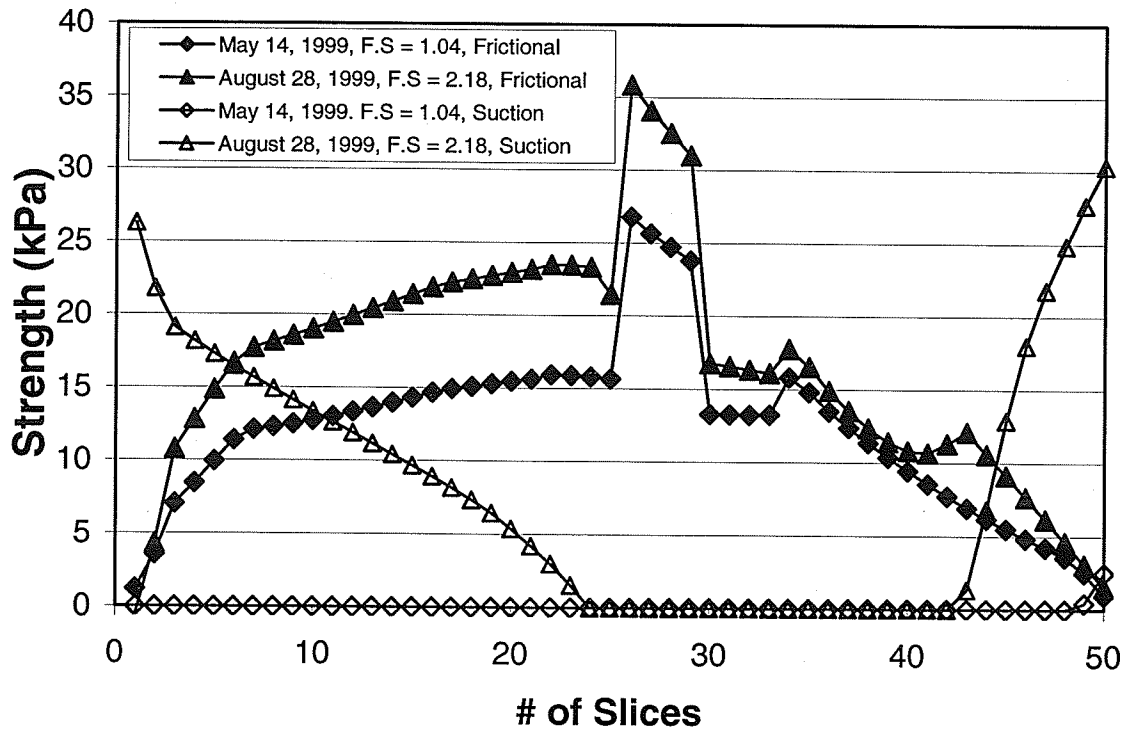


Figure 6.27 Frictional and suction component of available shear strength.

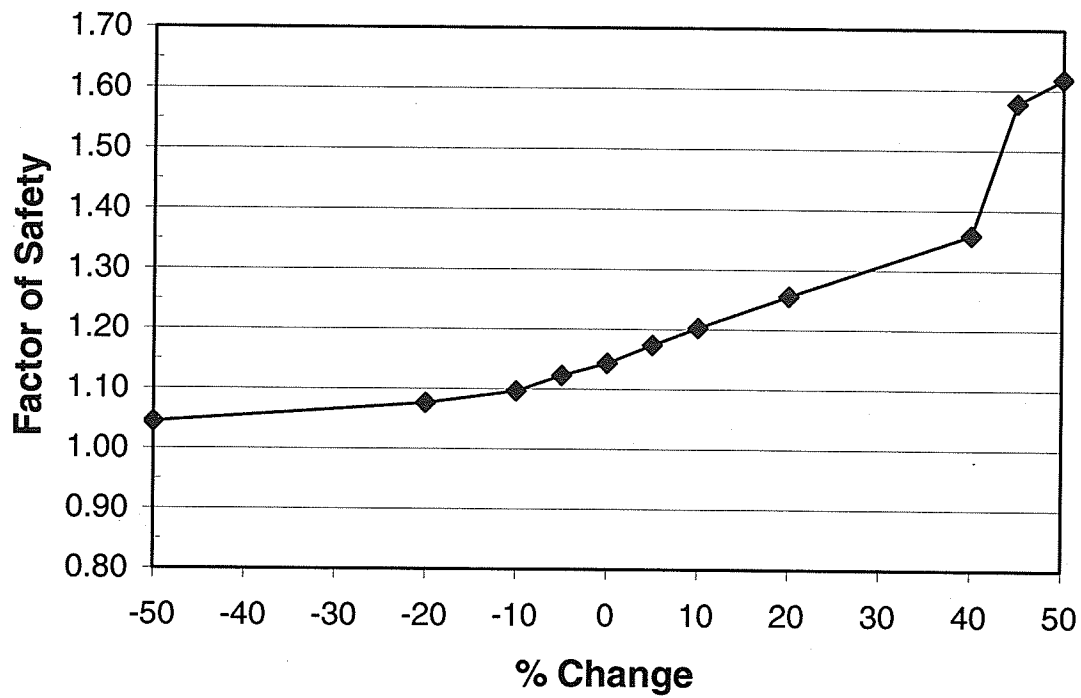


Figure 6.28 Factor of safety *versus* percent change in evapotranspiration for May 15, 1999.

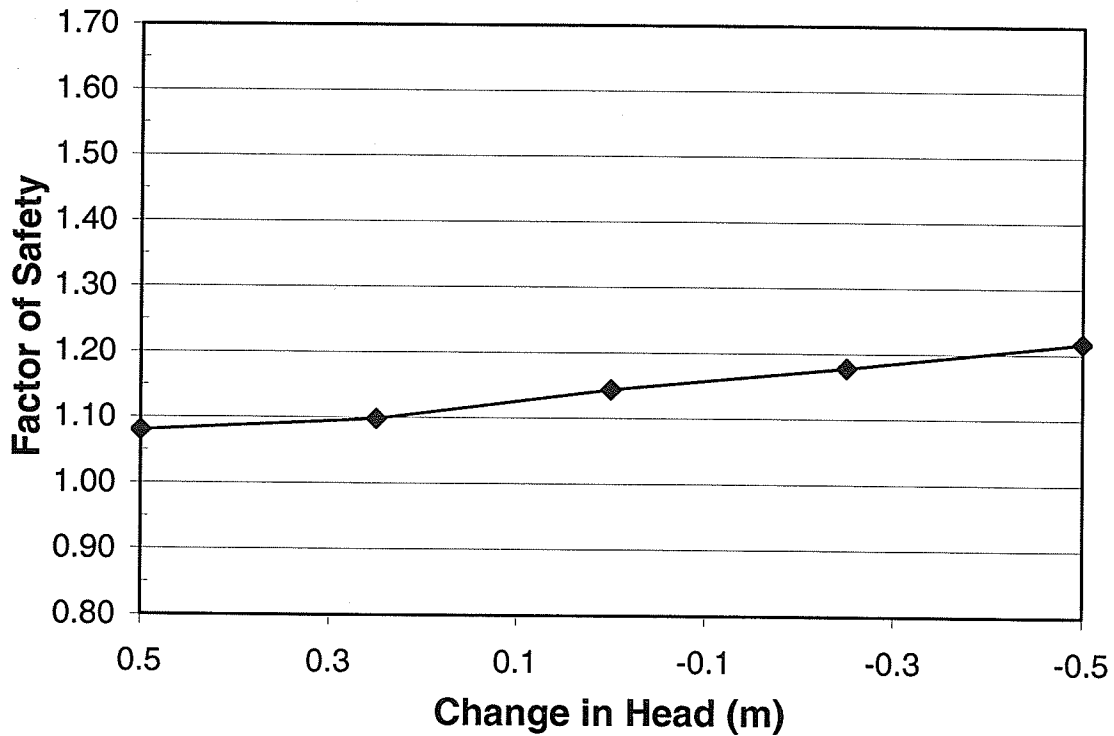


Figure 6.29 Factor of safety *versus* change in head at the left boundary of the detailed model domain for May 15, 1999.

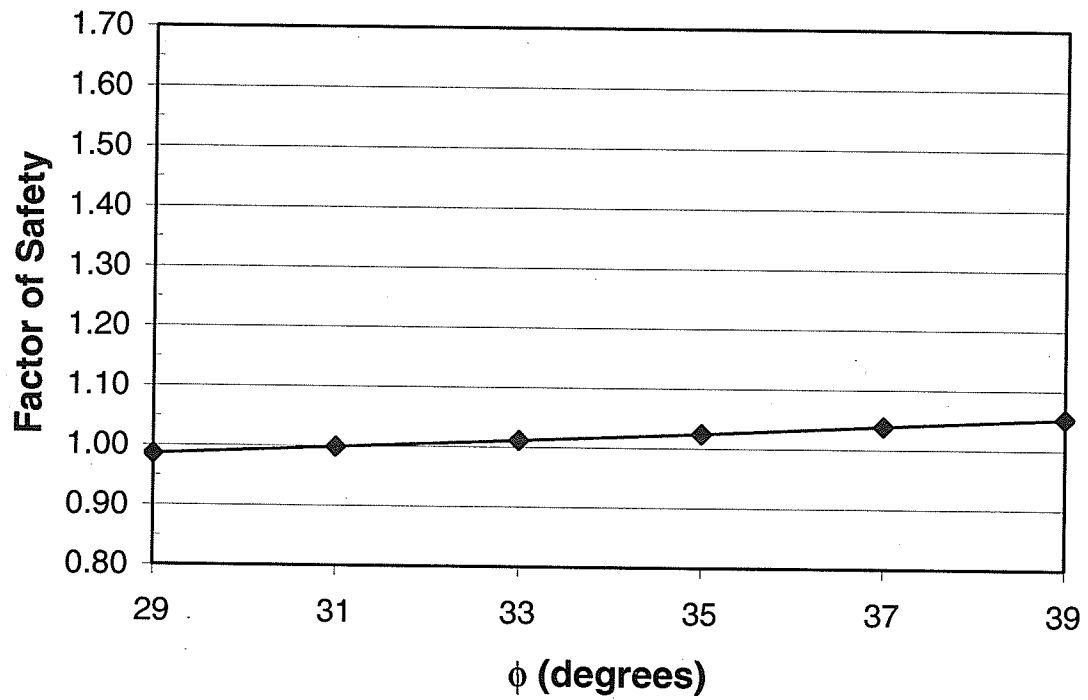


Figure 6.30 Factor of safety *versus* ϕ of the silty fine sand seam for May 15, 1999.

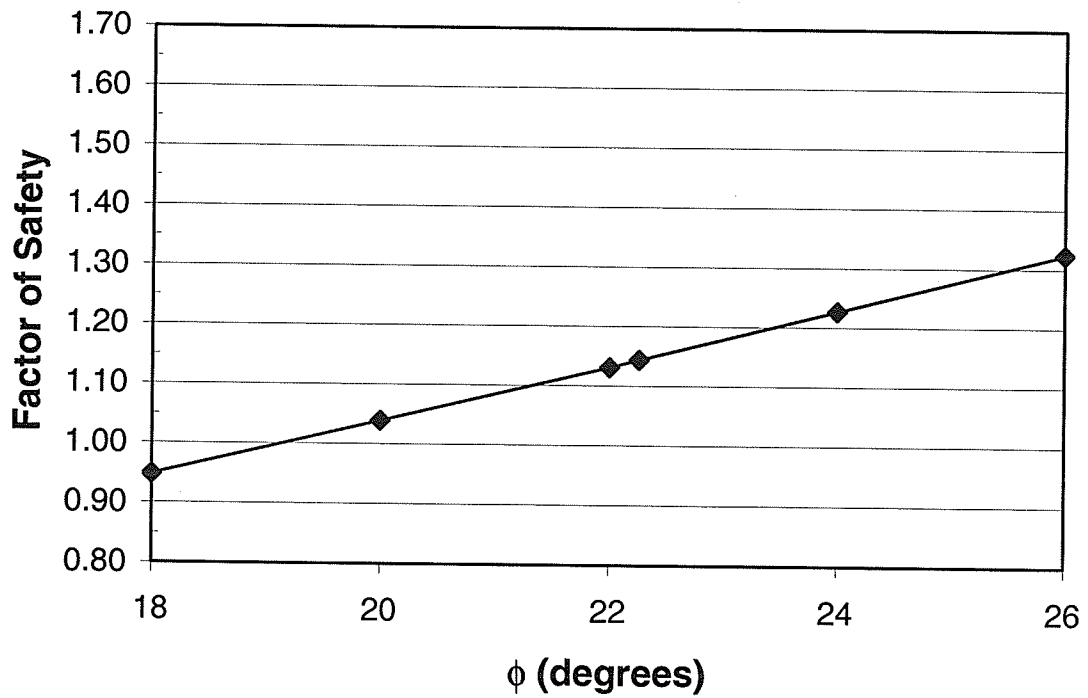


Figure 6.31 Factor of safety *versus* ϕ of the weathered and unweathered clay for May 15, 1999.

Chapter 7

Summary and Conclusions

7.0 Summary

Two bowl-shaped failures that occurred along the PR 259 highway cut were a direct result of the slope geometry, nature of material, and dissipation of soil suction that caused a significant reduction of available shear strength.

The soil profile at the location of the two failures was heterogeneous. The material encountered during the field investigation included glacial till, lacustrine clay, alluvium and colluvium, silt, and fine sand. The complex soil profile was a direct result of the complex geology and geomorphology. The field investigation included four boreholes, two test pits and several hand augured holes with several standpipe piezometer installations.

A Quick-draw Tensiometer was used to obtain matric suction profiles in the soil during excavation of the test pits. Readings with the Tensiometer were taken at 0.5 metre intervals during the excavation. The suction profile was then used to

calibrate the detailed transient Seep/W model. The tensiometer was a valuable tool and played a significant role in determining the stability of the slope.

During the field investigation, failure surfaces were observed in two test pits and in extracted samples retrieved from the study area. A majority of the fractures were in-filled with gray, silty, fine sand and were surrounded by lacustrine clay or "till like" material (Figure 4.20). The presence of the silty fine sand in a fracture of clay or till implies that the material is not native and was transported by water from its origin. The remaining failure surfaces were slickensided in nature as exhibited in Test pit 2 (Figure 4.14 – 4.16). A slickensided failure surface was observed in Test pit 1 in what was previously thought to be intact material. The inclination of the failure surface ($\sim 22^\circ$) was slightly above the inclination of the slope ($\sim 17^\circ$). The inclination of the slope and the observed failure surface is close to ϕ'_{nc} determined from the laboratory program and used in the slope stability analysis. The ϕ_{nc} (ϕ_r for Direct Shear) frictional angle was chosen based on the block/friable nature of the material and the fact the slope has undergone past movements.

Information from the field investigation and laboratory testing program was compiled, organized and incorporated into an integrated seepage and slope analysis using the Seep/W and Slope/W computer applications. A preliminary model was constructed in Seep/W and Slope/W to obtain an understanding of the role and effect that soil suction has on slope stability. The preliminary model

defined only one representative soil with averaged soil parameters. The results from the preliminary model showed that during normal dry conditions the slope was stable, while during normal wet conditions the slope remained stable only because of the contribution of soil suction to available shear strength.

Upon completion of the preliminary model, a more detailed transient model was constructed to improve the understanding of the influence of rainfall duration and intensity on dissipation of soil suction. An environmental flux boundary was incorporated into the detailed transient model to simulate rainfall and evapotranspiration. Construction of the more detailed Seep/W model used four distinct soil layers. Several assumptions were required for constructing the model. The effects of these assumptions were examined in the sensitivity section (6.4). The detailed Seep/W model used the same cross-section and mesh design as the preliminary model. The majority of boundary conditions used the detailed Seep/W model were the same as the preliminary model with the exception for an environmental flux boundary applied to the slope face and a recharge flux applied to the silty fine sand seam. The majority of the soil parameters were either determined or inferred from information gathered from the field investigation and the laboratory testing program. The SWCC and the hydraulic conductivity functions were determined from predictive models discussed in sections 2.3 and 2.4. The SWCC and the hydraulic conductivity function for the silty fine sand seam and the weathered clay layer were adjusted to provide a better representation of their inherent material properties.

Once the detailed transient Seep/W model was constructed, it was calibrated using measured water levels and *in-situ* suctions for the year 2000. The magnitude of evapotranspiration and the runoff coefficients based on return period were adjusted during calibration. The evapotranspiration was determined using an empirical equation developed by Meyer (1944). The equation requires temperature, relative humidity and wind speed data. During the early stages of calibration, modeling of the slope was extremely sensitive to intense rainfall events since the upper soil never became de-saturated, nullifying storage capabilities. Consequently, a storage function was built into the Seep/W model by shifting the SWCC of the weathered clay layer to allow de-saturation of the upper soil. After calibration, it was evident (96.3% reduction in evapotranspiration) that the Meyer (1944) equation could not estimate evapotranspiration effectively in this application. The results of the calibrated model showed good agreement with the measured water levels and reasonable correlation with the measured suction profile. Due to the coupled nature of the water levels and suction profile, further refinement was not undertaken.

After calibration, 1998, 1999 and calibration year 2000 were analyzed using the detailed transient Seep/W model. The seepage results showed that there was direct correlation between the selected environmental flux boundary condition and the change of total head at a node (Figures 6.20 - 6.22). In addition, the environmental flux boundary condition produced almost identical trends when compared to change in suction at node (Figure 6.23). It is evident that the

environmental flux boundary condition plays a major role in controlling the soil/water conditions in the slope.

The detailed Slope/W model incorporated the same geometry and soil layers as the Seep/W model. The strength and density parameters assigned to the soil layers, except for the silty fine sand seam, were determined during the laboratory testing program. Typical values of strength and density parameters were assigned to the silty fine sand seam.

Pore water pressures calculated for 1998 and 1999, the suspected years of slope movements, and for the calibration year of 2000 were incorporated into the detailed Slope/W model. The calibration year 2000 produced calculated Factors of Safety that were never lower than 1.72 (Figures 6.24). The results for 1998, and 1999 indicated several periods where the slope was unstable ($F.S. \approx 1.04$, Figures 6.24 and 6.25) and numerous periods with only marginal stability ($F < 1.4$). Both 1998 and 1999 exhibited roughly the same numbers of periods that were unstable or only marginally stable, all of them occurring in May to June. Since significant rainfall events of 1998 were of short duration and high intensity while the 1999 significant rainfall events were of low intensity and long duration, it is suspected that slope movements occurred in June 1999. After June, in all three years, the calculated factors of safety fell within the same range ($F.S. \approx 2.0$), suggesting a natural equilibrium.

The influence of suction on available shear strength during unstable and stable years, differed considerably. It is evident in Figures 6.26 and 6.27 that shear strength due to suction contributed significantly to the available frictional shear strength during normal operating conditions. However, during significant rainfall events of low intensity and long duration, rainfall infiltration dissipates the soil suction, and produces 'unstable' factors of safety that can trigger slope movements. Significant rainfall events most likely occur during wetter periods from spring thaw to early summer.

A sensitivity analysis was performed to determine the impact of adjusted, assumed or estimated model parameters on the outcome of the integrated model. The sensitivity analysis was performed by adjusting the following model parameters; recharge into the silty fine sand seam, ϕ' of the silty fine sand seam and the magnitude of evapotranspiration. The amount of recharge into the silty fine sand seam and its estimated ϕ' , have little influence the factor of safety (Figure 6.29, 6.30). However, the magnitude of evapotranspiration has considerable impact on the calculated factor of safety, especially at higher values. The effect of evapotranspiration on stability, the inability to estimate evapotranspiration effectively, and the fact that the soil/water conditions of the slope depend on the defined environmental flux boundary warrants further development of methods for estimating or obtaining accurate evapotranspiration data to increase the confidence level in determining the stability of a slope like the one examined.

7.1 Conclusions

The primary conclusions that can be drawn from this research project are as follows:

1. Soil suction can contribute significantly to the total available shear strength in unsaturated materials. In many cases suction may be the dominant strength component to maintain stable conditions for a slope.
2. Infiltration of rainfall into a soil profile reduces the suction, thereby reducing available shear strength.
3. Near surface soil/water conditions are dominated by the weather conditions that can be modeled using known theories that incorporate time-dependent environmental parameters.
4. The sensitivity analysis of the strength and flow boundary conditions in this project demonstrated that the most significant parameter for the determination of stability was the characterization of the environmental boundary conditions.
5. The integrated use of finite element seepage analysis and limit equilibrium stability analysis allowed for examination and quantification of the time-dependent environmental conditions which dominated the stability.
6. Extensive rainfall events of long duration and short intensities facilitate infiltration over high intensity, low duration events. These events are

most likely to occur in spring to early summer and are critical in terms of slope stability.

The secondary conclusions are;

1. Reduction of available shear strength due to dissipation of soil suction will generally cause shallow sliding failures where the failure will initiate below the crest and exit above the toe.
2. Methods for predicting the SWCC and hydraulic conductivity function can be used with confidence when no experimental methods are feasible.
3. Hydraulic properties of medium plastic clays can facilitate rainfall infiltration if the material is block/friable and within a zone of weathering, and freeze/thaw cycles.
4. Preliminary modeling is a necessary step in order to develop detailed models that effectively represents *in-situ* soil conditions.

7.2 Limitations of the Research

The limitations of the research for the most part were directly related to the heterogeneity of the profile and the soil itself. As with most research projects, the limited amount of money available for the field program restricted the number of boreholes, tests pits, and instruments that can be installed.

The limited number of boreholes made it difficult to get a clear picture of the soil profile in this heterogeneous study area. This difficulty was especially evident in determining the location and thickness of the seam of silty fine sand. In addition, the limited number and depth of the boreholes minimized the quantity of retrieved soil samples that were available for the laboratory program. The minimal amount of soil samples restricted the possibilities of the laboratory testing program to the essentials and eliminated auxiliary tests like determining SWCC using a desiccator.

The "till-like" heterogeneous material decreased the flexibility of the laboratory testing program and restricted the potential for suitable laboratory samples. The nature of the material restricted the triaxial sample size to the size of Shelby tubes used. Difficulties were also encountered in selecting representative samples to obtain proper *in-situ* soil parameters. A laboratory sample tested in the either triaxial, direct shear or flexible wall permeameter apparatuses needs to be intact, and be able to withstand the installation process with only a limited amount of sample disturbance. Selecting the most "ideal" laboratory sample can deviate considerable from the most "representative" sample. Laboratory samples used in the research were selected to best represent the *in-situ* soil, while having the ability to produce good laboratory results.

Due to the limited amount of field data, there were several limitations to the coupled modelling component of the research. The limited number of boreholes increased the number of assumptions in the both the Seep/W and Slope/W transient models. Some of these assumptions included several aspects of the soil profiles, the boundary condition at the crest, and the depth of the weathered clay above the silty fine sand seam. The one assumption that could potentially have the largest impact is the no flow boundary condition along the left boundary of the domain. This would probably be better represented by a variable head boundary. A variable head boundary would allow for changes in the groundwater elevation with respect to time based on environmental conditions of infiltration and evapotranspiration.

The lack of a storage component in the Seep/W computer model was one limitation that was not a result of the limited number of boreholes. As previously mentioned in Section 6.2.1.4, storage capabilities had to be built into the seepage model to allow for de-saturation the upper soil material. Adjusting the soil properties of the weathered soil to incorporate storage (primary and secondary) somewhat takes away from the premise of computer modelling. Computer modelling represents the physical model based on observations and retrieved data. The author hopes that a suitable storage function can be incorporated into later versions of the Seep/W computer program.

References

- Aubertin, M., Ricard, J-F., Chapuis, R.P., 1998. A predictive model for the water retention curve: application to tailings from hard rock mines. *Canadian Geotechnical Journal* **35**: 55-69.
- Bear, J. Dynamics of fluids in porous media. New York: Dover Publications, 1972
- Bedient, P.B., Huber, W.C. Hydrology and Floodplain Analysis. 2nd edition. USA: Addison-Wesley Publishing Company, 1992
- Betcher, R.N. 1983. Groundwater Availability Map Series, Manitoba Natural resources Water Resources, Virden Area (62-F)
- Brooks, R.H., and Corey, A.T. 1964. Hydraulic properties of porous media. Colorado State University, Hydrology paper **3**.
- Brooks, R.H., and Corey, A.T. 1966. Properties of porous media affecting fluid flow. *Transactions of the American Society of American Engineers*, **24**: 335-339
- Brunsdeon, D., and Prior, D.B., *editors*. Slope Instability; Graham, J. Methods of stability analysis. Chapter **6**: 171-215 . Toronto: John Wiley and Sons, 1984 Inc.,
- Burdine, N. T. 1953. Relative permeability calculations from pore-size distribution data. *Petr. Trans., Am. Inst. Mining Metall. Eng.* **198**: 71-77
- Domaschuk, L. 1977. Soil Block Sampler. *Canadian Geotechnical Journal* **14**: 262-265
- Edlefsen, N.E., Anderson, A.B.C. 1943. Thermodynamics of soil moisture. *Hilgardia* **15**:31-298.
- Ferreira, N.J., Blatz, J.A., Graham, J., and Kenyon, R.M. 2001 Examination of instability in an unsaturated highway cut. *In Proceedings of 54th Canadian Geotechnical Conference, Calgary, Alberta.*
- Fredlund, D.G, and Krahn, J. 1977. Comparison of slope stability methods of analysis. *Canadian Geotechnical Journal* **14**: 429-439.
- Fredlund, D.G., and Morgenstern, N. R. 1977. Stress state variables for unsaturated soils. *American Society for Civil Engineers, Geotech.Eng. Div.,GT5* **103**: 447-466.
- Fredlund, D.G., and Morgenstern, N. R., and Widger, R.A. 1978. The Shear strength of unsaturated soils. *Canadian Geotechnical Journal* **15**: 313-321

- Fredlund, D.G., and Rahardjo, H., Soil mechanics for unsaturated soils. New York: John Wiley & Sons, Inc., 1993.
- Fredlund, D.G., and Xing, A. 1994. Equations for the soil-water characteristic curve. *Canadian Geotechnical Journal* **31**: 521-532.
- Fredlund, D.G., Xing, A and Huang, S. 1994. Predicting the permeability function for an unsaturated soil using the soil-water characteristic curve. *Canadian Geotechnical Journal* **31**: 533-546.
- Geo-slope International Ltd. User's Guide Seep/W for finite element seepage analysis. Canada: Geo-slope International Ltd., Version 3: Chapter 8: 8-9 – 8-10.
- Gonzalez, P.A., and Adams, B.J. 1980. Mine tailings disposal: laboratory characterization of tailings. Department of Civil Engineering, University of Toronto, Canada. 1-14.
- Hillel, D. Applications of soil physics. New York: Academic Press, 1980.
- Klassen, R.W. and Wyder, J.E. 1970. Bedrock topography, buried valleys and nature of drift, Virden map-area, Geological Survey of Canada, Paper 70-56
- Klassen, R.W. 1975. Quaternary Geology and Geomorphology of Assiniboine and Qu'Appelle Valleys of Manitoba and Saskatchewan, Geological Survey of Canada, Bulletin 228
- Kovács, G. Seepage hydraulics. Amsterdam: Science Publishers, 1981
- Krahn, J., Fredlund, D.G. and Klassen, M. J. 1989. Effect of soil suction on slope stability at Notch Hill. *Canadian Geotechnical Journal*, **26**: 269-278.
- Meyer, A.F., 1944. Evaporation from lakes and reservoirs. Minnesota Resources Commission, St Paul.
- Mitchell, J.K. Fundamentals of soil behavior. 2nd edition. New York: John Wiley & Sons, Inc., 1993.
- Morgenstern, N.R. and Price, V.E. 1965. Stability of General Slip Surfaces. *Geotechnique* **15**: 79-93
- Morris, P.H., Graham, J. and Williams, D.J. 1992. Cracking in drying soils. *Canadian Geotechnical Journal* **29**: 263-277.
- Mualem, Y. 1976. A new model for predicting the hydraulic conductivity of unsaturated porous media. *Water Resources Res.* **12**: 513-522

- Penman, H.L. 1948., Natural evapotranspiration from open water, bare soils and grass. *In* Proceedings of the Royal Society of London, Series A, **193**: 120-145
- Prior, D.B., and Graham, J. 1974. Landslides in the Magho district of Fermanagh, Northern Ireland. *Engineering Geology* **8**:341-359.
- Richards, B.G. 1965. Measurement of the free energy of soil moisture by the Psychrometric technique using Thermistors. Moisture equilibria and moisture changes in soils beneath covered areas, a symposium in print. Australia: Butterworths: 39-46.
- Rivard, P.J. and Lu, Y. 1978. Shear Strength of Soft Fissured Clay. *Canadian Geotechnical Journal*, **15**: 382-390.
- Ross, P.J., Williams, J., and Bristow, K.L. 1991. Equation for extending water-retention curves to dryness. *Soil Society of America Journal* **5**: 923-927.
- Skempton, A.W. 1964. Long-term stability of clay slopes. *Geotechnique* **14**:77-102.
- Spencer, E. 1967. A method of analysis of the stability of embankments assuming parallel inter-slice forces. *Geotechnique* **17**: 11-26.
- Shaw, R.J., Hendry, M.J. 1998. Hydrogeology of a thick clay till and Cretaceous clay sequence, Saskatchewan, Canada. *Canadian Geotechnical Journal* **35**: 1041-1052
- Terzaghi, K. 1936. The shear resistance of saturated soils. *Proceedings 1st international conference on soil mech. found. eng., Cambridge, MA.* **1**: 54-56
- Vanapalli, S.K., Fredlund, D.G., Pufahl, D.E., and Clinton, A.W. 1996. Model for prediction of shear strength with respect to soil suction. *Canadian Geotechnical Journal* **33**: 379-392.
- van Genuchten, M. Th. 1980. A close form equation for predicting the hydraulic conductivity of unsaturated soils. *Soil Science Society of American Journal* **44**: 892-898
- Viklander, P. 1998. Permeability and volume change in till due to cyclic freeze/thaw *Canadian Geotechnical Journal* **35**: 471-477
- Wilson, G.W., Fredlund, D.G., and Barbour, S.L. 1997. The effect of soil suction on evaporative from soil surfaces. *Canadian Geotechnical Journal* **34**: 145-155

Appendix A: Hand Augured Field Logs



Geotechnical Laboratory - Field Drilling Log

Department of Civil and Geological Engineering
University of Manitoba
Winnipeg, Manitoba, R3T 5V6

HOLE# A1

SHEET 1 of 3

SITE/LOCATION PR 259

CLIENT Dept. of Highways

CONTRACTOR _____

PROJECT _____

DRILL RIG _____

PROJECT No. M. Sc.

METHOD Hand Auger

LOGGED BY Nelson Ferreira

DATE July 12, 2000

PLASTIC SOILS

SOIL TYPE- COLOUR, MOISTURE CONTENT
CONSISTENCY, PLASTICITY, MISC. OBSER.
(ie. ORGANICS, OXIDATION, STRUCTURES, ETC.)

SOIL DESCRIPTION KEY

TRACE: 0- 10% BOULDERS: > 200 mm ϕ COARSE SAND: 2-4.75 mm ϕ
SOME: 10- 20% COBBLES: 75- 200 mm ϕ MEDIUM SAND: .425-2 mm ϕ
WITH: 20- 35% COARSE GRAVEL: 19-75 mm ϕ FINE SAND: .075-.425 mm ϕ
AND: 35- 50% FINE GRAVEL 4.75- 19 mm ϕ FINES: <.075 mm ϕ

PLASTIC SOILS

SOIL TYPE- COLOUR, MOISTURE CONTENT
DENSITY, GRADATION, GRAIN SIZE, MISC. OBSER.
(ie. FINES, COBBLES, OXIDATION, DEPOST. STR., ETC.)

DEPTH	SOIL DESCRIPTION	SAMPLE					MISC. TESTS
		Sample #	Type	Depth	Sample Cont.	Recov. Length	
0 - 5"	Silty, fine sand loam - Dark gray, dry, no consistency, no plasticity, trace oxidation, trace clay, shale and organics, 0-4.75mm	A1-1	A	6"			
5" - 9"	same as above except grey, some clay, moist, medium plasticity,	A1-2	A	9"			
9" - 15"	same as above	A1-3	A	13"			
15" - 24"	Clayey silt - dark gray, moist, soft, low plasticity, trace of oxidation, some fine sand, trace clay shale 15mm	A1-4	A	20"			
24" - 34"	Clayey silt - dark gray, moist, soft, low plasticity, trace of oxidation, some fine sand, trace of clay shale	A1-5	A	26"			
34" - 41"	Silty clay - dark grey, moist, soft, medium plasticity, trace of oxidation, trace of fine sand, trace blocky friable structure, trace of clay shale <4.75mm	A1-6	A	37"			
41" - 48"	Silty clay - dark gray, moist, low to medium plasticity, stiff, trace blocky/friable structure, some oxidation, some fine sand	A1-7	A	44"			
48" - 55"	Silty Clay - dark gray, moist, low stiffness, blocky friable, some oxidation, some fine sand, medium plasticity, trace of organics	A1-8	A	52"			
55" - 60"	Silty Clay - dark grey, moist, low stiffness, blocky friable, medium plasticity, some oxidation, some fine sand	A1-9	A	59"			

SAMPLE TYPE

T - SHELBY TUBE
A - AUGER CUTTINGS
C - CORE
SB - SPLIT BARREL
W - WASH

SAMPLE CONTAINERS

O - TUBE
G - GLASS JAR
P - MOISTURE TIN
B - BAG

MISC. TESTS

T - TORVANE
H - HEADSPACE VAPOURS
SPT - STD. PENETR. TEST
DCT - DYN CONE TEST

WELL DETAILS/NOTES:

_____	_____
_____	_____
_____	_____
_____	_____
_____	_____
_____	_____

_____	Depth (ft.)
_____	_____
_____	_____
_____	_____
_____	_____
_____	_____



Geotechnical Laboratory - Field Drilling Log

Department of Civil and Geological Engineering
University of Manitoba
Winnipeg, Manitoba, R3T 5V6

HOLE# A1

SHEET 2 of 3

SITE/LOCATION PR 259

CLIENT Dept. of Highways

CONTRACTOR _____

PROJECT _____

DRILL RIG _____

PROJECT No. M. Sc.

METHOD Hand Auger

LOGGED BY Nelson Ferreira

DATE July 12, 2000

PLASTIC SOILS
SOIL TYPE- COLOUR, MOISTURE CONTENT
CONSISTENCY, PLASTICITY, MISC. OBSER.
(ie. ORGANICS, OXIDATION, STRUCTURES, ETC.)

SOIL DESCRIPTION KEY
TRACE: 0-10% BOULDERS: > 200 mmφ
SOME: 10-20% COBBLES: 75-200 mmφ
WITH: 20-35% COARSE GRAVEL: 19-75 mmφ
AND: 35-50% FINE GRAVEL: 4.75-19 mmφ
COARSE SAND: 2-4.75 mmφ
MEDIUM SAND: .425-2 mmφ
FINE SAND: .075-.425 mmφ
FINES: <.075 mmφ

PLASTIC SOILS
SOIL TYPE- COLOUR, MOISTURE CONTENT
DENSITY, GRADATION, GRAIN SIZE, MISC. OBSER.
(ie. FINES, COBBLES, OXIDATION, DEPOST. STR., ETC.)

DEPTH	SOIL DESCRIPTION	SAMPLE					MISC. TESTS
		Sample #	Type	Depth	Sample Cont.	Recov. Length	
60" - 68"	Silty Clay - dark gray, moist, soft, blocky, friable, some oxidation, some fine sand, medium plasticity	A1-10	A	64"			
68" - 73"	Silty Clay - dark gray, moist, soft, blocky, friable, some oxidation, some tan fine sand, medium plasticity	A1-11	A	70"			
73" - 78"	Silty Clay - dark gray, moist, soft, blocky, friable, some oxidation, some tan fine sand, medium plasticity	A1-12	A	75"			
78" - 83"	Silty Fine Sand - dark tan sand and silt, wet, soft, no structure, trace clay, no plasticity, trace of clay shale, 0 - 4.75mm	A1-13	A	80"			
83" - 89"	Silty Fine Sand - Dark tan, wet, soft, no plasticity, free water, dilative, trace of clay	A1-14	A	85"			
89" - 95"	Silty Fine Sand - Dark tan, wet, no consistency, no plasticity, free water, dilative, trace of oxidation, trace of clay, trace of clay shale 0-4.75 mm	A1-15	A	91"			
95" - 103"	Silty Fine Sand - tan, wet no consistency, no plasticity, free water, dilative, trace of oxidation	A1-16	A	97"			
103" - 109"	Silty Fine Sand - dark tan, wet, no consistency, no plasticity, free water, dilative, very soft	A1-17	A	106"			

SAMPLE TYPE

T - SHELBY TUBE
A - AUGER CUTTINGS
C - CORE
SB - SPLIT BARREL
W - WASH

SAMPLE CONTAINERS

O - TUBE
G - GLASS JAR
P - MOISTURE TIN
B - BAG

MISC. TESTS

T - TORVANE
H - HEADSPACE VAPOURS
SPT - STD. PENETR. TEST
DCT - DYN CONE TEST

WELL DETAILS/NOTES:

_____	_____
_____	_____
_____	_____
_____	_____
_____	_____
_____	_____

Depth (ft.)



SHEET 3 of 3

SITE/LOCATION PR 259

CLIENT Dept. of Highways

CONTRACTOR

PROJECT

DRILL RIG

PROJECT No.

METHOD Hand Auger

LOGGED BY Nelson Ferreira

DATE July 12, 2000

PLASTIC SOILS

SOIL TYPE- COLOUR, MOISTURE CONTENT
CONSISTENCY, PLASTICITY, MISC. OBSER.
(i.e. ORGANICS, OXIDATION, STRUCTURES, ETC.)

SOIL DESCRIPTION KEY

TRACE: 0- 10%	BOULDERS: > 200 mmφ	COARSE SAND: 2-4.75 mmφ
SOME: 10- 20%	COBBLES: 75- 200 mmφ	MEDIUM SAND: .425-2 mmφ
WITH: 20 -35%	COARSE GRAVEL: 19-75 mmφ	FINE SAND: .075-.425 mmφ
AND: 35- 50%	FINE GRAVEL 4.75- 19 mmφ	FINES: <.075 mmφ

PLASTIC SOILS

SOIL TYPE- COLOUR, MOISTURE CONTENT
DENSITY, GRADATION, GRAIN SIZE, MISC. OBSER.
(ie. FINES, COBBLES, OXIDATION, DEPOST. STR.,
ETC.)

[illegible]

SAMPLE TYPE T - SHELBY TUBE A - AUGER CUTTINGS C - CORE SB - SPLIT BARREL W - WASH	SAMPLE CONTAINERS O - TUBE G - GLASS JAR P - MOISTURE TIN B - BAG	WELL DETAILS/NOTES: <div> <div></div> <div></div> <div></div> <div></div> <div></div> <div></div> <div></div> <div></div> <div></div> <div></div> </div>	<div> <div></div> <div></div> <div></div> <div></div> <div></div> <div></div> <div></div> <div></div> <div></div> <div></div> </div>	Depth (ft.) <div> <div></div> <div></div> <div></div> <div></div> <div></div> <div></div> <div></div> <div></div> <div></div> <div></div> </div>
	MISC. TESTS T - TORVANE H - HEADSPACE VAPOURS SPT - STD. PENETR. TEST DCT - DYN CONE TEST			



LOGGED BY N. Ferreira/G. Siemens DATE Aug. 17, 2000

PLASTIC SOILS
SOIL TYPE- COLOUR, MOISTURE CONTENT
DENSITY, GRADATION, GRAIN SIZE, MISC. OBSER.
(ie. FINES, COBBLES, OXIDATION, DEPOST. STR.,
ETC.)

0.3 m

1.7 m

3.3 m

3.8 m

SITE/LOCATION PR 259

CLIENT Dept. of Highways

CONTRACTOR

PROJECT

DRILL RIG


PROJECT No.	M. Sc.
-------------	--------

METHOD

LOGGED BY N. Ferreira/G. Siemens DATE Aug. 17, 2000

PLASTIC SOILS	SOIL DESCRIPTION KEY			PLASTIC SOILS
SOIL TYPE- COLOUR, MOISTURE CONTENT CONSISTENCY, PLASTICITY, MISC. OBSER. (ie. ORGANICS, OXIDATION, STRUCTURES, ETC.)	TRACE: 0- 10% SOME: 10- 20% WITH: 20- 35% AND: 35- 50%	BOULDERS: > 200 mm ϕ COBBLES: 75- 200 mm ϕ COARSE GRAVEL: 19-75 mm ϕ FINE GRAVEL 4.75- 19 mm ϕ	COARSE SAND: 2-4.75 mm ϕ MEDIUM SAND: .425-2 mm ϕ FINE SAND: .075-.425 mm ϕ FINES: < .075 mm ϕ	SOIL TYPE- COLOUR, MOISTURE CONTENT DENSITY, GRADATION, GRAIN SIZE, MISC. OBSER. (ie. FINES, COBBLES, OXIDATION, DEPOST. STR., ETC.)

[illegible]

SAMPLE TYPE	SAMPLE CONTAINERS	WELL DETAILS/NOTES:				Depth (ft.)
	MISC. TESTS					
T - SHELBY TUBE	O - TUBE					
A - AUGER CUTTINGS	G - GLASS JAR				Cuttings	3.3 m
C - CORE	P - MOISTURE TIN					
SB - SPLIT BARREL	B - BAG				Bentonite	4.1 m
W - WASH						
			</			



Geotechnical Laboratory - Field Drilling Log

Department of Civil and Geological Engineering
University of Manitoba
Winnipeg, Manitoba, R3T 5V6

HOLE# **A4**

SHEET **1 of 2**

SITE/LOCATION **PR 259**

CLIENT **Dept. of Highways**

CONTRACTOR

PROJECT

DRILL RIG

PROJECT No. **M. Sc.**

METHOD **Hand Auger**

LOGGED BY **N. Ferreira/G. Siemens**

DATE **Aug. 17, 2000**

PLASTIC SOILS	SOIL DESCRIPTION KEY			PLASTIC SOILS
SOIL TYPE- COLOUR, MOISTURE CONTENT CONSISTENCY, PLASTICITY, MISC. OBSER. (ie. ORGANICS, OXIDATION, STRUCTURES, ETC.)	TRACE: 0- 10% SOME: 10- 20% WITH: 20 -35% AND: 35- 50%	BOULDERS: > 200 mm ϕ COBBLES: 75- 200 mm ϕ COARSE GRAVEL: 19-75 mm ϕ FINE GRAVEL 4.75- 19 mm ϕ	COARSE SAND: 2-4.75 mm ϕ MEDIUM SAND: .425-2 mm ϕ FINE SAND: .075-.425 mm ϕ FINES: <.075 mm ϕ	SOIL TYPE- COLOUR, MOISTURE CONTENT DENSITY, GRADATION, GRAIN SIZE, MISC. OBSER. (ie. FINES, COBBLES, OXIDATION, DEPOST. STR., ETC.)

DEPTH	SOIL DESCRIPTION	SAMPLE					MISC. TESTS
		Sample #	Type	Depth	Sample Cont.	Recov. Length	TYPE/RESULTS
	Location - 12.9 m west of BH-3, 1.65 m up from A2 along slope						
0' - 1'	Fine Sandy Silt - light to medium gray, dry, no consistence, no structure, no plasticity, trace of medium sand to coarse gravel, trace of organics, trace of gypsum	A4-1		1'			
1' - 2'	Silty Fine Sand - tan, dry, no consistency, no structure, no plasticity, trace of medium sand to coarse gravel, trace of organics, trace to some oxidation between 1'6" - 2', trace of gypsum	A4-2		1.5'			
2' - 3'	Silty Fine Sand - tan, dry, no consistency, no structure, no plasticity, trace of medium sand to coarse gravel, trace of organics, trace to some oxidation	A4-3		2.5'			
3' - 5'	Silty Clay - medium to dark grey, moist, no structure, low to medium plasticity, free water at 4' 6", with tan fine sand, trace of medium to coarse gravel, trace of oxidation, trace of clay shale	A4-4 A4-5		3' - 4' 4' - 5'			
5' - 6'	Silty Clay - medium to dark grey, moist, no structure, low to medium plasticity, free water, with tan fine sand, trace of medium to coarse gravel, trace of oxidation, trace of clay shale	A4-6		5.5'			
6' - 7'	Silty Clay - medium to dark grey, moist, no structure, low to medium plasticity, free water, with tan fine sand, trace of medium to coarse gravel, trace of oxidation, trace of clay shale	A4-7		6.5'			

SAMPLE TYPE	SAMPLE CONTAINERS	WELL DETAILS/NOTES:			Depth (ft.)
	T - SHELBY TUBE A - AUGER CUTTINGS C - CORE SB - SPLIT BARREL W - WASH				
	MISC. TESTS T - TORVANE H - HEADSPACE VAPOURS SPT- STD. PENETR. TEST DCT - DYN CONE TEST				



LOGGED BY N. Ferreira/G. Siemens DATE Aug. 17, 2000

SOIL TYPE- COLOUR, MOISTURE CONTENT
DENSITY, GRADATION, GRAIN SIZE, MISC. OBSER.
(ie. FINES, COBBLES, OXIDATION, DEPOST. STR.,
ETC.)

1

11' 2"



DATE Aug. 17, 2000

SOIL TYPE- COLOUR, MOISTURE CONTENT
DENSITY, GRADATION, GRAIN SIZE, MISC. OBSER.
(I.e. FINES, COBBLES, OXIDATION, DEPOST. STR.,
ETC.)

T - TORVANE
H - HEADSPACE VAPOURS
SPT - STD. PENETR. TEST
DCT - DYN CONE TEST

Depth (ft.)

Appendix B: Test Pit Field Logs



Geotechnical Laboratory - Field Drilling Log

Department of Civil and Geological Engineering
University of Manitoba
Winnipeg, Manitoba, R3T 5V6

HOLE# **TP-1**

SHEET **1 of 2**

SITE/LOCATION **PR259** CLIENT **M. Sc.**
CONTRACTOR **Department of Highways** PROJECT **PR259 Slope Failure**
DRILL RIG **Back Hoe** PROJECT No. _____
METHOD **Test Pit** LOGGED BY **N. Ferreira/G. Siemens** DATE **Jul. 24, 2000**

PLASTIC SOILS	SOIL DESCRIPTION KEY				PLASTIC SOILS
SOIL TYPE- COLOUR, MOISTURE CONTENT CONSISTENCY, PLASTICITY, MISC. OBSER. (ie. ORGANICS, OXIDATION, STRUCTURES, ETC.)	TRACE: 0- 10% SOME: 10- 20% WITH: 20 -35% AND: 35- 50%	BOULDERS: > 200 mm ϕ COBBLES: 75- 200 mm ϕ COARSE GRAVEL: 19-75 mm ϕ FINE GRAVEL 4.75- 19 mm ϕ	COARSE SAND: 2-4.75 mm ϕ MEDIUM SAND: .425-2 mm ϕ FINE SAND: .075-.425 mm ϕ FINES: <.075 mm ϕ		SOIL TYPE- COLOUR, MOISTURE CONTENT DENSITY, GRADATION, GRAIN SIZE, MISC. OBSER. (ie. FINES, COBBLES, OXIDATION, DEPOST. STR., ETC.)

DEPTH	SOIL DESCRIPTION	SAMPLE					MISC. TESTS TYPE/RESULTS
		Sample #	Type	Depth	Sample Cont.	Recov. Length	
0 - 0.5m	Silty Clay Loam - medium brown, dry, low to no plasticity, some organics, some oxidation, some clay shale, trace of fine sand	TP1-1	G	0-.5	B		Tens = 75 kPa
0.5 - 1m	Silty Clay Loam - medium brown, dry, low plasticity, clay intrusions, some organics, some clay shale, some oxidation	TP1-2	G	.5-1	B		Tens = 75 kPa
1 - 1.5m	Silty Clay - dark grey, moist, medium plasticity, clay intrusions, blocky friable, clay slickenslided, some fine sand, some clay shale, trace of oxidation	TP1-3	G	1.0-1.5	B		Tens = 36 kPa
1.5 - 2.0m	Silty Clay - grey, moist, low to medium plasticity, clay intrusions, blocky friable, clay slickenslided, some fine sand, trace of oxidation, trace of organics	TP1-4 BS-2	G	1.5-2.0 1.5-1.8	B		Tens = 40 kPa PP = 2.25, 2.3 2.40 kg/sq.cm
2.0 - 2.5m	Silty Clay - dark grey, moist, section of free water, clay intrusions of medium plasticity, low plasticity overall, some fine sand, some clay shale, some oxidation, blocky friable, slickenslided	TP1-5	G	2.0-2.5	B		Tens = 0 kPa No more Tensiometer Readings
2.5 - 2.8M	Silty Clay - grey-brown, moist free water some oxidation low palsticity possible failure surface @ 2.7m angle = 15 degrees from horiz.	TP1-6 BS-3	G	2.5-2.8 2.5-2.9	B		PP = 2.5, 3.6, 2.5, 3.8 kg/sq. cm
2.8 - 3.4m	Silty Clay - dark grey, moist, free water, med. plasticity trace sand, trace oxidation, blocky friable, somewhat slickensided	TP1-7	G	2.8-3.4	B		

SAMPLE TYPE	SAMPLE CONTAINERS	WELL DETAILS/NOTES:		Depth (ft.)
	O - TUBE G - GLASS JAR P - MOISTURE TIN B - BAG MISC. TESTS T - TORVANE H - HEADSPACE VAPOURS SPT- STD. PENETR. TEST DCT - DYN CONE TEST			
T - SHELBY TUBE A - AUGER CUTTINGS C - CORE SB - SPLIT BARREL W - WASH				



DATE Jul. 25, 2000

PLASTIC SOILS
SOIL TYPE- COLOUR, MOISTURE CONTENT
density, GRADATION, GRAIN SIZE, MISC. OBSER.
(ie. FINES, COBBLES, OXIDATION, DEPOST. STR.,
ETC.)

Depth (ft.)



Geotechnical Laboratory - Field Drilling Log

Department of Civil and Geological Engineering
University of Manitoba
Winnipeg, Manitoba, R3T 5V6

HOLE# TP-2

SHEET 1 of 2

SITE/LOCATION PR259 CLIENT M. Sc.
CONTRACTOR Department of Highways PROJECT PR259 Slope Failure
DRILL RIG Back Hoe PROJECT No.
METHOD Test Pit LOGGED BY N. Ferreira/G. Siemens DATE Jul. 25, 2000

PLASTIC SOILS	SOIL DESCRIPTION KEY	PLASTIC SOILS
SOIL TYPE- COLOUR, MOISTURE CONTENT CONSISTENCY, PLASTICITY, MISC. OBSER. (ie. ORGANICS, OXIDATION, STRUCTURES, ETC.)	TRACE: 0- 10% BOULDERS: > 200 mm SOME: 10- 20% COBBLES: 75- 200 mm WITH: 20- 35% COARSE GRAVEL: 19-75 mm AND: 35- 50% FINE GRAVEL 4.75- 19 mm	SOIL TYPE- COLOUR, MOISTURE CONTENT DENSITY, GRADATION, GRAIN SIZE, MISC. OBSER. (ie. FINES, COBBLES, OXIDATION, DEPOST. STR., ETC.)

DEPTH	SOIL DESCRIPTION	SAMPLE					MISC. TESTS
		Sample #	Type	Depth	Sample Cont.	Recov. Length	
0 - 0.25m	Silty clay - light to medium grey, moist, slightly blocky friable, medium to high plasticity, trace of organics, trace of clay shale, all gradation, trace of oxidation, trace of fine sand, trace of fine gravel	TP2-1	G	0-0.25m	B		
0.25 - .6m	Silty Clay Loam - medium grey-brown, moist, no structure, some organics, no to low plasticity, some clay inclusions of medium plasticity, some fine sand, trace of clay shale, trace of oxidation	TP2-2	G	.25-.6	B		
0.6 - 1.1m	Silty Clay loam - medium grey-brown, moist, no structure, some organics, no to low plasticity, some tan fine sand, trace of clay shale, trace of oxidation, trace of fine gravel to boulders	TP2-3	G	.6-1.1	B		Tens = 36 kPa
1.1 - 1.5m	Silty Clay - medium grey-brown, moist, no structure, trace organics, trace oxidation, trace clay-shale, low plasticity, trace coarse sand	TP2-4	G	1.1-1.5	B		Tens = 42 kPa
1.5 - 1.8m	Silty Clay - medium grey-brown, trace sand, some clay shale, moist, no structure, trace organics, trace oxidation, trace coarse sand, sand pockets, clay pockets	TP2-5	G	1.5-1.8	B		Tens = 2 kPa
1.8 - 2.1m	Silty Clay - medium grey-brown, trace sand, trace organics, some oxidation, tan silt pockets, trace fine gravel, some clay-shale, low to medium plasticity, free water	TP2-6	G	1.8-2.1	B		Tens = 2 kPa
2.1 - 2.5m	Silty Clay - grey-brown, some fine sand, moist, free water, some structure, some oxidation, trace clay shale	TP2-7	G	2.1-2.5	B		

SAMPLE TYPE	SAMPLE CONTAINERS	WELL DETAILS/NOTES:		Depth (ft.)
	MISC. TESTS			
T - SHELBY TUBE	O - TUBE			
A - AUGER CUTTINGS	G - GLASS JAR			
C - CORE	P - MOISTURE TIN			
SB - SPLIT BARREL	B - BAG			
W - WASH				
	T - TORVANE			
	H - HEADSPACE VAPOURS			
	SPT - STD. PENETR. TEST			
	DCT - DYN CONE TEST			

Geotechnical Laboratory - Field Drilling Log

Department of Civil and Geological Engineering
University of Manitoba
Winnipeg, Manitoba, R3T 5V6

HOLE# TP-2

SHEET 2 of 2

SITE/LOCATION PR259

CLIENT

M. Sc.

CONTRACTOR Department of Highways

PROJECT

PR259 Slope Failure

DRILL RIG	Back Hoe
-----------	----------

PROJECT No. _____

METHOD	Test Pit
--------	----------

LOGGED BY

N. Ferreira/G. Siemens

DATE Jul. 25, 2000

PLASTIC SOILS	SOIL DESCRIPTION KEY			PLASTIC SOILS
SOIL TYPE- COLOUR, MOISTURE CONTENT CONSISTENCY, PLASTICITY, MISC. OBSER. (ie. ORGANICS, OXIDATION, STRUCTURES, ETC.)	TRACE: 0- 10% SOME: 10- 20% WITH: 20- 35% AND: 35- 60%	BOULDERS: > 200 mm COBBLES: 75- 200 mm COARSE GRAVEL: 19-75 mm FINE GRAVEL: 4.75- 19 mm	COARSE SAND: 2-4.75 mm MEDIUM SAND: .425- 2 mm FINE SAND: .075- .425 mm FINES: < .075 mm	SOIL TYPE- COLOUR, MOISTURE CONTENT DENSITY, GRADATION, GRAIN SIZE, MISC. OBSER. (ie. FINES, COBBLES, OXIDATION, DEPOST. STR., ETC.)

[illegible]

<div>SAMPLE TYPE</div> <div>T - SHELBY TUBE</div> <div>A - AUGER CUTTINGS</div> <div>C - CORE</div> <div>SB - SPLIT BARREL</div> <div>W - WASH</div>	<div>SAMPLE CONTAINERS</div> <div>O - TUBE</div> <div>G - GLASS JAR</div> <div>P - MOISTURE TIN</div> <div>B - BAG</div>	<div>WELL DETAILS/NOTES:</div> <div></div> <div></div> <div></div> <div></div> <div></div> <div></div> <div></div> <div></div> <div></div> <div></div>	<div></div> <div></div> <div></div> <div></div> <div></div> <div></div> <div></div> <div></div> <div></div> <div></div>	<div></div> <div></div> <div></div> <div></div> <div></div> <div></div> <div></div> <div></div> <div></div> <div></div>	<div></div> <div></div> <div></div> <div></div> <div></div> <div></div> <div></div> <div></div> <div></div> <div></div>	<div></div> <div></div> <div></div> <div></div> <div></div> <div></div> <div></div> <div></div> <div></div> <div></div>	<div></div> <div></div> <div></div> <div></div> <div></div> <div></div> <div></div> <div></div> <div></div> <div></div>	<div></div> <div></div> <div></div> <div></div> <div></div> <div></div> <div></div> <div></div> <div></div> <div></div>	<div></div> <div></div> <div></div> <div></div> <div></div> <div></div> <div></div> <div></div> <div></div> <div></div>	<div></div> <div></div> <div></div> <div></div> <div></div> <div></div> <div></div> <div></div> <div></div> <div></div>	<div></div> <div></div> <div></div> <div></div> <div></div> <div></div> <div></div> <div></div> <div></div> <div></div>	<div></div> <div></div> <div></div> <div></div> <div></div> <div></div> <div></div> <div></div> <div></div> <div></div>	<div></div> <div></div> <div></div> <div></div> <div></div> <div></div> <div></div> <div></div> <div></div> <div></div>	<div></div> <div></div> <div></div> <div></div> <div></div> <div></div> <div></div> <div></div> <div></div> <div></div>	<div></div> <div></div> <div></div> <div></div> <div></div> <div></div> <div></div> <div></div> <div></div> <div></div>	<div></div> <div></div> <div></div> <div></div> <div></div> <div></div> <div></div> <div></div> <div></div> <div></div>	<div></div> <div></div> <div></div> <div></div> <div></div> <div></div> <div></div> <div></div> <div></div> <div></div>	<div></div> <div></div> <div></div> <div></div> <div></div> <div></div> <div></div> <div></div> <div></div> <div></div>	<div></div> <div></div> <div></div> <div></div> <div></div> <div></div> <div></div> <div></div> <div></div> <div></div>	<div></div> <div></div> <div></div> <div></div> <div></div> <div></div> <div></div> <div></div> <div></div> <div></div>	<div></div> <div></div> <div></div> <div></div> <div></div> <div></div> <div></div> <div></div> <div></div> <div></div>	<div></div> <div></div> <div></div> <div></div> <div></div> <div></div> <div></div> <div></div> <div></div> <div></div>	<div></div> <div></div> <div></div> <div></div> <div></div> <div></div> <div></div> <div></div> <div></div> <div></div>	<div></div> <div></div> <div></div> <div></div> <div></div> <div></div> <div></div> <div></div> <div></div> <div></div>	<div></div> <div></div> <div></div> <div></div> <div></div> <div></div> <div></div> <div></div> <div></div> <div></div>	<div></div> <div></div> <div></div> <div></div> <div></div> <div></div> <div></div> <div></div> <div></div> <div></div>	<div></div> <div></div> <div></div> <div></div> <div></div> <div></div> <div></div> <div></div> <div></div> <div></div>	<div></div> <div></div> <div></div> <div></div> <div></div> <div></div> <div></div> <div></div> <div></div> <div></div>	<div></div> <div></div> <div></div> <div></div> <div></div> <div></div> <div></div> <div></div> <div></div> <div></div>	<div></div> <div></div> <div></div> <div></div> <div></div> <div></div> <div></div> <div></div> <div></div> <div></div>	<div></div> <div></div> <div></div> <div></div> <div></div> <div></div> <div></div> <div></div> <div></div> <div></div>	<div></div> <div></div> <div></div> <div></div> <div></div> <div></div> <div></div> <div></div> <div></div> <div></div>	<div></div> <div></div> <div></div> <div></div> <div></div> <div></div> <div></div> <div></div> <div></div> <div></div>	<div></div> <div></div> <div></div> <div></div> <div></div> <div></div> <div></div> <div></div> <div></div> <div></div>	<div></div> <div></div> <div></div> <div></div> <div></div> <div></div> <div></div> <div></div> <div></div> <div></div>	<div></div> <div></div> <div></div> <div></div> <div></div> <div></div> <div></div> <div></div> <div></div> <div></div>	<div></div> <div></div> <div></div> <div></div> <div></div> <div></div> <div></div> <div></div> <div></div> <div></div>	<div></div> <div></div> <div></div> <div></div> <div></div> <div></div> <div></div> <div></div> <div></div> <div></div>	<div></div> <div></div> <div></div> <div></div> <div></div> <div></div> <div></div> <div></div> <div></div> <div></div>	<div></div> <div></div> <div></div> <div></div> <div></div> <div></div> <div></div> <div></div> <div></div> <div></div>	<div></div> <div></div> <div></div> <div></div> <div></div> <div></div> <div></div> <div></div> <div></div> <div></div>	<div></div> <div></div> <div></div> <div></div> <div></div> <div></div> <div></div> <div></div> <div></div> <div></div>	<div></div> <div></div> <div></div> <div></div> <div></div> <div></div> <div></div> <div></div> <div></div> <div></div>	<div></div> <div></div> <div></div> <div></div> <div></div> <div></div> <div></div> <div></div> <div></div> <div></div>	<div></div> <div></div> <div></div> <div></div> <div></div> <div></div> <div></div> <div></div> <div></div> <div></div>	<div></div> <div></div> <div></div> <div></div> <div></div> <div></div> <div></div> <div></div> <div></div> <div></div>	<div></div> <div></div> <div></div> <div></div> <div></div> <div></div> <div></div> <div></div> <div></div> <div></div>	<div></div> <div></div> <div></div> <div></div> <div></div> <div></div> <div></div> <div></div> <div></div> <div></div>	<div></div> <div></div> <div></div> <div></div> <div></div> <div></div> <div></div> <div></div> <div></div> <div></div>	<div></div> <div></div> <div></div> <div></div> <div></div> <div></div> <div></div> <div></div> <div></div> <div></div>	<div></div> <div></div> <div></div> <div></div> <div></div> <div></div> <div></div> <div></div> <div></div> <div></div>	<div></div> <div></div> <div></div> <div></div> <div></div> <div></div> <div></div> <div></div> <div></div> <div></div>	<div></div> <div></div> <div></div> <div></div> <div></div> <div></div> <div></div> <div></div> <div></div> <div></div>	<div></div> <div></div> <div></div> <div></div> <div></div> <div></div> <div></div> <div></div> <div></div> <div></div>	<div></div> <div></div> <div></div> <div></div> <div></div> <div></div> <div></div> <div></div> <div></div> <div></div>	<div></div> <div></div> <div></div> <div></div> <div></div> <div></div> <div></div> <div></div> <div></div> <div></div>	<div></div> <div></div> <div></div> <div></div> <div></div> <div></div> <div></div> <div></div> <div></div> <div></div>	<div></div> <div></div> <div></div> <div></div> <div></div> <div></div> <div></div> <div></div> <div></div> <div></div>	<div></div> <div></div> <div></div> <div></div> <div></div> <div></div> <div></div> <div></div> <div></div> <div></div>	<div></div> <div></div> <div></div> <div></div> <div></div> <div></div> <div></div> <div></div> <div></div> <div></div>	<div></div> <div></div> <div></div> <div></div> <div></div> <div></div> <div></div> <div></div> <div></div> <div></div>	<div></div> <div></div> <div></div> <div></div> <div></div> <div></div> <div></div> <div></div> <div></div> <div></div>	<div></div> <div></div> <div></div> <div></div> <div></div> <div></div> <div></div> <div></div> <div></div> <div></div>	<div></div> <div></div> <div></div> <div></div> <div></div> <div></div> <div></div> <div></div> <div></div> <div></div>	<div></div> <div></div> <div></div> <div></div> <div></div> <div></div> <div></div> <div></div> <div></div> <div></div>	<div></div> <div></div> <div></div> <div></div> <div></div> <div></div> <div></div> <div></div> <div></div> <div></div>	<div></div> <div></div> <div></div> <div></div> <div></div> <div></div> <div></div> <div></div> <div></div> <div></div>	<div></div> <div></div> <div></div> <div></div> <div></div> <div></div> <div></div> <div></div> <div></div> <div></div>	<div></div> <div></div> <div></div> <div></div> <div></div> <div></div> <div></div> <div></div> <div></div> <div></div>	<div></div> <div></div> <div></div> <div></div> <div></div> <div></div> <div></div> <div></div> <div></div> <div></div>	<div></div> <div></div> <div></div> <div></div> <div></div> <div></div> <div></div> <div></div> <div></div> <div></div>	<div></div> <div></div> <div></div> <div></div> <div></div> <div></div> <div></div> <div></div> <div></div> <div></div>	<div></div> <div></div> <div></div> <div></div> <div></div> <div></div> <div></div> <div></div> <div></div> <div></div>	<div></div> <div></div> <div></div> <div></div> <div></div> <div></div> <div></div> <div></div> <div></div> <div></div>	<div></div> <div></div> <div></div> <div></div> <div></div> <div></div> <div></div> <div></div> <div></div> <div></div>	<div></div> <div></div> <div></div> <div></div> <div></div> <div></div> <div></div> <div></div> <div></div> <div></div>	<div></div> <div></div> <div></div> <div></div> <div></div> <div></div> <div></div> <div></div> <div></div> <div></div>	<div></div> <div></div> <div></div> <div></div> <div></div> <div></div> <div></div> <div></div> <div></div> <div></div>	<div></div> <div></div> <div></div> <div></div> <div></div> <div></div> <div></div> <div></div> <div></div> <div></div>	<div></div> <div></div> <div></div> <div></div> <div></div> <div></div> <div></div> <div></div> <div></div> <div></div>	<div></div> <div></div> <div></div> <div></div> <div></div> <div></div> <div></div> <div></div> <div></div> <div></div>	<div></div> <div></div> <div></div> <div></div> <div></div> <div></div> <div></div> <div></div> <div></div> <div></div>	<div></div> <div></div> <div></div> <div></div> <div></div> <div></div> <div></div> <div></div> <div></div> <div></div>	<div></div> <div></div> <div></div> <div></div> <div></div> <div></div> <div></div> <div></div> <div></div> <div></div>	<div></div> <div></div> <div></div> <div></div> <div></div> <div></div> <div></div> <div></div> <div></div> <div></div>	<div></div> <div></div> <div></div> <div></div> <div></div> <div></div> <div></div> <div></div> <div></div> <div></div>	<div></div> <div></div> <div></div> <div></div> <div></div> <div></div> <div></div> <div></div> <div></div> <div></div>	<div></div> <div></div> <div></div> <div></div> <div></div> <div></div> <div></div> <div></div> <div></div> <div></div>	<div></div> <div></div> <div></div> <div></div> <div></div> <div></div> <div></div> <div></div> <div></div> <div></div>	<div></div> <div></div> <div></div> <div></div> <div></div> <div></div> <div></div> <div></div> <div></div> <div></div>	<div></div> <div></div> <div></div> <div></div> <div></div> <div></div> <div></div> <div></div> <div></div> <div></div>	<div></div> <div></div> <div></div> <div></div> <div></div> <div></div> <div></div> <div></div> <div></div> <div></div>	<div></div> <div></div> <div></div> <div></div> <div></div> <div></div> <div></div> <div></div> <div></div> <div></div>	<div></div> <div></div> <div></div> <div></div> <div></div> <div></div> <div></div> <div></div> <div></div> <div></div>	<div></div> <div></div> <div></div> <div></div> <div></div> <div></div> <div></div> <div></div> <div></div> <div></div>	<div></div> <div></div> <div></div> <div></div> <div></div> <div></div> <div></div> <div></div> <div></div> <div></div>	<div></div> <div></div> <div></div> <div></div> <div></div> <div></div> <div></div> <div></div> <div></div> <div></div>	<div></div> <div></div> <div></div> <div></div> <div></div> <div></div> <div></div> <div></div> <div></div> <div></div>	<div></div> <div></div> <div></div> <div></div> <div></div> <div></div> <div></div> <div></div> <div></div> <div></div>	<div></div> <div></div> <div></div> <div></div> <div></div> <div></div> <div></div> <div></div> <div></div> <div></div>	<div></div> <div></div> <div></div> <div></div> <div></div> <div></div> <div></div> <div></div> <div></div> <div></div>	<div></div> <div></div> <div></div> <div></div> <div></div> <div></div> <div></div> <div></div> <div></div> <div></div>	<div></div> <div></div> <div></div> <div></div> <div></div> <
--	--	--	---	---	---	---	---	---	---	---	---	---	---	---	---	---	---	---	---	---	---	---	---	---	---	---	---	---	---	---	---	---	---	---	---	---	---	---	---	---	---	---	---	---	---	---	---	---	---	---	---	---	---	---	---	---	---	---	---	---	---	---	---	---	---	---	---	---	---	---	---	---	---	---	---	---	---	---	---	---	---	---	---	---	---	---	---	---	---	---	---	---	---	---	---	---	---	---	---	---	---	---	---

Appendix C: Field Borehole Logs



Geotechnical Laboratory - Field Drilling Log

Department of Civil and Geological Engineering
University of Manitoba
Winnipeg, Manitoba, R3T 5V6

HOLE# **BH 1**

SHEET **1 of 4**

SITE/LOCATION **PR 259** CLIENT **Dept. of Highways & Transportation**
CONTRACTOR **Paddock Drilling Ltd.** PROJECT **PR 259 Slope Failures**
DRILL RIG **Pads** PROJECT No. _____
METHOD **HAS & SSA** LOGGED BY **N. Ferreira/ G. Siemens** DATE **Jul 27, 2000**

PLASTIC SOILS	SOIL DESCRIPTION KEY			PLASTIC SOILS
SOIL TYPE- COLOUR, MOISTURE CONTENT CONSISTENCY, PLASTICITY, MISC. OBSER. (ie. ORGANICS, OXIDATION, STRUCTURES, ETC.)	TRACE: 0- 10% SOME: 10- 20% WITH: 20 -35% AND: 35- 50%	BOULDERS: > 200 mmφ COBBLES: 75- 200 mmφ COARSE GRAVEL: 19-75 mmφ FINE GRAVEL 4.75- 19 mmφ	COARSE SAND: 2-4.75 mmφ MEDIUM SAND: .425-2 mmφ FINE SAND: .075-.425 mmφ FINES: <.075 mmφ	SOIL TYPE- COLOUR, MOISTURE CONTENT DENSITY, GRADATION, GRAIN SIZE, MISC. OBSER. (ie. FINES, COBBLES, OXIDATION, DEPOST. STR., ETC.)

DEPTH	SOIL DESCRIPTION	SAMPLE			MISC. TESTS	
		Sample #	Type	Depth	Sample Cont.	Recov. Length
	- Surfical Boulders and Cobbles	BH1-1		10"		
0 - 20"	Silty Fine Sand Loam - medium brown to gray, dry, no structure, no plasticity, some organics, coarse sand to boulders, trace of clayshale, trace of oxidation	BH1-2	SB	15"		
20" - 40"	Silty Clay - medium gray, moist, slightly blocky, very stiff, low to medium plasticity, some fine sand to coarse gravel, some oxidation, some fine sand seams less than 2 mm	BH1-3	SB	18"		T = 1.5 kg/cm2
40" - 60"	Silty Clay - medium gray, moist, slightly blocky, very stiff, low to medium plasticity, trace of fine sand to coarse gravel, trace of oxidation, several fractures	BH1-4	SB			
	Fracture @ 45" - trace of organics					
	Fracture @ 55" - some gypsum, and oxidation					
60" - 66"	Silty Clay - medium gray, moist, blocky/friable, stiff, same as above	BH1-5	SB	60-66	18	
	Fracture @ 64" - sand seam, completely oxidized					
66" - 80"	Silty Clay - medium grey to tan brown, fine tan sand, moist, blocky/friable, very stiff in clay part, some oxidation, some fractures with gypsum in all directions, some coarse sand to coarse gravel, trace of organics, clay - low to medium plasticity	BH1-6	SB	66-80	B	

SAMPLE TYPE	SAMPLE CONTAINERS	WELL DETAILS/NOTES:		Depth (ft.)
	MISC. TESTS			
T - SHELBY TUBE	O - TUBE			
A - AUGER CUTTINGS	G - GLASS JAR			
C - CORE	P - MOISTURE TIN			
SB - SPLIT BARREL	B - BAG			
W - WASH	T - TORVANE			
	H - HEADSPACE VAPOURS			
	SPT- STD. PENETR. TEST			
	DCT - DYN CONE TEST			



Geotechnical Laboratory - Field Drilling Log

Department of Civil and Geological Engineering
University of Manitoba
Winnipeg, Manitoba, R3T 5V6

HOLE# **BH 1**
SHEET **3 of 4**

SITE/LOCATION **PR 259** CLIENT **Dept. of Highways & Transportation**
CONTRACTOR **Paddock Drilling Ltd.** PROJECT **PR 259 Slope Failures**
DRILL RIG **Pads** PROJECT No. _____
METHOD **SSA & Push Samples** LOGGED BY **N. Ferreira/ G. Siemens** DATE **Jul 27, 2000**

PLASTIC SOILS	SOIL DESCRIPTION KEY	PLASTIC SOILS
SOIL TYPE- COLOUR, MOISTURE CONTENT CONSISTENCY, PLASTICITY, MISC. OBSER. (ie. ORGANICS, OXIDATION, STRUCTURES, ETC.)	TRACE: 0- 10% BOULDERS: > 200 mmφ SOME: 10- 20% COBBLES: 75- 200 mmφ WITH: 20- 35% COARSE GRAVEL: 19-75 mmφ AND: 35- 50% FINE GRAVEL 4.75- 19 mmφ	SOIL TYPE- COLOUR, MOISTURE CONTENT DENSITY, GRADATION, GRAIN SIZE, MISC. OBSER. (ie. FINES, COBBLES, OXIDATION, DEPOST. STR., ETC.)
	COARSE SAND: 2-4.75 mmφ MEDIUM SAND: .425-2 mmφ FINE SAND: .075-.425 mmφ FINES: <.075 mmφ	

DEPTH	SOIL DESCRIPTION	SAMPLE					MISC. TESTS
		Sample #	Type	Depth	Sample Cont.	Recov. Length	
23' - 25'	Silty Clay - dark grey, moist, low to medium plasticity, some sand, some silt pockets, very stiff	BH1-12		24'	B		T = 1.9 kg/cm2
25' - 31'	Silty Clay - dark grey, low to medium plasticity, some sand, silt pockets @ 26' - 4" thick, very stiff	BH1-13		27'	B		T = 1.7 kg/cm2
31' - 34'	Fine Sand/Silt - medium grey some tan colour, moist, no plasticity, trace of oxidation, trace of clay with section of some clay	BH1-14		33'	B		
34' - 35'	Clayey Silt - varved medium grey, stiff, low to medium plasticity, some silt including pockets, some oxidation and fine sand trace of gypsum	BH1-15		34'	B		T = 1.0 kg/cm2
35' - 40'	Clayey Silt - medium to dark grey, moist, varved, stiff, some silt pockets, low to medium plasticity	BH1-16		37'	B		T = 1.95 kg/cm2
40' - 45'	Clayey Silt - medium to dark grey, moist, varved, stiff, some silt pockets, low to medium plasticity	BH1-17		43'	B		T = 1.75 kg/cm2
45' - 50'	Silty Clay - medium to dark grey, moist, slightly varved, very stiff, trace silt pockets, except from 47' - 47.5' some silt, medium to high plasticity	BH1-18		46'	B		T = 1.5 kg/cm2
50' - 55'	Silty Clay - medium to dark grey, moist slightly varved, very stiff, trace of silt pockets, except from 53' - 53.5' some silt, medium to high plasticity	BH1-19		52'	B		T = 2.0 kg/cm2

SAMPLE TYPE	SAMPLE CONTAINERS	WELL DETAILS/NOTES:		Depth (ft.)
	MISC. TESTS			
T - SHELBY TUBE	O - TUBE			
A - AUGER CUTTINGS	G - GLASS JAR			
C - CORE	P - MOISTURE TIN			
SB - SPLIT BARREL	B - BAG			
W - WASH	T - TORVANE			
	H - HEADSPACE VAPOURS			
	SPT- STD. PENETR. TEST			
	DCT - DYN CONE TEST			



Geotechnical Laboratory - Field Drilling Log

Department of Civil and Geological Engineering
University of Manitoba
Winnipeg, Manitoba, R3T 5V6

HOLE# **BH 3**

SHEET **1 of 5**

SITE/LOCATION **PR 259** CLIENT **Dept. of Highways & Transportation**
CONTRACTOR **Paddock Drilling Ltd.** PROJECT **PR 259 Slope Failures**
DRILL RIG **Pads** PROJECT No. _____
METHOD **SSA & Push Samples** LOGGED BY **N. Ferreira/ G. Siemens** DATE **Jul 27, 2000**

PLASTIC SOILS	SOIL DESCRIPTION KEY			PLASTIC SOILS
SOIL TYPE- COLOUR, MOISTURE CONTENT CONSISTENCY, PLASTICITY, MISC. OBSER. (ie. ORGANICS, OXIDATION, STRUCTURES, ETC.)	TRACE: 0- 10% SOME: 10- 20% WITH: 20 -35% AND: 35- 50%	BOULDERS: > 200 mmφ COBBLES: 75- 200 mmφ COARSE GRAVEL: 19-75 mmφ FINE GRAVEL: 4.75- 19 mmφ	COARSE SAND: 2-4.75 mmφ MEDIUM SAND: .425-2 mmφ FINE SAND: .075-.425 mmφ FINES: <.075 mmφ	SOIL TYPE- COLOUR, MOISTURE CONTENT DENSITY, GRADATION, GRAIN SIZE, MISC. OBSER. (ie. FINES, COBBLES, OXIDATION, DEPOST. STR., ETC.)

DEPTH	SOIL DESCRIPTION	SAMPLE					MISC. TESTS
		Sample #	Type	Depth	Sample Cont.	Recov. Length	
0- 3.5'	Silty Clay Loam - Dark gray, moist, firm, closed small fissures, low plasticity, some oxidation, trace of organics, gypsum and fine sand	BH3-1	A	1.5	B		T = 1.35 kg/cm2
3.5' - 5'	Silty Clay - Dark gray, moist, soft, small fissures that are closed, low to medium plasticity, some fine sand, trace of oxidation and organics	BH3-2	A	4'	B		
5' - 7'	Silty Clay - Dark gray, moist. Soft, small fissures that are closed, low to medium plasticity, some light gray silt and fine sand	BH3-3	T		O	22"	Pocket Pen = 3.5, beyond range T = 1.38 kg/cm2 @ 7'
7' - 9'	Silty Clay - Dark gray, moist, very stiff, slickensided at bottom of Shelby, medium plasticity, trace of light gray silt and fine sand	BH3-4	T		O	23.5"	PP beyond range T = 1.3 kg/cm2
9' - 11'	Silty Clay - Dark gray, moist, very stiff, medium to high plasticity, trace of light gray silty pockets	Bh3-5	T		O		PP beyond range @ 9' 4.0, 3.75, 3.7 Kg/cm2 @ 11' T = 1.75 kg/cm2
11' - 13'	Silty Clay - Dark gray, moist, very stiff, medium to high plasticity, trace of light gray silty pockets	BH3-6	T		O		PP beyond range @ 13' T = 2.0 kg/cm2

SAMPLE TYPE	SAMPLE CONTAINERS	WELL DETAILS/NOTES:		Depth (ft.)
	MISC. TESTS			
T - SHELBY TUBE A - AUGER CUTTINGS C - CORE SB - SPLIT BARREL W - WASH	O - TUBE G - GLASS JAR P - MOISTURE TIN B - BAG T - TORVANE H - HEADSPACE VAPOURS SPT- STD. PENETR. TEST DCT - DYN CONE TEST	STICK-UP ABOVE GROUND - 47 1/4" above ground level		
		Bentonite		2'
		Cuttings		13'
		Bentonite		15'
		Silica Sand		17'



Geotechnical Laboratory - Field Drilling Log

Department of Civil and Geological Engineering
University of Manitoba
Winnipeg, Manitoba, R3T 5V6

HOLE# **BH 3**

SHEET **2 of 5**

SITE/LOCATION **PR 259** CLIENT **Dept. of Highways & Transportation**
CONTRACTOR **Paddock Drilling Ltd.** PROJECT **PR 259 Slope Failures**
DRILL RIG **Pads** PROJECT No. _____
METHOD **SSA & Push Samples** LOGGED BY **N. Ferreira/ G. Siemens** DATE **Jul 27, 2000**

PLASTIC SOILS	SOIL DESCRIPTION KEY	PLASTIC SOILS
SOIL TYPE- COLOUR, MOISTURE CONTENT CONSISTENCY, PLASTICITY, MISC. OBSER. (ie. ORGANICS, OXIDATION, STRUCTURES, ETC.)	TRACE: 0- 10% BOULDERS: > 200 mmφ SOME: 10- 20% COBBLES: 75- 200 mmφ WITH: 20- 35% COARSE GRAVEL: 19- 75 mmφ AND: 35- 50% FINE GRAVEL: 4.75- 19 mmφ	SOIL TYPE- COLOUR, MOISTURE CONTENT DENSITY, GRADATION, GRAIN SIZE, MISC. OBSER. (ie. FINES, COBBLES, OXIDATION, DEPOST. STR., ETC.)

DEPTH	SOIL DESCRIPTION	SAMPLE					MISC. TESTS TYPE/RESULTS
		Sample #	Type	Depth	Sample Cont.	Recov. Length	
13' - 15'	Same as 9' - 11', shiny, possible fracture surface at bottom of shelby, except very stiff	BH3-7	T	9-11'	O	24"	T = DNR
15' - 17'	Silty Clay- Dark gray, moist, very stiff, medium to high plasticity, some silt, fine sand pockets	BH3-8	T	15-17'	O	24"	T = 1.9 kg/cm2 PP = 4.25, 4.3, 4.5 kg/cm2 @ 17'
17' - 19'	Same as 13 - 15' - bottom slickensided	BH3-9	T	17-19'	O	25"	T = 1.6 kg/cm2 @ 19' PP = DNR
20' - 25'	Silty Clay - dark gray, moist, stiff, medium plasticity, slickensided surfaces, trace of silt packets, small fissures that are closed	BH3-10	A	22'	B		T = 1.95 kg/cm2 @ 25'
	Fracture @ 5' 10" - dark grays and browns, somewhat slickensided with small closed fissures for half the cross-section, other half tan fine sand and silt, trace of oxidation, horizontal						
	Fracture @ 6' 3.5" - light and dark grays, sands and silt within the fracture, Dip = 20° from horizontal						
	Fracture @ 6' 6" - slickensided, dark gray and dark browns, some tan silt and sand, trace of oxidation, somewhat blocky						
	Fracture @ 6' 7 3/4" - slickensided, dark gray and dark browns, trace of gypsum, Dip = 15° from horizontal						

SAMPLE TYPE	SAMPLE CONTAINERS	WELL DETAILS/NOTES:		Depth (ft.)
	MISC. TESTS			
T - SHELBY TUBE A - AUGER CUTTINGS C - CORE SB - SPLIT BARREL W - WASH	O - TUBE G - GLASS JAR P - MOISTURE TIN B - BAG T - TORVANE H - HEADSPACE VAPOURS SPT- STD. PENETR. TEST DCT - DYN CONE TEST	STICK-UP ABOVE GROUND - 47 1/4 " above ground level		
		Bentonite		2'
		Cuttings		13'
		Bentonite		15'
		Silica Sand		17'



Geotechnical Laboratory - Field Drilling Log

Department of Civil and Geological Engineering
University of Manitoba
Winnipeg, Manitoba, R3T 5V6

HOLE# BH 3
SHEET 3 of 5

SITE/LOCATION PR 259 CLIENT Dept. of Highways & Transportation
CONTRACTOR Paddock Drilling Ltd. PROJECT PR 259 Slope Failures
DRILL RIG Pads PROJECT No. _____
METHOD SSA & Push Samples LOGGED BY N. Ferreira/ G. Siemens DATE Jul 27, 2000

PLASTIC SOILS	SOIL DESCRIPTION KEY			PLASTIC SOILS
SOIL TYPE- COLOUR, MOISTURE CONTENT CONSISTENCY, PLASTICITY, MISC. OBSER. (ie. ORGANICS, OXIDATION, STRUCTURES, ETC.)	TRACE: 0- 10% SOME: 10- 20% WITH: 20 -35% AND: 35- 50%	BOULDERS: > 200 mmφ COBBLES: 75- 200 mmφ COARSE GRAVEL: 19-75 mmφ FINE GRAVEL 4.75- 19 mmφ	COARSE SAND: 2-4.75 mmφ MEDIUM SAND: .425-2 mmφ FINE SAND: .075-.425 mmφ FINES: <.075 mmφ	SOIL TYPE- COLOUR, MOISTURE CONTENT DENSITY, GRADATION, GRAIN SIZE, MISC. OBSER. (ie. FINES, COBBLES, OXIDATION, DEPOST. STR., ETC.)

DEPTH	SOIL DESCRIPTION	SAMPLE					MISC. TESTS
		Sample #	Type	Depth	Sample Cont.	Recov. Length	
	Fracture @ 6' 9 3/4" - slickensided, dark gray and dark browns, trace of gypsum, Dip = 15° from horizontal						
	Fracture @ 8' 2" - Dark browns and grays, some what blocky, trace of fine sand, silt, and oxidation, Dip = 23° from horizontal						
	Fracture @ 8' 4" - Dark browns and grays, some what blocky, trace of fine sand, silt, and oxidation, Dip = 24° from horizontal						
	Fracture @ 8' 9" - Dark browns and grays, some what blocky, trace of fine sand, silt, and oxidation, Dip = 22° from horizontal						
	Fracture @ 9' - Dark browns and grays, slickensided						
	Fracture @ 10' 10" - light and dark grays, silt and fine sand seam, blocky						
	Fracture @ 11' 7" - dark gray, slickensided, horizontal						
	Fracture @ 11' 10" - dark gray, slickensided, horizontal						
	Fracture @ 12' 1" - dark gray, slickensided, Dip = 22° from horizontal						

SAMPLE TYPE	SAMPLE CONTAINERS	WELL DETAILS/NOTES:		Depth (ft.)
	MISC. TESTS			
T - SHELBY TUBE A - AUGER CUTTINGS C - CORE SB - SPLIT BARREL W - WASH	O - TUBE G - GLASS JAR P - MOISTURE TIN B - BAG T - TORVANE H - HEADSPACE VAPOURS SPT- STD. PENETR. TEST DCT - DYN CONE TEST	STICK-UP ABOVE GROUND - 47 1/4 " above ground level		
		Bentonite		2'
		Cuttings		13'
		Bentonite		15'
		Silica Sand		17'



Geotechnical Laboratory - Field Drilling Log

Department of Civil and Geological Engineering
University of Manitoba
Winnipeg, Manitoba, R3T 5V6

HOLE# BH 3
SHEET 4 of 5

SITE/LOCATION PR 259 CLIENT Dept. of Highways & Transportation
CONTRACTOR Paddock Drilling Ltd. PROJECT PR 259 Slope Failures
DRILL RIG Pads PROJECT No. _____
METHOD SSA & Push Samples LOGGED BY N. Ferreira/ G. Siemens DATE Jul 27, 2000

PLASTIC SOILS	SOIL DESCRIPTION KEY			PLASTIC SOILS
SOIL TYPE- COLOUR, MOISTURE CONTENT CONSISTENCY, PLASTICITY, MISC. OBSER. (ie. ORGANICS, OXIDATION, STRUCTURES, ETC.)	TRACE: 0- 10% SOME: 10- 20% WITH: 20 -35% AND: 35- 50%	BOULDERS: > 200 mm ϕ COBBLES: 75- 200 mm ϕ COARSE GRAVEL: 19-75 mm ϕ FINE GRAVEL 4.75- 19 mm ϕ	COARSE SAND: 2-4.75 mm ϕ MEDIUM SAND: .425-2 mm ϕ FINE SAND: .075-.425 mm ϕ FINES: <.075 mm ϕ	SOIL TYPE- COLOUR, MOISTURE CONTENT DENSITY, GRADATION, GRAIN SIZE, MISC. OBSER. (ie. FINES, COBBLES, OXIDATION, DEPOST. STR., ETC.)

DEPTH	SOIL DESCRIPTION	SAMPLE					MISC. TESTS
		Sample #	Type	Depth	Sample Cont.	Recov. Length	TYPE/RESULTS
	Fracture @ 12' 6" - light gray, fine sadn and silt seam looks like fine sand and silt is bedded on a angle near 70°, may be rotated into place,						
	Fracture @ 13' 4" - closed						
	Fracture @ 13' 8" - light gray, somewhat slickensided, some silt pockets, some blocky/friable structure, Dip = 25° from horizontal						
	Fracture @ 14' 1" - light gray, somewhat slickensided, trace of silt pockets, some blocky/friable structure, Dip = 25° from horizontal						
	Fracture @ 14' 6" - dark gray, slickensided, Dip = 23° from horizontal						
	Fracture @ 14' 7" - light and dark grays, silt seam, trace of fine sand, slightly laminated in the roughly vertical direction, Dip = 23o from horizontal						
	Fracture @ 14' 7.5" - dark gray, slickensided, horizontal, slightly nuggety						
	Fracture @ 14' 10" - dark gray, slickensided, horizontal, slightly nuggety						
	Fracture @ 16' - Dark gray, slickensided, no real plane						

SAMPLE TYPE	SAMPLE CONTAINERS	WELL DETAILS/NOTES:		Depth (ft.)
	MISC. TESTS			
T - SHELBY TUBE A - AUGER CUTTINGS C - CORE SB - SPLIT BARREL W - WASH	O - TUBE G - GLASS JAR P - MOISTURE TIN B - BAG T - TORVANE H - HEADSPACE VAPOURS SPT - STD. PENETR. TEST DCT - DYN CONE TEST	STICK-UP ABOVE GROUND - 47 1/4 " above ground level		
		Bentonite		2'
		Cuttings		13'
		Bentonite		15'
		Silca Sand		17'



Geotechnical Laboratory - Field Drilling Log

Department of Civil and Geological Engineering
University of Manitoba
Winnipeg, Manitoba, R3T 5V6

HOLE# **BH 4**

SHEET **1 of 2**

SITE/LOCATION **PR 259** CLIENT **Dept. of Highways & Transportation**
CONTRACTOR **Paddock Drilling Ltd.** PROJECT **PR 259 Slope Failures**
DRILL RIG **Pads** PROJECT No. _____
METHOD **HAS** LOGGED BY **N. Ferreira** DATE **Jul 27, 2000**

PLASTIC SOILS	SOIL DESCRIPTION KEY			PLASTIC SOILS
SOIL TYPE- COLOUR, MOISTURE CONTENT CONSISTENCY, PLASTICITY, MISC. OBSER. (ie. ORGANICS, OXIDATION, STRUCTURES, ETC.)	TRACE: 0- 10% SOME: 10- 20% WITH: 20- 35% AND: 35- 50%	BOULDERS: > 200 mm ϕ COBBLES: 75- 200 mm ϕ COARSE GRAVEL: 19-75 mm ϕ FINE GRAVEL: 4.75- 19 mm ϕ	COARSE SAND: 2-4.75 mm ϕ MEDIUM SAND: .425-2 mm ϕ FINE SAND: .075-.425 mm ϕ FINES: <.075 mm ϕ	SOIL TYPE- COLOUR, MOISTURE CONTENT DENSITY, GRADATION, GRAIN SIZE, MISC. OBSER. (ie. FINES, COBBLES, OXIDATION, DEPOST. STR., ETC.)

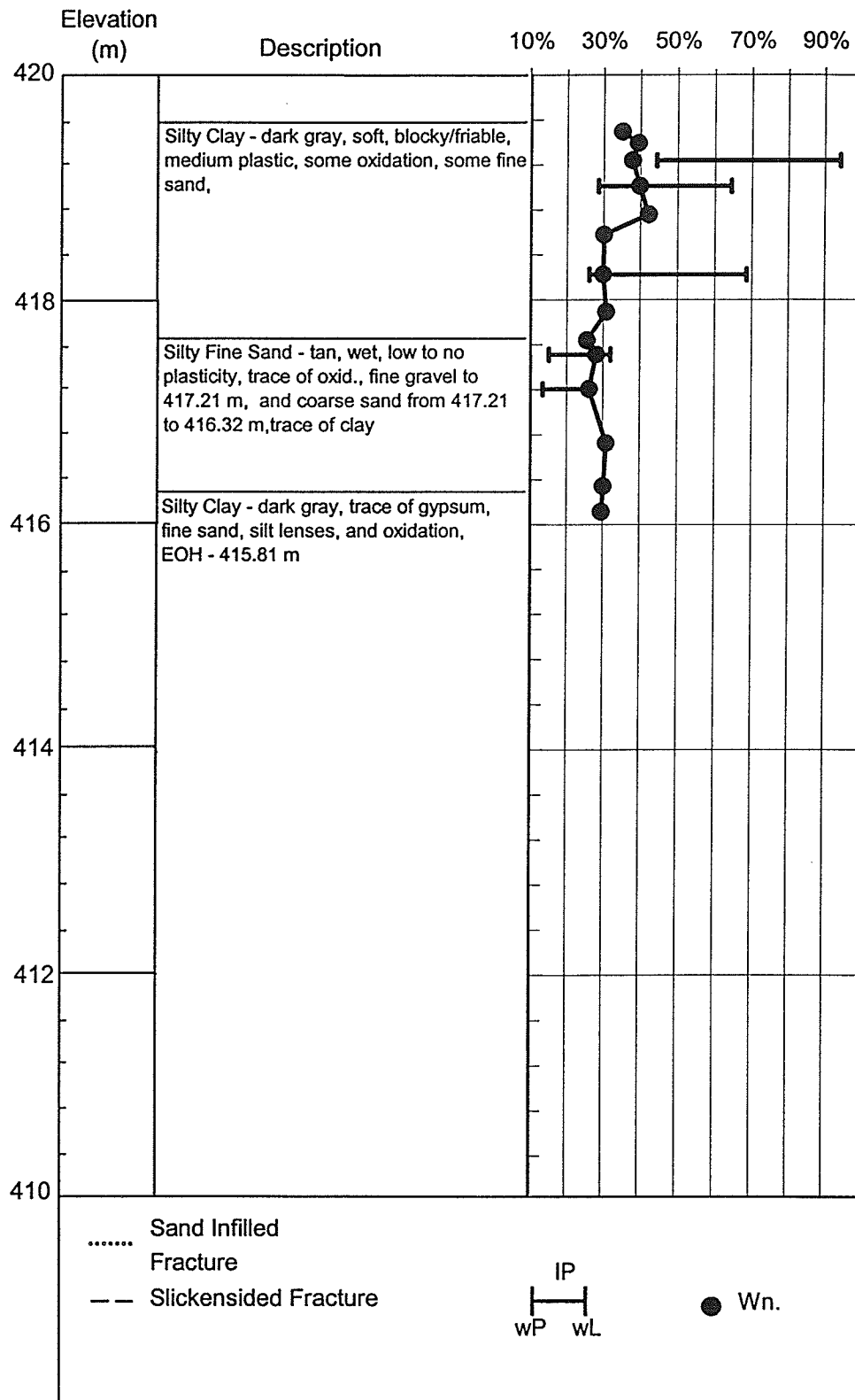
DEPTH	SOIL DESCRIPTION	SAMPLE					MISC. TESTS
		Sample #	Type	Depth	Sample Cont.	Recov. Length	
Surficial	Silty Fine Sand - Tan, moist, no structure, no plasticity, some	BH4-1			B		
Bench Cut	organics						
0- 6"	Silty Clay Loam - dary gray, moist, no structure, low plasticity,	BH4-2	SB		B		
	some organics, some tan fine sand						
6"- 20"	Silty Clay - light to medium gray, moist, blocky/friable, no to low	BH4-3	SB		B		
	plasticity, very stiff, trace of oxidation, some organics						
20" - 40"	Fine Sandy Silt - tan, moist, no structure, trace of oxidation,	BH4-4	SB		B		
	low density						
40" - 60"	Fine Sandy Silt - tan with some streaks of darker browns and gray,	BH4-5	SB		B		
	moist, no structure, trace of oxidation, low density						
60" - 80"	Fine Sandy Silt - tan, moist, no structure, layered with browns and	BH4-6	SB		B		
	grays, trace of oxidation, low density						
80" - 100"	Fine Sandy Silt - tan, moist, no structure, layered (laminated) with	BH4-7	SB		B		
	browns and grays, trace of oxidation, low density						
100"-120"	Fine Sandy Silt - tan, moist, no structure, layered (laminated) with	BH4-8	SB		B		
	browns and grays less than above, some of oxidation, dense,						
	oxidation along sand fractures						

SAMPLE TYPE	SAMPLE CONTAINERS	WELL DETAILS/NOTES:		Depth (ft.)
	O - TUBE G - GLASS JAR P - MOISTURE TIN B - BAG MISC. TESTS T - TORVANE H - HEADSPACE VAPOURS SPT - STD. PENETR. TEST DCT - DYN CONE TEST			
T - SHELBY TUBE A - AUGER CUTTINGS C - CORE SB - SPLIT BARREL W - WASH		STICK-UP ABOVE GROUND - 39.5" above ground level	Bentonite	2'
			Cuttings	18'
			Silca Sand	20'

Appendix D: Borehole Logs

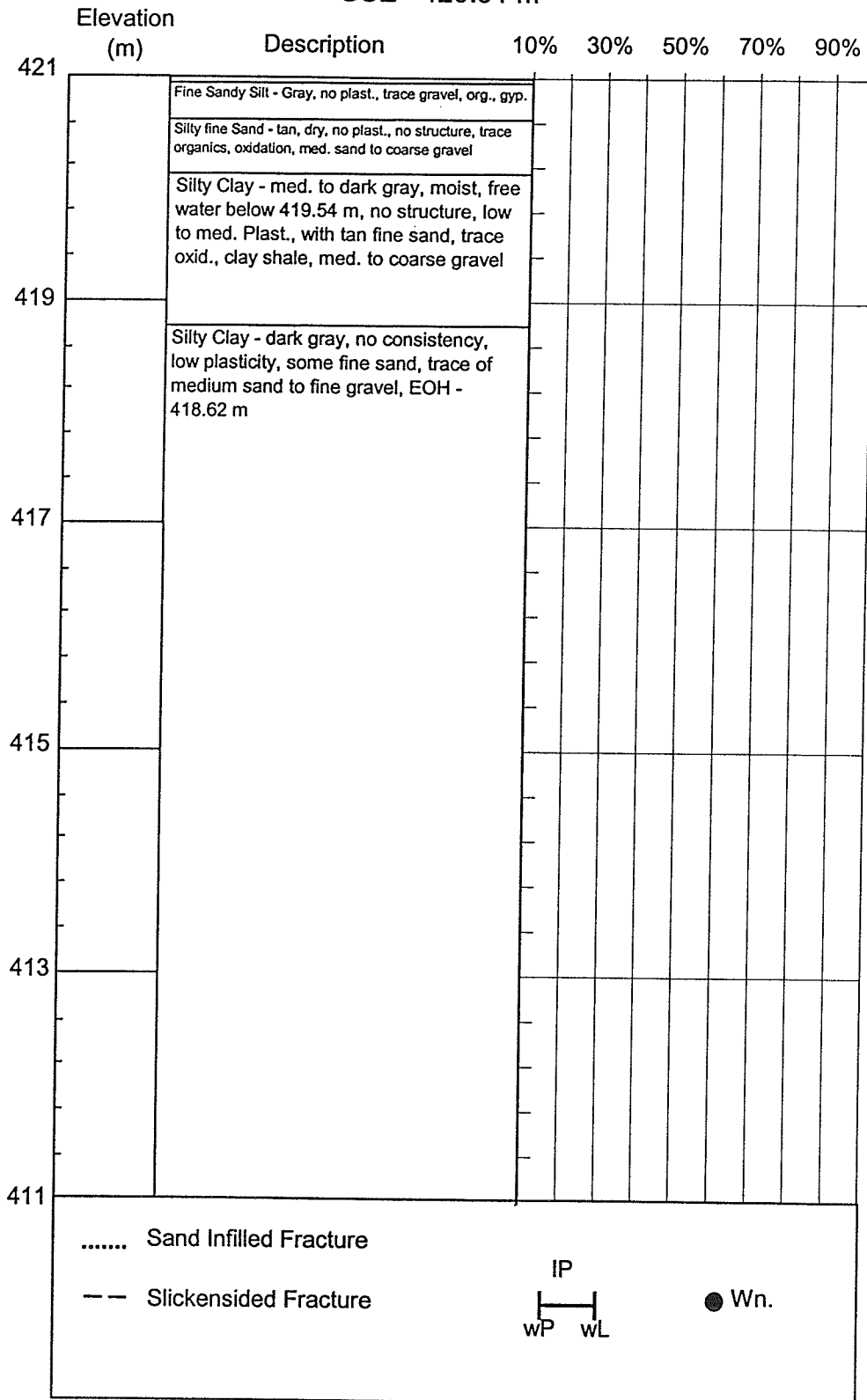
A-1

GSE - 419.62 m



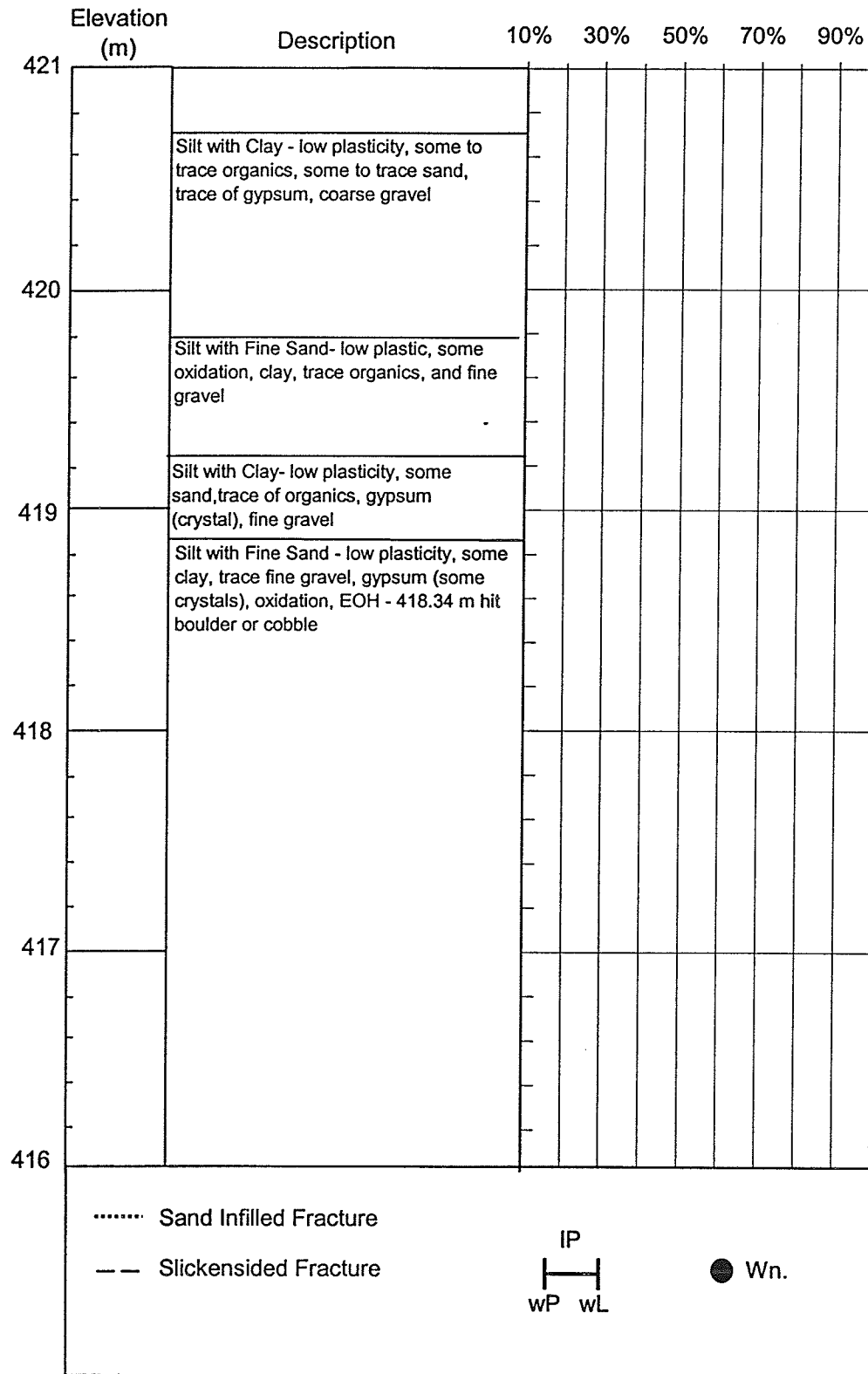
A-4

GSE - 420.91 m



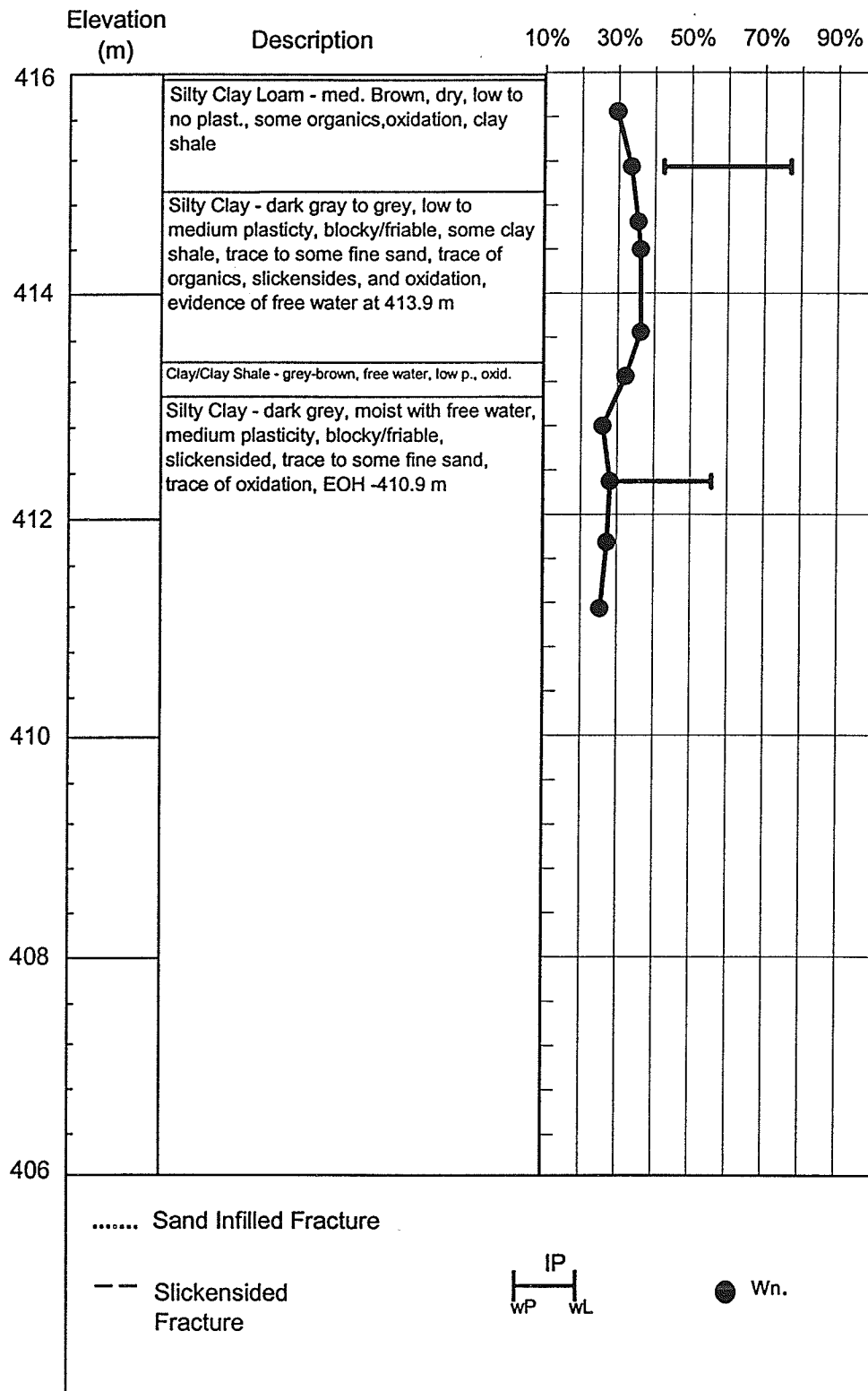
A-5

GSE - 420.46 m

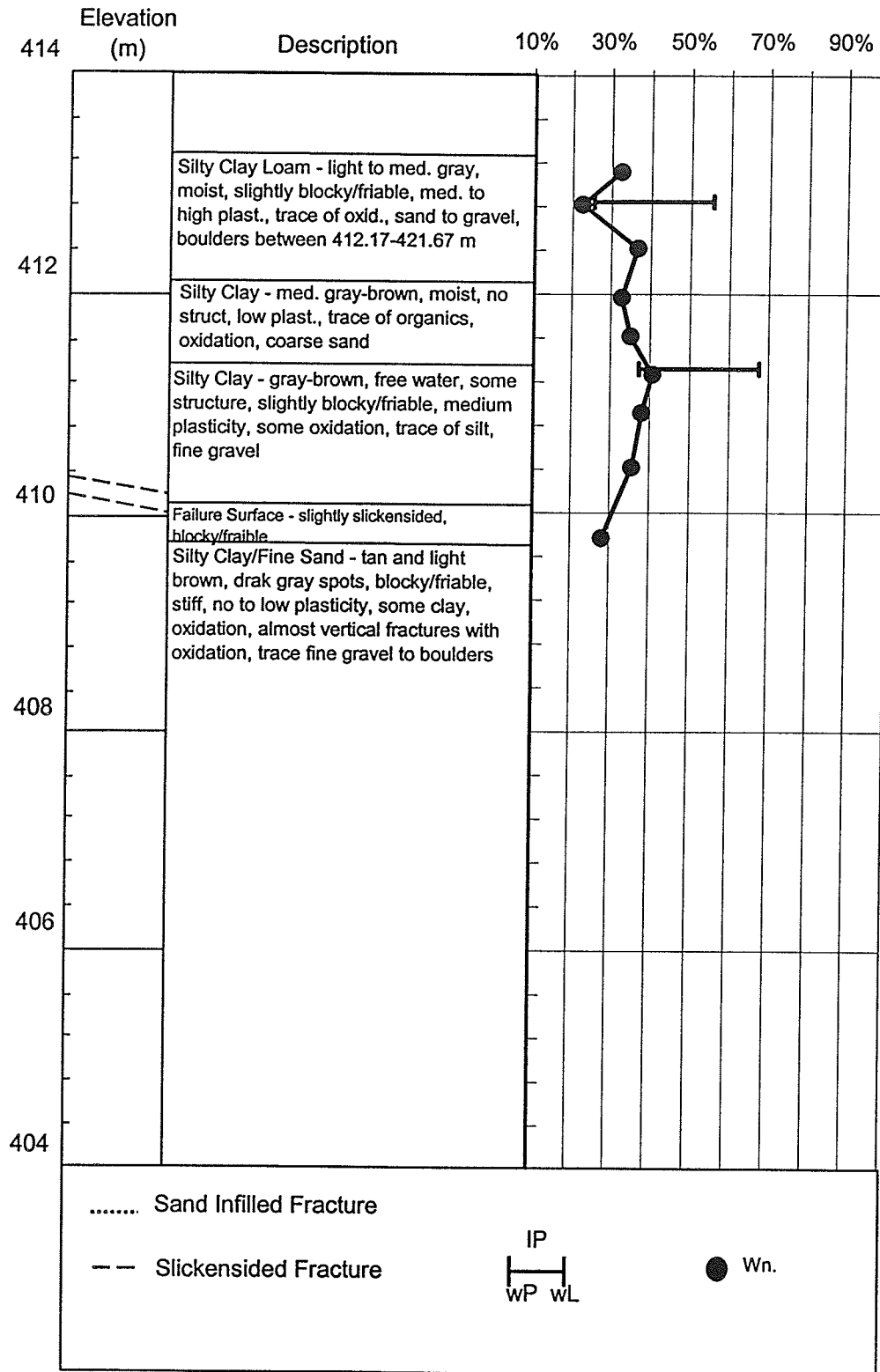


TP1

GSE - 415.90 m

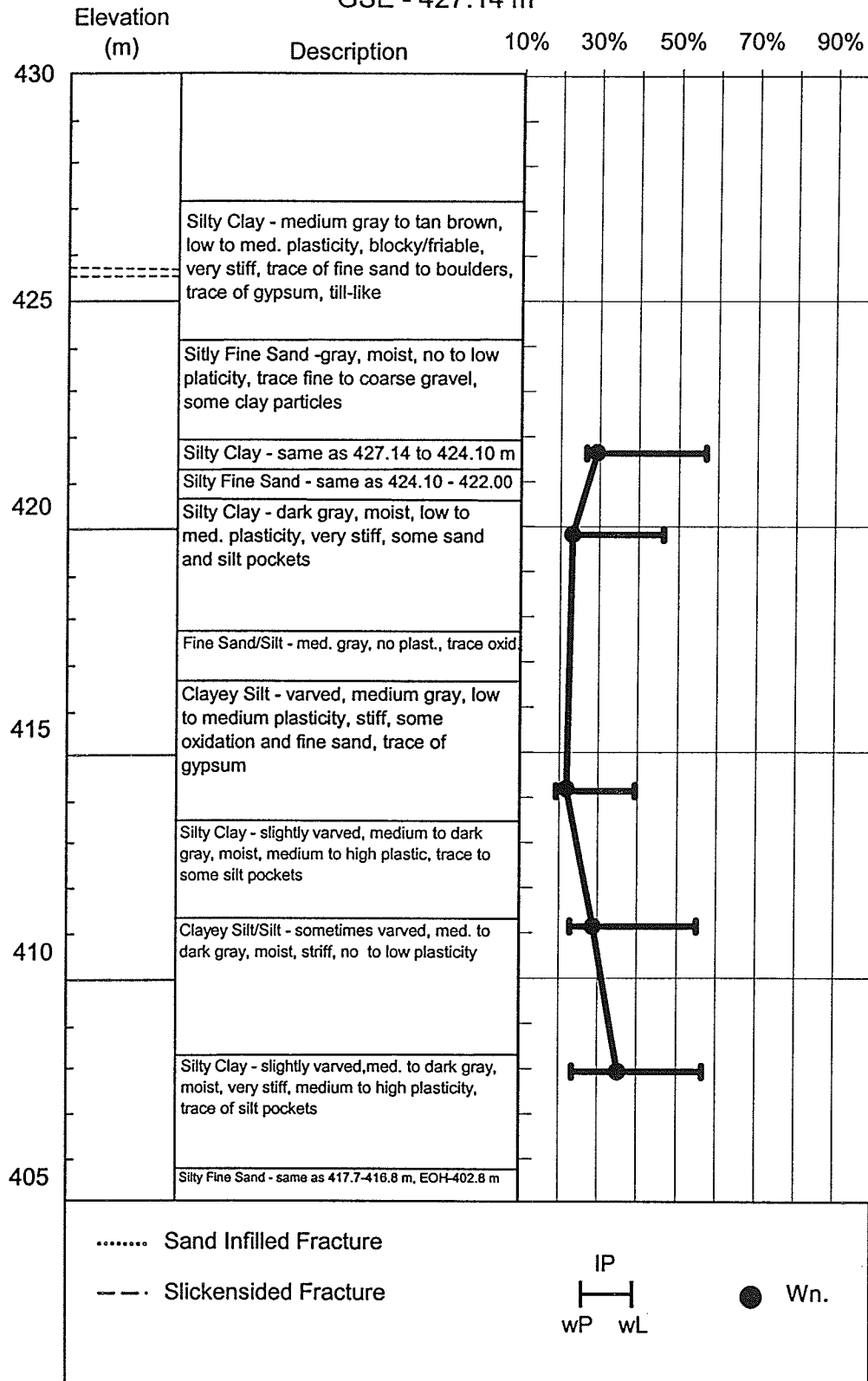


TP2 GSE - 413.27 m



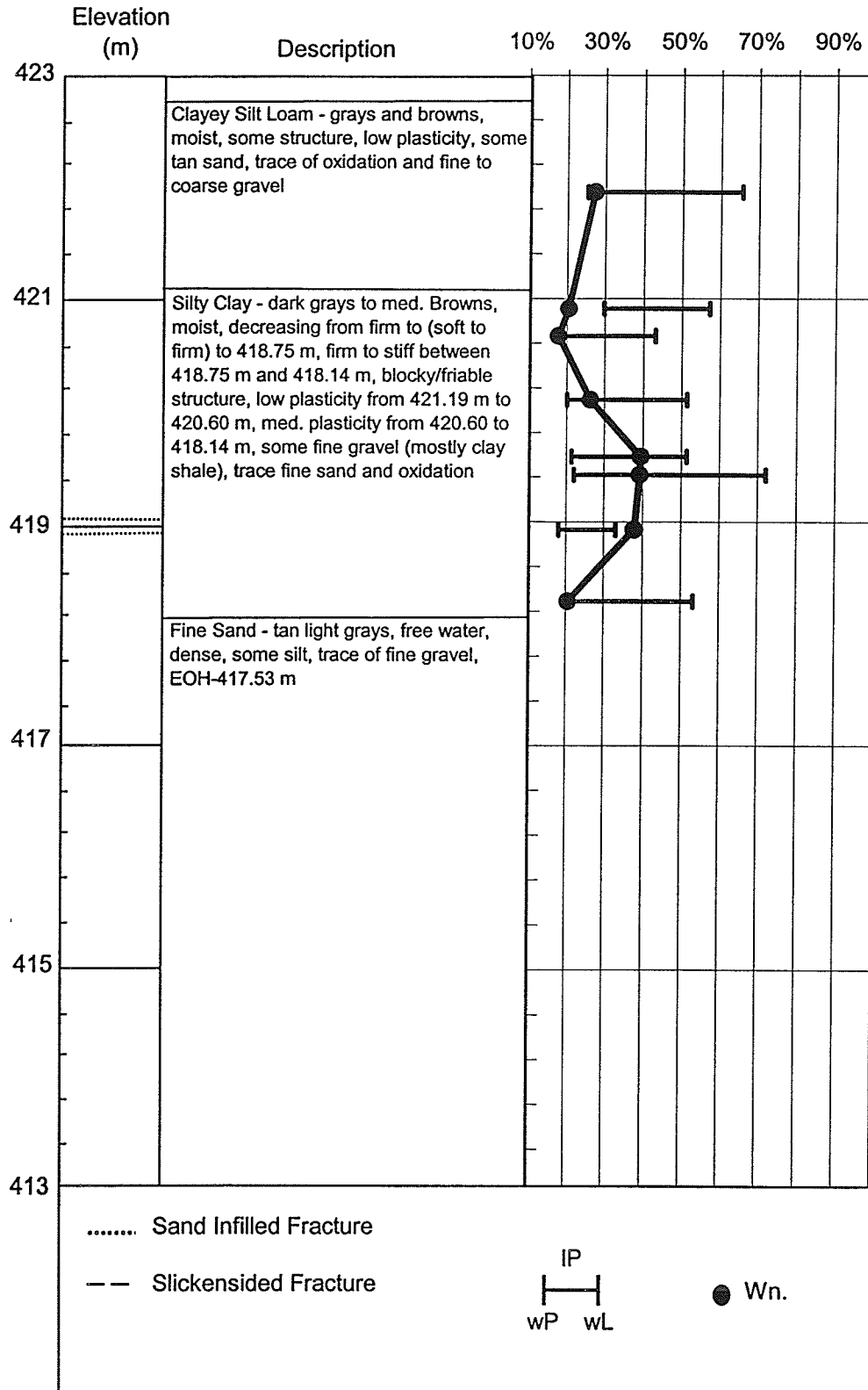
BH1

GSE - 427.14 m



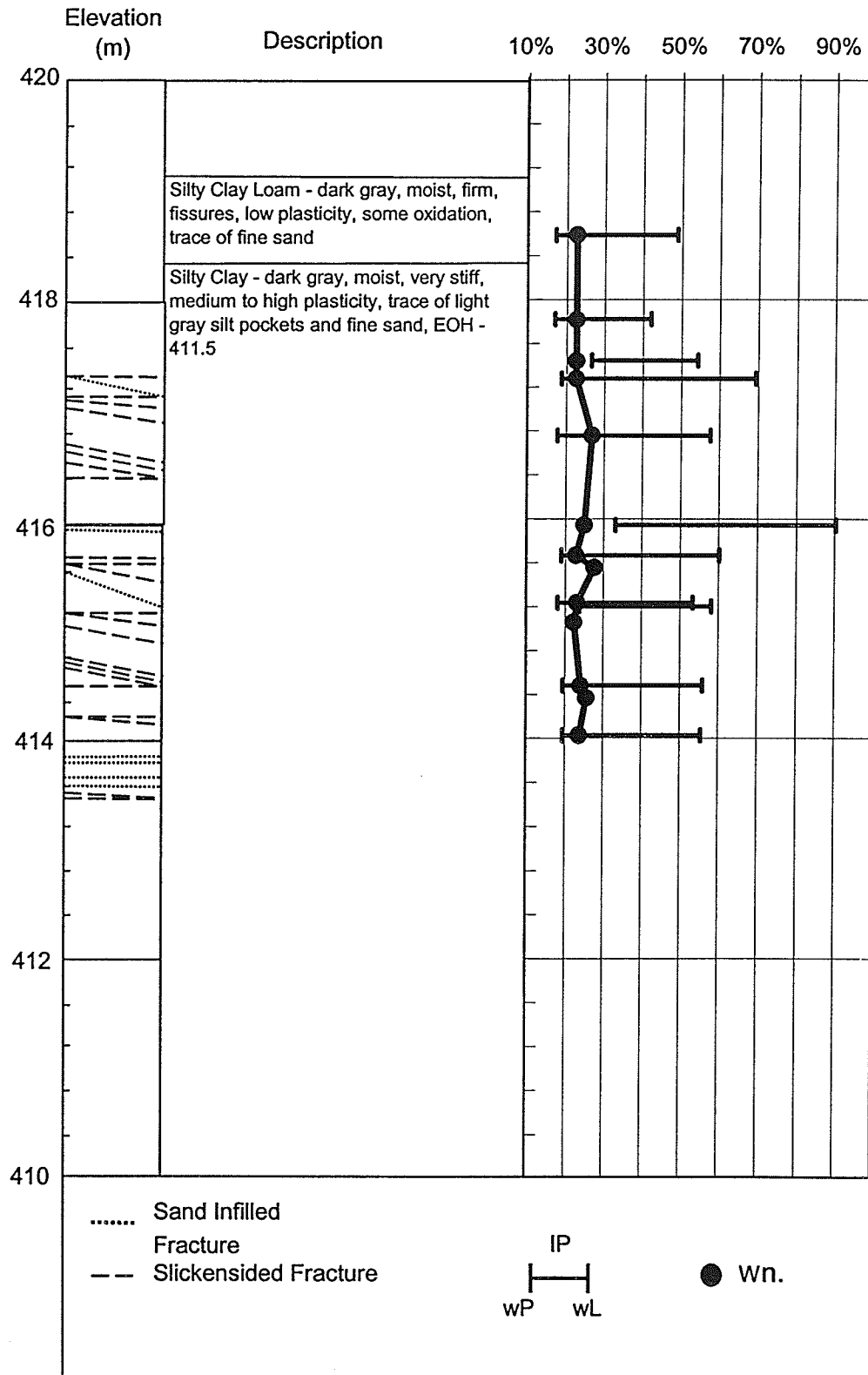
BH2

GSE - 422.71 m



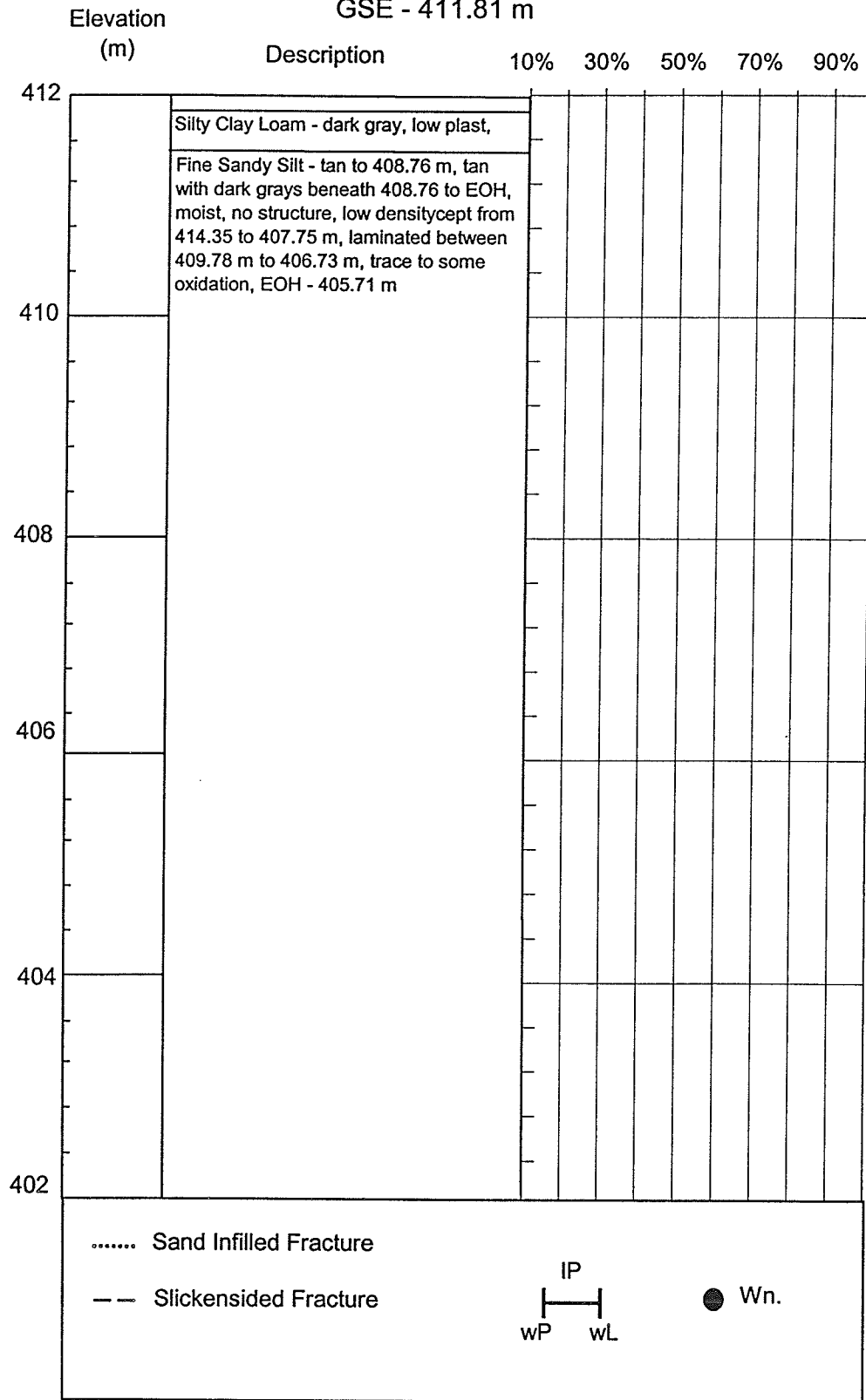
BH3

GSE - 419.12 m



BH4

GSE - 411.81 m



Appendix E: Grain Size Distribution

Grain Size Analysis Summary

Borehole: A1

Sample	Depth (m)	% Sand	% Silt	% Clay
A1-3	0.381	0.00%	24.00%	76.00%
A1-4	0.6096	0.00%	66.00%	34.00%
A1-8	1.397	0.00%	40.00%	60.00%
A1-13	2.1082	20.00%	51.00%	29.00%
A1-15	2.413	10.00%	59.00%	31.00%
A1-19	3.2766	55.00%	30.00%	15.00%

Borehole: BH1

Sample	Depth (m)	% Sand	% Silt	% Clay
BH1-10	5.50	0.00%	55.00%	45.00%
BH1-12	7.31	0.45%	61.55%	38.00%
BH1-17	13.00	0.00%	70.00%	30.00%
BH1-19	16.00	0.00%	50.00%	50.00%
BH1-22	19.20	0.00%	43.00%	57.00%

Borehole: BH2

Sample	Depth (m)	% Gravel	% Sand	% Silt	% Clay
BH2-1	0 - 1.52	21.68%	26.34%	32.50%	19.48%
BH2-2	1.80	12.00%	36.00%	26.00%	26.00%
BH2-2(2)	1.96 - 2.13	7.06%	40.50%	28.94%	23.50%
BH2-3	2.49 - 2.74	12.99%	45.22%	22.29%	19.50%
BH2-4	3.05 - 3.22	0.00%	0.00%	68.00%	42.00%
BH2-4(2)	3.23 - 3.35	0.03%	2.83%	51.62%	45.52%
BH2-5(2)	3.73 - 3.84	0.00%	12.35%	37.85%	25.50%
BH2-6	4.27 - 4.57	0.00%	2.00%	66.00%	42.00%

Borehole: BH3

Sample	Depth (m)	% Gravel	% Sand	% Silt	% Clay
BH3-1	0 - 1.07	0.00%	2.22%	40.42%	38.20%
BH3-2	1.07 - 1.52	0.00%	1.02%	68.98%	33.00%
BH3-3	1.68	0.10%	0.23%	49.67%	50.00%
BH3-3(2)	1.91 - 1.98	0.00%	0.00%	23.00%	57.00%
BH3-4	2.31 - 2.41	0.00%	0.73%	48.93%	48.20%
BH3-5	3.175	0.00%	12.00%	32.00%	56.00%
BH3-6(2)	3.4 - 3.51	0.00%	0.29%	47.71%	52.00%

BH3-6	3.81 - 3.96	0.00%	0.00%	48.00%	52.00%
BH3-7	3.96 - 4.17	0.00%	0.00%	45.00%	55.00%
BH3-8	4.57 - 4.70	0.00%	0.00%	48.00%	52.00%
BH3-8(2)	5.00 - 5.18	0.00%	2.28%	39.72%	58.00%

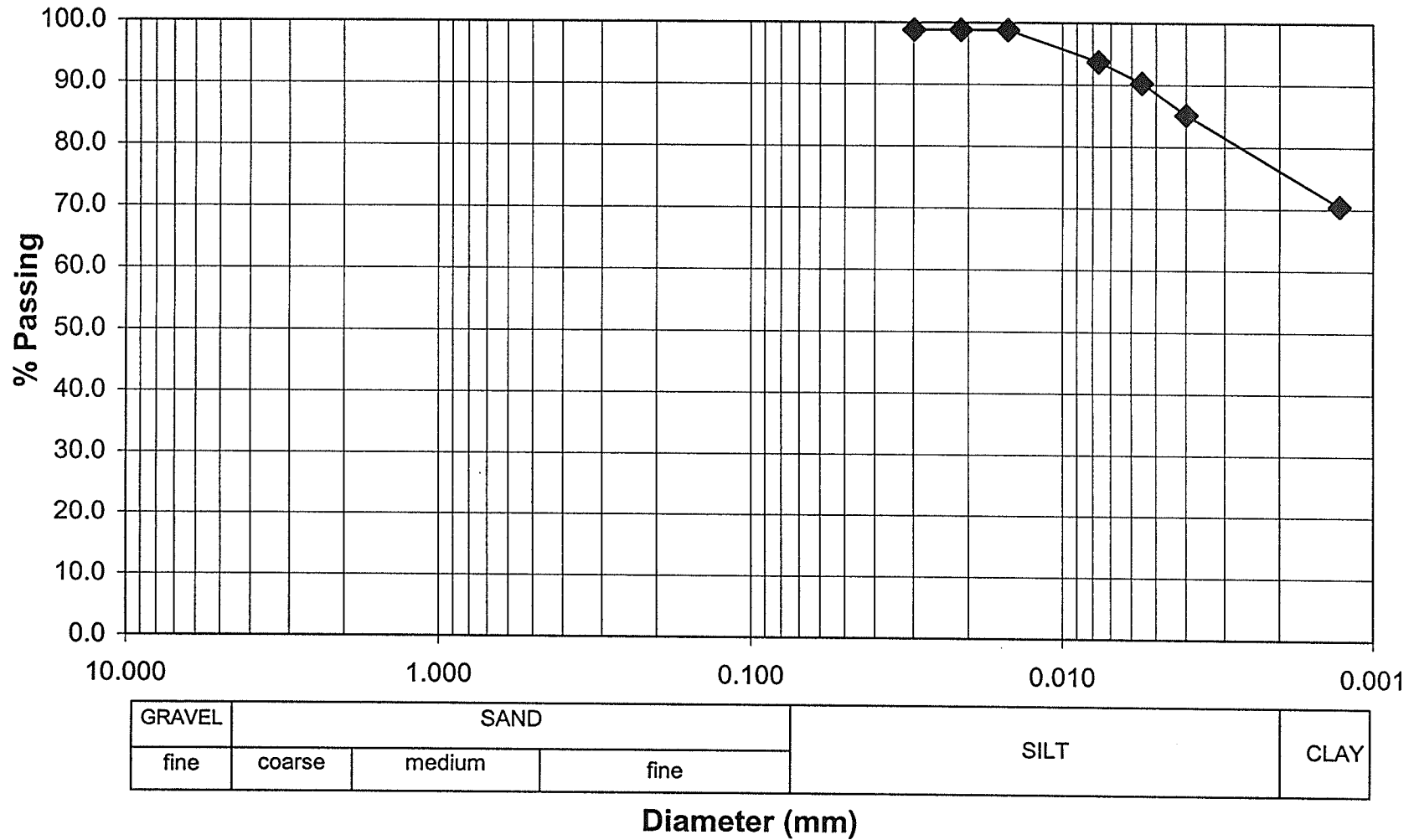
Borehole: TP1

Sample	Depth (m)	% Gravel	% Sand	% Silt	% Clay
TP1-2	0.5 - 1.0	40.00%	39.00%	10.00%	11.00%
TP1-8	3.4 - 3.8	0.00%	4.00%	22.00%	74.00%

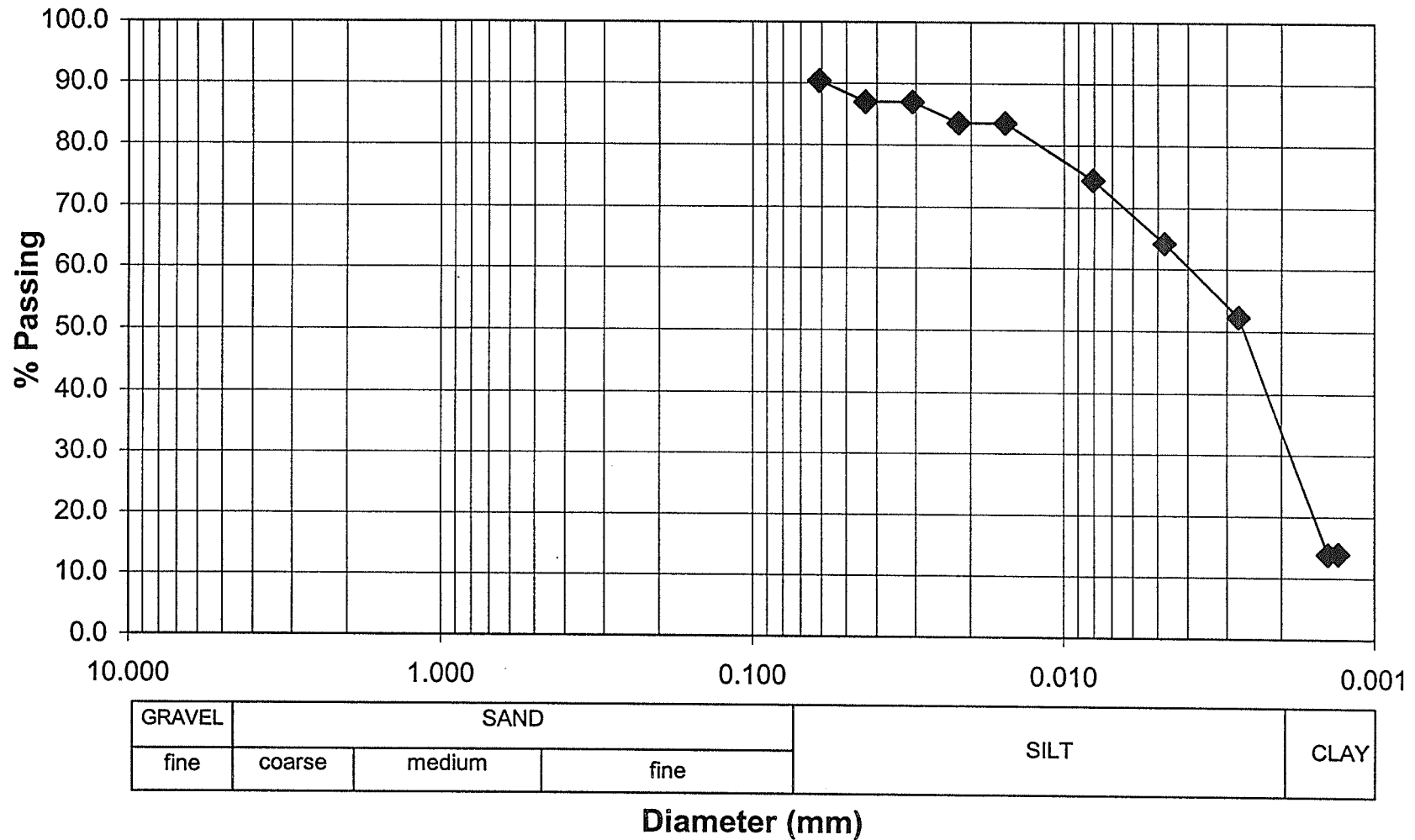
Borehole: TP2

Sample	Depth (m)	% Gravel	% Sand	% Silt	% Clay
TP2-2	0.25 - 0.6	1.00%	8.00%	23.00%	68.00%
TP2-6	1.8 - 2.1	7.00%	53.00%	21.00%	19.00%

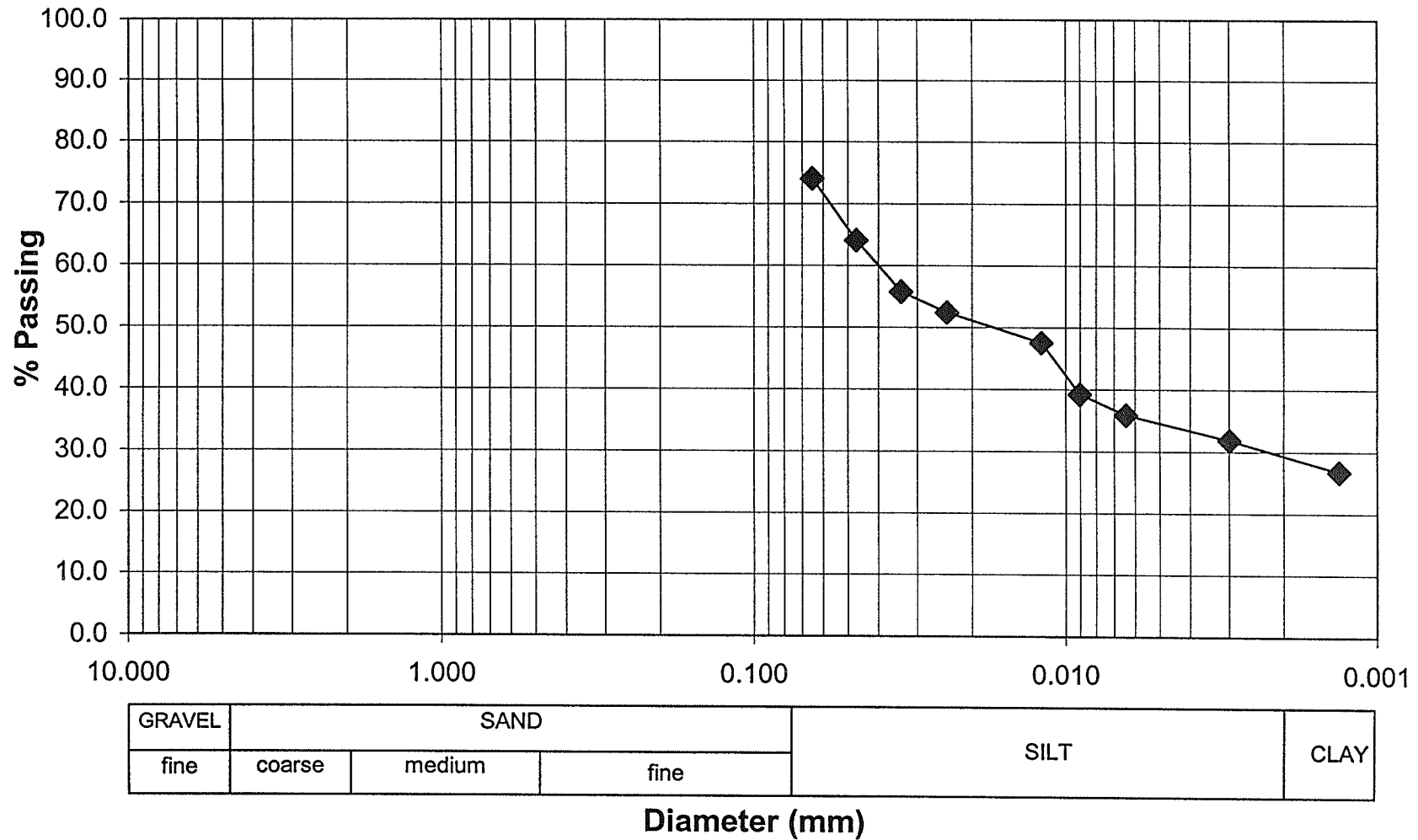
Project: PR259
Borehole: A1-3 Depth: 0.381 m
Date: July 26, 2000



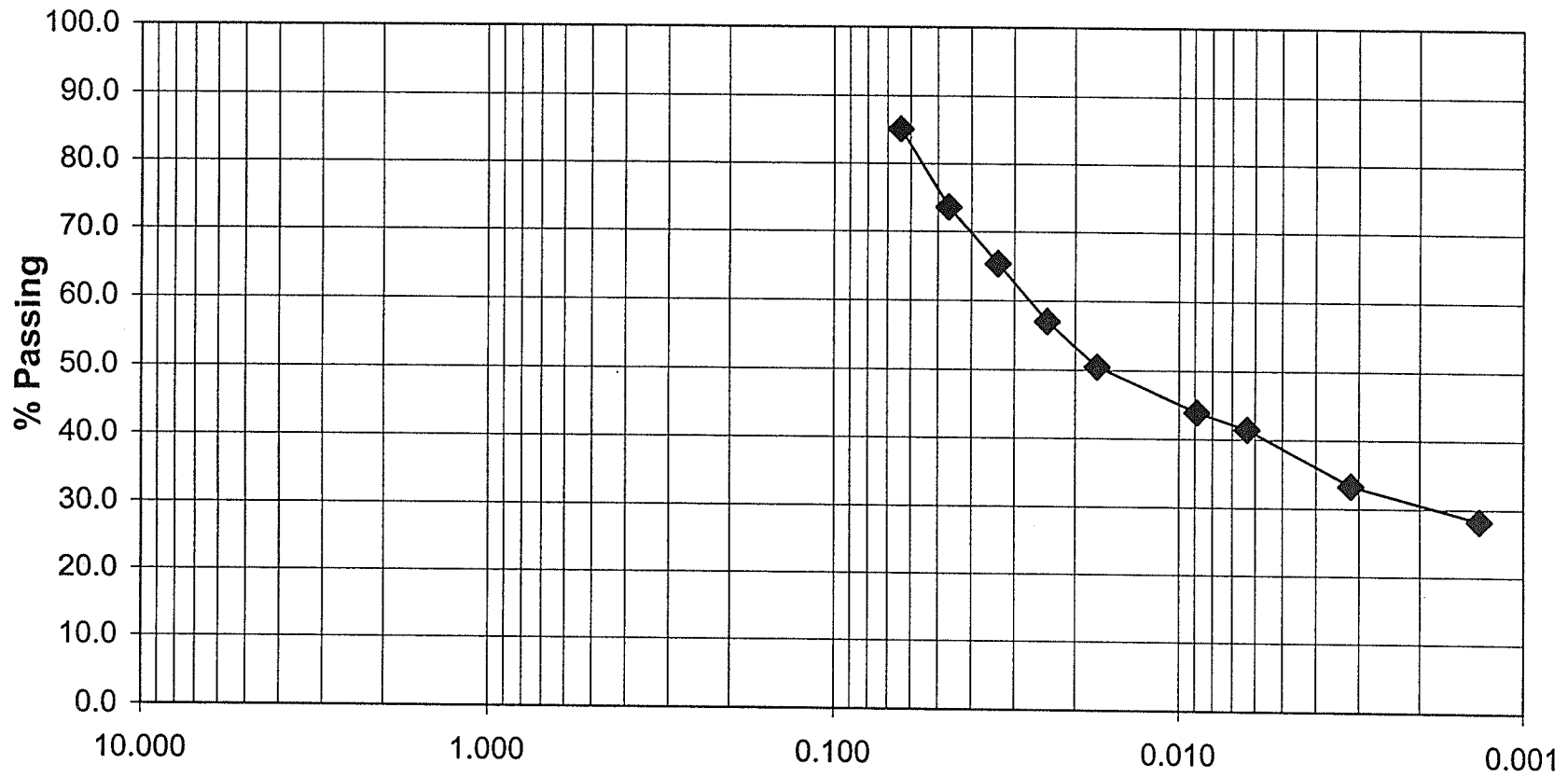
Project: PR259
Borehole: A1-4 Depth: 0.6096m
Date: August 1, 2000



Project: PR259
Sample: A1-13 Depth: 2.1082m
Date: August 4, 2000



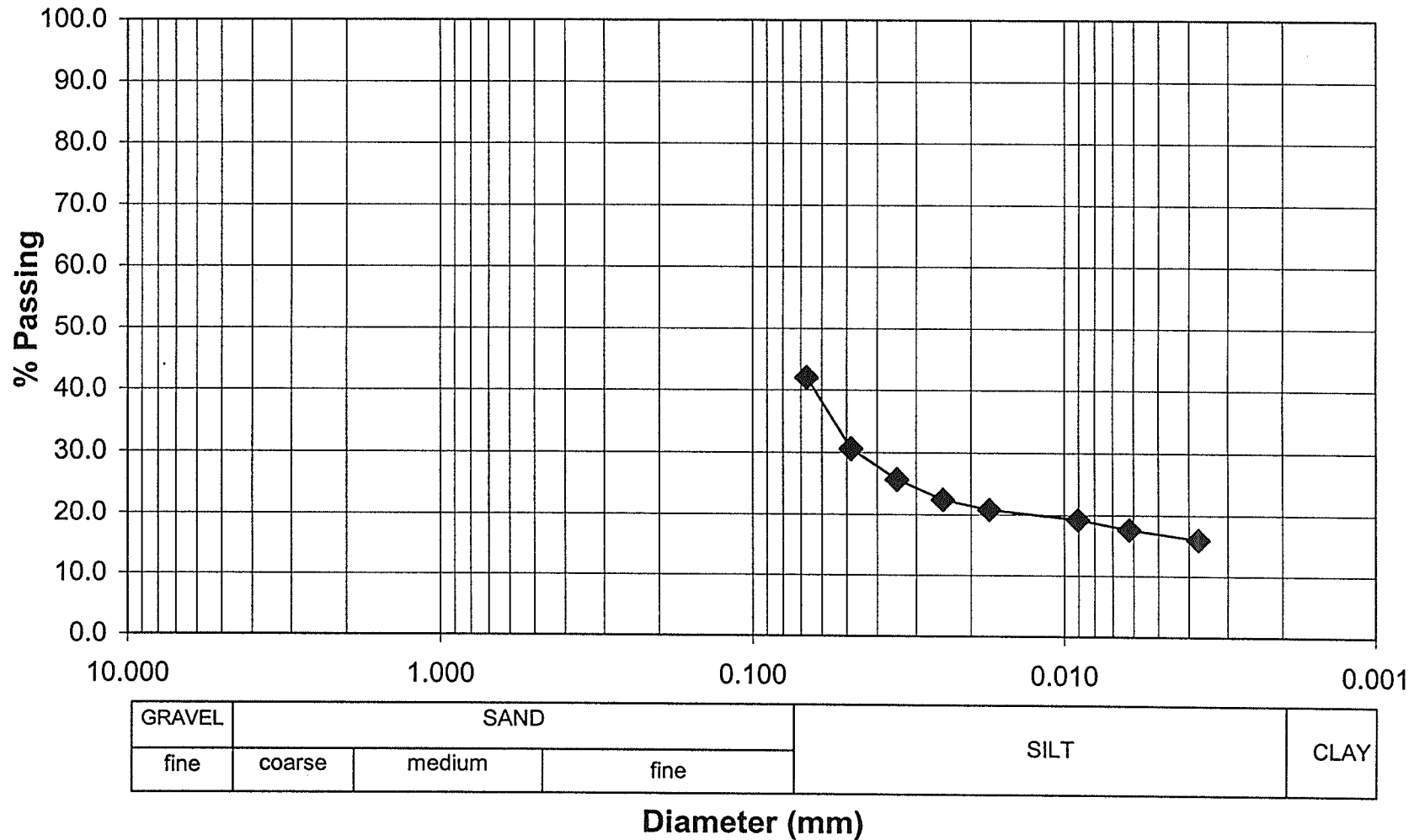
Project: PR259
Sample: A1-15 Depth: 2.413m
Date: August 4, 2000



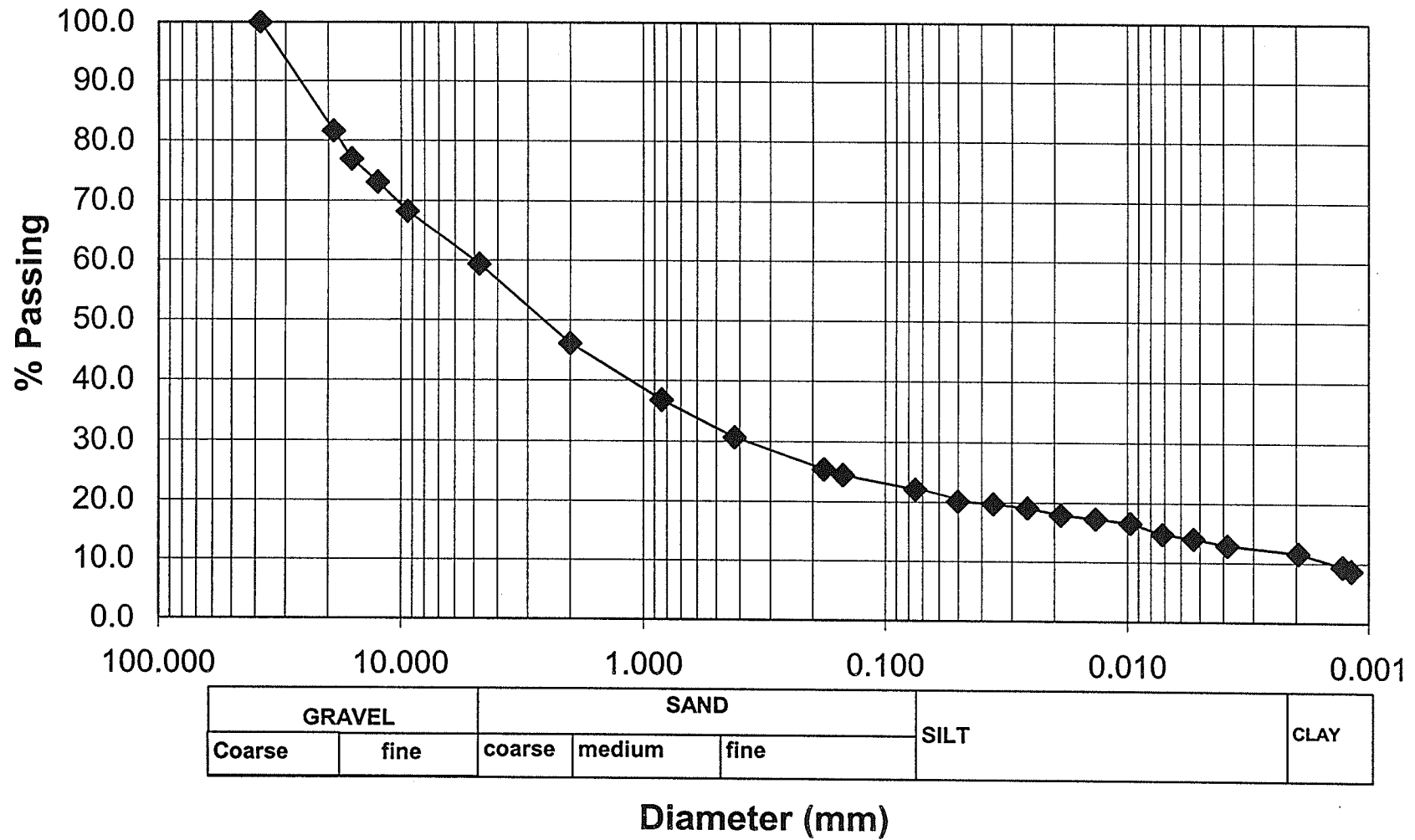
GRAVEL	SAND			SILT	CLAY
fine	coarse	medium	fine		

Diameter (mm)

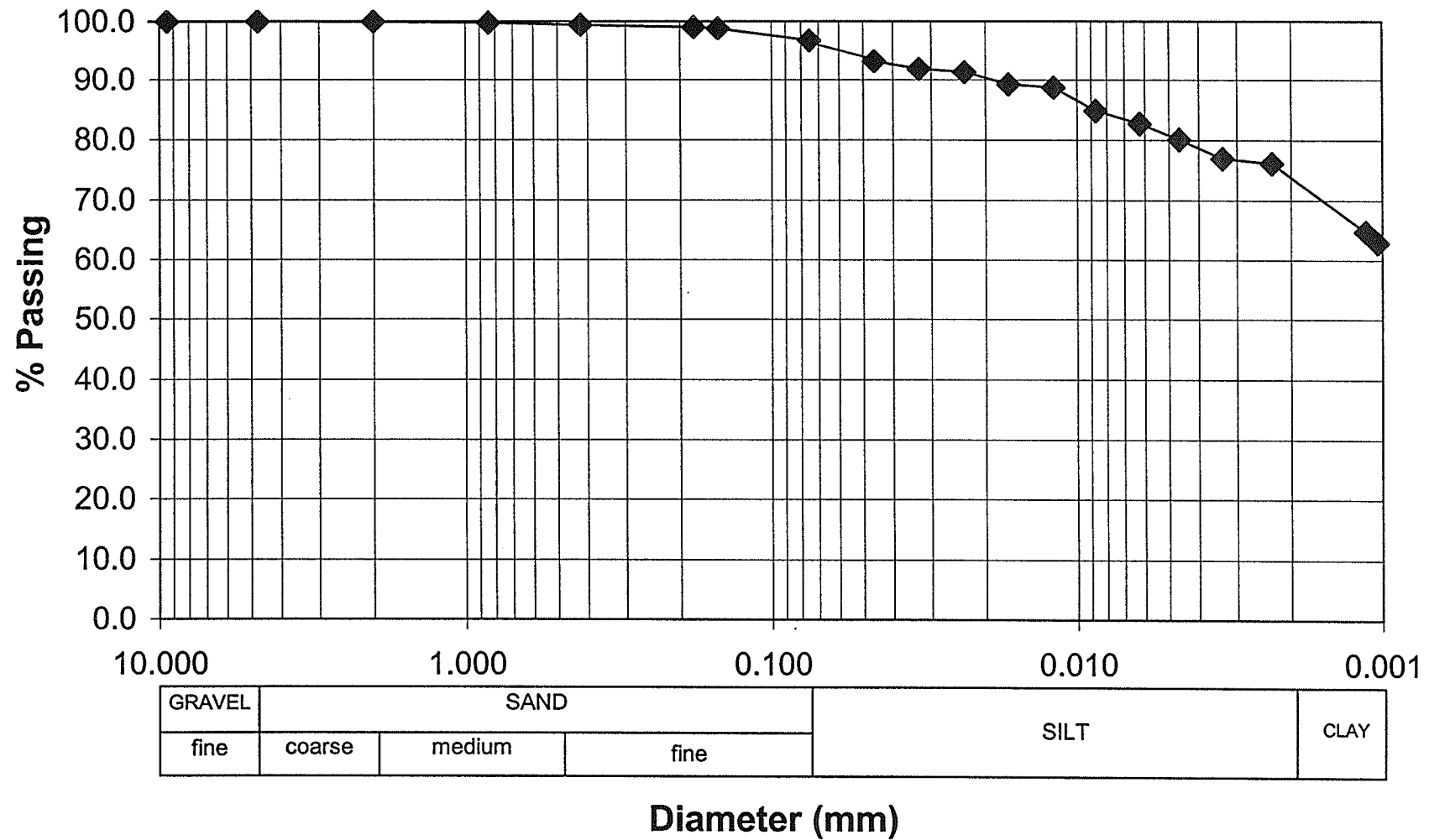
Project: PR259
Borehole: A1-19 Depth: 3.2766m
Date: Aug 2, 2000



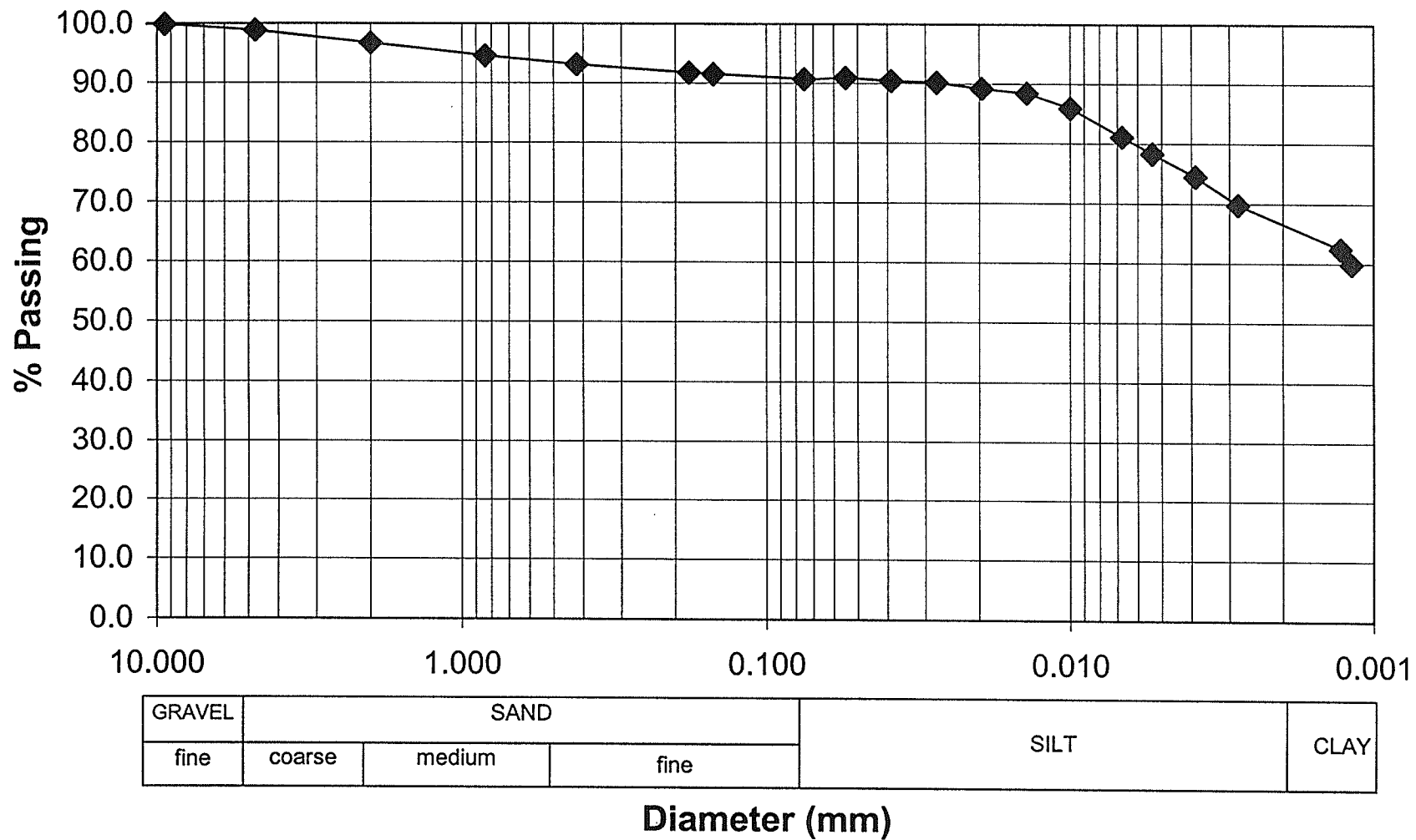
Project: PR259
Borehole: TP1-2 Depth: 0.75m
Date: Feburary 18, 2001



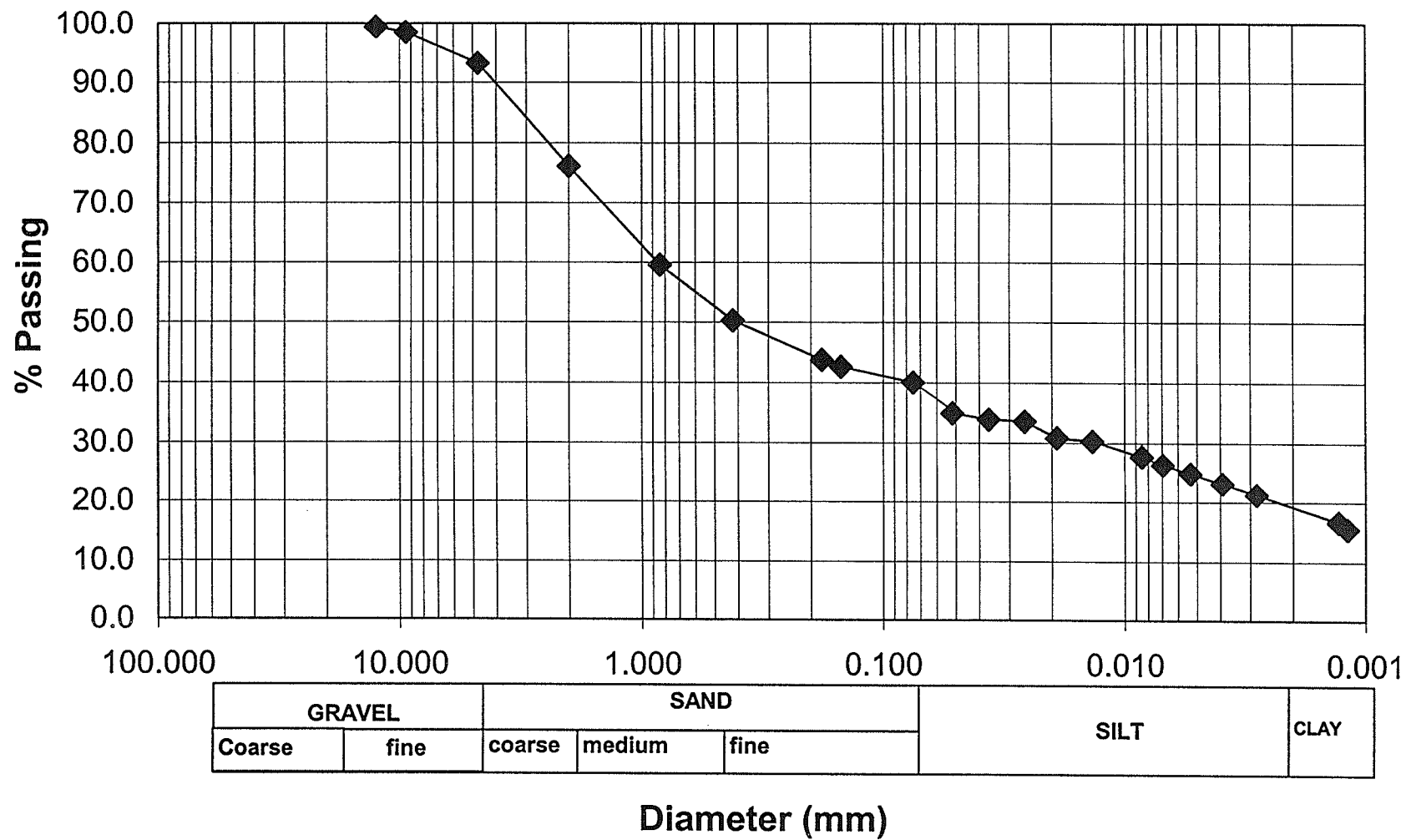
Project: PR259
 Borehole: TP1-8 Depth: 3.6 m
 Date: Feburary 18, 2001



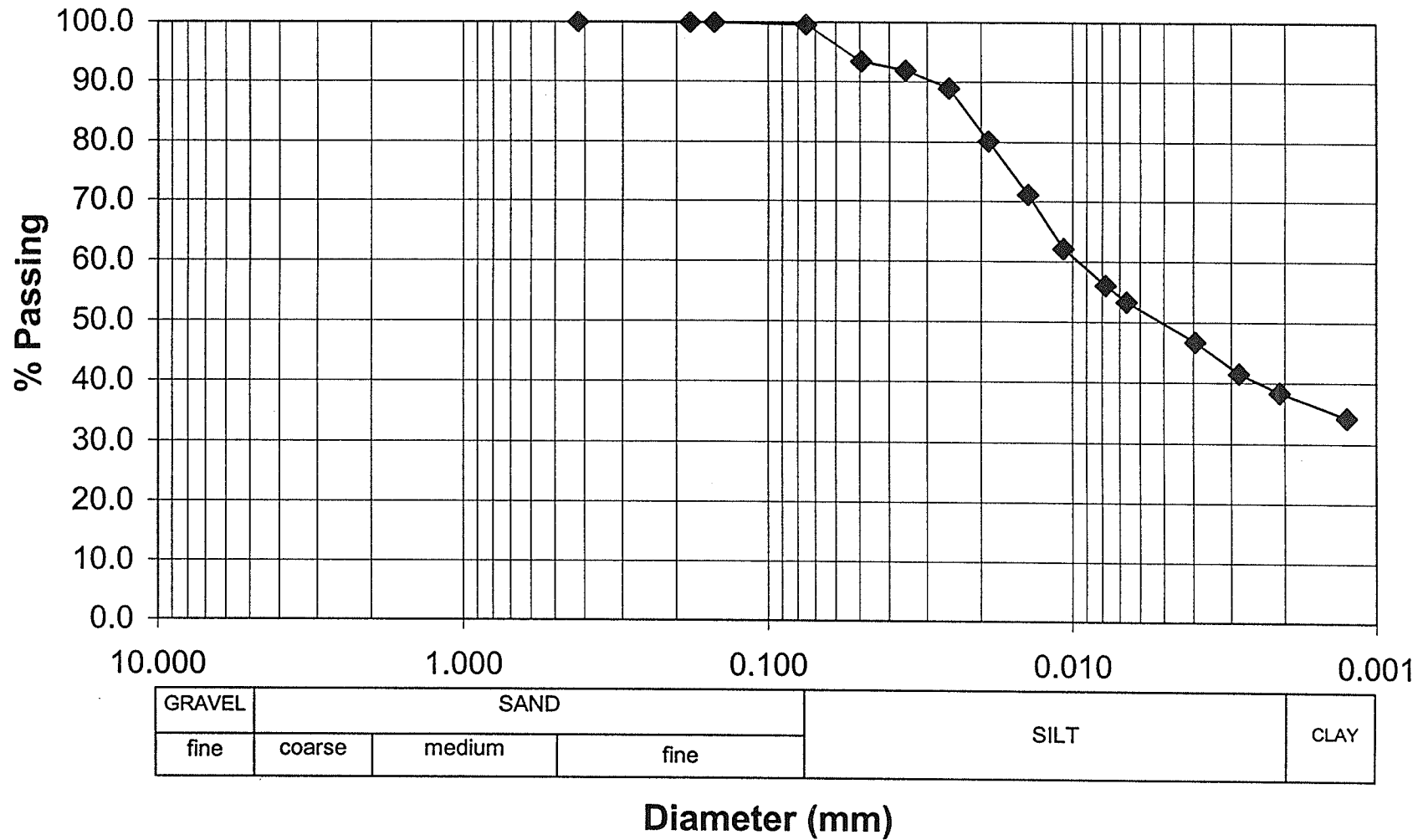
Project: PR259
 Borehole: TP2-2 Depth: .25 -.6 m
 Date: Feburary 18, 2001



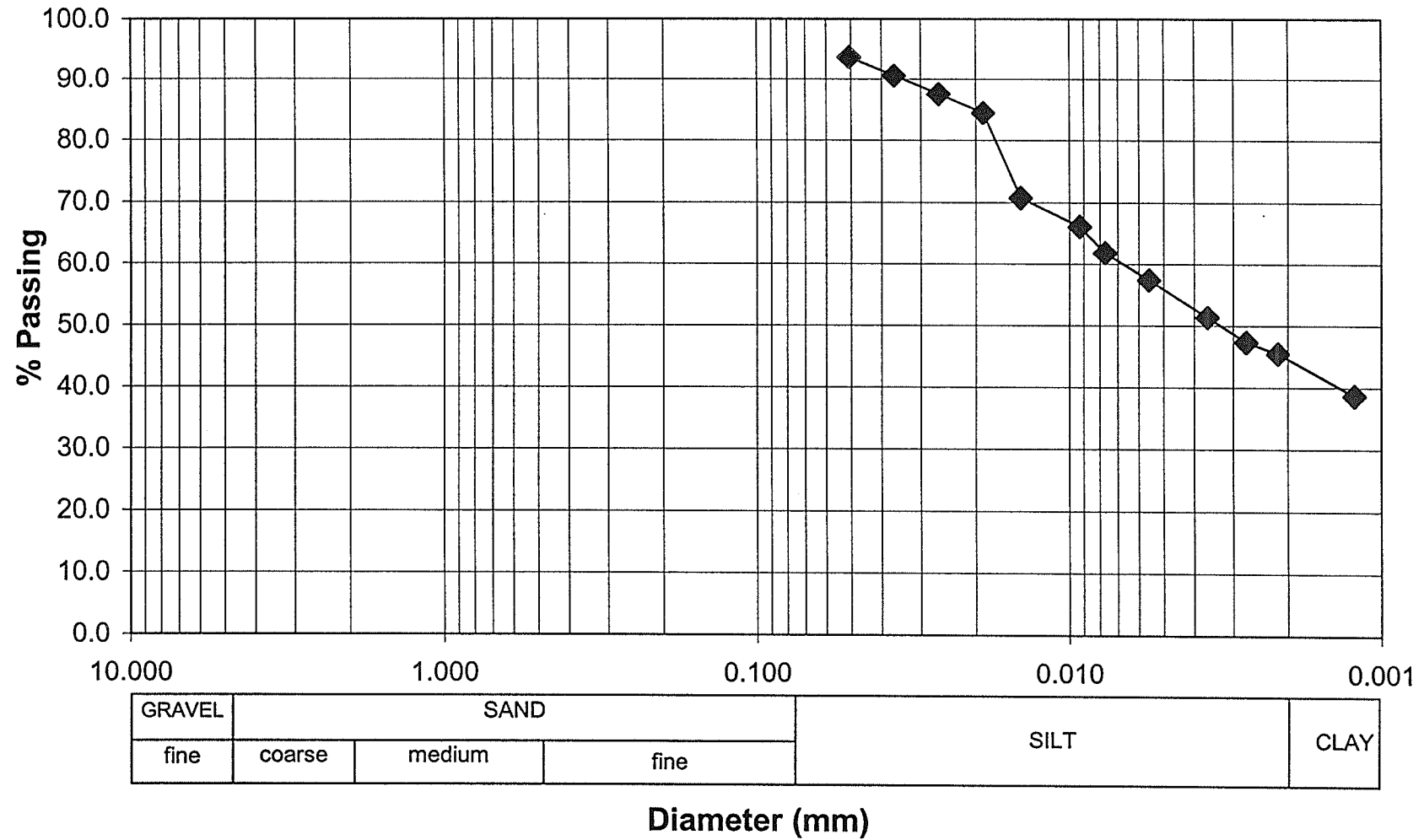
Project: PR259
Borehole: TP2-6 Depth: 2.00m
Date: Feburary 18, 2001



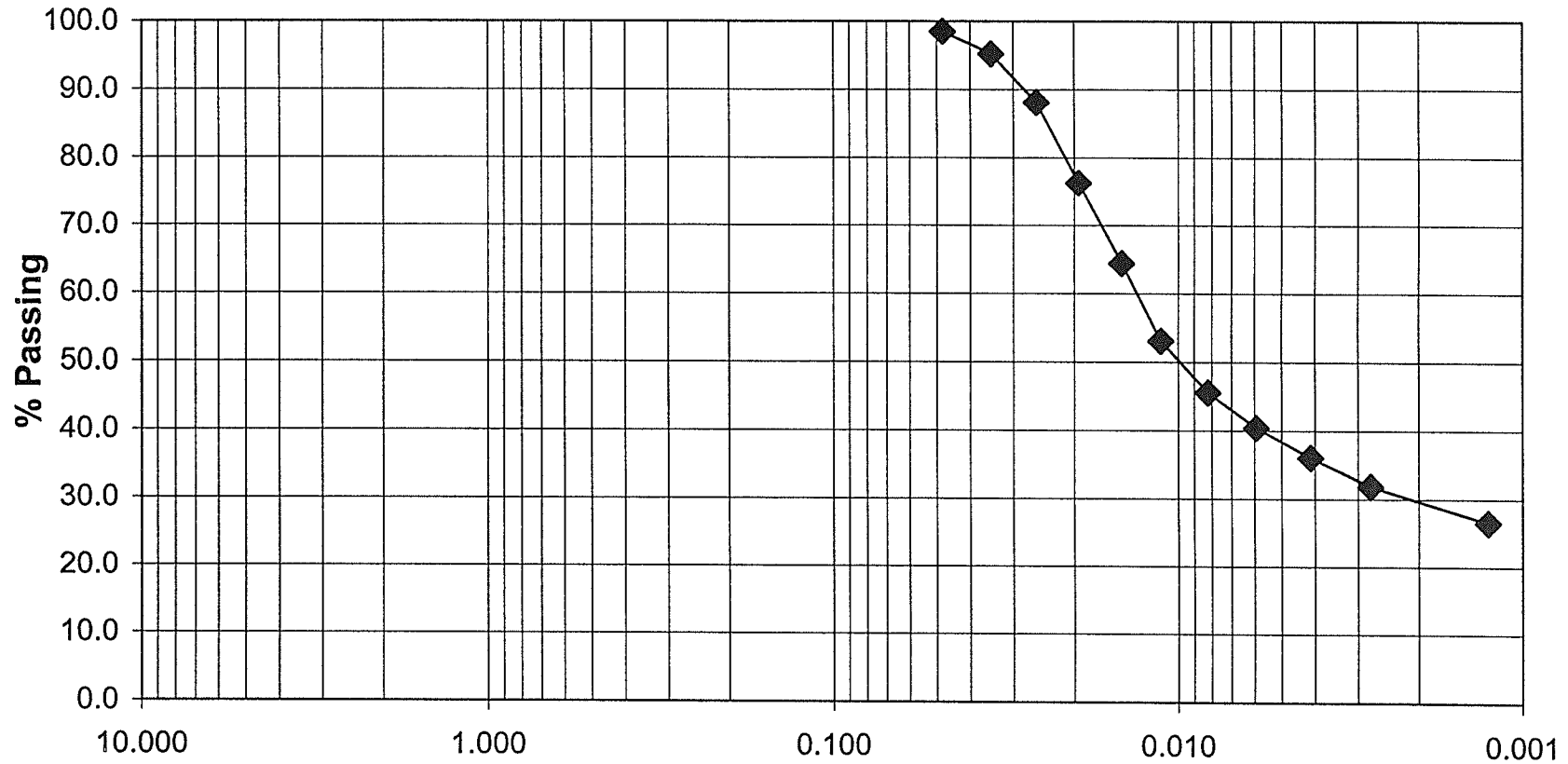
Project: PR259
 Borehole: BH1-12 Depth: 7.01 - 7.62 m
 Date: November 22, 2000



Date: November 20, 2000



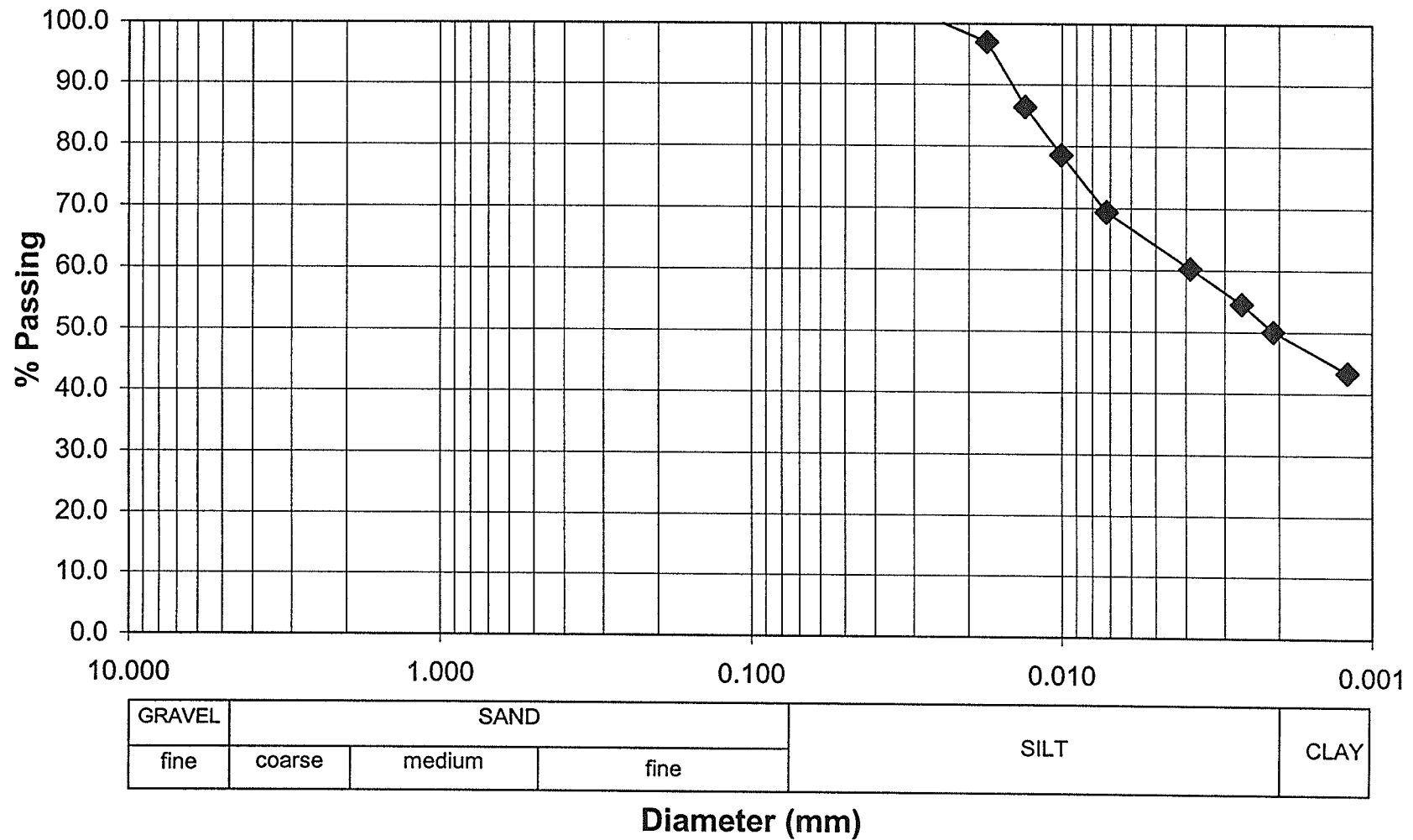
Project: PR259
Borehole: BH1-17 Depth: 12.19 - 13.72 m
Date: November 17, 2000



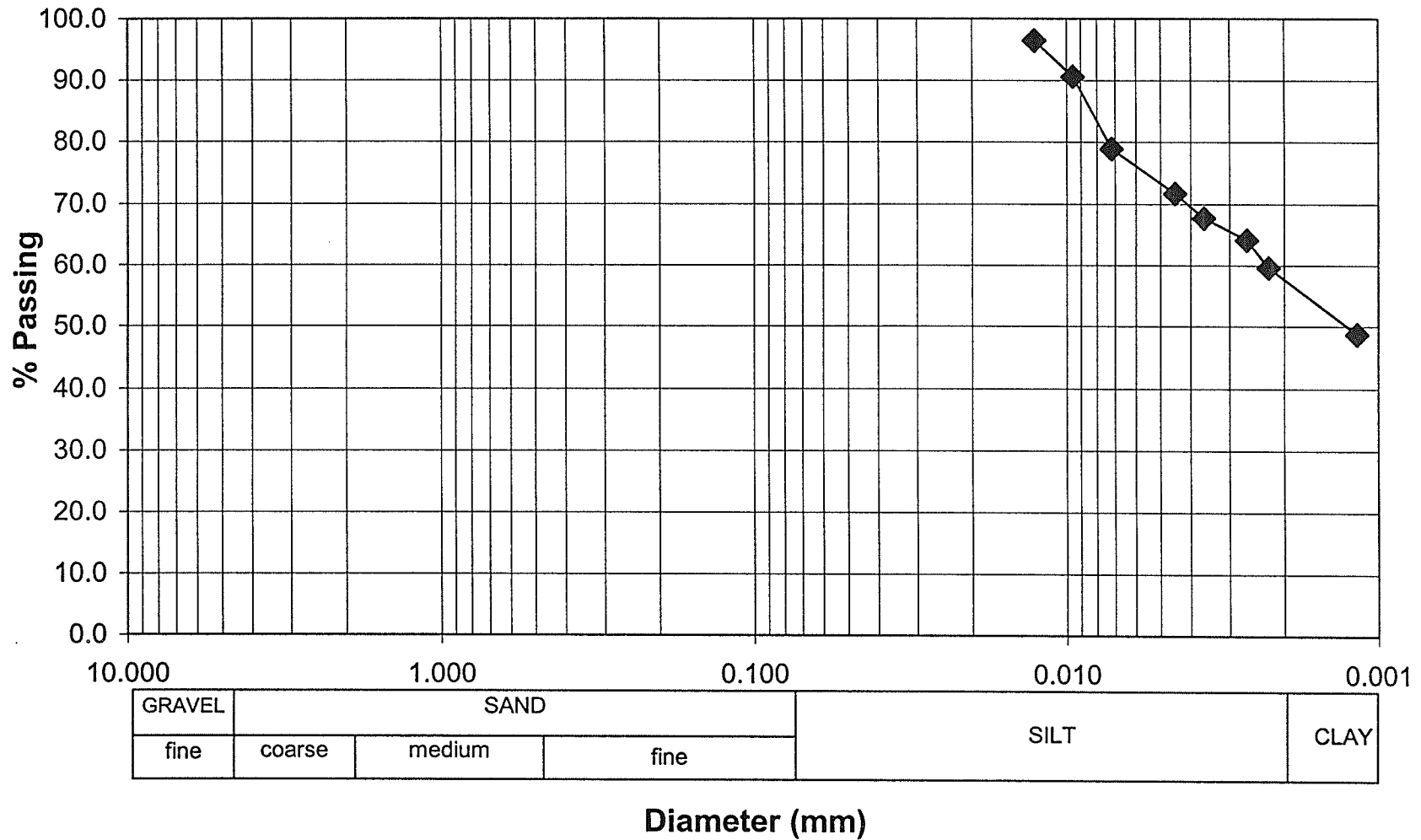
GRAVEL	SAND			SILT	CLAY
fine	coarse	medium	fine		

Diameter (mm)

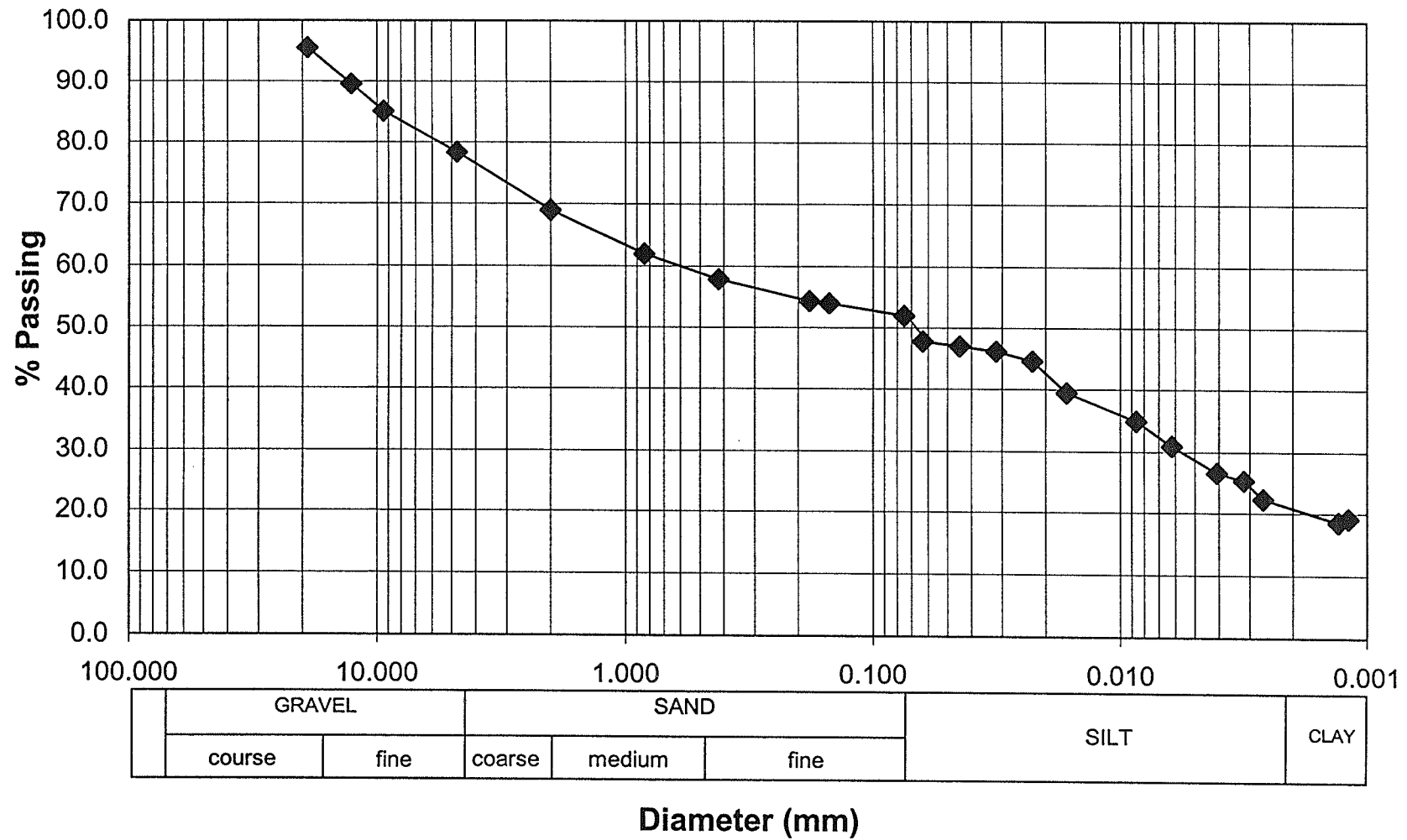
Project: PR259
Borehole: BH1-19 Depth: 15.24 - 16.76 m
Date: Nov 14, 2000



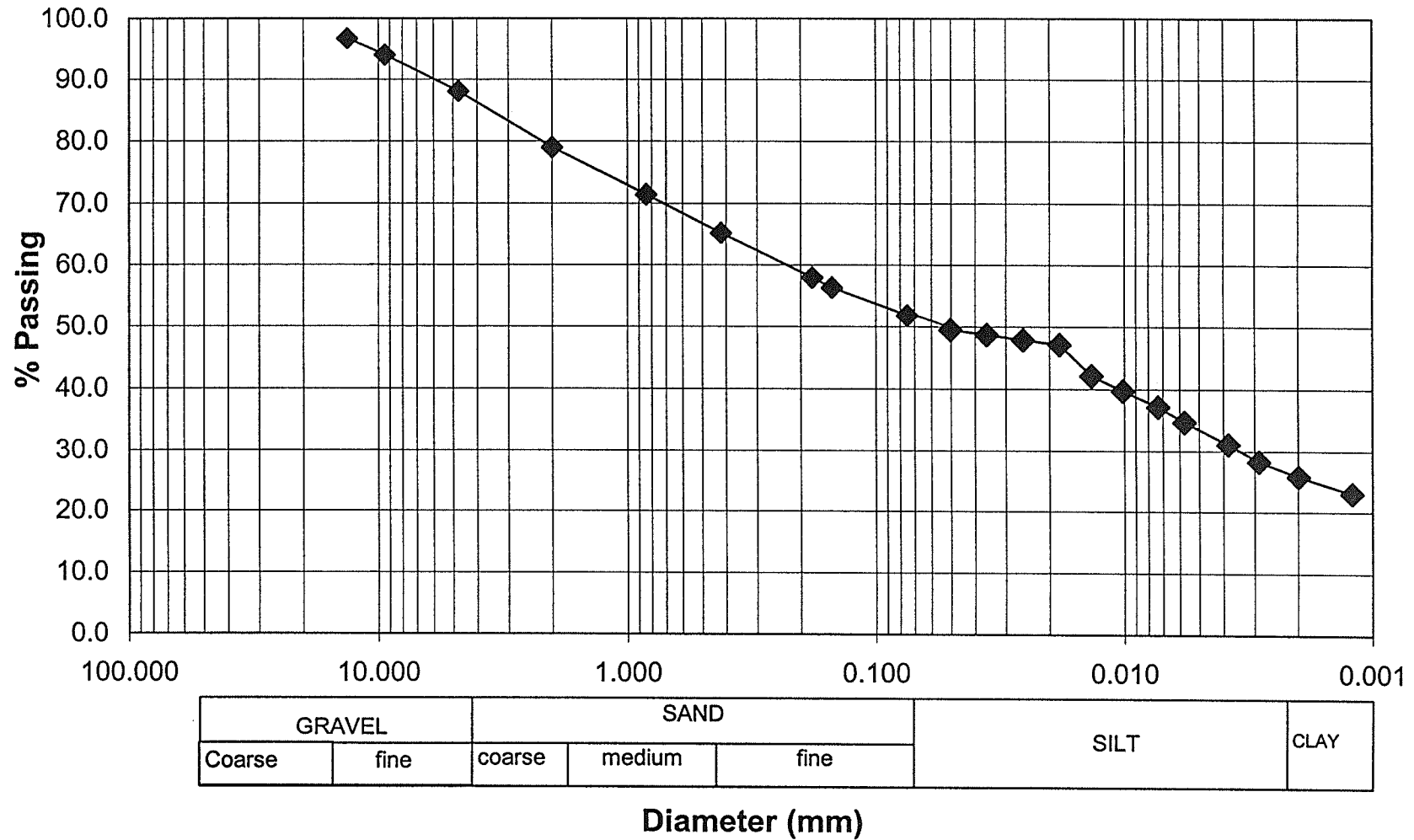
Project: PR259
 Borehole: BH1-22 Depth: 19.20 m
 Date: November 20, 2000



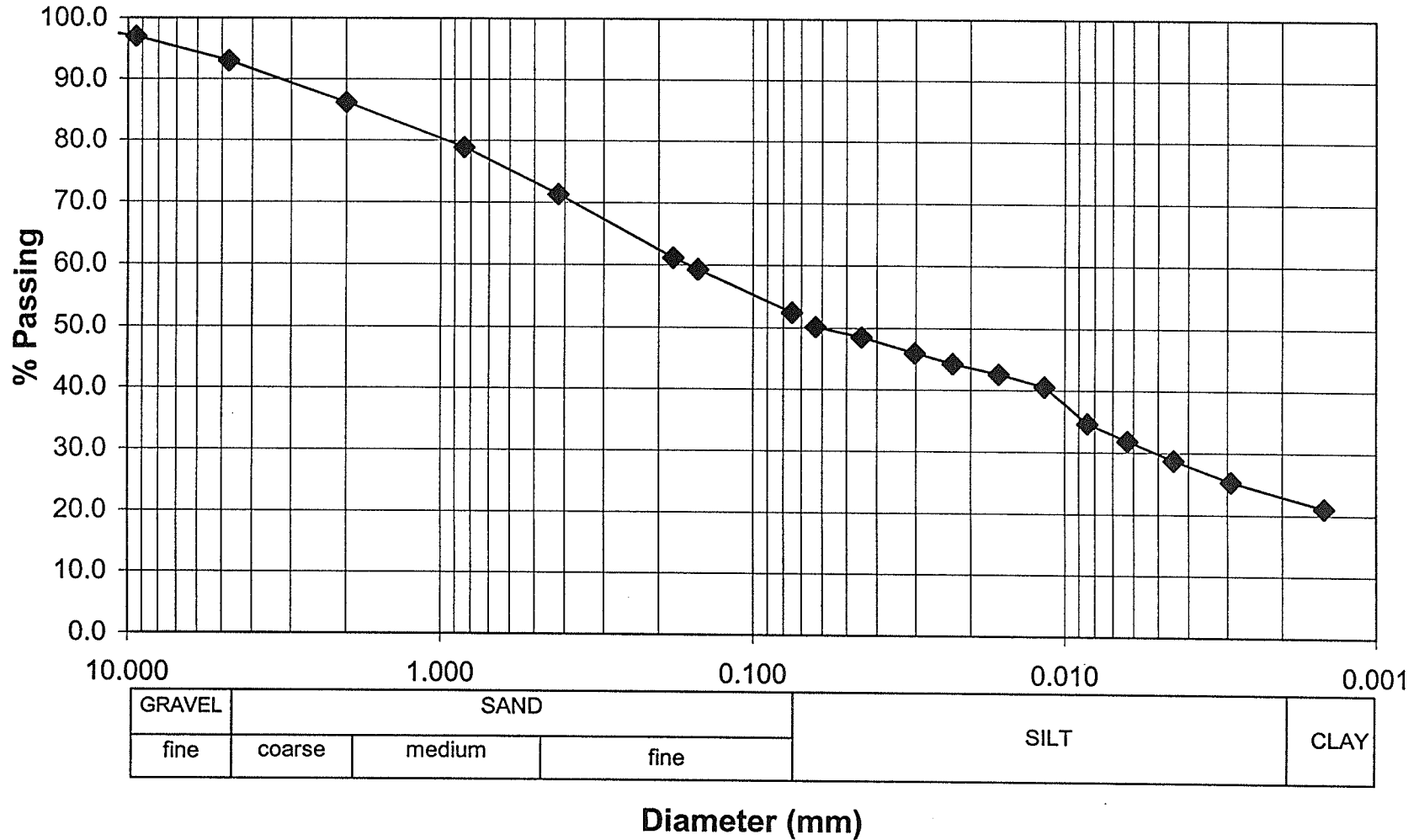
Project: PR259
Sample: BH2-1 Depth:0 - 1.52 m
Date: June 28, 2001



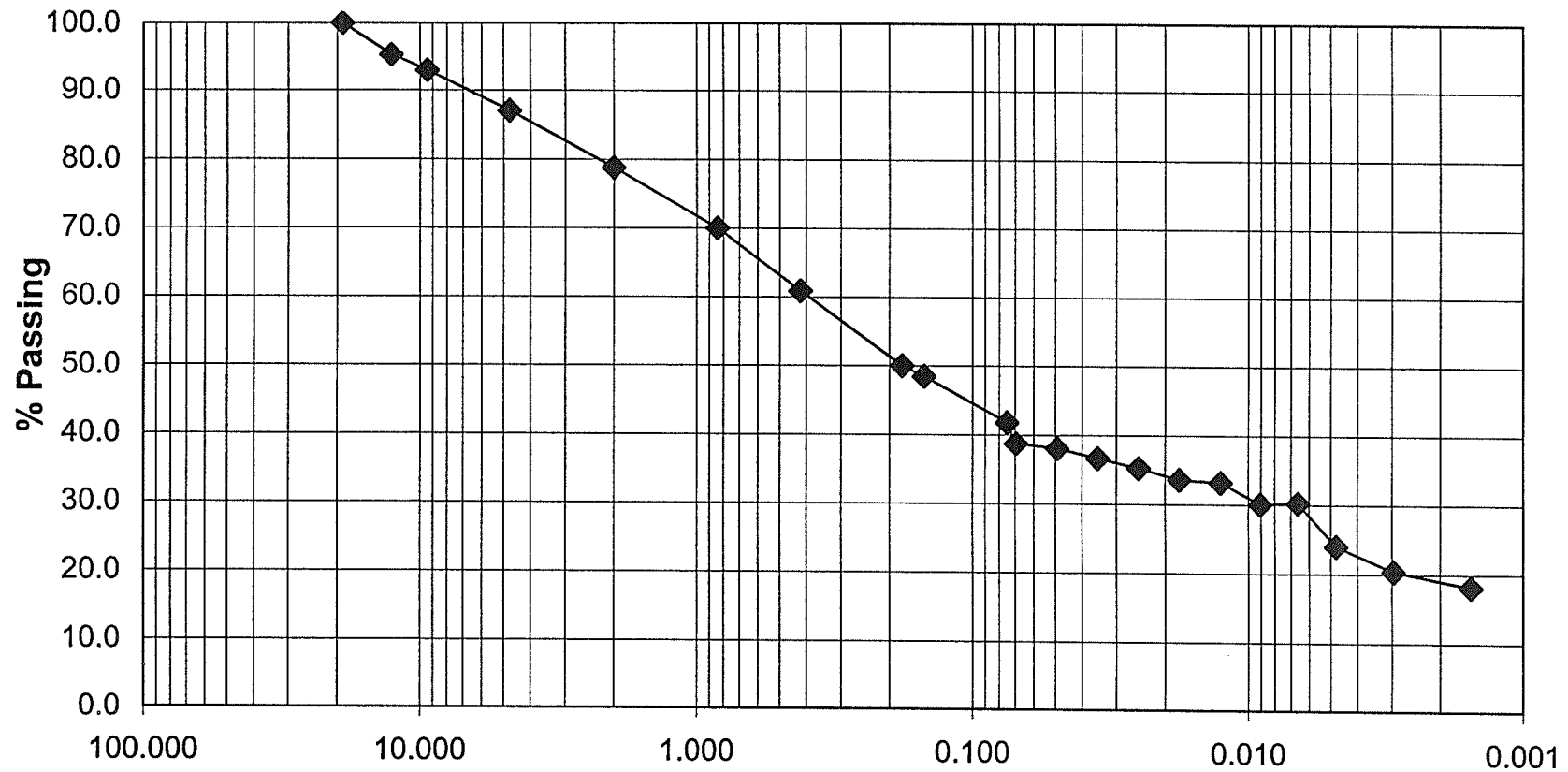
Project: PR259
Sample: BH2-2 Depth: 1.80 - 1.93 m
Date: November 6, 2000



Project: PR259
Sample: BH2-2(2) Depth: 1.96 - 2.13 m
Date: April 18, 2001



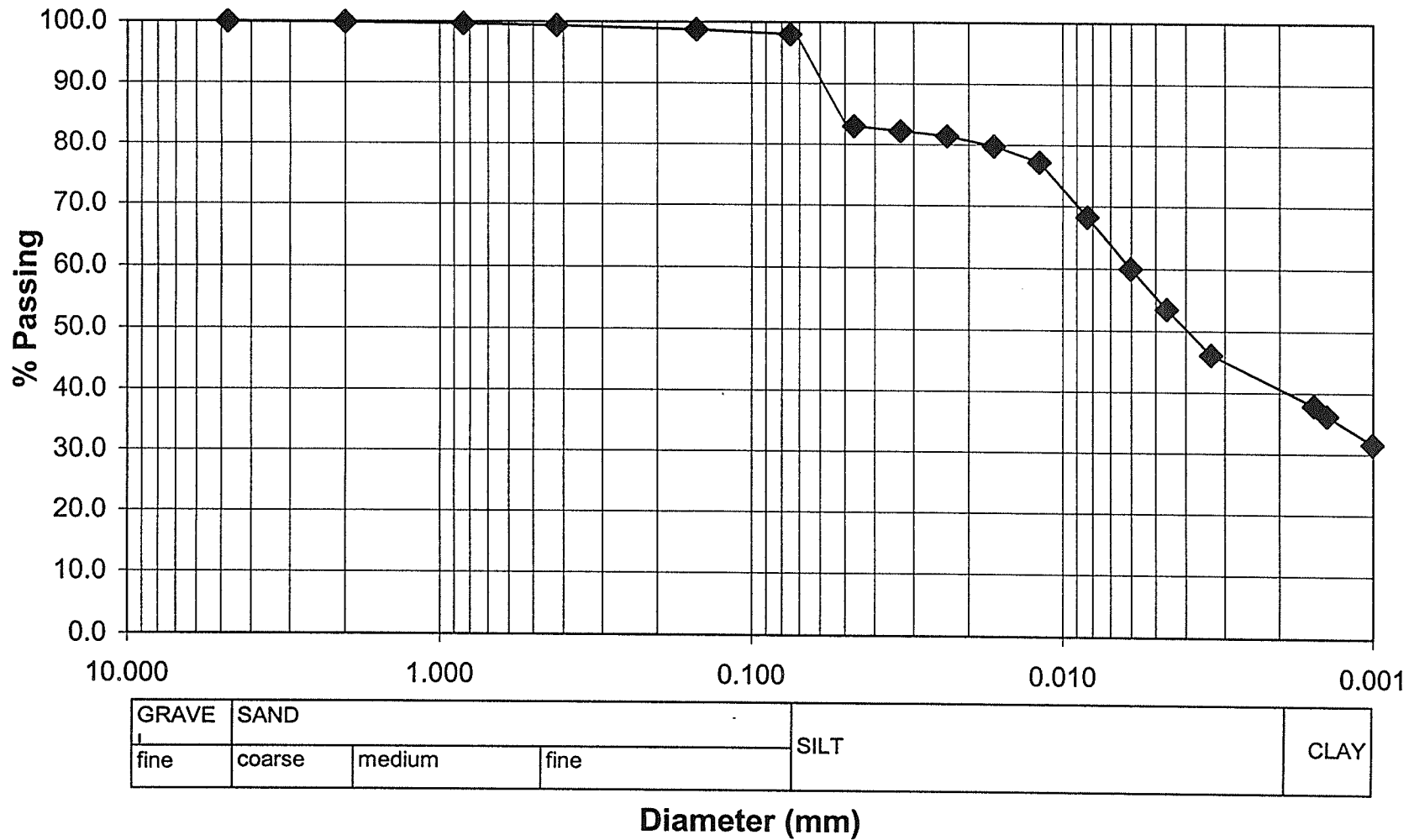
Project: PR259
Sample: BH2-3 Depth:2.49-2.74 m
Date: April 19, 2001



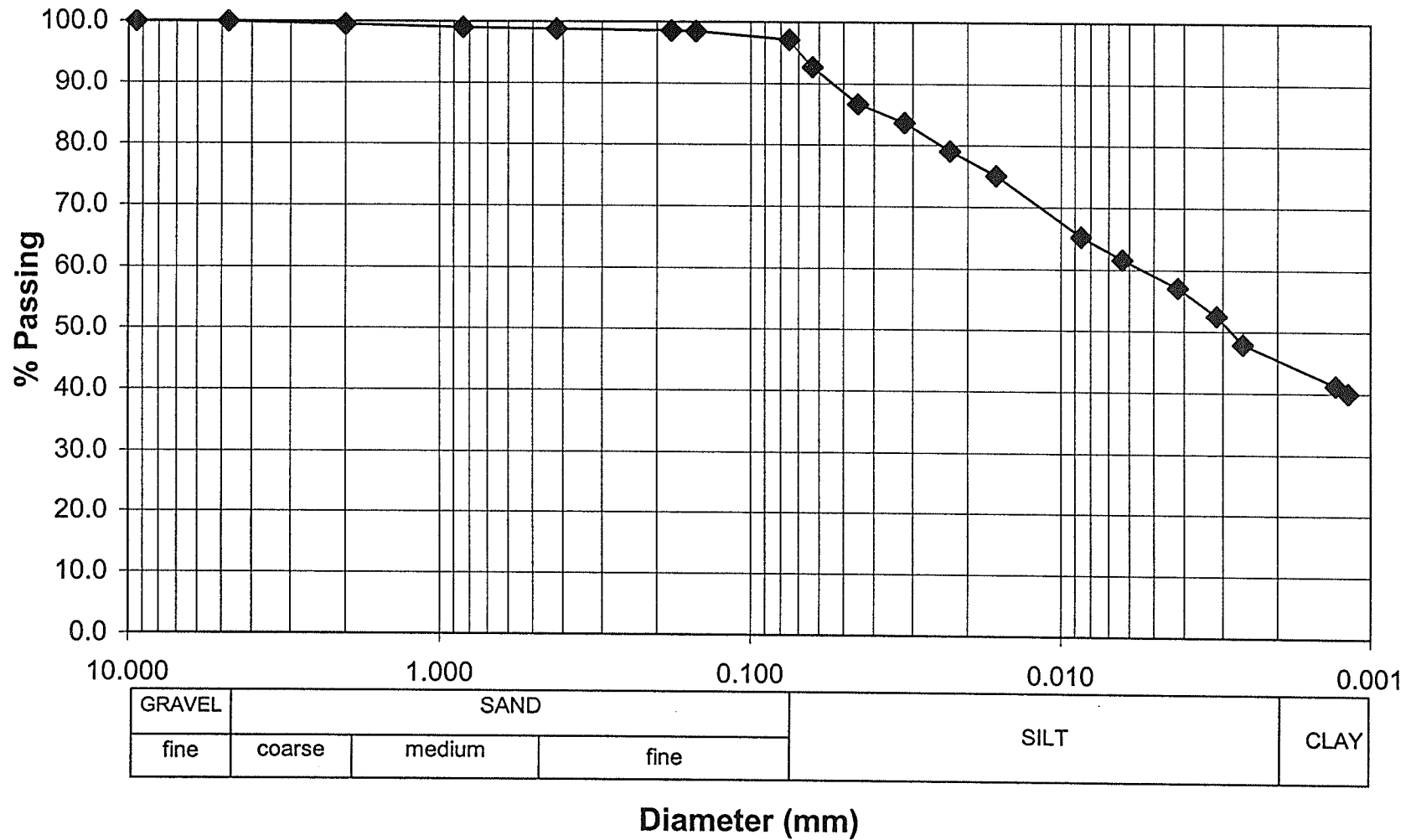
GRAVEL		SAND			SILT	CLAY
Coarse	fine	coarse	medium	fine		

Diameter (mm)

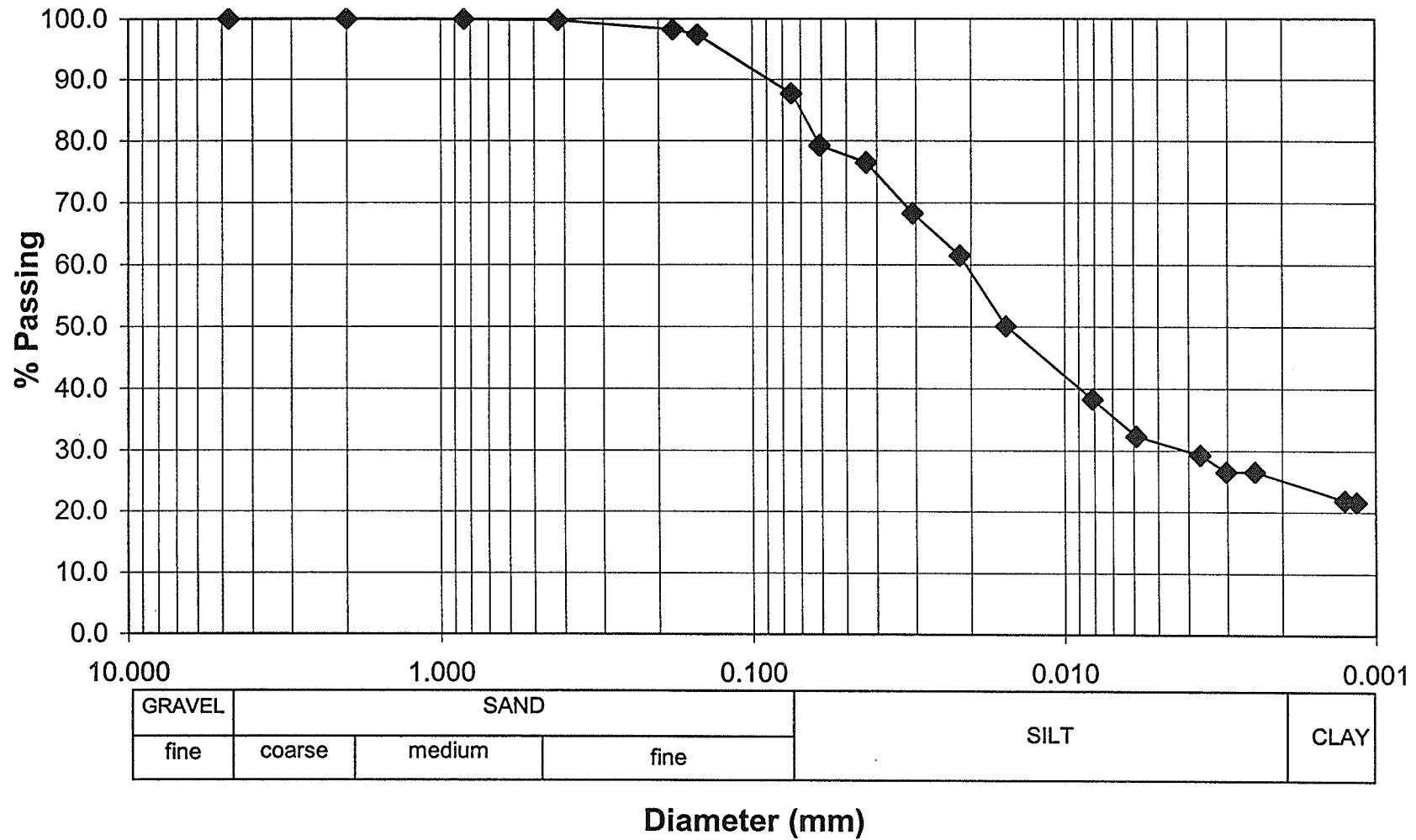
Project: PR259
Sample: BH2-4 Depth:3.06 m
Date: November 6, 2000



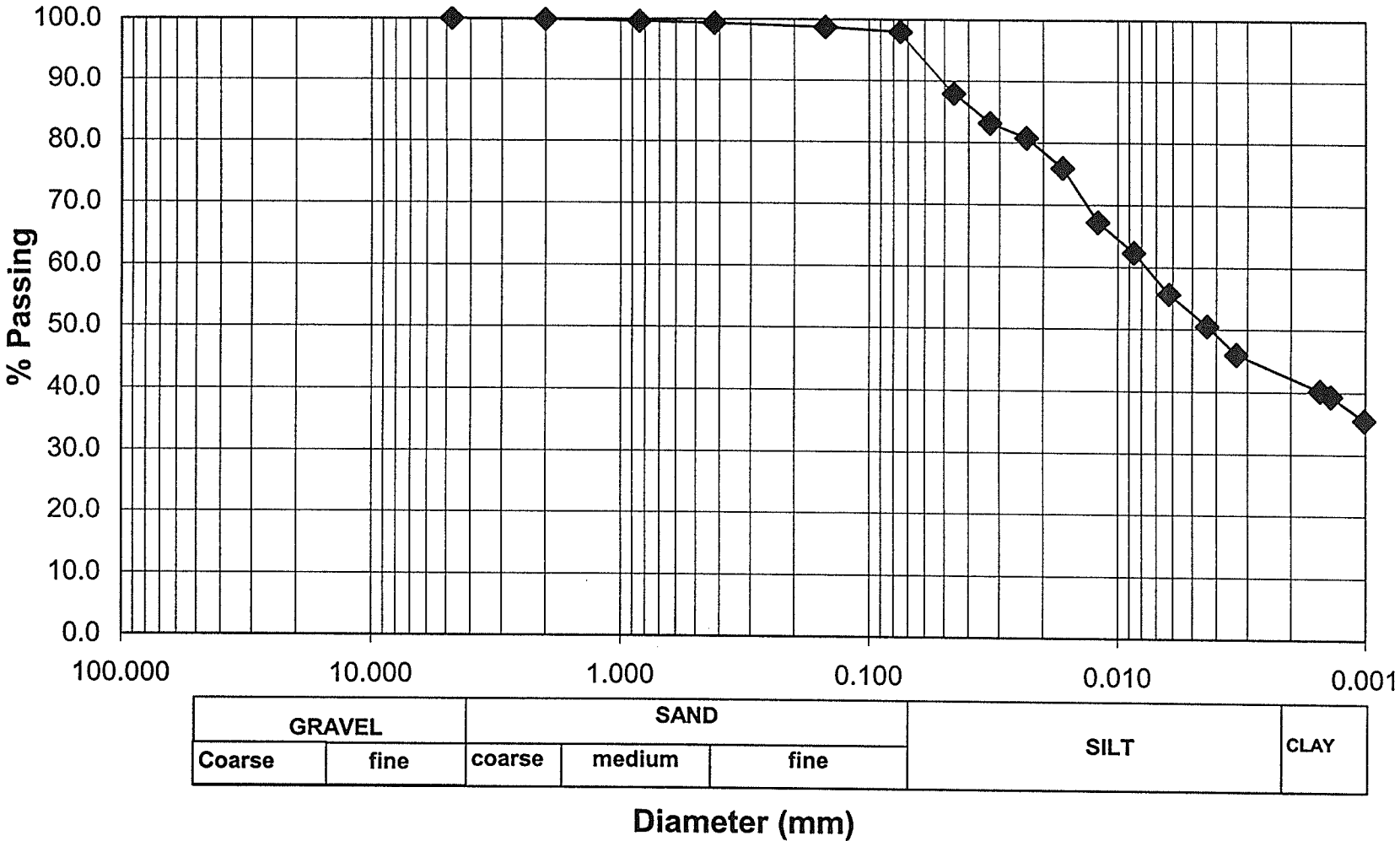
Project: PR259
Sample: BH2-4(2) Depth: 3.23 - 3.35 m
Date: June 28, 2001



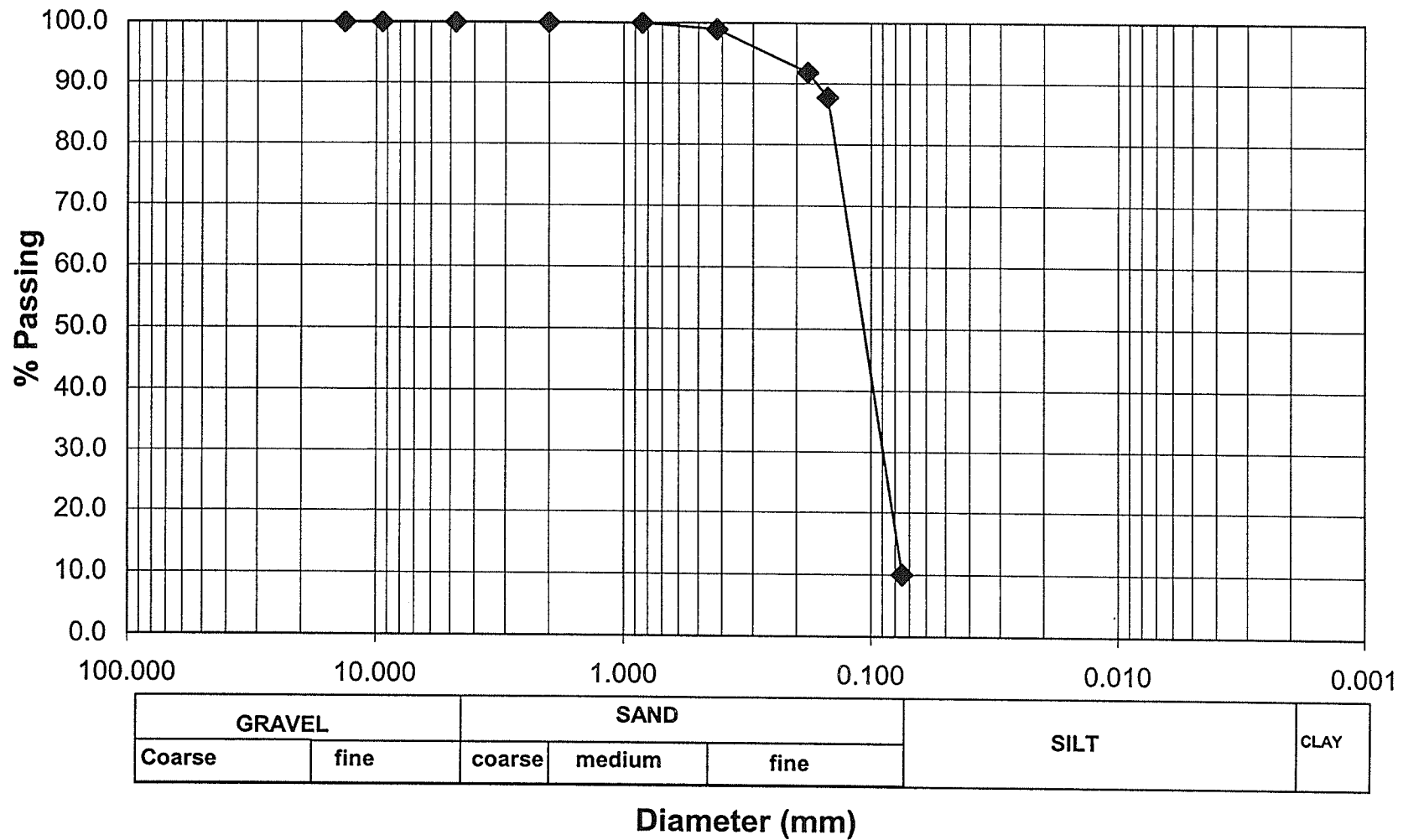
Project: PR259
Sample: BH2-5(2) Depth: 3.73 - 3.84 m
Date: June 28, 2001



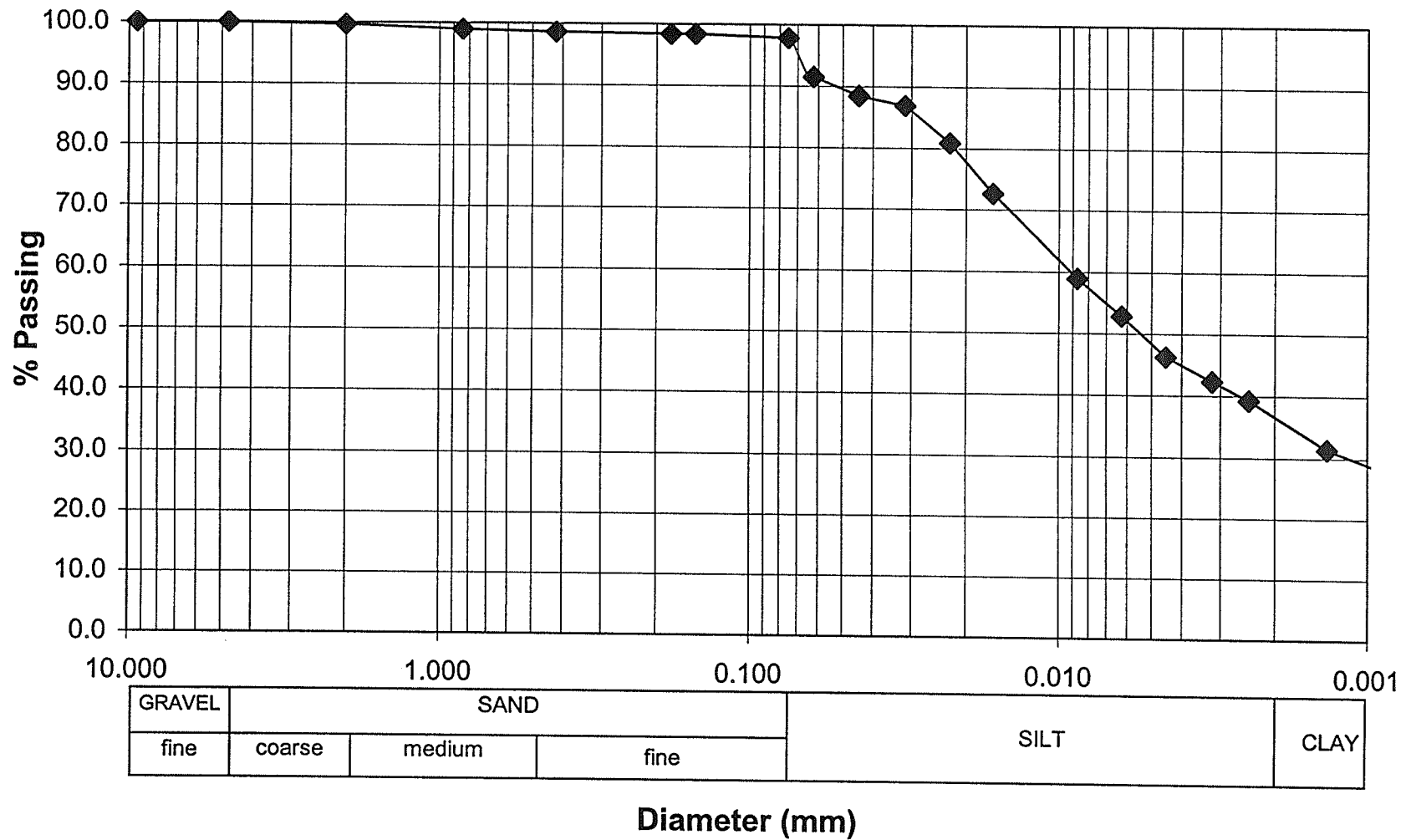
Project: PR259
Sample: BH2-6 Depth:4.267-4.572 m
Date: November 6, 2000



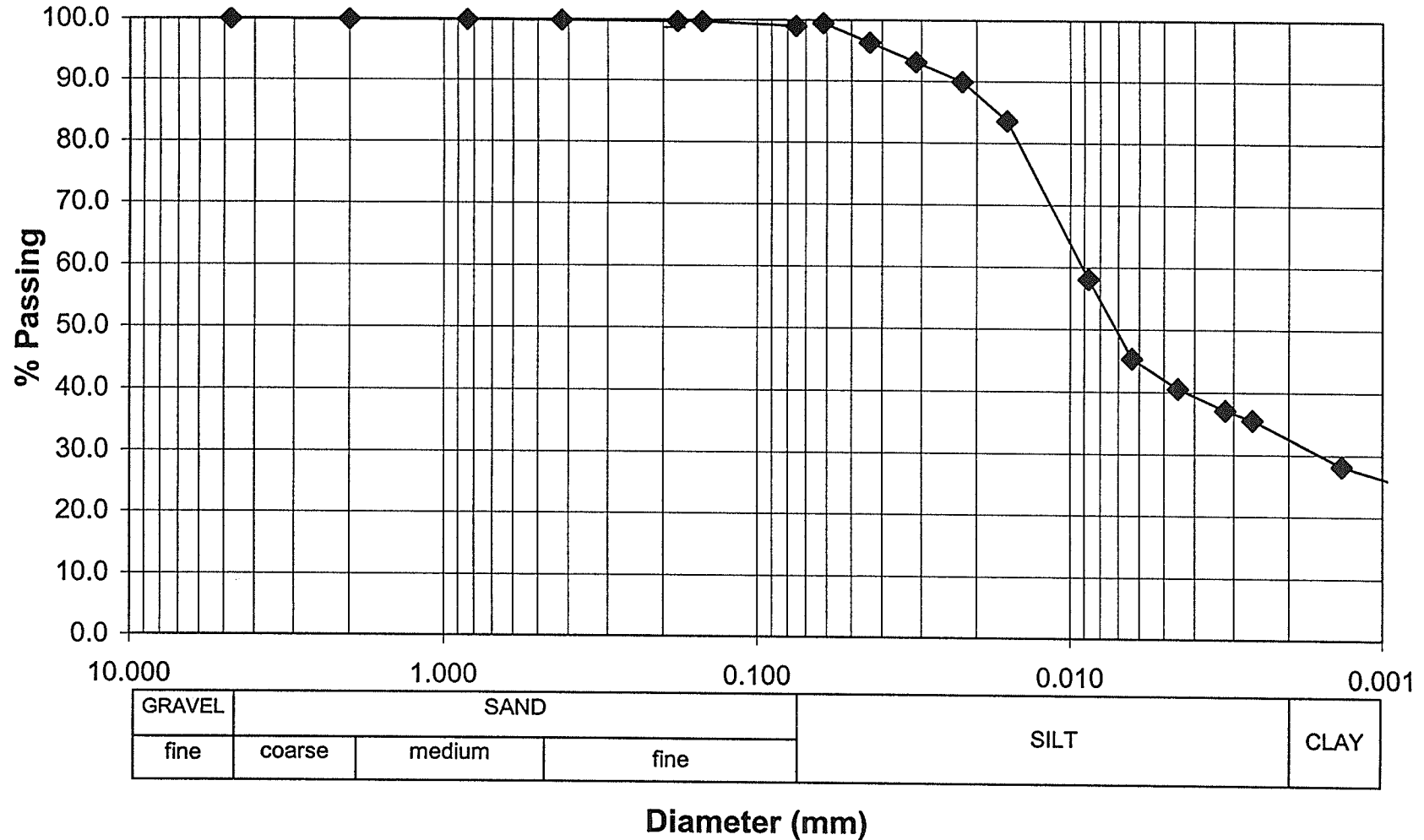
Date: December 28, 2001



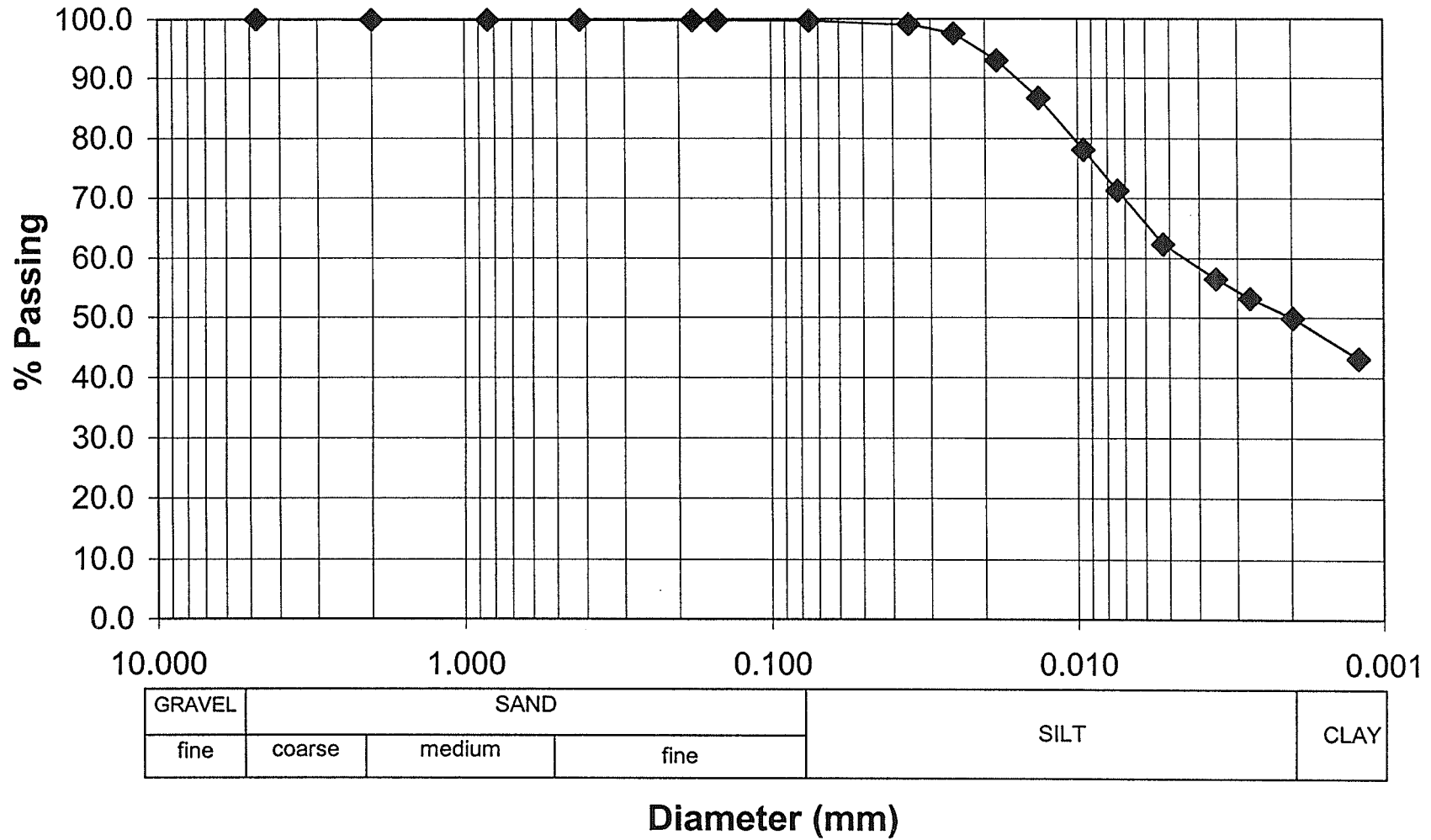
Project: PR259
Sample: BH3-1 Depth: 0 - 1.07 m
Date: June 26, 2001



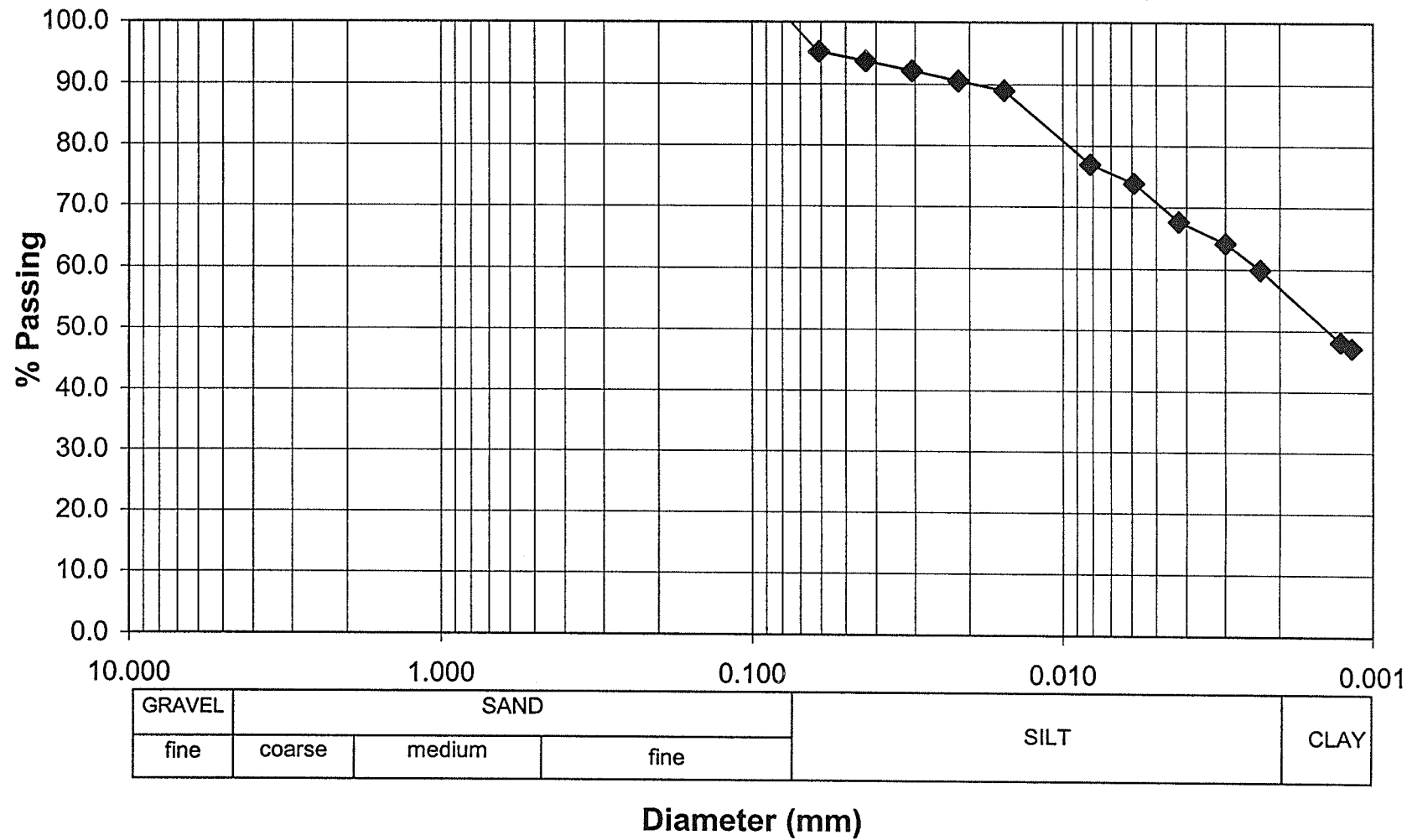
Project: PR259
Sample: BH3-2(2) Depth:1.07 - 1.52 m
Date: June 26, 2001



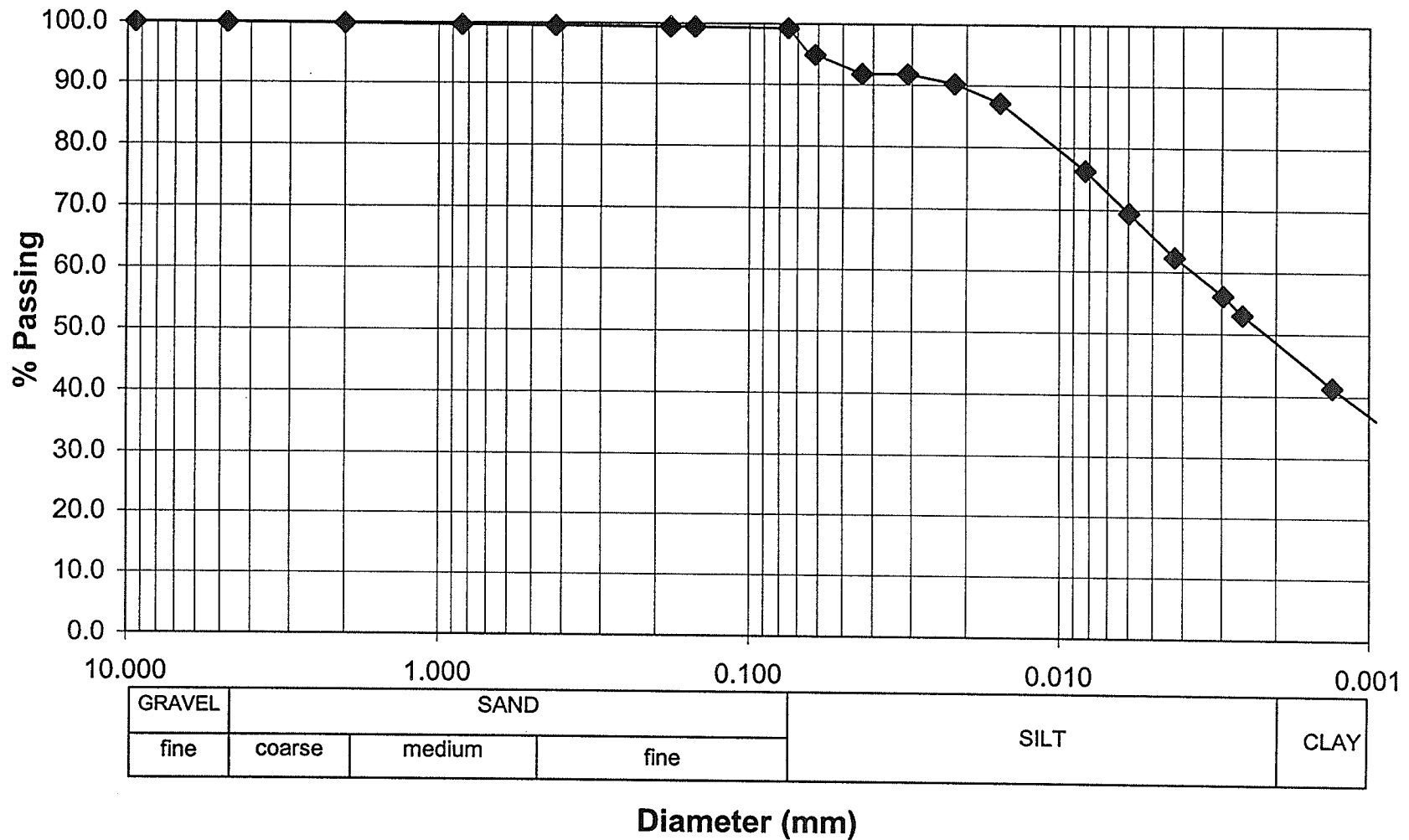
Project: PR259
Borehole: BH3-3 Depth: 1.57 - 1.78 m
Date: November 20, 2000



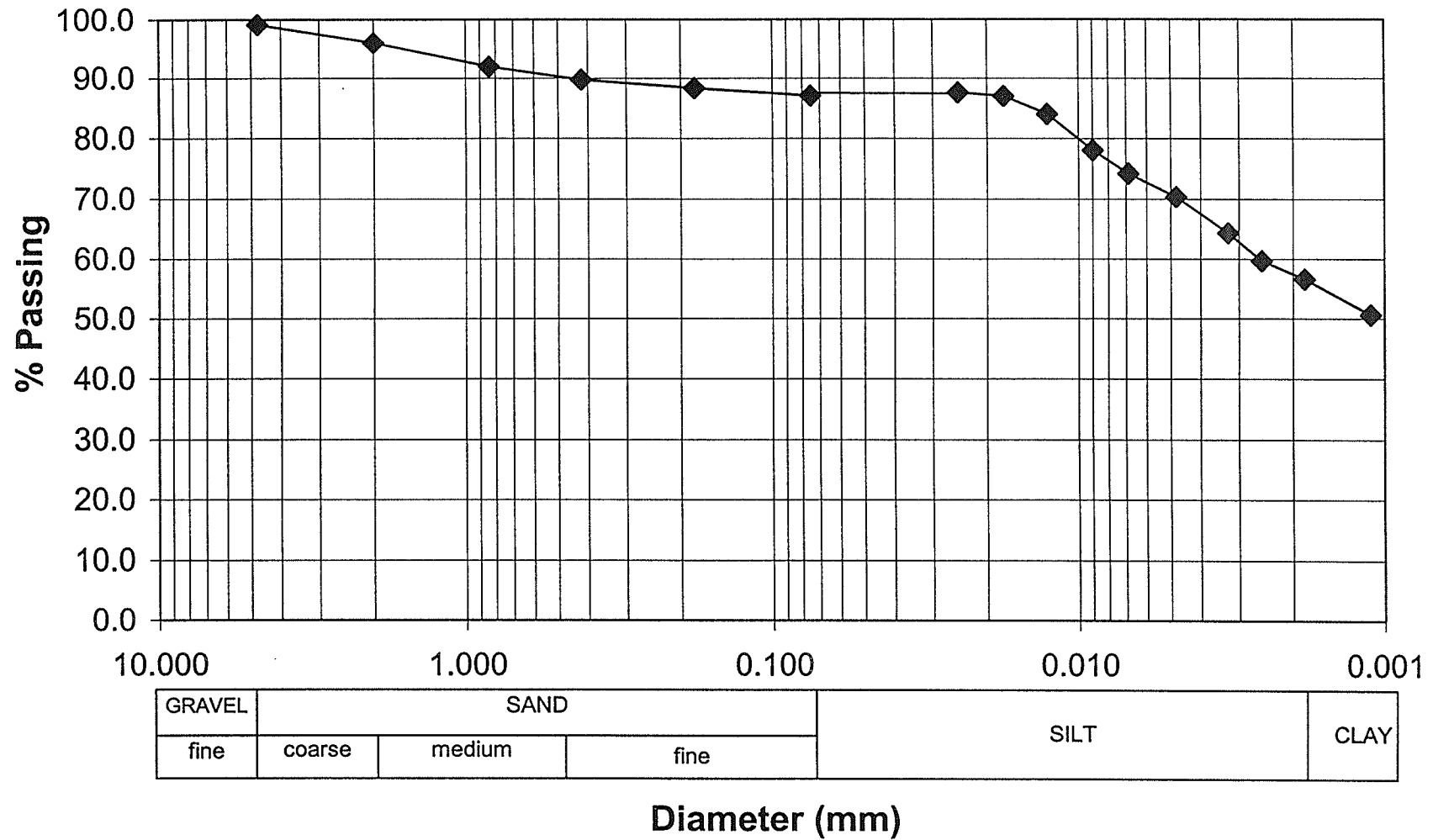
Project: PR259
Sample: BH3-3(2) Depth: 1.91 - 1.98 m
Date: June 28, 2001



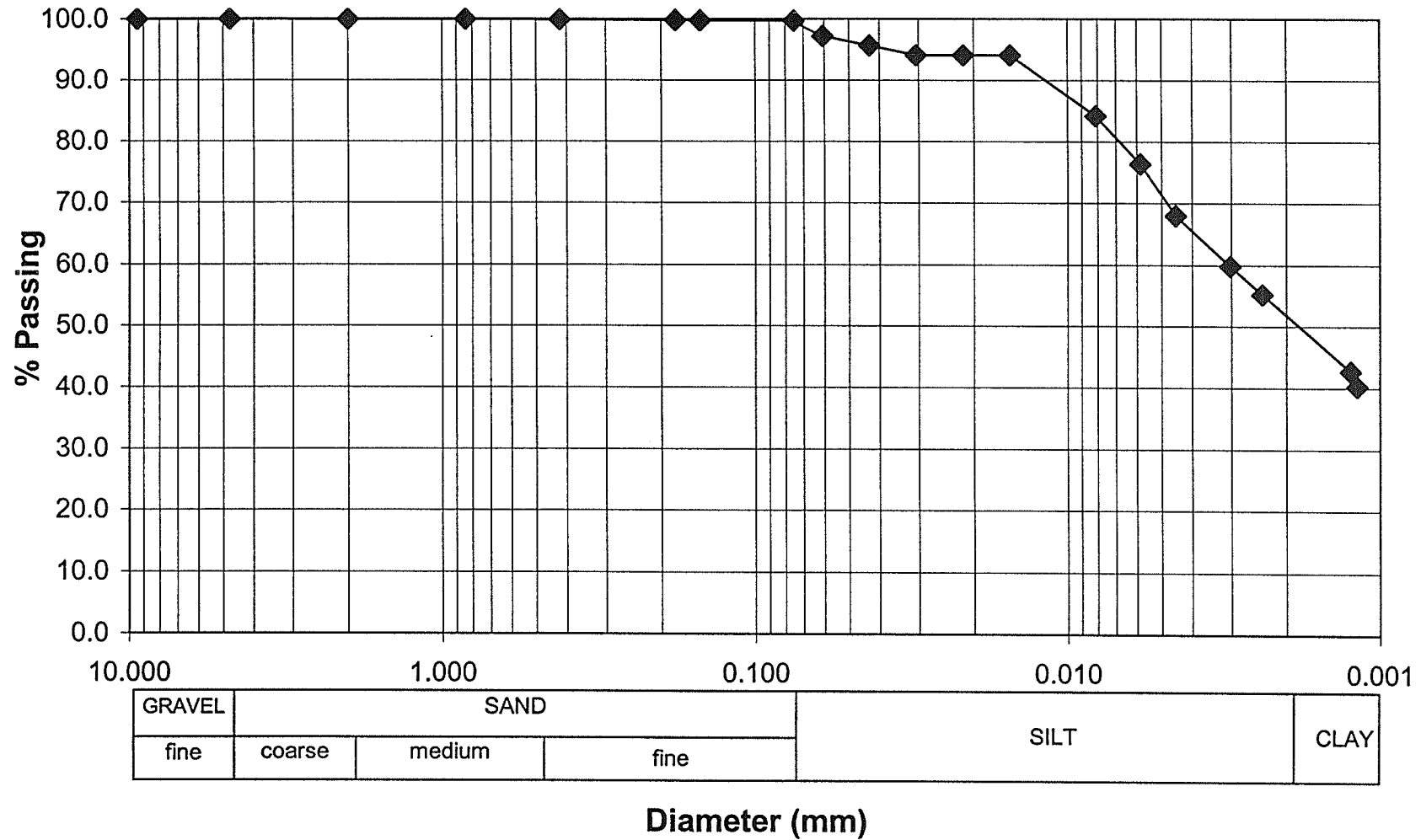
Project: PR259
Sample: BH3-4 Depth:2.331 - 2.413 m
Date: June 26, 2001



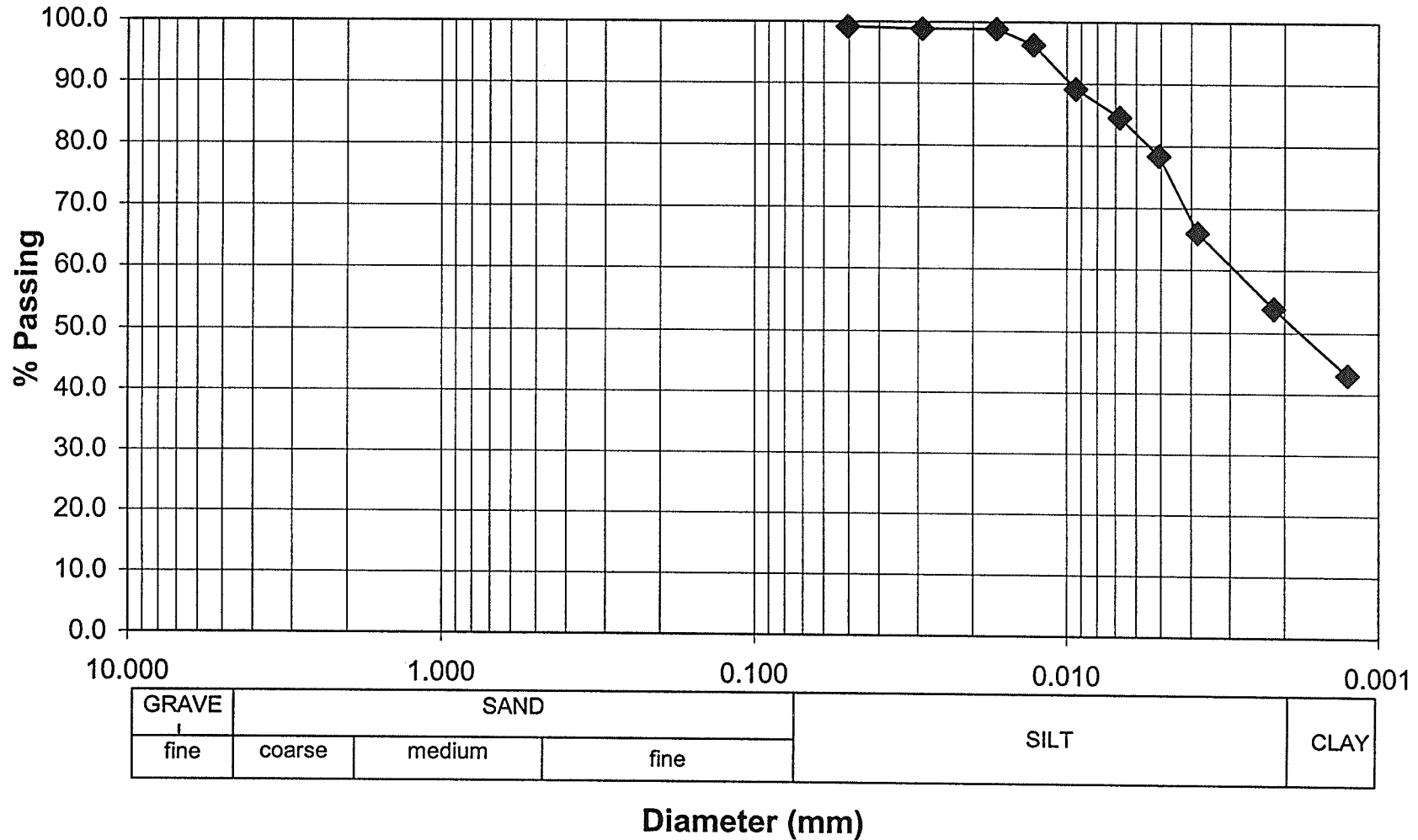
Project: PR259
Borehole: BH3-5 Depth: 3.175 m
Date: November 20, 2000



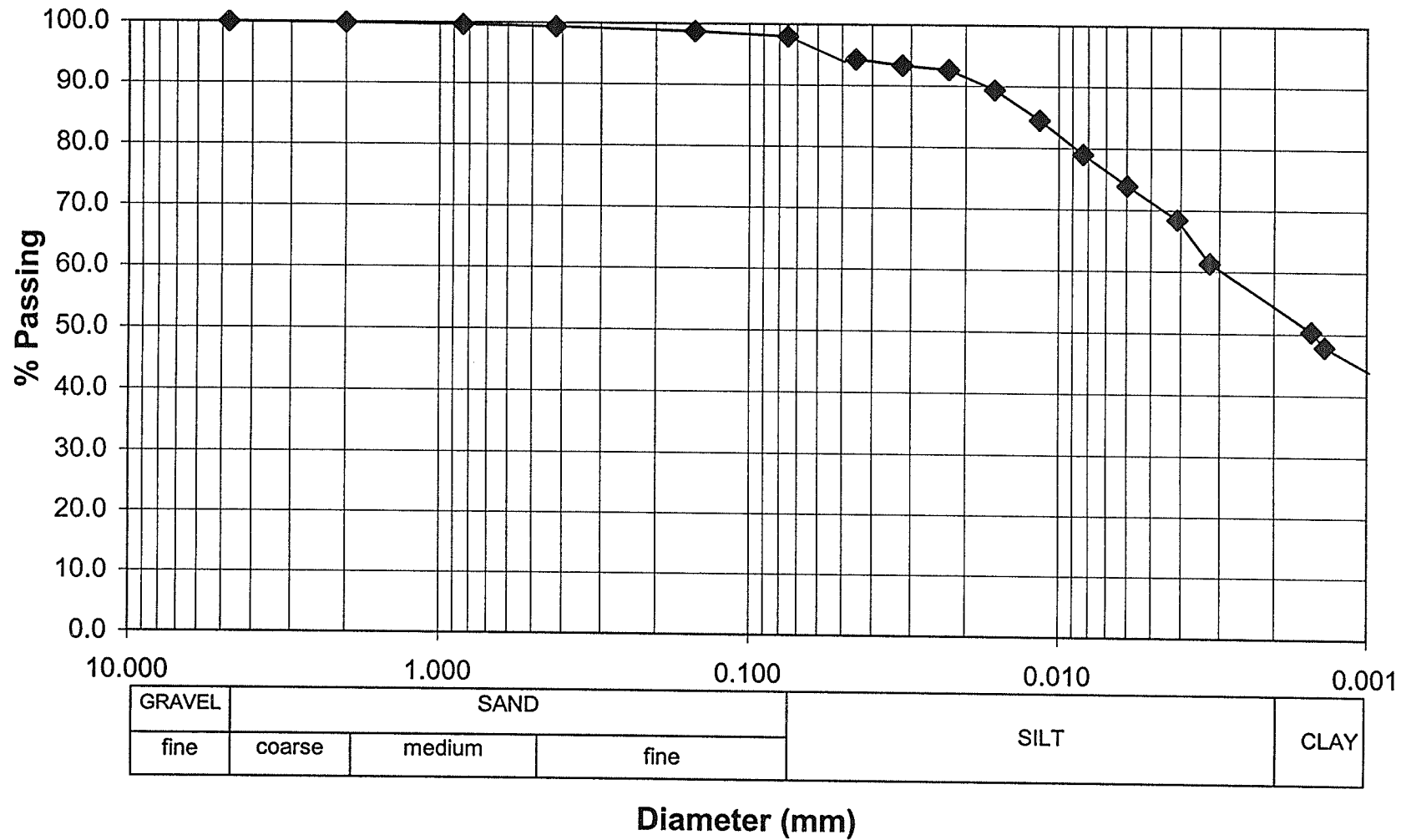
Project: PR259
Sample: BH3-6(2) Depth:3.40 - 3.51 m
Date: June 18, 2001



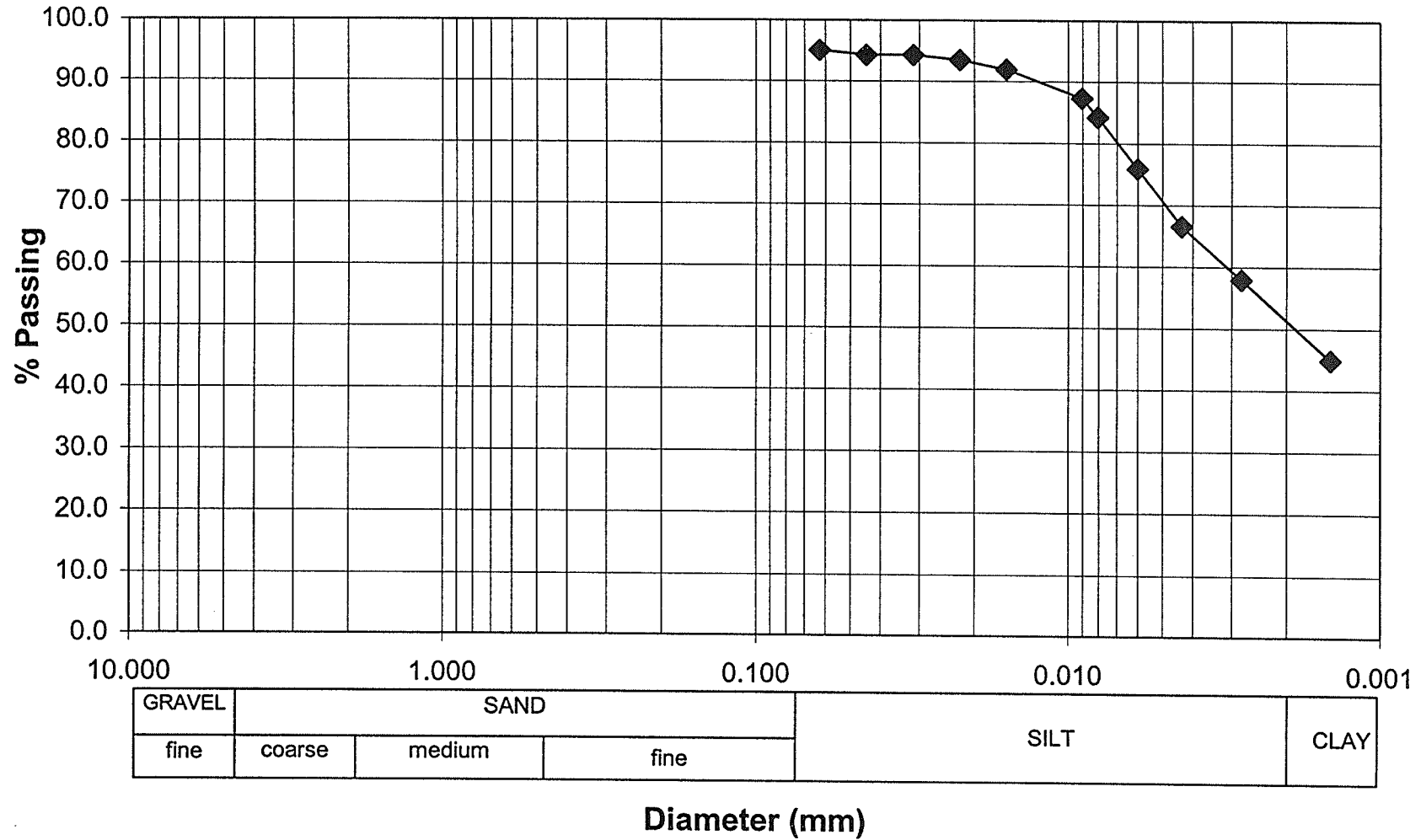
Project: PR259
Sample: BH3-6 Depth: 3.81 - 3.96 m
Date: April 18, 2000



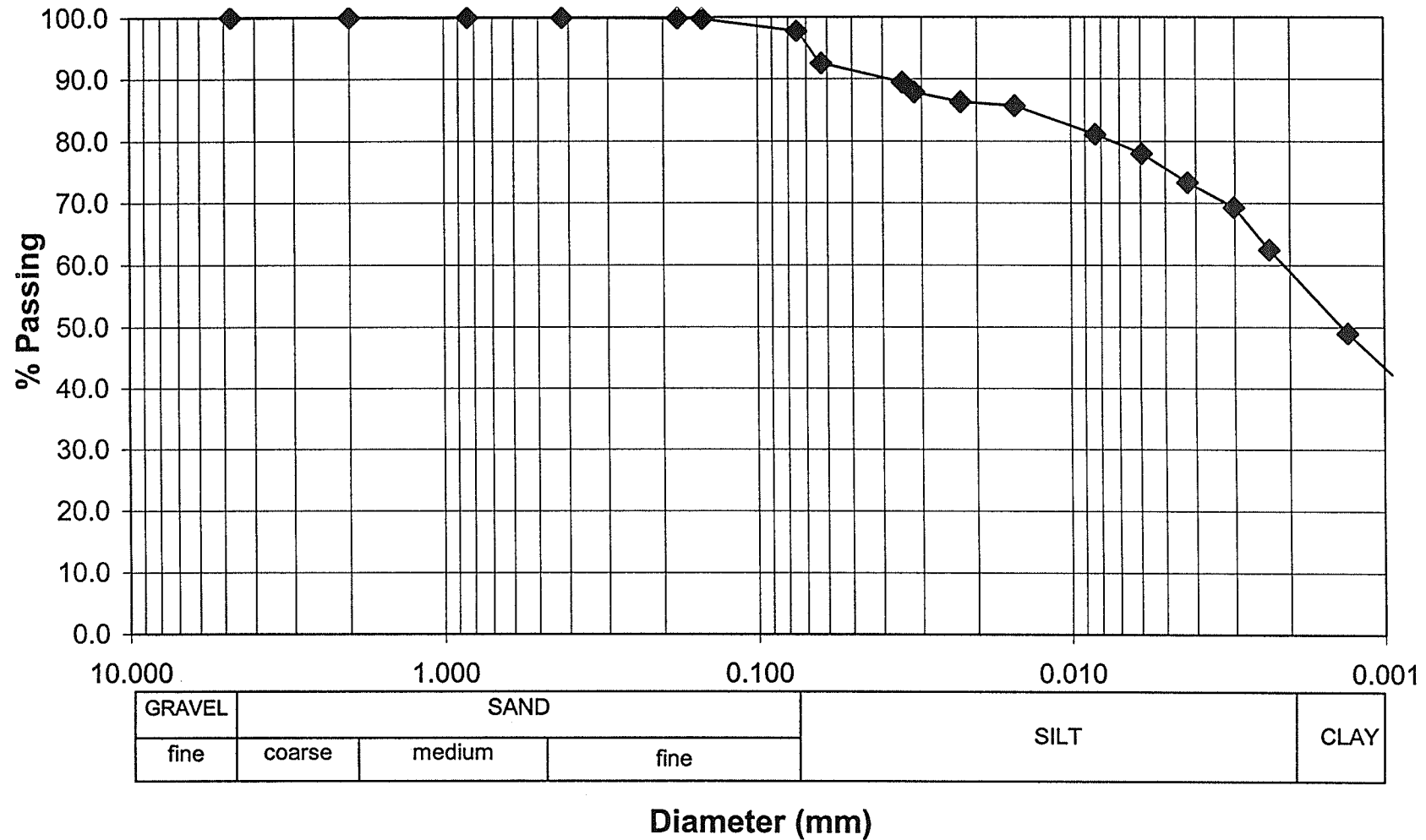
Project: PR259
Sample: BH3-7 Depth: 3.96 - 4.17 m
Date: November 6, 2000



Project: PR259
Sample: BH3-8 Depth:4.57-4.70 m
Date: April 19, 2001



Project: PR259
Sample: BH3-8(2) Depth: 5 - 5.18 m
Date: June 26, 2001



Appendix F: Gould Report



May 17, 1993

File No. 3016

M. M. Dillon Ltd.,
6 Donald Street South,
Winnipeg, MB
R3L 0K6

Attention; Mr. J. Ewing P.Eng

Dear Sir;

Re; Virden Water Supply Pipeline - Preliminary Geotechnical Considerations

1.0 General

A replacement water supply pipeline is proposed for the Town of Virden leading from a new well source to the existing reservoir, treatment plant and pumphouse. This pipeline is to be a buried line, below frost level 250 mm in diameter. The route selection of the pipeline is one facet of this preliminary investigation from which soil conditions, groundwater conditions and Assiniboine valley wall stability problems can be identified and assessed.

1.1 Subsurface Investigation

Following the site inspection of April 23, 1993 a subsurface investigation of the proposed pipeline route from the new well location SE1/4- 31-10-25W along PTH 259 to the Town of Virden was undertaken on May 3, 1993.

The subsurface investigation consisted of 10 augured tests holes extending to depths from 4.6m to 9.14m. The deeper test holes (TH-1, TH-2, TH-3, TH-4, TH-5, TH-10) concentrated upon subsurface conditions throughout the western Assiniboine Valley wall in an effort to determine soil and groundwater characteristics that may be responsible for indicated slope movements along PTH 259. These slope movements may influence the location of the supply line and the design.

2.0 Preliminary Soil Profile

2.1 Pipeline Route NE 25-10-26W to NE 22-10-26W

The soil profile along the PTH 259 right of way from the top of the Assiniboine valley wall to the Town of Virden, as determined from visual examination of soil samples obtained from test holes (TH-5 to TH-9) consists basically of fine sand overlying a silty clay. The depth of the fine sand varies from a minimum of 0.91m (TH-5) to 6.4m (TH-7). Coarse sand occurs immediately above the clay or in zones within the clay which is water bearing. Water levels below ground surface were found to vary along the route from a minimum of 2.3m (TH-8) with sand to the near surface clays (TH-5). Since these test holes were located within

the highway ditches, the water table is approximately 3.3m below the prairie level for the majority of the route. The position of the water table may vary seasonally with precipitation as indicated by the oxidation of the soil samples. Elevations and pipeline profile data have yet to be correlated to establish the problem areas.

2.2 Pipeline Route from New Wells to R.M. of Woodworth boundary

The pipeline route from the well to the crest of the valley wall has several alternatives from a geotechnical aspect. Surface indication of slope instability immediately adjacent PTH 259 is evident. The cause of this instability cannot be determined from this preliminary investigation, however the failure surfaces may be tangent to the shale surface indicated in TH-1, or within the stratified clays at higher elevations. TH-10, located at the toe of a slope in motion, high above the valley base, indicates a wet oxidized sand seam within the varved clay strata at a depth of 8.4m below the PTH 259 south ditch invert. TH-3 and TH-4 located along the south right of way, some distance from the road, suggest a direct route away from the road may be more stable. Soils indicated at the valley crest, consist of approximately 1.5m of a bouldery gravel till overlying a bouldery clay till. At the lower reaches the fine sand is dry, and extends to a depth of over 6.8 metres.

3.0 Depth of Pipeline Bury

The depth of bury required to protect the line from freezing during sustained low temperature periods is governed by the soil characteristics and the sustained temperatures under snow cover conditions. Moisture content and density, critical factors in computing the probable depth of frost penetration vary considerably but are estimated at 10% for sands above the water table at a dry density of 110 p.c.f. Applying the modified Berggren equation for a sand, and 3000 degree days of frost annually, the frost depth is computed between 64 inches and 43 inches depending upon the snow cover. Since the Virden area rarely has deep snow cover, it is wise to consider the deeper bury as a minimum, and 78 inches (2.0m) is recommended to provide additional protection for surface irregularities and material moisture and density variations.

4.0 Pumphouse Foundations

Informal logs of the test well produced by Paddock Drilling in April 1993 at the site of the permanent well indicate 60 feet (18 metres) of clay overlying sand and gravel to a maximum depth of 80 feet (24.4 metres). The permanent well and the formal log have yet to be produced. Pumphouse weights re M. M. Dillon will be in to order of 2000 lbs which produced relatively low unit loading on a slab or spread footing. The clay soils of the Virden area generally have high silt content and there is a high potential for frost heave. Foundations to provide stability can either be deep units which obtain support within clays below frost penetration depths or flexibility can be incorporated into the connections and lines to permit movement without stressing the joints. For high pressure lines, flexibility may be difficult mechanically to incorporate and expensive, consequently a deeper foundation may prove desirable.

A deep foundation alternative should consist of driven or cast-in-place pilings extending to minimum depths of 15 feet (4.5m) and pile caps or slabs should be provided with an underside void or compressible material of at least 150mm in thickness to permit soil movement without adding stress to the structure.

Alternatively, a Slab-on-grade structure may prove more economical, however, normally, soil surface movements can be up to 150mm annually, consequently considerable flexibility must be provided in all pipe and service connections. Frost action can be reduced with the provision of a heated space and 6-inches of rigid, high density, insulation installed below the base, extending for a minimum of 2 metres from the perimeter of the slab. The insulation should be covered with a minimum of (8-inches) 250mm of granular material for protection. The granular base material should be graded and the area of the pumphouse elevated (perched) to ensure drainage and minimize frost action.

5.0 Preliminary Summary

The pipeline route leading from the new wells, which would appear to present the least stability problems, appears from this preliminary review, favours a position away from PTH 259 rising from the valley floor directly up the valley wall to the prairie level along the south right of way limit. A highway ditch location for this pipeline section, may encounter high groundwater levels and trench instability. A potential does exist for adding to current highway embankment instability problems and the line maintenance, operation and liability consequences must be recognized. The boulders embedded into the soils will present excavation problems and require careful attention to pipe bedding and backfill.

From the valley crest to the Town of Virden, soils are predominately fine sands and the groundwater table which is known to fluctuate seasonally, may produce trench instability problems at lower pipeline sectors. A pipeline location at prairie level, above the highway ditch line is recommended, providing right-of-way is available at reasonable cost. A slightly higher location at prairie level, would enable depth of bury to be obtained for frost protection, yet significantly reduce the risk of trench instability.

Respectfully Submitted,



A. Dean Gould P.Eng.
Geotechnical Consultant



A. Dean Gould and Associates Geotechnical Engineers		Location; Town of Virden, Manitoba		Test Hole No. 1.		Project No. 3016	
PROJECT DESCRIPTION; Virden Water Supply Pipeline Replacement New Well to Reservoir				DRILLING DATE; May 3, 1993			
CLIENT; M. M. Dillon Ltd.,				DRILLER; Paddock Drilling Ltd. Brat 22 LOGGED BY; J. Kuchak C.E.T.			

SAMPLE NO.	DEPTH (m)	ELEV.	b	SOIL DESCRIPTION	MOISTURE CONTENT (%)			
					20	40	60	80
1R1	1.52m	381.085		0 - 0.3 m Brown, clayey moist sand				
		1 m		0.3 - 2.90 m Fine brown Sand some silt and frost				
		2 m						
1R2	3.81m 377.275	3 m		2.9 - 5.18 m Brown, firm, silty sandy clay Till with shale particles and oxide inclusions. Cobbles and boulders at 6.1 m				
		4 m						
1R3	5.33m 375.755	5 m		5.18 - 9.11 m Dark grey Shale, plastic, firm, as soapstone, greasy firmer below 6.85 m				
1R4	6.10m 374.985	5 m		9.14 m Bottom of Test Hole				
1R5	6.86m	6 m						
		7 m						

LEGEND	TOPSOIL	SILT	BROWN CLAY	TEST PIT No. 1
	SAND AND GRAVEL	TILL	GREY CLAY	
	PLASTIC LIMIT x LIQUID LIMIT N = Standard Penetration Value blows/ft qu = Unconfined Compression Strength (kPa)			

A. Dean Gould and Associates Geotechnical Engineers		Location: Town of Virden, Manitoba		Test Hole No. 2		Project No. 3016		
PROJECT DESCRIPTION: Virden Water Supply Pipeline Replacement New Well to Reservoir				DRILLING DATE: May 3, 1993				
CLIENT: M. M. Dillon Ltd.				DRILLER: Paddock Drilling Ltd. Brat 22 LOGGED BY: using 5-inch Flight Augers				
SAMP NO.	DEPTH (m)	ELEV.	b	SOIL DESCRIPTION	MOISTURE CONTENT (%)			
					20	40	60	80
2R1		388.151		0 - 3.05m Brown, fine clean Sand moist,				
		1 m						
		2 m						
		3 m		3.05 - 6.85 m Brown fine clean sand 385.101 with clay and shale particles water at 6.85 m (381.301)				
		4 m						
2R2	3.81m 384.341	5 m						
2R3	6.10m 382.051	6 m						
2R4	6.86m 381.291	7 m		6.85 - 8.08 Grey clayey Sand mix. wet 381.301 plastic				
	7.92m 380.231	8 m		8.08 - 9.14 m Brown wet, silty Sand 380.071 with occ. stones, slough @ 8.5m				
LEGEND <div style="display: flex; justify-content: space-around; align-items: flex-start;"> <div> TOPSOIL SAND AND GRAVEL </div> <div> SILT TILL </div> <div> BROWN CLAY GREY CLAY </div> <div> TEST HOLE No. 2 </div> </div> <div style="margin-top: 10px;"> PLASTIC LIMIT x _____ x LIQUID LIMIT N = Standard Penetration Value blows/ft qu = Unconfined Compression Strength (kPa) </div>								

A. Dean Gould and Associates Geotechnical Engineers		Location; Town of Virden, Manitoba		Test Hole No. 3.		Project No. 3016		
PROJECT DESCRIPTION; Virden Water Supply Pipeline Replacement New Well to Reservoir				DRILLING DATE; May 3, 1993				
CLIENT; M. M. Dillon Ltd.				DRILLER; Paddock Drilling Ltd. Brat 22 LOGGED BY; using 5 inch Flight Augers J. Kuchak C.E.T.				
SAMPLING NO.	DEPTH (m)	ELEV.	b	SOIL DESCRIPTION	MOISTURE CONTENT (%)			
					20	40	60	80
3R1	3.04 m 423.941	426.981		0 - 0.30m Black, organic Topsoil				
				0.3 - 0.76 m Dense, boulders and cobble Till				
		1 m		0.76 - 1.52 m Brown, moist, fine, silty Sand				
		2 m		1.52 - 7.62 m Brown, fine silty, sandy clay Till, with oxide inclusions Stone sizes to 2.5mm, Shale fragments. Cobbles and boulders throughout.				
3R2	4.57 m 422.411							
		3 m						
3R3	6.10 m 420.881							
		4 m						
3R4	7.62 m 419.361							
		5 m						
		6 m						
		7 m						
		8 m		7.62 - 8.53 m Grey, hard, oxidized silty clay. Varved, with oxidation of silt between clay				

LEGEND

TOPSOIL SILT BROWN CLAY TEST HOLE No. **3**

SAND AND GRAVEL TILL GREY CLAY

PLASTIC LIMIT x x LIQUID LIMIT

N = Standard Penetration Value blows/ft

qu = Unconfined Compression Strength (kPa)

A. Dean Gould and Associates Geotechnical Engineers		Location: Town of Virden, Manitoba		Test Hole No. 4.		Project No. 3016	
PROJECT DESCRIPTION: Virden Water Supply Pipeline Replacement New Well to Reservoir				DRILLING DATE: May 3, 1993			
CLIENT: M. M. Dillon Ltd.				DRILLER: Paddock Drilling Ltd., Brat 22 LOGGED BY: J. Kuchak C.E.T. using 5-inch Flight Augers			

SAMP PILE NO.	DEPTH (m)	ELEV.	b	SOIL DESCRIPTION	MOISTURE CONTENT (%)			
					20	40	60	80
4R1	1.52m 427.214	428.734		0 - 0.15m Black, organic sandy Topsoil				
				0.15 - 1.21m Sand, gravel and Boulders				
				428.584				
4R2	2 m 3.04m 425.694	1 m		1.21 - 2.28m Brown, firm, silty sandy, Till Mp-Hp clay till with oxidized silt inclusions. more sand and less clay 1.5-2.2m				
		2 m		2.28 - 3.04m Hard Clay Till with silt and alkali inclusions, shale pieces and occasional oxides.				
		3 m		3.04 - 6.10m Dark brown, hard, sandy silty Clay. mp-hp moist, small shale particles no oxidization				
4R3	4 m 4.57m 424.164	4 m						
		5 m						
		6 m						
4R4	6.10m 422.634	6 m						
		7 m		6.10 Bottom of Test Hole 422.634				
3R4	7.62 421.514	8 m						

LEGEND	TOPSOIL	SILT	BROWN CLAY	TEST HOLE No. 4
	SAND AND GRAVEL	TILL	GREY CLAY	
PLASTIC LIMIT x x LIQUID LIMIT N = Standard Penetration Value blows/ft qu = Unconfined Compression Strength (kPa)				

A. Dean Gould and Associates Geotechnical Engineers		Location; Town of Virden, Manitoba		Test Hole No. 5.		Project No. 3016	
PROJECT DESCRIPTION; Virden Water Supply Pipeline Replacement New Well to Reservoir				DRILLING DATE; May 3, 1993 DRILLER; Paddock Drilling Ltd. Brat 22 LOGGED BY; using 5 inch High Augers			
CLIENT; M. M. Dillon Ltd.							
SAMPLING NO.	DEPTH (m)	ELEV.	SOIL DESCRIPTION	MOISTURE CONTENT (%)			
				20	40	60	80
5R1	1.52m 440.138	441.658	0 - 0.91m Brown, silty sandy loam and gravel fill, with boulders				
		1 m	0.91 - 1.52m Grey-brown fine silty sandy clay Till. Contains shale and sand with oxidized inclusions. and less clay 1.5-2.2m				
		2 m	1.52 - 6.10m Dark brown firm highly plastic silty, sandy Till. Contains shale particals, very hard, some oxidization				
5R2	3.04m 438.618	440.748					
		440.138					
5R3	4.57m 437.088	3 m					
		4 m					
5R4	6.10m 435.558	5 m					
		6 m					
		7 m	6.10 Bottom of Test Hole 435.558				
		8 m					
LEGEND <div style="display: flex; justify-content: space-around; align-items: flex-start;"> <div> TOPSOIL SAND AND GRAVEL </div> <div> SILT TILL </div> <div> BROWN CLAY GREY CLAY </div> <div> TEST HOLE No. 5 </div> </div> <div style="margin-top: 5px;"> PLASTIC LIMIT x LIQUID LIMIT N = Standard Penetration Value blows/ft qu = Unconfined Compression Strength (kPa) </div>							

A. Dean Gould and Associates Geotechnical Engineers		Location; Town of Virden, Manitoba		Test Hole No. 6.		Project No. 3016	
PROJECT DESCRIPTION; Virden Water Supply Pipeline Replacement New Well to Reservoir				DRILLING DATE; May 3, 1993			
CLIENT: M. M. Dillon Ltd.				DRILLER; Paddock Drilling Ltd. Brat 22 LOGGED BY; using 5-inch High Augers			

SAMPLING NO.	DEPTH (m)	ELEV.	SOIL DESCRIPTION	MOISTURE CONTENT (%)			
				20	40	60	80
6R1	1.52m 439.519	441.039	0 - 0.30m Brown, organic sandy topsoil				
			0.30 - 1.07m Brown, loose, silty Sand				
		440.739					
		1 m	1.07 - 1.52m Brown, sandy Silty. 439.969 Contains lenses of sand, oxidized.				
6R2	4.57m 436.469	439.519	1.52 - 3.35m Brown, moist to wet, silty Sand. water enters hole at 2.4 m depth. Elev. 438.639				
		2 m					
		3 m	3.35 - 4.57m Grey uniform, silty Clay. 437.689 Highly plastic, firm, uniform no visible inclusions.				
		4 m	4.57 Bottom of Test Hole 436.469				
		5 m					
		6 m					
		7 m					
		8 m					

LEGEND

TOPSOIL SILT BROWN CLAY TEST HOLE No. 6

SAND AND GRAVEL TILL GREY CLAY

PLASTIC LIMIT x x LIQUID LIMIT

N = Standard Penetration Value blows/ft

qu = Unconfined Compression Strength (kPa)

A. Dean Gould and Associates Geotechnical Engineers		Location; Town of Virden, Manitoba		Test Hole No. 7.		Project No. 3016		
PROJECT DESCRIPTION; Virden Water Supply Pipeline Replacement New Well to Reservoir				DRILLING DATE; May 3, 1993				
CLIENT; M. M. Dillon Ltd.				DRILLER; Paddock Drilling Ltd. Brat 22 using 5-inch Flight Augers				
LOGGED BY; T. Kuchak C.E.T.								
SAMPLE NO.	DEPTH (m)	ELEV.	b	SOIL DESCRIPTION	MOISTURE CONTENT (%)			
					20	40	60	80
7R1	2.29m 438.226	440.516		0 - 0.76m Silty Clay Fill				
				0.76 - 6.40m Tan, moist, very silty fine Sand. Occassional oxide				
7R2	4.57m 435.946	439.756						
7R3	6.10m 434.416	434.116		6.40 - 8.38m Grey, firm silty, highly plastic Clay. Contains sand seams. Water Inflow @ 8.38m				
				8.38 - 9.14m Wet, oxidized, very silty fine Sand. Some clay 8.5-9.1m				
7R4	8.53m 431.986	432.136						
	8 m	431.376		9.14m Bottom of Test Hole				

LEGEND	TOPSOIL	SILT	BROWN CLAY	TEST HOLE No. 7
	SAND AND GRAVEL	TILL	GREY CLAY	
	PLASTIC LIMIT x LIQUID LIMIT N = Standard Penetration Value blows/ft qu = Unconfined Compression Strength (kPa)			

A. Dean Gould and Associates Geotechnical Engineers		Location; Town of Virden, Manitoba		Test Hole No. 8.		Project No. 3016	
PROJECT DESCRIPTION; Virden Water Supply Pipeline Replacement New Well to Reservoir				DRILLING DATE; May 3, 1993			
CLIENT; M. M. Dillon Ltd.				DRILLER; Paddock Drilling Ltd. Brat 22 LOGGED BY; using 5-inch Flight Augers J. Kuchak C.E.T.			

SAMPLING REF	DEPTH (m)	ELEV.	SOIL DESCRIPTION	MOISTURE CONTENT (%)			
				20	40	60	80
8R1	2.74m 438.001	440.741	0 - 2.29m Brown, moist clean, fine - medium Sand				
		1 m					
		2 m	2.29 - 2.74m Coarse grey Sand. Wet 438.451 Water at 2.29 m (438.451) 2.74 - 4.57m Grey, firm silty Clay 438.001 dark brown @ 2.74m				
		3 m					
8R2	4.57m 436.171	4 m					
		5 m	4.57 Bottom of Test Hole 436.171				
		6 m					
		7 m					
		8 m					

LEGEND

TOPSOIL
SAND AND GRAVEL
SILT
TILL
BROWN CLAY
GREY CLAY

TEST HOLE No. 8

PLASTIC LIMIT x LIQUID LIMIT
N = Standard Penetration Value blows/ft
qu = Unconfined Compression Strength (kPa)

A. Dean Gould and Associates Geotechnical Engineers		Location: Town of Virden, Manitoba		Test Hole No. 9.		Project No. 3016		
PROJECT DESCRIPTION: Virden Water Supply Pipeline Replacement New Well to Reservoir				DRILLING DATE: May 3, 1993				
CLIENT: M. M. Dillon Ltd.				DRILLER: Paddock Drilling Ltd., Brat 22 LOGGED BY: using 5-inch Flight Augers J. Kuchak C.E.T.				
SAMPLE NO.	DEPTH (m)	ELEV.	b	SOIL DESCRIPTION	MOISTURE CONTENT (%)			
					20	40	60	80
9R1		441.340		0 - 0.09m Topsoil				
				0.09 - 4.57m Fine, moist, clean brown Sand.				
	1 m							
	2 m							
	3 m							
	4 m							
	5 m							
	6 m							
	4.57m 436.770			4.57 Bottom of Test Hole 436.770				
	7 m							
	8 m							

LEGEND	TOPSOIL	SILT	BROWN CLAY	TEST HOLE No. 9
	SAND AND GRAVEL	TILL	GREY CLAY	
PLASTIC LIMIT x ——— x LIQUID LIMIT N = Standard Penetration Value blows/ft qu = Unconfined Compression Strength (kPa)				

A. Dean Gould and Associates Geotechnical Engineers		Location; Town of Virden, Manitoba		Test Hole No. 10.		Project No. 3016	
PROJECT DESCRIPTION; Virden Water Supply Pipeline Replacement New Well to Reservoir				DRILLING DATE; May 3, 1993			
CLIENT; M. M. Dillon Ltd.				DRILLER; Paddock Drilling Ltd. Brat 22 LOGGED BY; using 5-inch Flight Augers			

SAMPLING NO.	DEPTH (m)	ELEV.	b	SOIL DESCRIPTION	MOISTURE CONTENT (%)			
					20	40	60	80
10R1	2.29 408.250	410.540		0 - 0.76m Silty clay Fill				
				0.76 - 6.4m Tan, moist, very silty 409.780 fine sand, occasional oxide inclusion				
10R2	4.57m 405.970	5 m						
10R3	6.10m 404.440	6 m		6.4 - 8.38m Grey firm silty Clay. 404.140 Highly plastic, varved with sand seams. - water enters hole @ 8.38m Elev. 402.160				
10R4	8.53m 402.010	8 m		8.38 - 9.14m Silty fine Sand, wet 402.160 oxidized, some clay seams 9.14 Bottom of Test Hole 401.100				

LEGEND

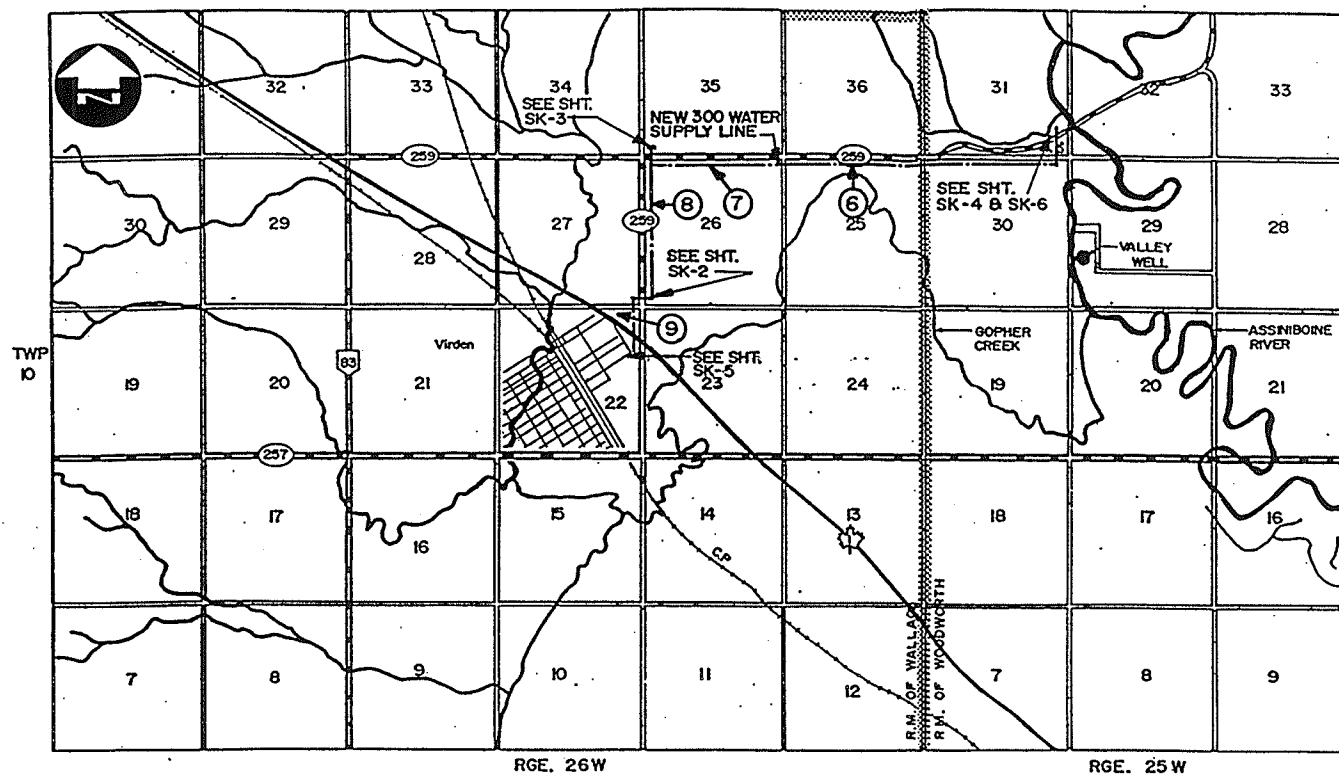
TOPSOIL
SAND AND GRAVEL

SILT
TILL

BROWN CLAY
GREY CLAY

TEST HOLE No. 10

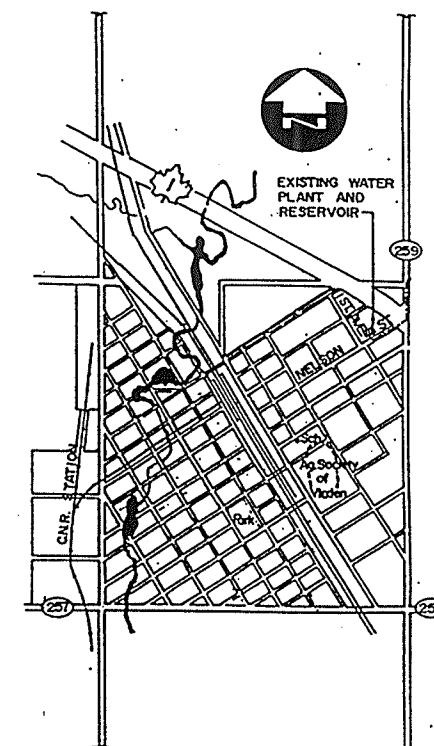
PLASTIC LIMIT x LIQUID LIMIT
N = Standard Penetration Value blows/ft
qu = Unconfined Compression Strength (kPa)



SITE PLAN
N.T.S.

LEGEND

⑧ → TEST HOLE LOCATION



TOWN OF VIRDEN
SECTION 22 - TWP 10 - RGE. 26W
N.T.S.

DILLON
Consulting Engineers • Planners
Environmental Scientists

DATE MAY • 1993

**TOWN OF VIRDEN
WATER SUPPLY LINE**

PIPELINE ROUTE & TEST HOLE LOCATIONS

PROJECT NO.
93-1097

FIGURE NO.
SK-1

